Fakultät Mathematik und
Naturwissenschaften der
Technischen Universität Dresden

TECHNISCHE
UNIVERSITÄT
DRESDEN

Single-Molecule Measurements of Complex Molecular Interactions in Membrane Proteins using Atomic Force Microscopy

Dissertation

zur Erlangung des akademischen Grades
Doctor rerum naturalium
(Dr. rer. nat.)

vorgelegt von

K. Tanuj Sapra

geboren am 16. Januar 1978 in Bombay (India)

International Max Planck
Research School for
Molecular Cell Biology and
Bioengineerging

CBG
Max Planck Institute
of Molecular Cell Biology
and Genetics

1) Gutachter: Prof. Dr. Daniel J. Müller
Technische Universität Dresden, Germany

2) Gutachter: Prof. Dr. Petra Schwille
Technische Universität Dresden, Germany

3) Gutachter: Prof. Krzysztof Palczewski
Case Western Reserve University, USA

Why would God show us that He exists in all those forms that mankind has known,
for us to kill each other?

Only if we could see that He exists in just that one form called Life,
wouldn't all miseries cease to exist?

Foreword

Being a scientist is a privilege. Not only does one get the opportunity to do what he or she wants, but also get paid for that. With this also comes great responsibility to give back to the society something meaningful and beneficial. In our quest for knowledge sometimes we forget to choose the ‘right’ type of questions. To a scientist’s thirsty brain every question is worth answering. Ironically, this is what has advanced science since ages. Though sometimes it is difficult to convince a layperson about the importance of one’s work, every scientific work needs some attention. The seed of an idea in a mind is not without a reason. For what might seem illogical to one person could create a whole new field of investigation. History is proof that great minds that were crushed by the ignorance of time stood up again as giants to usher in a new era of thinking. It is with respect that we should treat not only each other’s lives, but also ideas and work.

The whole experience of doing a PhD was a great roller coaster ride for me. I treat this thesis as my prayer through the last 7 years, and each word of it a hymn. In this book I have tried to logically present what I could accomplish in the last 3 years. Any work on membrane proteins could be aptly started with an introduction to the origin of life. The very requirement of life as we know today was the formation of a mixture of complex molecules, their intricate interactions and the necessity for these to have their own space. Compartmentalization was the starting point of complex life forms. In the first few pages of my introduction (**sections 1.1** & **1.2**), I have tried to summarize what happened before, during and after the birth of cell. In the rest of the **Chapter 1**, it has been an earnest attempt to give an overview of the membrane protein field, what has been done in the past years and where we stand now.

The other important aspect of my thesis, the atomic force microscope (AFM), is introduced in **Chapter 2**. I have started with a historical overview of development of AFM, continuing with the technical aspects of the instrument and the cantilever, followed by introducing the technique of single-molecule force spectroscopy (SMFS). The chapter finishes with a very condensed description of recent work done using AFM. Though I tried to at least briefly touch upon all the topics most relevant to my thesis, it is in no way exhaustive.

The next chapters (**3-5**) form the focus of my doctoral thesis on the single-molecule studies of membrane protein unfolding, using bacteriorhodopsin and rhodopsin as model systems. These chapters start with an introduction to these membrane proteins, followed by the conventional sequence of experimental procedures, results, discussion and conclusions. **Chapter 6** wraps up my work by giving an overview of the whole thesis, connecting the different chapters.

Throughout the text where and when necessary, I have tried to correlate the conventional biochemical and molecular biology studies with my biophysical results and conclusions. Since it is not possible to do during one’s thesis all the experiments one would like to and is burning to do, in the conclusion sections of the main chapters and the outlook section (**Chapter 7**) I have proposed what could be done using SMFS to advance our knowledge of membrane proteins.

To my family
who is always there to support me
in good times and bad

IN A NUT-SHELL

Single-molecule force spectroscopy (SMFS) with atomic force microscope (AFM) has advanced our knowledge of the mechanical aspects of biological processes, and helped us take big strides in the hitherto unexplored areas of protein (un)folding. One such virgin land is that of membrane proteins, where the advent of AFM has not only helped to visualize the difficult to crystallize membrane proteins at the single-molecule level, but also given a new perspective in the understanding of the interplay of molecular interactions involved in the construction of these molecules. My PhD work was tightly focused on exploiting this sensitive technique to decipher the intra- and intermolecular interactions in membrane proteins, using bacteriorhodopsin and bovine rhodopsin as model systems.

Using single-molecule unfolding measurements on different bacteriorhodopsin oligomeric assemblies - trimeric, dimeric and monomeric - it was possible to elucidate the contribution of intra- and interhelical interactions in single bacteriorhodopsin molecules. Besides, intriguing insights were obtained into the organization of bacteriorhodopsin as trimers, as deduced from the unfolding pathways of the proteins from different assemblies. Though the unfolding pathways of bacteriorhodopsin from all the assemblies remained the same, the different occurrence probability of these pathways suggested a kinetic stabilization of bacteriorhodopsin from a trimer compared to that existing as a monomer.

Unraveling the knot of a complex G-protein coupled receptor, rhodopsin, showed the existence of two structural states, a native, functional state, and a non-native, non-functional state, corresponding to the presence or absence of a highly conserved disulfide bridge, respectively. The molecular interactions in absence of the native disulfide bridge mapped onto the three-dimensional structure of native rhodopsin gave insights into the molecular origin of the neurodegenerative disease *retinitis pigmentosa*. This presents a novel technique to decipher molecular interactions of a different conformational state of the same molecule in the absence of a high-resolution X-ray crystal structure. Interestingly, the presence of $ZnCl_2$ maintained the integrity of the disulfide bridge and the nature of unfolding intermediates. Moreover, the increased mechanical and thermodynamic stability of rhodopsin with bound zinc ions suggested a plausible role for the bivalent ion in rhodopsin dimerization and consequently signal transduction.

Last but not the least, I decided to dig into the mysteries of the real mechanisms of mechanical unfolding with the help of well-chosen single point mutations in bacteriorhodopsin. The monumental work has helped me to solve some key questions regarding the nature of mechanical barriers that constitute the intermediates in the unfolding process. Of particular interest is the determination of altered occurrence probabilities of unfolding pathways in an energy landscape and their correlation to the intramolecular interactions with the help of bioinformatics tools.

The kind of work presented here, in my opinion, will not only help us to understand the basic principles of membrane protein (un)folding, but also to manipulate and tune energy landscapes with the help of small molecules, proteins, or mutations, thus opening up new vistas in medicine and pharmacology. It is just a matter of a lot of hard work, some time, and a little bit of luck till we understand the key elements of membrane protein (un)folding and use it to our advantage.

Abbreviations

aa	Amino acid
AFM	Atomic force microscope
BFP	Biomembrane force probe
BR	Bacteriorhodopsin
CD	Circular dichroism
CFTR	Cystic fibrosis transmembrane regulator
DAGK	Diacylglycerol kinase
DFS	Dynamic force spectroscopy
DLVO	Derjaguin-Landau-Verwey-Overbeek
DOPC	Dioleoylphosphatidyl-choline
DPPC	Dipalmitoylphosphatidyl-choline
DTAC	*n*-dodecyl trimethyl ammonium chloride
DTT	Dithiothreitol
EDL	Electrostatic double-layer
EM	Electron microscopy
EPR	Electron paramagnetic resonance
ER	Endoplasmic reticulum
F-D	Force-distance
FEP	Free energy perturbation
FJC	Freely jointed chain
GpA	Glycophorin A
GPCR	Guanine nucleotide-binding protein-coupled receptor
IgG	Immunoglobulin
LacY	Lactose permease
LOT	Laser optical tweezer
MCP	Major coat protein
MD	Molecular dynamics
NEM	*N*-ethylmaleimide
NMR	Nuclear magnetic resonance
PE	Phosphatidylethanolamine
PSRC	Photosynthetic reaction center
ROS	Rod outer segment
RPE	Retinal pigment epithelium
SD	Standard deviation
SDS	Sodium dodecyl sulfate
SEM	Standard error of mean
SFA	Surface force apparatus
SFM	Surface force microscope
SMFS	Single-molecule force spectroscopy
SNOM	Scanning near-field optical microscope
SPM	Scanning probe microscope
S-S	Disulfide bond
SSID	Site-specific infrared dichroism
STM	Scanning tunneling microscope
TM	Transmembrane
WLC	Worm-like chain
WT	Wild-type
2-D, 3-D	Two-dimensional, three-dimensional

Symbols

E	Potential energy (J)
E	Young's modulus (N/m^2)
EC_{50}	Concentration of a compound where 50% of its maximal effect is observed (M)
F, F_{attr}, F_{rep}, F_{ext}, F_{vdW}	Force, attractive force, repulsive force, external force, Van der Waals force (N)
f_r, ν, ω	Resonance frequency, vibrational frequency, angular frequency (s^{-1} or rad$\cdot$s^{-1})
G_n, G^*, ΔG^*_u, $\Delta G^*_{u(F)}$	Free energy of, native state, transition state, unfolding (no force), unfolding (under force) (J)
H	Hamaker constant (J)
k_B	Boltzmann constant (1.381 x 10^{-23} J$\cdot$K^{-1})
k_{off}	Rate constant (s^{-1})
k_u, $k_{u(F)}$	Unfolding rate, unfolding rate under force (s^{-1})
K_D	Equilibrium dissociation constant (M)
L	Length (m)
l_p	Persistence length (m)
L_c	Contour length (m)
M, m^*, m_o	Mass, end loaded mass, effective mass (kg)
n	Total number (dimensionless)
N	Refractive index (dimensionless)
P_e	Percent probability (dimensionless)
Q	Quality factor (dimensionless)
r_f	Loading rate (N$\cdot$s^{-1})
R	Distance, radius (m)
s	Segment length of a freely jointed chain (m)
T	Thickness (m)
t_D	Relaxation time (s)
t_{off}	Lifetime (s)
t_r	Response time (s)
tss	Tip-sample separation (m)
T	Temperature (K = ^{o}C + 273.15)
$\langle U \rangle$	Mean energy (J)
w	Width (m)
x, Δx, z	Deflection, displacement, extension (m)
x_u	Width of potential barrier (m)
$\langle x^2 \rangle$	Variance of deflection (m)
ε	Dielectric constant (F$\cdot$m^{-1}, C$^2\cdot$J$^{-1}\cdot$m^{-1})
κ	Force/Spring constant (N$\cdot$m^{-1})
λ	Wavelength (m)
ρ	Density (kg$\cdot$m^{-3})
μ^{-1}	Debye length (m)
ψ	Surface potential (J)
χ	Transmission coefficient (W$\cdot$m$^{-2}\cdot$K^{-1})

CONTENTS

CHAPTER 1

INTRODUCTION 1

1.1 CELL AS A COMPLEX FACTORY 1

1.2 MEMBRANES 2

1.3 MEMBRANE PROTEINS 3

- 1.3.1 THE IMPORTANCE OF STUDYING MEMBRANE PROTEINS 5
- 1.3.2 MEMBRANE PROTEIN FOLDING, MISFOLDING AND MISASSEMBLY 6
  - *Model membrane proteins for studying folding, misfolding and misassembly 14*
- 1.3.3 WHY ARE MEMBRANE PROTEINS SO DIFFICULT TO STUDY? 16
- 1.3.4 METHODS FOR STUDYING MEMBRANE PROTEINS 17
- 1.3.5 WHY STUDY MEMBRANE PROTEINS WITH ATOMIC FORCE MICROSCOPY? 20

CHAPTER 2

ATOMIC FORCE MICROSCOPY 22

2.1 ATOMIC FORCE MICROSCOPE 22

- 2.1.1 A BRIEF HISTORY 22
- 2.1.2 PRINCIPLE AND SET-UP 22
- 2.1.3 CANTILEVER 24
  - *Calibrating the cantilever 26*
- 2.1.4 RELEVANT FORCES 29
  - *Short-range forces 30*
  - *Electrostatic double-layer force 30*
  - *van der Waals force 31*
- 2.1.5 AFM MODES 33
  - *Contact or dc mode 33*
  - *Non-contact ac modes 34*

2.2 SINGLE-MOLECULE FORCE SPECTROSCOPY 36

- 2.2.1 BACKGROUND OF MECHANICAL UNFOLDING 39
- 2.2.2 A VARIETY OF PROTEINS RIPPED APART BY SMFS 41
- 2.2.3 WHAT CAN BE LEARNT FROM SMFS ON MEMBRANE PROTEINS? 43

CHAPTER 3

DISSECTING THE INTER- AND INTRAMOLECULAR INTERACTIONS OF BACTERIORHODOPSIN 46

3.1 INTRODUCTION 46

3.2 EXPERIMENTAL PROCEDURES 49

- 3.2.1 PURPLE MEMBRANE PREPARATION, DIMERIZATION AND MONOMERIZATION OF BR 49
- 3.2.2 PREPARATION OF SUPPORTS FOR SINGLE-MOLECULE FORCE SPECTROSCOPY 50
- 3.2.3 AFM SETUP FOR MEASUREMENTS 51
- 3.2.4 SINGLE-MOLECULE FORCE SPECTROSCOPY AND IMAGING 51
- 3.2.5 SELECTION OF FORCE-DISTANCE CURVES 52
- 3.2.6 ANALYSIS OF FORCE-DISTANCE CURVES 54
  - *Models used to describe stretching under force 55*

3.3 RESULTS 58

- 3.3.1 HIGH-RESOLUTION AFM IMAGING OF MONOMERIC, DIMERIC AND TRIMERIC BR ASSEMBLIES 58
- 3.3.2 UNFOLDING PATHWAY OF A SINGLE BR MOLECULE 59
- 3.3.3 UNFOLDING PATHWAYS DO NOT DEPEND ON BR ASSEMBLY 61
- 3.3.4 SINGLE BR MOLECULES FROM DIFFERENT ASSEMBLIES UNFOLD AT DIFFERENT FORCES 63

3.3.5 Unfolding probability via a certain trajectory depends on BR assembly ... 64

3.4 DISCUSSION ... 65

3.4.1 Unfolding pathways remain the same but their probability depends on BR assembly ... 65
3.4.2 Location of stable structural segments is independent of BR assembly ... 67
3.4.3 Membrane protein assembly changes stability of structural segments ... 67
3.4.4 Deciphering contributions of inter- and intramolecular interactions ... 68
3.4.5 Can the results from single-molecule measurements correlated to chemical and thermal denaturation experiments? ... 69

3.5 FUNCTIONAL IMPLICATIONS AND OUTLOOK ... 69

3.6 CONCLUSIONS ... 70

... ***CHAPTER 4***

UNRAVELING MOLECULAR INTERACTIONS THAT STABILIZE NATIVE BOVINE RHODOPSIN ... 71

4.1 BACKGROUND & SCOPE ... 71

4.1.1 Rhodopsin ... 72

4.2 EXPERIMENTAL PROCEDURES ... 75

4.2.1 Preparation of ROS disc membranes ... 75
4.2.2 Attaching a single rhodopsin molecule to the AFM cantilever tip ... 76
4.2.3 Imaging and single-molecule force spectroscopy ... 76
4.2.4 Selection of force-distance curves and data analyses ... 77
4.2.5 Assigning the stable structural segments in rhodopsin ... 79

4.3 RESULTS ... 80

4.3.1 Imaging native ROS disc membranes ... 80
4.3.2 Mechanical unfolding of single native rhodopsin molecules ... 81
4.3.3 Unfolding rhodopsin from the N-terminal end ... 83
4.3.4 Mapping the stable structural segments in dark state native rhodopsin ... 84
4.3.5 Unfolding rhodopsin in absence of the structurally stabilizing native Cys110-Cys187 bond ... 86

4.4 DISCUSSION ... 87

4.4.1 Molecular interactions in the N-terminal region and transmembrane helix I ... 88
4.4.2 Unfolding of helices I and II with extracellular loop C-I: Proof of ‘third stage’ of membrane protein folding ... 89
4.4.3 Origin of two stable structural segments in transmembrane helix II ... 89
4.4.4 Stability of extracellular loop E-I ... 90
4.4.5 Extracting the helical hairpin structure held together by the native Cys110-Csy187 bond ... 90
4.4.6 Stable structural segments of helix V and cytoplasmic loop C-III, and helix VI ... 91
4.4.7 Extracellular loop E-III, helix VII, and cytoplasmic helix VIII establish independently stable structural segments ... 91
4.4.8 Molecular interactions are altered in absence of the native disulfide bond ... 92
4.4.9 Functional implications of changing molecular interactions ... 95
4.4.10 Cleaving cytoplasmic loop C-III does not affect molecular interactions ... 95
4.4.11 Conserved residues are localized within stable structural segments ... 96

4.5 CONCLUSIONS & OUTLOOK ... 97

... ***CHAPTER 5***

ZINC MEDIATED INCREASE IN STABILITY OF NATIVE BOVINE RHODOPSIN ... 98

5.1 INTRODUCTION ... 98

5.1.1 Role of zinc in biology ... 98
5.1.2 Physiological role of Zn^{2+} in the eye ... 99

5.2 EXPERIMENTAL PROCEDURES **101**
5.2.1 ROS disc membrane preparation 101
5.2.2 AFM imaging and SMFS 101
5.2.3 Selection and analysis of force-extension curves 102
5.2.4 Molecular dynamics simulations 102
5.2.5 Free energy calculations 102
5.3 RESULTS **103**
5.3.1 Unfolding single native rhodopsin molecules in presence of Zn^{2+} 103
5.3.2 Zn^{2+} binding increases the mechanical stability of rhodopsin 107
5.3.3 Stabilization of rhodopsin by Zn^{2+} is specific 110
5.3.4 Zn^{2+} stabilizes the native disulfide bond between Cys110-Cys187 111
5.3.5 Unfolding probability of secondary structure elements is altered on Zn^{2+} binding .. 113
5.3.6 Effect of Zn^{2+} on the free energy of rhodopsin 114
5.4 DISCUSSION **116**
5.4.1 Specific effect of Zn^{2+} 117
5.4.2 Zn^{2+} binding has a global effect on rhodopsin 117
5.4.3 Is the effect of Zn^{2+} binding in rhodopsin physiologically relevant? 118
5.4.4 Increase in thermodynamic stability by Zn^{2+} 119
5.4.5 Zn^{2+} binding and dimerization of rhodopsin 120
5.5 CONCLUSIONS & FUTURE GOALS **122**

.... ***CHAPTER 6***

GENERAL CONCLUSIONS **124**

.... ***CHAPTER 7***

OUTLOOK & FUTURE GOALS: MECHANICAL UNFOLDING OF MEMBRANE PROTEINS – AN UNEXPLORED GOLDMINE? **126**
7.1 MECHANISM OF HELIX UNFOLDING UNDER FORCE – A HYPOTHESIS **126**
7.2 EFFECT OF POINT MUTATIONS ON THE COMPLEX UNFOLDING ENERGY LANDSCAPE OF BR **129**
7.2.1 Changes in intramolecular interactions alter the preferred unfolding routes on the energy landscape 130
7.2.2 Mutations and unfolding energy landscape 133
7.2.3 Physiological relevance of energy landscapes 134
7.3 CAN WE PROBE THE RELATIONSHIP BETWEEN MEMBRANE PROTEIN STABILITY AND FOLDING EFFICIENCY WITH SMFS? **135**
7.4 THE KLONDIKE GOLD RUSH? **136**
BIBLIOGRAPHY **137**
PUBLICATIONS **165**
ACKNOWLEDGEMENTS **166**

Chapter

1

INTRODUCTION

1.1 CELL AS A COMPLEX FACTORY

The cell is the basic morphological unit of all modern organisms. A cell in its simplest form can be considered as a small sac or balloon filled with the chemicals of life. A variety of life sustaining processes take place in the cell. Individual cells group to form tissues, which further associate to form more complex organs that perform complex functions and are linked by intricate systems of communication, thus giving rise to an organism (Alberts et al., 2002). Any explanation about how this fascinating and efficient machine originated is not without many missing links, but a pinch of imagination with science helps us to understand the important steps in the whole process.

The raw materials of life came into existence during the chemical evolution in the prebiotic environment. Even with these raw materials in her hands, Mother Nature couldn't produce life in a matter of days or months. It was necessary that our ancient pool of organics and inorganics be modified and learns to work in tandem. It was required that different macromolecules with complementary arrangements of functional groups associate with each other to give rise to more complex molecular assemblies with a greater range of functional and structural possibilities (Voet et al., 1999).

Life, it seems, is not without a sense of irony. Where on the one hand these evolving basic systems needed to coexist, on the other hand the pressure to compete for the available resources in the primordial pond and the ever changing environment made it essential for them to have their own boundaries. Evolution, ever seeking to exploit the natural tendencies of molecules, has seized the opportunity to craft functional associations of protein complexes, separated lipid compositional areas and regions of functional specialization. Thus the cell was born.

The compartmentation of cell lead to its evolution as the most efficient nano-machine known to mankind. Even with only an outer cell membrane (surrounded by a cell wall in most cases) prokaryotes perform different metabolic functions in different regions of the cytoplasm. Eukaryotes, on the other hand, delegate their functions to different membrane bound organelles – endoplasmic reticulum (**ER**), Golgi apparatus, mitochondria, chloroplasts, lysosomes and peroxisomes, and vacuoles (Voet et al., 1999). These compartments maintain the characteristic and essential differences between the contents of each organelle and the cytosol (Alberts et al., 2002).

1.2 MEMBRANES

One of the crucial events leading to the formation of the first cell must have been the development of the outer membrane (Alberts et al., 2002). From the pool of various saturated and unsaturated lipids with different head groups, nature has very beautifully constructed the thin, self-sealing, insulating boundaries that are used by cells to create regions of different composition and electrochemical potential[1]. The lipid bilayer has been firmly established as the universal basis for cell-membrane structure. Apart from imparting the basic structure of the membrane, the lipid bilayer serves as a relatively impermeable barrier to the passage of most water-soluble molecules. The liquid crystallographic structure of a L_α-phase dioleoylphosphatidyl-choline (**DOPC**) bilayer revealed that the membrane is typically divided into two regions – a 30 Å wide hydrocarbon core in the centre dominated by aliphatic lipid chains, and a ~15 Å thick interfacial region of the bilayer comprising of lipid headgroups and considerable bound water (Wiener and White, 1992).

The three major classes of membrane lipid molecules – phospholipids, cholesterol and glycolipids - have different compositions in the inner and outer leaflets of the lipid bilayer reflecting the different functions of the two faces of a cell membrane, a property which might be helpful in deciding the topology of the protein during insertion influenced by the 'positive-inside' rule (von Heijne, 1986). Moreover, the variations in lipid composition may have relevance to membrane protein misassembly (Bogdanov and Dowhan, 1999; Eidelman et al., 2002; Hampton, 2002).

---

[1] A high electrochemical gradient across the cell membrane could create an electric field of 100,000 volt/cm (Alberts et al., 2002).

In the year 1972, S. Jonathan Singer and Garth Nicolson put forth the 'fluid mosaic model' (Singer and Nicolson, 1972). The model visualized the cell membrane to be a dynamic, fluid structure where most of the molecules are able to move about in the plane of the membrane and not a static structure as thought previously. Since this model, our understanding of the cell membrane has advanced tremendously to the point where we now know that the cell membrane is more mosaic than fluid (Engelman, 2005). Further refinements in this barrier led to the use for its energy-storage properties and to the creation of ways to pass information across this boundary.

1.3 MEMBRANE PROTEINS

Though the lipid bilayer is the scaffold of the membrane and is the key player in cellular homoeostasis and metabolic-energy transduction, the membrane must be modified by macromolecules for the uptake of nutrients and the disposal of waste. Owing to their strategic localization at the interfaces between the interior and exterior of the cell and between cellular compartments, besides the inevitable function of mediating communication between both sides of the membrane (receptors, pores and channels are all signal transducers), membrane proteins have pivotal roles in many cellular processes, including photosynthesis, cell-cell signaling and adhesion, transport of ions and small molecules, maintenance of osmotic balance and cellular organization. Due to the physical and chemical constraints imposed by the hydrophobic environment, only two structural motifs have been observed for protein structure within the bilayer: β-barrel and bundles of transmembrane (**TM**) α-helices (**Figure 1.1**), the former being predominant (Bigelow et al., 2004; Bowie, 2005; White and Wimley, 1999). A frequently observed submotif is the interfacial helix connected to adjacent TM helices, illustrated by the coat protein of fd bacteriophage (McDonnell et al., 1993).

The general structural features of membrane proteins compare remarkably well with those of soluble proteins. E.g., the interior amino acids in the photosynthetic reaction center (**PSRC**) of *Rhodobacter sphaeroides* are almost exclusively nonpolar, packed just as tightly as those of soluble proteins (Rees et al., 1989). Also, like the soluble proteins, the interiors of membrane proteins are comprised of internally hydrogen bonded α-helices and β-sheets. The distinguishing characteristics of membrane proteins are the preferred locations of some amino acids along the TM axis, e.g., arginine and lysine are much more abundant in the cytoplasmic domains relative to the periplasmic domains of bacterial membrane proteins (von Heijne, 1986), and the aromatic amino acids like tryptophan and tyrosine are highly preferred at the interfacial locations (Schiffer et al., 1992).

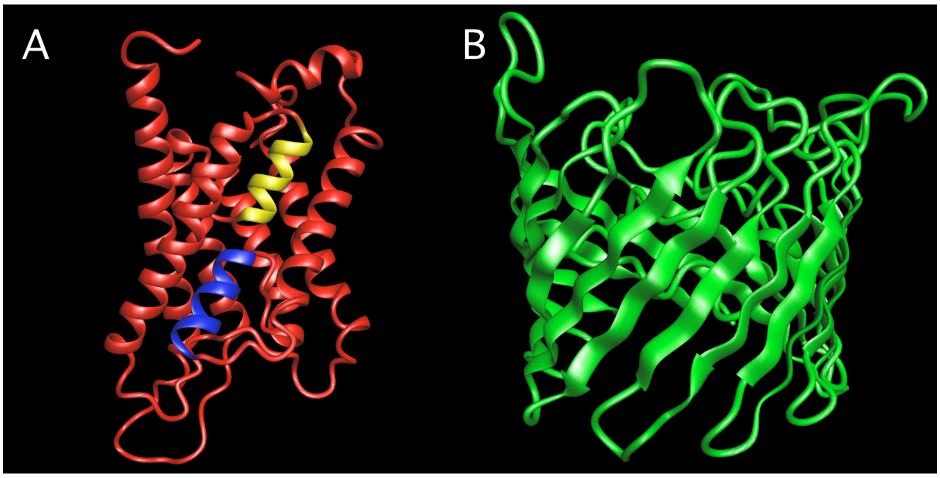

Figure 1.1 Structural motifs of membrane proteins

The two most common structural architectures of membrane proteins, (**A**) the α-helix bundle, and (**B**) the β-barrel. (**A**) Aquaporin-1 (PDB: 1J4N) (Sui et al., 2001) from *Bos taurus*, example of an α-helical protein, shows two half helices (blue and yellow) in the middle of the lipid bilayer. (**B**) The β-barrel structure of porin (PDB: 1PRN) from *Rhodopseudomonas blastica* (Kreusch and Schulz, 1994) with anti-parallel β-strands.

β-Strands are found in the outer membranes of the Gram-negative bacteria[2], mitochondria and chloroplasts, forming rigid pores known as β-barrels (Wimley, 2003). Membranes are spanned by antiparallel β-strands of 9-11 residues with a tilt of 20-45° out of the TM axis (Wimley, 2003). The smallest known barrels contain 8 TM strands, and the largest barrels of known structure (Sansom and Kerr, 1995), the TonB-dependent importers, contain 22 strands each; however, evidence points to the existence of much larger ones (Ramachandran et al., 2002). Although unified by many common structural features, there is an immense diversity of distribution, function and architecture of β-barrel proteins in diverse organisms. Examples from the many different functional categories include OmpF (non-specific porin), maltoporin (facilitated transporter), TolC (energy-dependent transporter-efflux), Tom40 (mitochondria protein import pore) and α-hemolysin (protein pore-forming toxin), to mention a few (Wimley, 2003).

---

[2] Approximately 2-3% of the genes in Gram-negative bacterial genomes encode β-barrels (Wimley, 2003)

Single and bundled TM α-helices, held together by a delicate balance of electrostatic and van der Waals interactions, have a much broader range of functionalities and complexities (Torres et al., 2003). Our early views of membrane protein structure were largely based on the pioneering work on bacteriorhodopsin (**BR**) by Henderson and colleagues (Henderson and Unwin, 1975), besides those of Baldwin (Baldwin, 1993) and Kuhlbrandt (Kühlbrandt and Wang, 1991). The notion that these structures were just bundles of long helical rods traversing the membrane was shaken by the elucidation of the structure of the glycerol/water channel GlpF (Fu et al., 2000) and ion channel structures (Doyle et al., 1998; Dutzler et al., 2002). These molecules turned out to be complex architectural feats constructed of kinked and distorted helices, some of them penetrating half way into the bilayer (Fu et al., 2000). The constraints of an anisotropic lipid environment force the TM helices to adapt a narrower distribution of packing angles around 20^o with a strong preference for left-handed helices, compared to right-handed helices with a packing angle at -35^o found in water-soluble proteins (Bowie, 1997). A packing angle of 20^o is favourable due to facilitation of inter-helix side chain interdigitation (Chothia et al., 1981). In fact, more than 60% of all TM-helix-packing angles are in the range of 0^o to 40^o. Another reason for this preference is the favourable orientation of TM helices along membrane normal, which tends to favour small packing angles (Huschilt et al., 1989). The general packing of α-helices in membrane proteins has been described by the 'knob-into-holes' packing model first described for soluble coiled coils (Langosch and Heringa, 1998) (see **section 1.3.2**). In **section 3.1**, I would give an overview on the light-driven proton pump BR, and in **section 4.1.1**, I would describe the well-studied model Guanine nucleotide-binding protein-coupled receptor (**GPCR**) molecule rhodopsin, the two membrane proteins I worked with during my PhD.

1.3.1 The importance of studying membrane proteins

Since membrane proteins carry out a plethora of functions and are involved in almost every process in the cell, their importance cannot be overstated. We can never hope to understand how cells work if we ignore the molecules encoded by a quarter of the genome. Besides, studies of membrane protein folding *in vitro* (Booth and Curran, 1999) are of considerable interest at several levels. Intellectually, folding is an intriguing problem, both for soluble and membrane proteins alike. Moreover, improving our understanding of membrane protein structure could have a significant impact on medicine. The pharmaceutical importance of membrane proteins stems from the fact that they include structural proteins, channels and receptors that are accessible through the exterior of cells and thus formidable drug targets. Mutations in genes encoding membrane proteins are the causative agents of various diseases, including cystic fibrosis, retinitis pigmentosa, congenital nephrogenic diabetes insipidus, arrhythmias, hearing loss, and also amyloid diseases[3] (Sanders and Myers, 2004; Sanders and Nagy, 2000; Tamarappoo et al., 1999). A better understanding of these defects is important for designing new therapies. The GPCRs form the largest known family of cell-surface receptors responding to diverse stimuli such as hormones, neurotransmitters, odorant molecules and light, thus implicating them in virtually all physiological processes and making them targets for ~60% of the new drug molecules. Structural, biochemical and biophysical information from different sources could greatly improve our understanding of these fascinating molecules and increase the efficiency of drug discovery.

1.3.2 Membrane protein folding, misfolding and misassembly

Apart from predicting the correct three dimensional folded structure of a protein from its sequence, the key problem in protein folding is how a chain of amino acids folds and acquires the conformation of this native, folded, biologically active protein from its denatured state, thus making protein folding one of the most perplexing problems in molecular biology. The first milestone in deciphering the central dogma of molecular biology, DNA → RNA → Proteins, was reached in 1961 when Anfinsen elegantly showed the spontaneous formation of disulfide bonds in ribonuclease A (RNaseA) driven by the free energy of folding (Anfinsen and Haber, 1961). Anfinsen's 'thermodynamic hypothesis' was challenged by a brilliant thought experiment of Levinthal's. Since 1968, when Levinthal first expressed his dilemma about the impossibility of a protein folding into its native functional state by a random search (Levinthal, 1968), there has been progress by leaps and bounds in our understanding about protein folding. Levinthal's paradox, as it is most commonly known as, is that if a small protein were to fold by randomly checking all possible conformations of its unfolded state, the process would take longer than the age of the universe! He proposed that the folding process should follow a set of well-defined pathways under kinetic control. The 'New view' or the

---

[3] The precursor of the peptide that forms amyloid proteins in Alzheimer's disease is a membrane protein (Selkoe, 2001)

'Ensemble view' of protein folding has solved in part the Levinthal's paradox by introducing the concept of folding energy landscapes pictorially represented as funnel shaped landscapes (**Figure 1.2**) (Dill, 1999; Dill and Chan, 1997). Besides, energy landscapes provide the framework for relating the thermodynamics and kinetics of protein folding. Folding studies on small globular proteins suggest that the basic folding information needed to specify the three-dimensional (**3-D**) structure of a protein is encoded in the amino acid sequence of the polypeptide chain (Dill, 1999), and studies point in the same direction for membrane proteins. Though a number of models, like the hydrophobic collapse, the nucleation-condensation, and the framework model, have been proposed to explain the folding of globular proteins, there is no general consensus about the universal appeal of any one of them (Daggett and Fersht, 2003a; Daggett and Fersht, 2003b).

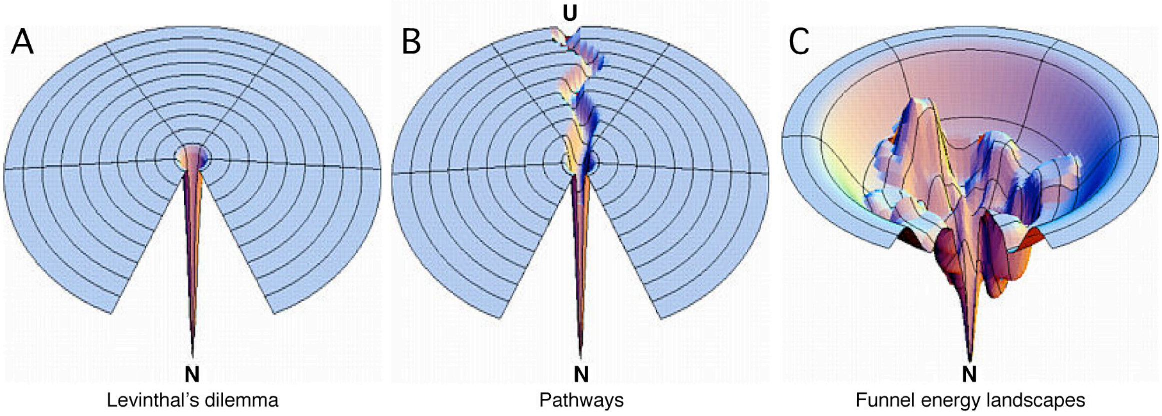

Figure 1.2 From Levinthal to pathways to funnels

Levinthal's thought experiment of the impossibility of a protein to fold through a random search of all possible conformations, denoted as a flat energy surface (**A**), led to the idea that protein folding is guided through well-defined pathways to their native, folded states (**B**). The failure to find pathway led mechanisms in proteins, and the observation that many proteins could refold enormously fast after unfolding *in vitro* suggested that the fold of a protein is encoded in its primary sequence, thus giving birth to the concept of funnel-shaped energy landscapes. On such a funnel-shaped landscape proteins could fold via numerous trajectories being taken through a funnel, signifying the reduction in their energies as the protein folds[4].

The best point to start in the case of membrane proteins is from the early models of membrane protein folding. Based on structural and thermodynamic measurements of the partitioning of small hydrophobic peptides and the so-called helical hairpin insertion model (Engelman and Steitz, 1981), Jacobs and White (Jacobs and White, 1989) proposed a three-step thermodynamic model for protein folding involving interfacial partitioning, interfacial folding and insertion. At about the same time Popot and

---

[4] The caption title of this figure is the title of an excellent review by Prof. Ken A. Dill (Dill and Chan, 1997).

Engelman proposed a 'two-stage hypothesis' for the assembly of α-helical proteins in their landmark papers (Popot et al., 1987; Popot and Engelman, 1990). According to the two-stage model the process of membrane protein folding can be divided into two very simple intuitive stages: insertion and folding (**Figure 1.3**).

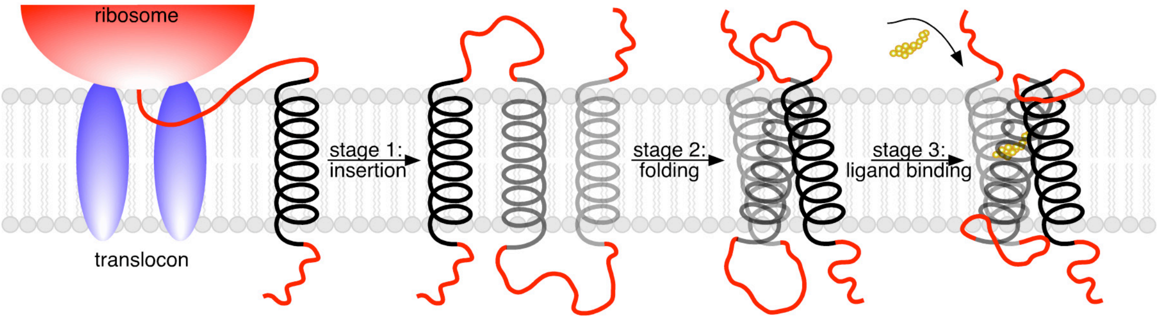

Figure 1.3 The two-stage model of membrane protein folding

The cartoon here shows the insertion of a constitutive membrane protein, the polypeptide being synthesized at the ribosome and inserted via the translocon machinery. Stage 1 involves the formation of stable helices across the membrane bilayer. The helices, in a later step (stage 2), interact with one another to form higher order structures. In a possible third stage (stage 3), these higher order structures can facilitate partitioning of additional polypeptide regions such as loops connecting the helices or even short helices (Engelman et al., 2003). The binding of a ligand can be a stabilizing force in this final folding stage. Except the translocon-mediated insertion of the helices, the mechanism should remain the same for non-constitutive membrane proteins.

In the first stage, the TM segments driven by the thermodynamically favored formation of backbone hydrogen bonds in the lipid environment form independently stable α-helices across the membrane lipid bilayer, thus establishing some of the membrane-inserted segments and their topology. In the second stage, more interactions are established between helices building the tertiary and quaternary structures. As simple as it may seem, this is just an attempt to explain an utterly complex mechanism. Kinetic analysis of retinal binding to BR showed that the retinal binds after the fragments associate, effectively in a 'third stage' of the folding process (Popot et al., 1987). During this possible third stage, higher order structures can facilitate partitioning of additional polypeptide regions such as coil regions or short helices or prosthetic groups into the membrane. Consequently the loops connecting transmembrane helices may adopt their native conformation thereby pulling secondary structures into the functional structure.

A decade later, White and Wimley (White and Wimley, 1999) proposed a four-step thermodynamic cycle for membrane protein folding. The four steps - partitioning, folding, insertion and association - can process along an interfacial path, a water path or a combination of the two (**Figure 1.4**).

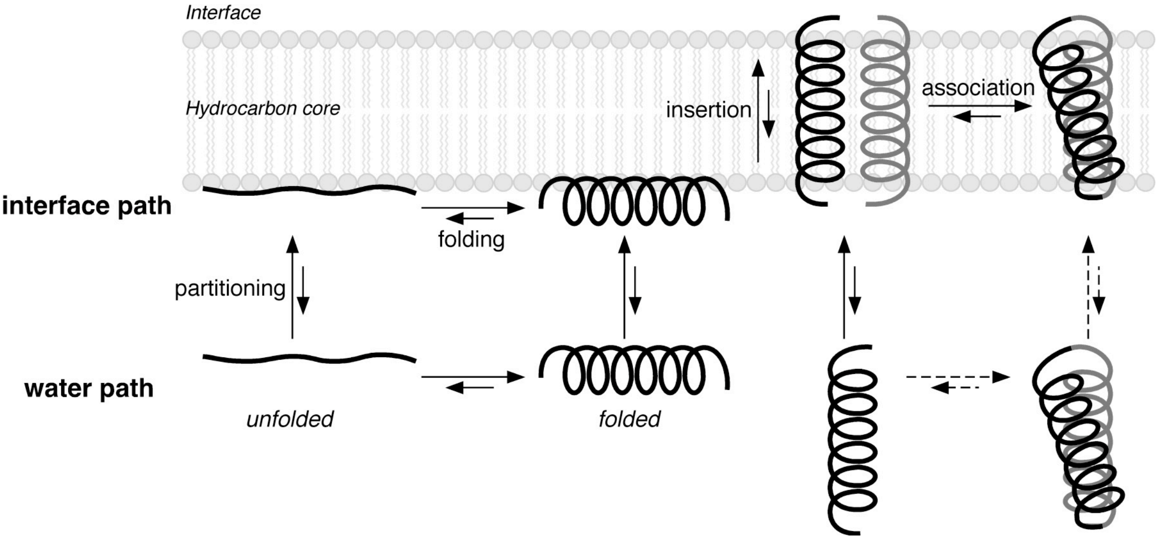

Figure 1.4 A four-step thermodynamic model describing the energetics of partitioning, folding, insertion, and association of an α-helix

The steps can follow either an interfacial path or an aqueous path or a combination of the two. It should be noted that the lipid chains and the head-groups of the membrane bilayer are not drawn to scale. The thickness of a single interface extends upto ~15 Å, enough to accommodate the unfolded and folded (~10 Å in diameter) polypeptide chains (White and Wimley, 1999).

However, unlike the assembly of BR fragments *in vitro* (Popot and Engelman, 1990), helix fragments of mammalian rhodopsin do not associate *in vitro* and only a subset associates *in vivo* (Ridge et al., 1995a). Taking into account the point mutation and deletion studies on rhodopsin that suggest the tight structural coupling of the extracellular and the transmembrane domains of rhodopsin (Hwa et al., 2001), the ‘three-stage model’ for membrane protein folding does not provide a framework for understanding rhodopsin folding (Klein-Seetharaman, 2005). This leads to an important conclusion that long-range interactions[5] determine the formation of early conformational ensembles and partially folded structures during the folding of rhodopsin (Klein-Seetharaman, 2005; Rader et al., 2004). Regardless of the insertion/assembly process, stably folded membrane proteins reside in a free energy minimum determined by the net energetics of the interactions of the peptide chains with each other, the lipid bilayer hydrocarbon core, the bilayer interface, cofactors and with water (White and Wimley, 1999)

---

[5] These long-range interactions include interactions between (i) amino acids of different soluble loops, (ii) residues of loops and TM helices, and (iii) TM helices.

Like the soluble-protein-folding problem, the folding of membrane proteins probably proceeds down a funnel-shaped energy landscape to an energy minimum (Dill and Chan, 1997). Consistent with a folding funnel view is the observation of multiple pathways in the folding of bacteriorhodopsin (Lu and Booth, 2000) (**section 7.2**). A major difference between soluble protein folding and membrane protein folding, however, is that the starting point in membrane proteins is much more constrained because the secondary structure and topology is set by the insertion process within the strict confines of the hydrophobic membrane. Thus, the unfolded protein is much farther down the folding funnel and closer to the folded state compared to that in soluble proteins. It seems clear that the folding-energy landscape is defined by a complex interplay between various forces, including polypeptide partitioning in the bilayer, interactions between the lipid chains and the protein, and interactions within the protein itself.

The descriptions of membrane-protein folding energetics will need to vary as a function of bilayer depth due to the anisotropic nature of the lipid bilayer. For a polypeptide chain to partition in the lipid milieu from water, there needs to be an existence of equilibrium between the two phases. Though the average 20-residue segment is just long enough to span a typical bilayer in a helical conformation, hydrophobicity is an important feature defining TM helices, thus implying that thermodynamic partitioning between water and the lipid bilayer plays an important role in membrane protein insertion and/or maintenance of the protein in the bilayer.

To have a thermodynamic perspective to insertion of helices, a thermodynamic scale based on a water-octanol system was developed by White and Wimley (White and Wimley, 1999; Wimley et al., 1996). This scale beautifully describes the contribution of each of the 20 amino acids in the energetics of polypeptide partitioning in the lipid bilayer. E.g., transferring a glycine residue is unfavourable ($\Delta G = 1.25$ kcal mol^{-1}), and a ΔG of 10 kcal mol^{-1} for transferring a 20-residue polyalanine sequence suggests that the segment is not sufficiently hydrophobic to partition into the membrane. On the other hand, replacing five alanines with five leucines would make the insertion favorable ($\Delta G = -1.25$ kcal mol^{-1}) indicating a hydrophobicity threshold to drive the equilibrium in favor of bilayer insertion (Liu et al., 1996a). Though these and such results of ΔG measurements on substituting amino acids and altering their insertion preference are in excellent agreement with the recent experiments on translocon-catalysed TM insertion (Hessa et al., 2005a), octanol being an isotropic medium is not a perfect model of the hydrocarbon core in which the transfer energies vary as a function of bilayer depth (Wimley and White, 1996).

As simple as it may seem *in vitro*, the real scenario in a cell is always complex involving a lot of protein machines, controls and feedbacks. The recent elucidation of the structure of SecY/Sec61 translocon complex from *Methanococcus jannaschii* shed light on the elegant working of this molecular machine (Rapoport et al., 2004; Van den Berg et al., 2004). The SecY/Sec61 complex has quite a few difficult jobs on its hands, like to decide the topology of the inserted segments, the partitioning of the segment to the aqueous compartment on the other side or in the membrane laterally, to mention a couple. The former has been explained at least partially on the basis of the 'positive-inside rule' (von Heijne, 1986), charge reversal studies on *Saccharomyces cerevisiae* Sec61 α subunit (Goder et al., 2004), synthesis rate and the length of the hydrophobic segment (Goder et al., 2004; Rapoport et al., 2004). Though the structure solved is of the closed form of the channel without a translocating polypeptide, coupled with considerable biochemical data, it enabled Rapoport and colleagues (Rapoport et al., 2004; Van den Berg et al., 2004) to suggest a plausible model for the general protein translocation process, thus markedly advancing our ideas about how these complex functions can be accomplished. In brief, the ribosome secretes nascent chains into the membrane-resident translocon, where the polypeptide chains are assembled and released into the membrane by a process that is much better understood now than before (Blobel and Dobberstein, 1975). After completion of the process, the ribosome-translocon complex dissociates leaving the protein stably folded in the membrane. Nonconstitutive membrane proteins, such as melittin (Dempsey, 1990), colicins (Cramer et al., 1995), diphtheria toxin (Zhan et al., 1995) and the β-barrel protein staphylococcal α-hemolysin (Song et al., 1996), bypass this elaborate machinery by spontaneously entering the membrane from the aqueous phase.

The elegant work of von Heijne and co-workers has helped to improve our understanding of the insertion code significantly (Hessa et al., 2005a; Hessa et al., 2005b). By substituting different amino acids in a test polypeptide segment it was possible to measure an apparent free energy of biological partition for each of the 20 amino acids. The biological scale correlates reasonably well with the measured free energies for transferring amino acid chains from water to octanol. This study clearly shows that the insertion probability not only depends on the composition, but also on the location of individual residues within the TM segments. This is a big stride in our understanding of the defining factors that contribute to insertion probability of a segment, and a major milestone on the way to solving the membrane protein folding problem.

Besides insertion and folding, the 'two-stage hypothesis' has provided the conceptual basis for the packing of TM α-helices as an important factor contributing to the stability of the structure (Curran and Engelman, 2003). Any defect in packing could lead to misfolding/misassembly and a subsequent manifestation as a disease. Many concepts of how helices interact in membranes come from the work on the TM domain of erythrocyte dimeric protein glycophorin A (**GpA**). Early mutagenesis (Lemmon et al., 1992), computational modeling (Adams et al., 1996; Petrache et al., 2000) and thermodynamic characterization (Fisher et al., 2003; Fleming et al., 1997) of the GpA TM dimer emphasized the central role of GxxxG (GG_4) in the $L^{75}IxxGVxxGVxxT^{87}$ interfacial motif. The GG_4 sequence dimerization motif is found in many helix oligomers (Curran and Engelman, 2003), including the major coat protein (**MCP**) from bacteriophage (Melnyk et al., 2002), ErbB family of growth factor receptor tyrosin kinases (Mendrola et al., 2002), F_0F_1-ATP synthase (Arselin et al., 2003), GPCRs (Overton et al., 2003), integrins (Li et al., 2004b) and *Escherichia coli* (***E. coli***) lactose permease (**LacY**) (Abramson et al., 2003). The glycine residues in this motif face each other in the dimer allowing close packing of the helices (Jiang and Vakser, 2004). Besides GG_4, other over-represented dimerization motifs are II_4, GA_4, and IG_4. The GxxxG motif along with the AxxxA or SxxxS motifs minimizes the steric hindrance of helix backbones. Recent structural data have revealed that small side chains are able to allow both conformational changes and stabilization of helical membrane protein structure by the formation of C_αH---O hydrogen bonds across the helical backbone (Senes et al., 2001). However, whether isolated C_αH---O interactions (e.g., T24 in BR, (Yohannan et al., 2004a)) are as stabilizing as those present in extensive networks (G79 in GpA) is still debatable.

As surprising as it may seem, studies have shown that several polar residues, namely glutamine, glutamic acid, aspartic acid and asparagine, are able to promote strong homo-oligomerization in a polyleucine or GCN4 zipper sequence context, whereas the more frequently occurring serine and threonine[6] residues do not (Gratkowski et al., 2001; Zhou et al., 2000). The strong interactions involving polar side chains often contribute to protein misfolding or malfunction. The mutation of a nonpolar residue to a polar one is commonly associated with disease, e.g. cystic fibrosis transmembrane conductance regulator (**CFTR**) (Partridge et al., 2002). Later it was found that other factors, such as ligand binding (Moriki et al., 2001; Schlessinger, 2002) and the folding of extramembranous loops (Allen et al., 2001; Kim et al., 2001), also contribute to the packing of TM helices.

Protein folding studies could be excellent starting points to help us understand the effects of point mutations in membrane protein misassembly and misfolding[7] in the cell, which could be extremely complex processes involving insertion in the ER, trafficking to the Golgi, the quality control of the ER (ER-associated degradation or ERAD) followed by degradation by proteasomes (Brodsky and McCracken, 1999; Tsai et al., 2002). Medical genetics so far has identified ~16,000 missense mutations leading to single amino acid changes in protein sequences that are linked to human diseases (Sanders and Myers, 2004). The exact mechanisms by which single amino acid changes lead to disease phenotypes are largely unknown. The most common class of mechanism is perturbation of normal protein folding or trafficking, as opposed to mutations that just perturb protein function (Kaushal and Khorana, 1994; Stojanovic and Hwa, 2002; Wang and Moult, 2001), thus making protein misassembly an extremely common contributor to the etiology and pathology of heritable human disease. Many disease-linked mutations also occur in integral membrane proteins causing the protein to misfold or misassemble (Sanders and Myers, 2004; Sanders and Nagy, 2000) leading to diseases like cystic fibrosis, retinitis pigmentosa, Charcot-Marie-Tooth disease and hereditary hearing loss

---

[6] Serine and threonine account for approximately 7% of the amino acids in TM helices (Curran and Engelman, 2003).

[7] It should be noted here that 'misassembly' is a broad term in the sense that it encompasses kinetically trapped protein intermediates, which lead to aberrant conformations, proteins not properly folded due to mutations which might also affect protein trafficking and function. 'Misfolding' on the other hand could be described as a subset of misassembled proteins that lead to incorrectly folded proteins (Sanders and Myers, 2004).

(Aridor and Hannan, 2000; Aridor and Hannan, 2002; Cotton and Horaitis, 2002). Other fatal diseases like Parkinson, Alzheimer's, Creutzfeldt-Jakob and atherosclerosis have also been attributed to the misassembly of proteins (Dobson, 1999; Dobson, 2002).

Model membrane proteins for studying folding, misfolding and misassembly

While there have been a number of kinetic studies of membrane protein folding (Booth et al., 2001b; Dale and Krebs, 1999; Kleinschmidt and Tamm, 2002), and of the partitioning of water-soluble proteins between folding and misfolding pathways (Dobson, 1999; Jaenicke, 1995; Kiefhaber et al., 1991), molecular biophysical studies of membrane protein misfolding are in their infancy. Besides BR, rhodopsin, GpA and LacY (Abramson et al., 2004), diacylglycerol kinase (**DAGK**) and CFTR have served as excellent model systems to address this deficiency.

Mutations in CFTR lead to cystic fibrosis, a common (and deadly) Mendelian disorder. Approximately 1000 different disease-linked single point mutations have been documented in this ATP-regulated chloride channel (Zielenski and Tsui, 1995). Wild-type (**WT**) CFTR is known to fold with only modest efficiency (~50%) under normal conditions, with most of the remainder being targeted by ERAD for retrotranslocation out of the ER, polyubiquitination, and proteasomal degradation (Gelman et al., 2002; Xiong et al., 1999). The most common disease form of CFTR is the ΔF508 mutant, a deletion of Phe508 in the NBD1 domain (cytosolic domain composed of a nucleotide binding subdomain). The low assembling and trafficking efficiency (near 0%) of ΔF508 CFTR to the cell surface results in an almost complete loss of cellular CFTR function (Kopito, 1999; Seibert et al., 1997). The ΔF508 fraction that escapes, does fold, trafficks beyond the ER to the cell surface and is functional can be increased by lowering the temperature or by chemical chaperones such as glycerol (Gelman and Kopito, 2002). In **Chapter 7**, I have suggested the possibility of using force-clamp single-molecule force spectroscopy (**SMFS**) to study the kinetics of membrane protein unfolding under different conditions that perturb the stability of a protein. Protein folding studies on synthetic peptides also help identify 'negative design elements' as illustrated by the example of a disease-linked transmembrane mutation P205S in CFTR, where replacing proline with serine leads to misassembly and aggregation of the protein (Wigley et al., 2002).

E. coli DAGK, a homotrimer of 13 kDa subunits, is an integral membrane protein that serves as an important model system for studies of membrane protein catalysis and stability (Badola and Sanders, 1997; Wen et al., 1996; Zhou and Bowie, 2000). It was found that there exists an excellent correlation between the thermodynamic and kinetic stability of DAGK mutants and their folding efficiency (Nagy and Sanders, 2004). In particular, mutants that are significantly less stable than the wild-type protein always exhibit a higher degree of misfolding[8]. On the other hand for some mutants like the Y16C, which has both kinetic and thermodynamic stability similar to that of the wild-type, a detailed analysis of folding under a variety of conditions revealed a specific difficulty in inserting into lipid bilayers, thus suggesting an evident role during the folding process to assist the transmembrane domain of DAGK into the membrane. But once folding is complete, Tyr16 is unimportant for stability or catalysis, making Y16C a pathway-defective mutant (Nagy and Sanders, 2002). For membrane proteins it needs to be determined if there exists a correlation between the thermodynamic and mechanical stability as probed by SMFS.

Besides defects in the ER machinery or mutations in the protein, misassembly of membrane proteins may be promoted by several membrane characteristics. The quasi-two-dimensionality of the bilayer (McCloskey and Poo, 1986), protein crowding effects in native membranes (protein content is often >50% by weight relative to lipid content) (Grasberger et al., 1986), and spatial-orientational entropy effects imposed by membrane insertion or tethering (Grasberger et al., 1986; McCloskey and Poo, 1986) can each contribute to misassembly of membrane proteins. Interactions of both soluble and peripheral membrane proteins with the complex lipid backbone/polar head group region can profoundly stabilize or destabilize their structures (Christensen et al., 2001; Shin et al., 1997; Silvestro and Axelsen, 2000; White and Wimley, 1999), leading to misfolding diseases like Parkinson's (α-synuclein), Alzheimer's (β-amyloid peptide) and the prion diseases (Jo et al., 2002; Kazlauskaite et al., 2003; Lee et al., 2002). Thus, the conformational behavior and the unfolding pathways of protein tethered to or embedded in the membrane surface could be expected to be strongly influenced by this milieu. The example of LacY and its activation by phosphatidylethanolamine (**PE**) (Bogdanov and Dowhan, 1999) shows that certain lipids may play highly specific roles in protein folding and misfolding. In the case of DAGK, once refolded, it retains its native conformational state even if model membrane conditions are changed to match the composition in which the misfolded protein was originally detected following purification (Nagy et al., 2001). Thus, the formation of these misfolded states likely results from kinetic competition between the correct and incorrect folding pathways.

---

[8] The different DAGK mutants that misfold into different structures resulting in aberrant oligomeric structures do not represent global free-energy minima since they can be refolded (Gorzelle et al., 1999)

The rapidly expanding crop of membrane protein structures has enhanced our view of the structure universe, which combined with an increasingly quantitative understanding of fold determination is revolutionizing understanding of the principles that govern the folding of these proteins and engenders optimism that a solution to the folding problem for membrane proteins can be achieved (Bowie, 2005). A tremendous advance of cellular biology during the past 15 years has been the study of protein folding in the cell, and there is a great need to integrate the results of test tube studies of protein folding with cellular results.

1.3.3 Why are membrane proteins so difficult to study?

In their short experimental history, membrane proteins have turned out to be very tactful warriors. They have eluded detailed molecular level study and the task of determining their structures has been hampered by experimental difficulties due to their strict confinements in the lipid bilayer. This has nick-named them the ‘Wild West’ of structural biology (Torres et al., 2003). Analyses of the complete genomic sequences for several organisms indicate that 20-30% of all open reading frames code for the helix-bundle motif, thus constituting a third of the proteomes (Arkin et al., 1997; Wallin and von Heijne, 1998). Given the fact, it is surprising that <1% of the structures in the Protein Data Bank (Berman et al., 2000) are membrane proteins[9]. This disturbing discrepancy emphasizes the challenges in the structure determination of membrane proteins. The situation has improved markedly in recent years, and we now know over 90 unique structures (Bowie, 2005). The molecular-level understanding of membrane proteins lags far behind that of water-soluble proteins owing to the difficulty in obtaining high-resolution structural information.

---

[9] 238 membrane protein structures of a total 38479 structures, as on Aug 29, 2006 (http://www.rcsb.org).

Membrane proteins are hard to handle and consequently the purification of functional protein in milligram quantities is a major problem. A common problem that precludes the characterization of many membrane proteins is their metastable nature once outside the membrane and their tendency to aggregate in solution, which leads to rapid inactivation (Booth, 2003; Bowie, 2001). Apart from designing new mutant proteins (Bowie, 2001), the expression, solubilization, purification and crystallization require an urgent need for new detergent mixtures and manipulation of lipid properties to improve the efficiency of folding as well as the stability and function of the protein (Booth, 2003; Booth et al., 2001a). The use of heat (Privalov, 1992) or denaturants (Pace, 1986) in the thermodynamic studies of the folding/unfolding process has not been used so widely for membrane proteins as for soluble proteins (Richards, 1992). The main difficulty is the resistance of membrane proteins to complete denaturation because of the great stability of secondary structure elements in membranes.

As explained before (**section 1.3.2**), knowledge of membrane protein folding mechanisms *in vitro* will take us to the root of these problems and help us work toward strategies to disaggregate and fold proteins correctly. Kinetic and stability studies are emerging on membrane protein folding, mainly on bacterial proteins due to their ease of expression in large quantities in bacterial hosts. In the absence of high-resolution structures, mutagenesis and cross-linking assays have long been used to probe structure-function relationships (Kaback et al., 2001; Karlin, 1993; Nakayama and Khorana, 1990), besides being useful for studying specific structural features or bonds in membrane proteins (Booth, 2003; Davidson et al., 1994; Liu et al., 1996b). The need of the time is to have new methods which help us study membrane proteins in their native lipid environment.

1.3.4 Methods for studying membrane proteins

The study of membrane proteins remains an important challenge for the structural biologist (**section 1.3.3**). There are a number of experimental methods and predictive tools that are employed in the investigation of membrane proteins, though each comes with its own bag of advantages and disadvantages. Because of the experimental difficulties associated with their hydrophobic span, classical techniques such as X-ray crystallography and solution nuclear magnetic resonance (**NMR**) have been producing structures at a very slow pace (Opella and Marassi, 2004; White, 2004), the huge size of membrane proteins adding to the problem. The growth of well-ordered 3-D crystals is a major constraint in attaining high-resolution structures of membrane proteins of any size due to the instability of membrane proteins outside the native membrane, making this process run on the time-scale of years. The advent of new methods, like cubic lipid phases bilayer-like environment, though promising are not generally applicable (Luecke et al., 1999b). The problem of crystallizing membrane proteins can be overcome by the use of electron microscopy (**EM**)[10], where membrane proteins arranged into two-dimensional (**2-D**) planar ordered structures are used. Structures solved by this method are those of bacteriorhodopsin (Unwin and Henderson, 1975), photosystem II (Rhee et al., 1998), the gap junction (Unger et al., 1999), the bacterial translocon complex SecYEG (Breyton et al., 2002), the bacterial multidrug-resistance transporter EmrE (Ubarretxena-Belandia et al., 2003) and aquaporin-1 (Walz et al., 1997).

There have been a number of alternative methods devised to overcome the difficulties in each method. Large proteins, which are difficult to organize into 2-D or 3-D periodic arrays, can be studied using EM at intermediate resolution (8-30 Å) using single-particle techniques (Frank, 1996). Solution NMR (Klein-Seetharaman et al., 2002), solid-state NMR, oriented samples NMR (**OS NMR**), magic-angle spinning NMR (**MAS NMR**) (Eilers et al., 2002) are different NMR methods put to use to study membrane proteins (MacKenzie et al., 1997). Site-directed spin labeling electron paramagnetic resonance, (**SDSL**)-**EPR**, is a commonly used method which provides a wealth of information about the membrane protein structure (Farahbakhsh et al., 1995). A series of elegant experiments on rhodopsin and bacteriorhodopsin combining cysteine mutagenesis and EPR by Khorana and co-workers proves the indispensability of these techniques to study membrane proteins in the absence of 3-D structures (Altenbach et al., 1990; Altenbach et al., 1996; Farahbakhsh et al., 1995; Steinhoff et al., 1995). Site-specific infrared dichroism (**SSID**) is a new approach that can be used to determine helix tilt and rotational orientation of TM α-helices incorporated in uniaxially oriented lipid bilayers. Mass spectrometric studies have helped identify the non-native bonds implicated in misfolded states of membrane proteins (Hwa et al., 2001). Though the challenges are immense in each of these methods[11], nevertheless, complementary information such as orientational constraints relative to the membrane plane, torsional constraints, secondary structure (Altenbach et al., 1990), topography maps (Zhan et al., 1995), the depth of a residue in a membrane and in α-helical TM homo-oligomers (Altenbach et al., 1994) and oligomeric size of a protein can be obtained. It is possible to measure distances of upto ~20 Å using continuous wave EPR (Borbat et al., 2002), and over a broad range (20-50 Å) using novel pulsed EPR methodologies (Altenbach et al., 2001). Covalent cross-linking strategies have been employed to study transient protein-receptor complexes (Cai et al., 2001). Circular dichroism (**CD**) (near- and far-UV) is an excellent method to do a comparative structural and biochemical analysis of mutant proteins implicated in misfolding and malfunction (Liu et al., 1996b).

---

[10] Higher resolution structures can be achieved with cryo-EM because of the frozen hydrated state of the membrane proteins, and reduction of the radiation damage at low imaging temperatures (-180 ^{0}C - -260 ^{0}C) (Baker and Henderson, 2001).

Besides the experimental methods, a number of computational tools have been developed to strengthen or validate the experimental data for the different methods. Using computational methods not only circumvents the problems associated with solubility of membrane proteins but also, in many respects, makes it easier to investigate the interactions of single TM helices due to the uniformity of their structure and interactions (e.g., nearly parallel helices packed together) (Lehnert et al., 2004). E.g., global search molecular dynamics simulations explores interhelical interactions in homo-oligomeric α-helical bundles (Adams et al., 1995). The power of computational work is illustrated by a recent work to identify the core amino acid residues in the folding of rhodopsin (Rader et al., 2004), and the first examples of *in silico* unfolding of bacteriorhodopsin (Cieplak et al., 2006; Seeber et al., 2006).

Part of the reason why eukaryotic membrane proteins have not seen a fast track progress as bacterial membrane proteins is due to the fact that >50% of the membrane protein families in eukaryotes lack bacterial homologs (Fleishman et al., 2006). The complex nature of eukaryotic membrane proteins makes their expression, purification and crystallization more difficult as compared to the bacterial ones. Therefore, it is conceivable that many more years will elapse before high-resolution structures of eukaryotic TM proteins emerge. Until then, integrated approaches that combine biochemical and computational analyses with low-resolution structures are likely to have increasingly important roles in providing frameworks for the mechanistic understanding of membrane-protein structure and function.

---

[11] Solution NMR requires that the molecule be not too large, a big problem for membrane proteins because they are embedded in the large lipid bilayer fragments.

1.3.5 Why study membrane proteins with atomic force microscopy?

Structure determination of eukaryotic membrane proteins remains too slow to sustain hypothesis-driven experimentation aimed at understanding structure-function relationships in integral membrane proteins (Fleishman et al., 2006). The atomic force microscope (**AFM**) (see **Chapter 2** for a detailed description) provides novel ways to characterize structure-function relationships of native membrane proteins at the single-molecule level (Engel and Müller, 2000; Fotiadis et al., 2003; Müller and Engel, 1999). Membrane proteins make good samples for AFM bypassing the difficulties of X-ray crystallography. Characterizing membrane proteins with single-molecule techniques provides structural and functional insights into the different oligomeric and conformation states in their native environment that are difficult to obtain with conventional approaches as mentioned before (**section 1.3.4**). Another key advantage is that AFM does not require labeling of proteins and enables measurements in physiological buffer at ambient temperature. Although AFM provides only surface information, a lateral resolution of ~0.5 nm and a vertical of ~0.1 nm with an outstanding signal-to-noise ratio enables observation of structural details of single membrane proteins. E.g., time lapse recording of nuclear pore complexes (Stöffler et al., 1999), of gap junction hemichannels under different Ca^{2+} conditions (Müller et al., 2002a), and cytolysin pores (Czajkowsky et al., 2004).

Based on the structural rigidity of the molecule it is possible to map the energy landscape of the protein (Scheuring et al., 2002), and the effect of environmental changes and ligand binding on the energy landscape (Nevo et al., 2005; Strunz et al., 2000). Moreover, it is possible to detect the electrostatic potential as for OmpF (Philippsen et al., 2002), and to measure the current in the pA range as demonstrated in the case of hexagonally packed intermediate layer of *Deinococcus radiodurans* (Frederix et al., 2005). AFM has been put to good use to study the structure, assembly and oligomeric state of membrane proteins as illustrated by specific studies of F_oF_1-ATP synthases from different organisms and species showing different number of identical subunits in the rotor of the membrane embedded F_o motor (Pogoryelov et al., 2005; Seelert et al., 2000;

Stahlberg et al., 2001); the structural investigation of the proteins of the photosynthetic apparatus in native membranes of *Rhodopseudomonas* (Goncalves et al., 2005; Scheuring et al., 2006; Scheuring et al., 2003), *Rhodospirillum* (Scheuring and Sturgis, 2005), and *Rhodobacter* (Bahatyrova et al., 2004; Scheuring et al., 2005) species to unravel the complex nature of the supramolecular assembly and its adaptation to different light intensities (Scheuring and Sturgis, 2005); the elucidation of the native oligomeric state of rhodopsin (Fotiadis et al., 2003; Fotiadis et al., 2004), a GPCR implicated in many key functions of the human body; and proposition of an atomic model of rhodopsin dimers in corroboration with the X-ray structure (Filipek et al., 2004; Liang et al., 2003).

Besides observing the structural details of individual protein molecules and assemblies, time-lapse AFM imaging of membrane proteins allows dynamic processes to be observed (Fotiadis et al., 1998; Hoh et al., 1991; Müller and Engel, 1999; Müller et al., 2002a). Considering that recently the trajectories of individual sodium-driven rotors of ATP synthase from *Ilyobacter tartaricus* in the membrane bilayer (Müller et al., 2003), and binding-dissociation of single chaperonin protein GroES molecules from individual GroEL proteins were observed directly (Viani et al., 2000), it is only a matter of time that AFM will be used to study the kinetic aspects of formation and disassembly of higher order structures like GPCRs.

In conjunction with high-resolution imaging, unfolding of membrane proteins using SMFS has gained tremendous importance in recent years (Cisneros et al., 2005; Kedrov et al., 2004; Oesterhelt et al., 2000; Sapra et al., 2006b). SMFS gives insights into interactions within and between membrane proteins. It allows the characterization of interactions that stabilize functional proteins, as well as those that destabilize them leading to malfunction and misfolding (Janovjak et al., 2006; Sapra et al., 2006a). A detailed description of the recent work and advances in SMFS will be given in **section 2.2**. Because of its practical use to characterize various parameters of membrane proteins in their native environment, AFM can be aptly described as a “lab on a tip” device (Müller et al., 2006).

Chapter

2

ATOMIC FORCE MICROSCOPY

2.1 ATOMIC FORCE MICROSCOPE

2.1.1 A brief history

Scanning probe microscopy began in the early 1980s when Binnig and Rohrer revolutionized microscopy through the invention of the scanning tunneling microscope (**STM**) (Binnig et al., 1982). The development of STM arose from an interest in the study of electrical properties of thin insulating layers, and it showed for the first time the atomic structure at the crystalline surface of silicon in real space and demonstrated the possibility to manipulate single atoms. The importance of this discovery was recognized through the award of the Nobel Prize in Physics in 1986. In the same year, Binnig together with Quate and Gerber demonstrated that the short-range van der Waals interactions could also be used to build a scanning probe microscope (**SPM**). Thus the birth of the second member of the SPM family – the atomic force microscope (AFM), also known as the scanning force microscope (**SFM**) (Binnig et al., 1986).

Commercial AFMs began to appear in the early 1990s and have evolved through several generations. The milestones are the development of the probe microscope with light microscope, cryo-AFM (Han et al., 1995), AFM-surface plasmon resonance (AFM-SPR) (Chen et al., 1996), ‘submarine AFM’ or the combined AFM-Langmuir trough (Eng et al., 1996), with patch-clamp and scanning near-field optical microscope (**SNOM**). Many types of SPMs have been developed and can be used not only for measuring surface topologies but also for measuring various material properties at or close to surfaces. This can be done in vacuum, in gas, or in liquids in a broad temperature range with a resolution down to either the atomic or the molecular level.

2.1.2 Principle and set-up

Despite its rather grandiose title, the AFM works on a very simple principle and is probably one of the easiest forms of microscopy to understand. The main parts of the

AFM setup are the cantilever, the tip or the tip, the piezoelectric transducer/actuator which has the sample stage on the top, the laser-head which houses the optical deflection system consisting of a laser diode and a quadrant photodetector, and a computer (illustrated in **Figure 2.1**). The fluid cell with the cantilever is mounted inside the head of the AFM. The piezoelectric transducer which has the piezo ceramic elements is voltage driven and can be made to move with an accuracy of atomic dimensions in the x, y and z directions. This movement in any of the orthogonal directions is assigned to three channels in the instruments' control electronics. The sample is mounted on the piezoelectric transducer which ensures three-dimensional positioning with sub-nanometer resolution. AFM images are created by scanning a sharp tip, mounted to a soft cantilever spring, in the x-y plane over a sample surface and by using the interaction force between the tip and the sample to map the topography of the surface (see **section 2.1.4** for a description on forces). The force between the tip and the sample is monitored by measuring the deflection (vertical bending) of the cantilever, which is usually detected by a laser beam focused on the free end of the cantilever and reflected onto a photodiode. This deflection is linearly proportional to the force as the cantilever behaves as a Hookean spring. A feedback loop connected between the detection system and the piezoelectric drive controls the vertical movement of the transducer to keep the applied force constant (constant force mode). This locks the vertical movement of the transducer to its lateral movement by the feedback loop during scanning, and the sample topography is contoured. The vertical information of the image is due to structural height differences, but can exhibit additional information based on the specific interactions between tip and sample. These can be of electrostatic, magnetic or chemical nature.

Another important feature of the instrument is the detection mechanism. Most instruments use the beam-deflection method. To monitor the motion of the tip as it traverses the sample, as mentioned before, the laser beam is focused onto the end of the cantilever, preferably directly over the tip, and then reflected off onto a quadrant photodiode detector (**Figure 2.1**). As the tip moves in response to the sample topography during scanning, the angle of the reflected laser beam changes the laser spot falling onto the photodiode producing changes in the intensity in each of its quadrants. This mechanical amplifier is sensitive enough to detect atomic scale movement of the tip as it traverses the sample. The difference in laser intensity between the top two segments and the bottom two segments produces an electrical signal which quantifies the normal (up and down) motion of the tip (**Figure 2.1**), and the difference between the laser intensity in the left and right pairs of segments quantifies any lateral or twisting motion of the tip. Thus frictional information can be distinguished from topographical information.

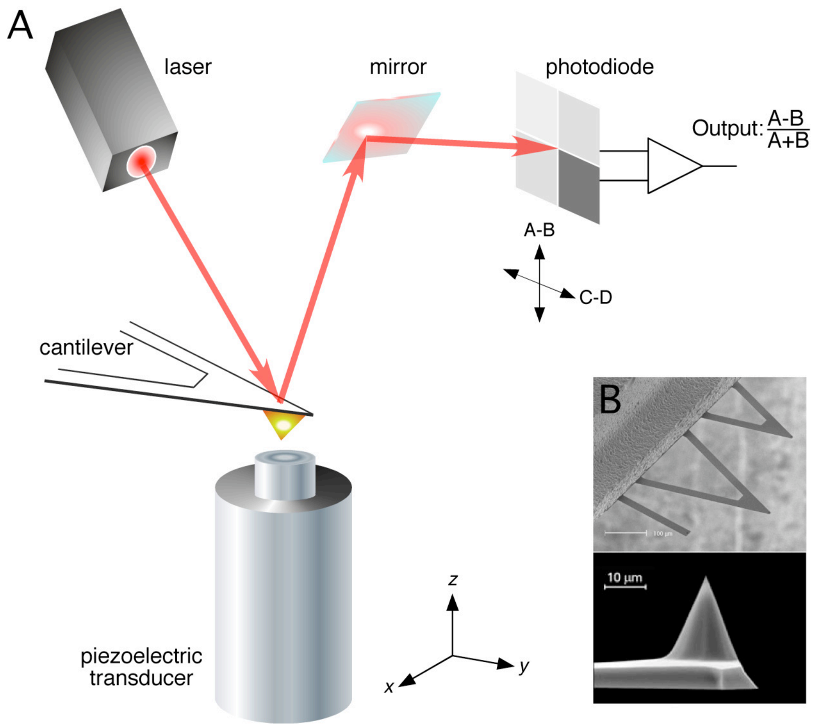

Figure 2.1 Setup of an AFM instrument

(**A**) The scheme shows the different parts and working of an AFM. Except the piezoelectric transducer, all the other components are housed in a so-called 'head' of the microscope. The cantilever (**B**) is fixed in a fluid cell (not shown) and placed in the head, which is then mounted on the piezoelectric actuator. A laser beam (λ = 625 nm) is adjusted on the edge of the cantilever so as to obtain a maximum sum signal on the photodiode. During sample scanning with the tip the beam is deflected with the up-down movement of the cantilever and the voltage signal is converted to force (pN) or deflection (nm) with the help of software. The output[12] of the deflection signal varies with the AFM mode. (**B**) V-shaped cantilevers with pyramidal tips most commonly used for single-molecule unfolding measurements (Cantilever images from www.veecoprobes.com).

For SMFS measurements (**section 2.2**) the piezoelectric transducer is moved only in the *z* (up-down) direction, thus enabling the unfolding of a molecule that was picked in a previous ramp cycle[13].

2.1.3 Cantilever

At the heart of the AFM is the most essential part - a cantilever with a tip or tip mounted at its end - which does the 'feeling'. Modern AFM styli and cantilevers are made from either silicon, silicon-nitride or diamond by microfabrication, using many of the techniques that have been developed for integrated circuit manufacture, such as lithographic photo-masking, etching and vapor deposition. Using the micro machining approach, sharp tips can be integrated onto cantilevers, a prerequisite for high-resolution imaging of biological samples. The structure of the tip determines the type of interaction with a surface, and the geometry area of interaction.

---

[12] The output signal shown in the figure is for contact mode. The RMS of the amplitude signal is measured in TappingMode™, and oscillation amplitude or frequency in non-contact mode.

[13] A ramp cycle is nothing but the up-down movement of the transducer.

A silicon-nitride tip is covered by a non-conducting layer of native oxide, and is often conical or pyramidal in geometry with a high aspect ratio. The pyramidal tip has a macroscopic cone angle of 50^o, which reduces at the apex. To increase the aspect ratio, apart from the sophisticated etching techniques, selective deposition of contaminants on the tip has been done, and carbon nanotubes have been used as tips. The tip may range in size from 2 μm to tens of microns in height, with a radius of 2-60 nm, and can be conducting or non-conducting.

Cantilevers are usually triangular or 'V' shaped, and rectangular or beam shaped with a length of 100-200 μm and thickness of 0.5-2 μm. Cantilevers are often coated with a thin layer of gold or aluminum to provide high reflectivity for beam deflection instruments, or ferromagnetic coating for magnetic measurements[14]. The V-shaped geometry minimizes the torsional motion or twisting of the cantilever while scanning a sample, making it the lever of choice for purely topographical imaging. A simple beam or rectangular geometry cantilever can be used for frictional measurements due to a greater degree of rotational freedom making it sensitive to lateral forces. Irrespective of the geometry, the force contribution, F, on the sample from the bending of the cantilever, x, is determined by Hooke's law,

$$F = -\kappa x \tag{2.1}$$

where κ is the force constant of the cantilever and x the displacement experienced. The force resolution of the AFM is in first approximation limited by the thermal noise of the cantilever, which in turn is determined by its spring constant. The typical values of stiffness for AFM cantilevers used in contact mode are 10-100 pN/nm, in non-contact mode between 0.5-5 pN/nm, and in tapping mode 30-60 pN/nm. Low values of cantilever stiffness represent high sensitivity to force for each nanometer deflection of the transducer. The subtle drawbacks of low stiffness are that the probe is susceptible to thermal fluctuations, and the response time, t_r, can be slow in an over damped viscous-water environment.

---

[14] An excellent source of information on cantilevers and styli is http://www.veeco.com.

$$\partial \mathrm{x}^2 \sim \frac{k_B T}{\kappa} \tag{2.2}$$

where k_B is the Boltzmann constant and T is the temperature. On the other hand, high probe stiffness results in large thermal fluctuations of the applied force (Evans, 2001),

$$\partial \mathrm{f}^2 \sim k_B T \bullet \kappa \tag{2.3}$$

Soft cantilevers are best for contact mode because they deflect without deforming the surface of the sample. Stiff cantilevers, on the other hand, are suitable for non-contact mode because they have high resonance frequencies. In addition, the resonance frequency, the quality factor, and the measurement bandwidth can also substantially contribute to the choice of the cantilever required for a specific application (Viani et al., 1999).

Calibrating the cantilever

As stated above, the force resolution, the thermal noise of the cantilever and its spring constant are all correlated. Moreover, to translate the deflection of the cantilever (x) to the units of force (F) in SMFS it is necessary to determine the spring constant, κ, of the cantilever, i.e., $F = -\kappa x$. Since the spring constant of the cantilever is a very important parameter, it needs to be accurately determined for quantitative studies.

κ for normal bending of a rectangular cantilever, as calculated from its geometry, is given by (Meyer et al., 2003),

$$\kappa = \frac{Ewt^3}{4l^3} \tag{2.4}$$

where w is the width, l the length, t the thickness of the cantilever and E the Young's modulus of the material. w and l can be measured by means of scanning electron microscopy, whereas t can be more precisely determined from the resonance frequency, f_r, of the cantilever,

$$t = \frac{2\sqrt{12\pi}}{1.875^2}\sqrt{\frac{\rho}{E}}f_r l^2 \tag{2.5}$$

where the mass density $\rho = 2330$ kg/m^3 and $E = 1.69 \times 10^{11}$ N/m^2 for silicon. To account for the effect of coating tips and/or manufacturer variability from cantilever to cantilever, it is necessary to determine κ using empirical methods.

f_r of a simple harmonic oscillator, for example a mass, m, on the end of a spring having spring constant κ, can be determined using the equation,

$$f_r = \frac{1}{2\pi}\sqrt{\frac{\kappa}{m}} \tag{2.6}$$

Rather than just measuring the resonance frequency of an AFM cantilever alone, the force constant, κ, can be determined more accurately by measuring the changes in the resonance frequency as small masses (in the form of tungsten spheres) are added using the following equation[15] (Cleveland et al., 1993)

$$\omega^2 = \frac{\kappa}{m^* + m_0} \qquad \text{since} \qquad f_r = \frac{\omega}{2\pi} \tag{2.7}$$

where m^* is the end loaded mass, m_0 the effective cantilever mass, and ω the angular frequency of the lever.

Assuming that one has accurate information on the length and width but not of the thickness, equation 2.8 allows calculation of κ with reasonable accuracy by just measuring the unloaded resonance of the cantilever (Cleveland et al., 1993),

---

[15] Since the AFM cantilever is not a simple point mass, but has its weight distributed along its length, equation 2.6 needs to be modified slightly by using an effective mass, m_0, which is governed by the lever geometry.

$$\kappa = 2w(\pi l f_r)^3 \sqrt{\frac{\rho^3}{E}} \tag{2.8}$$

where l, w, ρ and E have the same meaning as before, and f_r is the measured resonance frequency.

Recently a more accurate method corrected for the effects of air-damping and gold coating on the measurement of the resonance frequency of AFM cantilevers and requiring only the unloaded resonance of the cantilever to be measured has been proposed (Sader et al., 1995). The importance of load position in relation to force constant was also demonstrated, since the force constant of an AFM cantilever depends quite strongly on where it is being loaded. For this reason, a rather more direct measurement of the force constant of a cantilever could be obtained by pushing on the actual tip itself (where the force acts on the sample) using a wire of predetermined stiffness and monitoring the relative deflection (Gibson et al., 1996; Torii et al., 1996).

Routinely in the laboratory experiments the analysis of the thermal fluctuations of the vibrating lever is used to determine the stiffness of the cantilever. It is based on the equipartition theorem[16] (Florin et al., 1995). To avoid overestimation of the displacement of the lever and hence an underestimation of the measured stiffness, this approach requires that no additional noise is added to the thermal noise. The cantilever tip is treated as a simple harmonic oscillator whose power spectrum of thermal fluctuation is used to derive the spring constant. In brief, the cantilever is raised several microns from the surface and its natural frequency of vibration (resonance frequency) is monitored for 2-3 s. Since each vibration mode of the cantilever receives the thermal energy commensurated to one degree of freedom, $\frac{1}{2}k_B T$, the measured variance of the deflection $\langle x^2 \rangle$ can be used to calculate the spring constant,

---

[16] Principle of Equipartition of Energy states that if the energy of a molecule depends on the square of a parameter such as position or speed, then the mean energy associated with the degree of freedom measured by that parameter is $\langle U \rangle = \frac{1}{2} k_B T$ (Howard, 2001).

$$\frac{1}{2}k_B T = \frac{1}{2}\kappa\left\langle x^2\right\rangle \tag{2.9}$$

Using this approach, the spring constants of cantilevers can be calibrated in either air or in solution. It is important to note that the thermal noise is not white noise with equal contributions at all frequencies, but that the frequency spectrum of the thermal noise is dominated by peaks at the mechanical resonances of the cantilever. The quality factor, Q, of the cantilever determines the amplitude of thermal noise at the resonance (Meyer et al., 2003).

2.1.4 Relevant forces

Since the central concept of AFM and my thesis is measuring forces at the molecular level, it becomes of utmost importance that I give a brief overview of the different forces acting on molecules that play an important role in AFM measurements - imaging and SMFS (**Table 2.1**) (Howard, 2001). Moreover, any description of AFM and nano mechanics is incomplete without the mention of forces operating at the molecular level. This concept will be touched upon many times during the text of my thesis as molecular forces are at the crux of many biological questions.

Type of force	Approximate magnitude
Collisional	10^{-12} to 10^{-9} pN for 1 collision/s
Elastic	1-100 pN
Electrostatic and van der Waals	1-1000 pN
Viscous	1-1000 pN
Thermal	100-1000 pN
Covalent	10,000 pN

Table 2.1 Forces that play an important role at the molecular level with their approximate magnitudes

The interaction range of the different types of forces is of great importance for force microscopy, since different parts of the tip and cantilever contribute differently to the total measured force. Long-range van der Waals and electrostatic forces are always to be taken into account in force microscopy even though they may not be of any interest for the actual measurement. E.g., the typical situation in contact mode is determined by an equilibrium between the attractive long-range forces and the repulsive short-range forces, where only the latter provide good resolution (**Figure 2.2**) (Meyer et al., 2003).

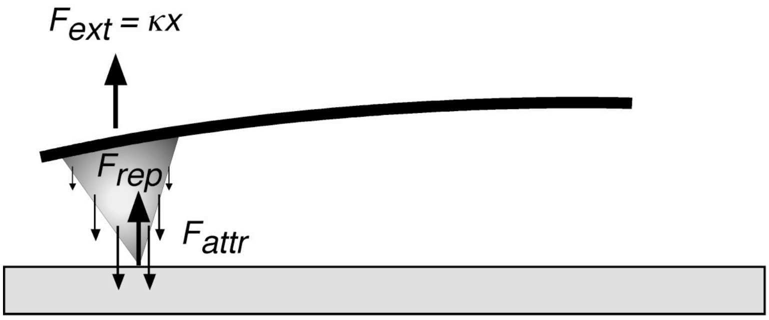

Figure 2.2 Equilibrium of forces in the contact mode

The attractive long-range force, F_{attr}, between the cantilever tip and the sample is balanced by the short range repulsive force, F_r, at the contact and the external force, F_{ext}, exerted by the cantilever bending.

Short-range forces

Short-range forces are more important to STM since contributions of the outermost atoms of the tip dominate the tunneling current due to the exponential decay with distance (Meyer et al., 2003). Short-range chemical forces arise from the overlap of electron wave functions and from the repulsion of the ion cores thus making their ranges comparable to the extension of the electron wave functions, i.e., <1 nm. Short-range forces can be both attractive and repulsive. Forces are attractive when the overlap of electron waves reduces the total energy. On the other hand, the Pauli exclusion principle can lead to repulsive forces due to strong electron wave overlap. The variation of short-range forces on the atomic scale makes atomic resolution possible in force microscopy. At a distance of 0.5 nm from the surface, short-range forces between tip apex and surface atoms become comparable to long-range forces between tip and sample. Consequently, this is a characteristic distance at which atomic resolution in non-contact modes is obtained (Meyer et al., 2003).

Electrostatic double-layer force

The electrostatic double-layer force (**EDL**) between charged particles is one of the principal long-range forces that govern biological interactions. A surface in a liquid can acquire a charge either by the ionization or dissociation of surface groups, or by the adsorption of ions from solution onto a previously uncharged or oppositely charged surface. Whatever the charging mechanism, the final surface charge is compensated by an equal but oppositely charged region of counter ions. Some of these counter ions are bound to the surface within the so-called *Stern* or *Helmholtz* layer, while others form an atmosphere of ions in rapid thermal motion close to the surface, known as the diffuse *electric double layer* (Israelachvili, 1991), thus increasing the concentrations of ions between the interacting particles. A similar thing happens when imaging under aqueous media where mica is negatively charged and can attract oppositely charged ions from solution. This causes the ions to cluster at the solid-liquid interface leading to the formation of a positively charged layer. The double layer can interact with other double layers or with polarizable surfaces. The repulsive interaction of electric double layers has been exploited to achieve high-resolution in force microscopy (Müller et al., 1999b). The potential decays exponentially away from the surface with the thickness of the ionic atmosphere, known as the Debye screening length ($1/\mu$). μ^{-1} depends on the solution dielectric constant and the ion concentrations (Israelachvili, 1991). For low surface potentials (ψ_0), the potential at a distance (ψ_r) is related to the Debye length through the Debye-Hückel approximation (Israelachvili, 1991),

$$\psi_r \approx \psi_0 e^{-\mu r} \tag{2.10}$$

Generally, greater the ionic strength of the imaging medium, lower the electrostatic repulsion that an approaching AFM tip experiences. The double-layer repulsion, unlike the van der Waals attraction, is much more sensitive to the type and concentration of electrolyte present, the pH, and the surface charge density or potential. The interplay between the attractive van der Waals forces and the repulsive double-layer forces forms the basis of the so-called **DLVO** (Derjaguin-Landau-Verwey-Overbeek) theory of colloid science (Israelachvili, 1991).

van der Waals force

The van der Waals force is the second most important long-range interaction in biology. These are dipole-dipole forces that act between all atoms and molecules and can be effective from 0.2-10 nm. The most important forces are not those between permanent dipoles but the so-called *dispersion* forces. These act between dipoles that arise from fluctuations and dipoles induced in their electric field. The van der Waals force at short distances decays as $F \propto \frac{1}{r^7}$, whereas beyond r ≈ 5 nm this power law reduces to $F \propto \frac{1}{r^8}$ (Israelachvili, 1991). The distance dependence has the same form, whether van der Waals forces are calculated by summing up the molecular forces for each geometry and assuming that they are pairwise additive and non-retarded, or by using the more rigorous approach of the Lifshiftz theory, which treats the macroscopic bodies as a continuum (Israelachvili, 1991).

The van der Waals interaction can be modeled to characterize both attractive and repulsive parts of the force-distance relationship between the tip and sample by varying the potential energy of one particle at the apex of the AFM tip, due to the interaction with a particle at the surface of the sample. The change in the value of potential energy with the change in separation (*r)* is described mathematically by the pair-potential energy function $E^{pair}(r)$. A special case of the well-known 'Mie' pair-potential energy function used to model this behavior is called the 'Lennard-Jones' or '6-12' function (**Figure 2.3**) (Israelachvili, 1991).

$$E^{pair}(r) = 4\varepsilon\left[\left(\frac{\sigma}{r}\right)^{12} - \left(\frac{\sigma}{r}\right)^{6}\right] \tag{2.11}$$

where ε and σ are constants that depend on the material.

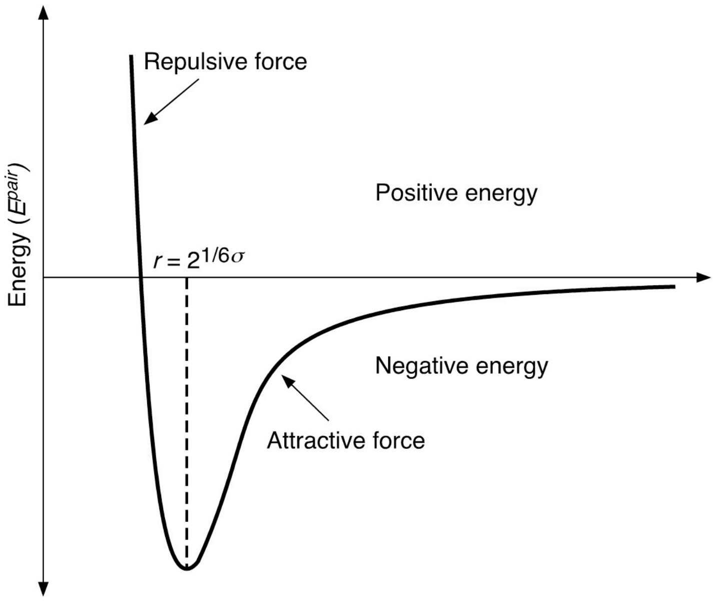

Figure 2.3 The Lennard-Jones function

Schematic diagram showing the variation in energy (E^{pair}) with separation (r) between two atoms.

Since the range of van der Waals force is limited, the tip-sample geometry of the force microscope can be well approximated as a sphere approaching a semi-infinite body. For this configuration the van der Waals force is (Meyer et al., 2003),

$$F_{vdW} = \frac{HR}{6r^2} \tag{2.12}$$

where H denotes the Hamaker constant, R the tip radius, and r the distance between the tip and the sample surface. Typical value for H, whether solid or liquid, is ~10^{-19} J for interactions across vacuum[17] (Israelachvili, 1991).

As a last comment it is important to mention that the medium between the tip and the sample has a great influence on the van der Waals force. The Lifshitz theory predicts that the force is proportional to $(\varepsilon_1 - \varepsilon_3)(\varepsilon_2 - \varepsilon_3)$ and $(n_1^2 - n_3^2)(n_2^2 - n_3^2)$, where ε and n denote the dielectric constant and the refractive index, respectively, of the tip (1), the sample (2), and the medium in-between (3) (Israelachvili, 1991). A medium with ε and n close to the respective values of the tip and sample will greatly reduce the van der Waals forces compared to the vacuum[18]. For most solid materials, this is the case when immersing the tip and the sample in water. A suitable choice of the immersing liquid can even lead to a negative Hamaker constant and consequently to repulsive van der Waals forces (Hutter and Bechhoefer, 1993). The immersion of the tip and the sample in a liquid can cause a dramatic reduction in the tip-sample force. In particular, the van der Waals forces can be reduced and the capillary forces removed.

2.1.5 AFM modes

Contact or dc mode

In contact mode AFM topographic images are recorded as the tip makes soft physical contact with the sample and scans the surface to monitor changes in the cantilever deflection with the photodiode detector. In this mode of operation the tip is brought into the repulsive force regime. The position of the tip is given by an equilibrium of forces:

---

[17] $H = 2.2 \times 10^{-20}$ J for two mica surfaces in water, and 8.3×10^{-21} J for two silicon oxide surfaces in water (Israelachvili, 1991).

[18] To give an idea about the strength of van der Waals force, for a tip of radius R = 30 nm, the van der Waals force in vacuum at a distance r = 0.5 nm is of the order of 2 nN (Meyer et al., 2003).

the attractive force between the tip and the sample has to be compensated by the repulsive force between the tip apex and the sample, and the external force exerted by the cantilever spring has to be added (**Figure 2.2**). The constant force of the scanner tracing the tip across the sample (or the sample under the tip) causes the cantilever to bend with the changes in topography. Topographic data is generated in one of two modes: constant-height or constant-force mode. Constant-height mode keeps the height of the scanner fixed while scanning and uses the spatial variation of the cantilever deflection to generate the topographic data set. It is most often used when speed is essential, e.g., real-time imaging of dynamic surfaces, or where cantilever deflections are small, e.g., atomic scale images of atomically flat surfaces. In constant-force mode the total applied force on the sample is kept constant by moving the scanner up and down in response to the topography. The preferred mode for most applications, contact-force mode is limited by the response time of the feedback circuit.

Due to specimen damage highest resolution in contact mode can be achieved only on sufficiently rigid samples (Baker et al., 2000). The problem is augmented by capillary forces while imaging in air, which could increase the normal force on the tip to about 50 nN thereby increasing proportionally the lateral force on the sample. Working in a liquid environment partially eliminates the problem by reducing the capillary force and consequently the normal force to 1 nN, which is still sufficient to cause damage to many biological samples. Though it has been estimated that forces as low as 50-100 pN are required for imaging membrane proteins and most biological samples to avoid destruction of the sample and obtain high-resolution (Müller et al., 1995; Müller and Engel, 2002), nevertheless, a valid criticism of the technique is its disturbance of the sample by the AFM tip. Structural comparison with atomic structures obtained by X-ray and electron crystallography demonstrates that the imaging process minimally disturbs the protein structures if the contact forces are kept around 100 pN.

Non-contact ac modes

A good way of avoiding the problems caused by the capillary layer is to use the long-range attractive forces to monitor the tip-sample interaction. These attractive forces are weaker than the repulsive force detected in contact dc mode, and consequently different techniques are required to utilize them. The two main types of ac modes are the TappingMode™ and the true non-contact ac mode.

TappingMode™ AFM

In TappingMode AFM the tip-sample separation is modulated while the sample is scanned by oscillating the cantilever at or close to its resonance frequency (100-400 kHz) with an amplitude ranging from 20 nm - 100 nm. The cantilever is oscillated either by applying a small sinusoidal electrical signal causing the main piezoelectric tube to vibrate in the vertical z direction causing in turn the cantilever to vibrate by viscous coupling, or alternatively by a small piezoelectric transducer at the fixed end of the cantilever, or by an oscillating magnetic field where the cantilever must be coated with a magnetic material. The feedback loop maintains a constant oscillation amplitude by maintaining a constant RMS of the oscillation signal, thus a constant tip-sample interaction is maintained during imaging.

Contact mode AFM is not suitable for imaging weakly immobilized structures such as single macromolecules since these are often sweeped away by the AFM tip while raster scanning the surface (Karrasch et al., 1993). TappingMode AFM overcomes this disadvantage by touching the sample at each minimum of the tip oscillation at the end of its downward movement, thus reducing the contact time, the friction and the lateral forces (~1 pN) considerably compared to contact mode, making it ideal for studying soft or elastic samples. A variety of macromolecules have been observed using TappingMode AFM which could not be imaged before (Bezanilla et al., 1994; Dunlap et al., 1997; Fritz et al., 1995; Guthold et al., 1999; Möller et al., 1999).

Unfortunately, the TappingMode images lack the spatial resolution of ≤1 nm exclusively acquired using the AFM in the contact mode. Nevertheless, the use of drive frequencies close to the resonance frequency of the cantilever enables precise control of the cantilever oscillation and to obtain high-resolution topographs of native proteins (Möller et al., 1999). Recent developments, such as the use of magnetically activated cantilever (MAC) mode AFM (Han et al., 1997), allow the resonance frequency of cantilevers to be adjusted and their oscillation to be precisely controlled enabling high-resolution images.

Non-contact ac mode

The main difference between this mode and the TappingMode is that the cantilever is oscillated at a frequency which is slightly above the cantilever's resonance frequency with an amplitude of a few nanometers (<10 nm) to obtain an AC signal from the cantilever. As the name implies, in this mode the oscillating cantilever never actually touches the surface of the sample but hovers a few nm above it. A clear advantage of such a technique is that no force is exerted on the sample. The initial use of this mode was limited to samples under vacuum, but recent developments have made the imaging of surfaces in an aqueous environment possible (Fukuma et al., 2005).

2.2 SINGLE-MOLECULE FORCE SPECTROSCOPY

SMFS with AFM allows measuring picoNewton forces at Ångstrom resolution associated with single molecules (Clausen-Schaumann et al., 2000; Fisher et al., 2000). This provides fundamental insights into the molecular basis of biological phenomena and properties as diverse as molecular recognition (Florin et al., 1994; Hinterdorfer et al., 1996; Lee et al., 1994), protein folding and unfolding (Kedrov et al., 2006a; Müller et al., 2002b; Oberhauser et al., 1998; Rief et al., 1997a), DNA mechanics (Rief et al., 1999a) and cell adhesion (Benoit et al., 2000).

In SMFS, individual molecules or molecular assemblies are pulled apart by attaching a spring to an anchored molecule or molecular assembly, possibly via molecular linkers, to learn about their structure, dynamics, interactions and mechanical properties (Cui and Bustamante, 2000; Florin et al., 1994; Merkel et al., 1999; Oesterhelt et al., 2000; Rief et al., 1997a). In particular, the pulling is done by the tip of the AFM cantilever (Binnig et al., 1986), and the force is sensed by the deflection of the cantilever. In other similar methods like the biomembrane force probe (**BFP**) (Evans et al., 1995; Simson et al., 1998) the force is sensed by the axial displacement of a glass microsphere glued to the pole of a micropipet-pressurized membrane capsule, and in the laser optical tweezer (**LOT**) (Ashkin, 1997; Ashkin et al., 1990) the displacement of a microsphere trapped in a narrowly focused beam of laser light is used to measure the force. Of the several powerful techniques available for probing the interaction forces between biosurfaces - use of shear flow detachment (Bongrand et al., 1988), surface force apparatus (**SFA**) (Leckband et al., 1992), BFP (Merkel et al., 1999), LOT (Ashkin, 1997) and AFM - AFM is the force-measuring method with the smallest force sensor (tip radii 2-60 nm range) and therefore provides the highest lateral resolution (**Figure 2.4**).

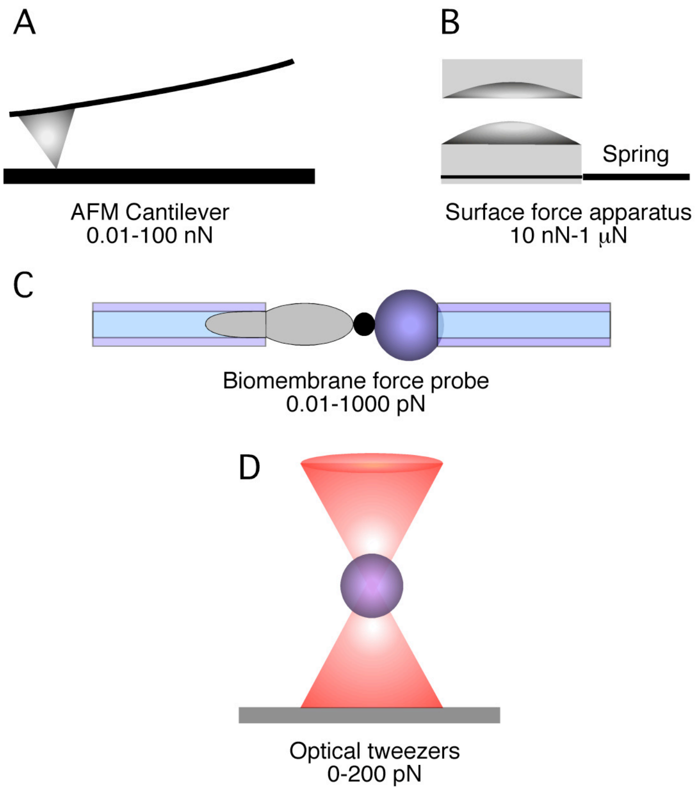

Figure 2.4 Techniques for determining forces in protein interactions

The force measuring components of the various instruments are shown; (**A**) an AFM cantilever, (**B**) the two plates and the spring in a SFS apparatus, (**C**) the micropipette aspiration with the membrane and the beads in a BFP set-up, and (**D**) the force generating photonic gradient in a LOT.

In SMFS by AFM, the surface is brought into contact with the tip and is retracted away at a certain velocity (approach-retract cycle) - the constant velocity or velocity-clamp mode. During certain approach-retract cycles a protein molecule attached to the tip is pulled away from the surface and stretched. Pulling induces mechanical stress in the molecular system and eventually forces a structural transition such as the unfolding of a nucleic acid or protein or the dissociation of a molecular complex. These transitions are of two kinds: (i) elongation of the polypeptide chain that requires an increasing force, and (ii) unfolding events that produce a relaxation of the chain (and a drop in the force) under mechanical stress (see **section 3.3.2**).

The elongation, unfolding and relaxation of the polypeptide chain results in the so-called force-distance (**F-D**) curve (**Figure 2.5**). F-D curves are obtained by monitoring the cantilever deflection (*d*) as a function of the vertical displacement of the piezoelectric scanner (*z*). This yields a raw 'voltage-displacement' curve which can be converted into a 'force-displacement' curve using two simple conversions. Firstly, the sensitivity of the AFM detector, i.e., the slope of the retraction curve in the region where the tip and the sample are in contact, is used to convert the voltage into a cantilever deflection (**Figure 2.5**). Secondly, the cantilever deflection is converted into a force (*F*) using Hooke's law as explained earlier (**section 2.1.3**).

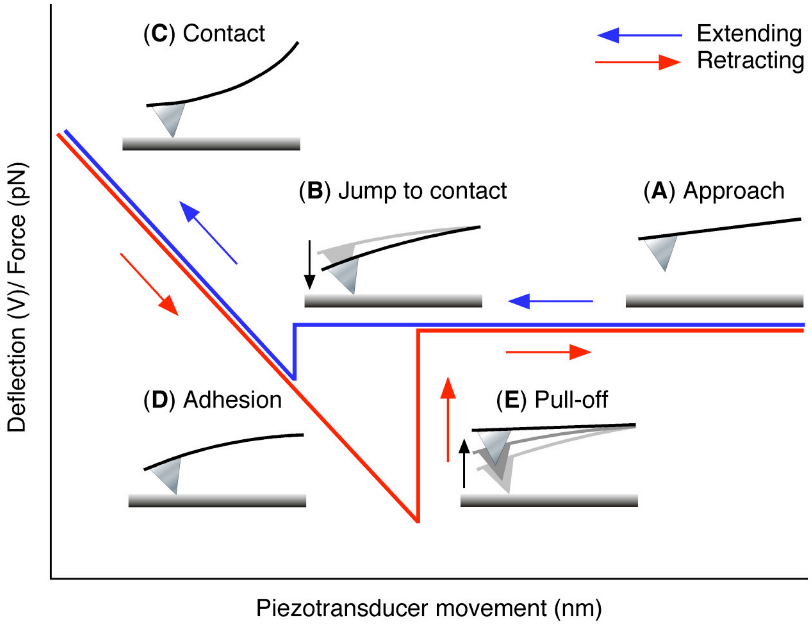

Figure 2.5 A typical force-distance curve

Schematic representation of a F-D curve with the corresponding stages in tip-sample interaction during the up-down movement of the piezoelectric transducer. The slope of the region between (**C**) and (**D**) is used to determine the deflection of the cantilever (nm) which is required to convert a 'voltage-displacement' curve into a 'force-displacement' curve if the spring constant of the cantilever is known. It should, however, be noted that the F-D curve (red) shown here does not represent the unfolding of a polypeptide chain, but rather denotes an adhesion peak between the cantilever and the surface.

The distance between distinct peaks in a F-D curve reflects the gain of distance after unfolding and stretching of a folded structure in the protein, and the amplitude is a measure of the force required to unfold the polypeptide chain. An unfolding event occurring at a given extension is thus specified by both the amplitude of the force peak at this extension and the distance from the same peak to the next one. These 'fingerprints' of the protein reveal different populations of unfolding events.

2.2.1 Background of mechanical unfolding

What exactly does the rupture force signify? Is it an absolute value that can be related to the strength of the bond? Apparently not! The conceptual basis of forced unfolding lies in the lifetime of a bond. To understand a reaction under force let's consider a classical two-state model. An energy profile diagram of a two-state reaction involves a low energy folded state and a high energy unfolded state separated by a barrier that should be overcome for interconversion between the two states (**Figure 2.6**). Folding and unfolding reactions of many small water-soluble proteins under no force can be described using this model (Baldwin and Rose, 1999a; Baldwin and Rose, 1999b). Mechanical unfolding experiments, too, are often described by a two-state model in which the protein adopts only a folded or unfolded state with a single intervening transition state (Evans and Ritchie, 1997; Rief et al., 1998a). If the transition state has a free energy, G^*, then the unfolding rate constant, k_u, is,

$$k_u = \left(\frac{1}{t_D}\right)\exp\left(-\frac{\Delta G_u^*}{k_B T}\right) \qquad \Delta G_u^* = G^* - G_n \qquad (2.13)$$

where t_D is the relaxation time[19] which includes the vibrational frequency, ν, and transmission coefficient, χ, of the transition state.

Weak bonds and structures have limited lifetimes, t_{off}, and so will dissociate under almost any level of force if pulled in for modest periods of time. Close to equilibrium in solution a large number of molecules continuously bond and dissociate under zero force. If exposed to a force gradient these reacting molecules reduce the ratio of bound-to-free constituents. On the other hand, at infinite dilution, which is the case in single-molecule experiments, an isolated single bond exists far from equilibrium and only has non-zero strength on time scales shorter than the time $\left(t_{off} = \frac{1}{k_{off}}\right)$ needed for spontaneous entropy-driven dissociation. If pulled apart faster than t_{off}, a bond resists detachment. Depending on the loading rate, the detachment force can range up to, and even exceed, the adiabatic limit, $F_\infty \sim \left|\frac{\partial E}{\partial x}\right|_{\max}$, defined by the intermolecular potential $E(x)$, if the bond is broken in less time than required for diffusive relaxation (t_D). In essence, higher loading rates give rise to higher unfolding or detachment forces, and lower loading rates to lower unfolding forces. This arises from the fact that when loaded at higher rates a bond experiences shorter lifetimes, and at low loading rates longer lifetimes (Evans, 1998; Evans, 2001).

---

[19] Though the correct value of the Arrhenius frequency factor is not known for protein folding, for most practical purposes a value of 10^9 s^{-1} is used (Bieri et al., 1999).

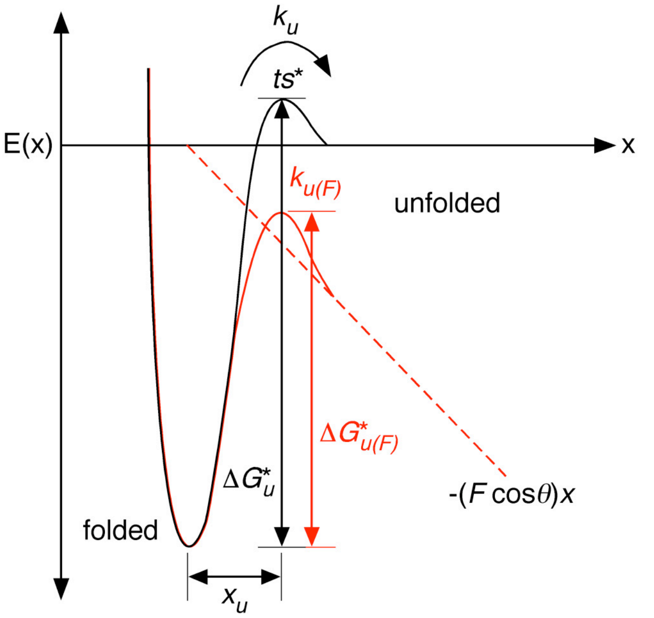

Figure 2.6 Energy landscapes under no force and an external force

A folded protein molecule confined in a well by an energetic barrier, ΔG^*_u, can be unfolded with an unfolding rate of k_u via a transition state ts^* at a distance x_u from the folded state. An external force, F, at an angle θ to the molecular coordinate x adds a mechanical potential $-(F\cos\theta)x$ that tilts the landscape and lowers the energy barrier to $\Delta G^*_{u(F)}$. The new unfolding rate under force is $k_{u(F)}$. However, the distance to the transition state, x_u, remains unchanged.

A very useful way of thinking about a reaction under force is that the force lowers the energy barrier of the underlying energy landscape (**Figure 2.6**). Application of an external pulling force, F, at an orientation, θ, relative to the selected microscopic reaction coordinate, x, adds a mechanical potential, $-(F\cos\theta)x$, that tilts the energy landscape, $E(x)$, along this coordinate thus lowering the energy barrier, G^*, at the transition state ($x = x_{ts}$) (**Figure 2.6**),

$$\Delta G^*_{u(f)} = \Delta G^*_u - F x_u \tag{2.14}$$

where $\Delta G^{*}_{u(f)}$ and ΔG^{*}_{u} represent the free energy difference under applied force and zero force, respectively, and $x_u = \langle x_{ts} \cos\theta \rangle$ is the thermally averaged projection.

Although force can displace and deform the width of the barrier, x_u, for a sharp energy barrier the shape and location of the transition state are insensitive to force (Evans, 1998). As first postulated by Bell thirty years ago (Bell, 1978), the rate of escape, k_{off}, increases exponentially with force,

$$k_{off} \approx \left(\frac{1}{t_{off}}\right) \exp\left(\frac{F}{F_u}\right) \tag{2.15}$$

where $F_u = \frac{k_B T}{x_u}$, the characteristic scale for force as introduced due to thermal activation, can be surprisingly small since the thermal energy $k_B T \approx 4.1$ pN nm at room temperature, and $x_u \approx 0.1$-1 nm. A similar relation is obtained on combining equations (2.13) and (2.14),

$$k_{u(F)} \cong \left(\frac{1}{t_D}\right) \exp\left(-\frac{\Delta G^{*}_{u} - F x_u}{k_B T}\right) = k_u \exp\left(\frac{F x_u}{k_B T}\right) \tag{2.16}$$

2.2.2 A variety of proteins ripped apart by SMFS

SMFS has been used extensively to characterize the mechanical properties of a range of biomolecules, including titin and its intermediates (Carrion-Vazquez et al., 1999; Marszalek et al., 1999; Rief et al., 1997a; Rief et al., 1998b), the triple helical coiled-coils of spectrin (Rief et al., 1999b), FN-III domains of tenascin (Oberhauser et al., 1998) and FN-III (Oberhauser et al., 2002; Oberhauser et al., 1998), polysaccharides (Marszalek et al., 2002; Rief et al., 1997b), integration strength of transmembrane α-helical peptides in lipid bilayers (Ganchev et al., 2004), diatom single adhesive nanofibers (Dugdale et al., 2005), the mechanical stability of dihydrofolate reductase (Junker et al., 2005), the molecular spring made of Ig and fibronectin type III (FN-III) domains - myomesin (Schoenauer et al., 2005), the nanospring behaviour of multidomain protein ankyrin (Lee et al., 2006), the ubiquitous collagen (Gutsmann et al., 2004), spider silk (Oroudjev et al., 2002), and even a non-mechanical protein barnase (Best et al., 2001).

Applied to novel uses – like the unbinding properties of ligand-receptor systems including avidin/biotin, antibody/antigen, and *p*-selectin/carbohydrate pairs (Fritz et al., 1998; Hinterdorfer et al., 1996; Merkel et al., 1999), determining misfolding events of single proteins (Oberhauser et al., 1999), the strength of a covalent bond (Grandbois et al., 1999), studying the effect of point mutations on the mechanical stability of Ig modules (Li et al., 2000), the unfolding kinetics of ubiquitin (Schlierf et al., 2004), mapping the energy landscape of GFP (Dietz and Rief, 2004), measurement of protein energy landscape roughness (Nevo et al., 2005), folding pathway of fast-folding Ig domain (Schwaiger et al., 2005), viscoelastic properties of single polysaccharide (Kawakami et al., 2004) and protein molecules (Janovjak et al., 2005), determining protein structure using a method termed ‘mechanical triangulation’ (Dietz and Rief, 2006) - experiments at the nanometer scale provide a complete new insight into processes which before the development of AFM and related instruments were not accessible by ensemble-average processes.

Different modes of application of force have been developed for single-molecule unfolding experiments. I have described the velocity-clamp mode which is most commonly used for unfolding single protein molecules. In 2001, Julio Fernandez and co-workers reported the construction of a force-clamp AFM instrument that allowed them to unfold titin mechanically either keeping the applied force constant at a set value or increasing it linearly with time[20] (Oberhauser et al., 2001). Whereas in the force-clamp mode the pulling force is maintained at a chosen value by continuously readjusting the cantilever-surface distance and thus the length of the bridging molecule through a feedback loop, in the force-ramp mode the force is increased linearly with time (Oberhauser et al., 2001).

The most interesting breakthrough came with the refolding study of ubiquitin using the force-clamp mode. Though no details or discrete folding steps were resolved in the rate-determining stage, a more or less continuous process akin to polymer collapse was found (Fernandez and Li, 2004). Important to note is that it is only during such segments of the stretching process where the external force applied to the protein is constant that the induced unfolding can start from an equilibrium state. Using these modes it has also been possible to estimate the natural lifetimes of the folded states and follow the refolding of other protein molecules, e.g., the insect flight muscle proteins projectin and kettin (Bullard et al., 2006), ubiquitin (Schlierf et al., 2004) and to determine the effect of force on the kinetics of disulfide exchange to measure the stability of the folded domain as a function of constant force (Wiita et al., 2006).

---

[20] Later the two modes were correctly named as ‘force-clamp’ and ‘force-ramp’, respectively.

With the available information on single components using scanning probe techniques we can now learn how processes are determined by the properties of the single elements of such ensembles, thus complementing more classical techniques involving the use of chemicals or denaturants.

2.2.3 What can be learnt from SMFS on membrane proteins?

The modular structure of proteins seems to be a general strategy for resistance against mechanical stress. As I have already mentioned in **section 2.2.2**, the mechanical properties of several modular proteins, like titin, have already been investigated by the AFM (Rief et al., 1997a). Such experiments have demonstrated that the elongation events observed during stretching of single proteins may be attributed to the unfolding of individual domains, and experiments with optical tweezers have corroborated these results (Kellermayer et al., 1997; Tskhovrebova et al., 1997). Here I will describe the progress that has been made in studying membrane proteins by SMFS.

The combination of AFM imaging and SMFS (Müller et al., 1999a; Oesterhelt et al., 2000) has yielded surprisingly detailed insights into the inter and intra-molecular interactions stabilizing membrane proteins like BR (Janovjak et al., 2003; Müller et al., 2002b), halorhodopsin (Cisneros et al., 2005), human aquaporin-1 (Möller et al., 2003), the Na^+/H^+ antiporter NhaA from *E. coli* (Kedrov et al., 2004), and more recently native bovine rhodopsin (**Chapter 4**) (Sapra et al., 2006b). The sensitivity of SMFS makes it possible to detect the interactions that stabilize secondary structures such as transmembrane α-helices, polypeptide loops and segments within (Möller et al., 2003; Müller et al., 2002b; Sapra et al., 2006b). Experiments over a wide range of temperature, and different protein-protein assemblies have shown that the positions of stable structural segments do not change, but their stabilities are changed as a consequence of altered molecular interactions. Such changes alter the probability of proteins to choose a certain unfolding pathway (**Chapter 3**) (Janovjak et al., 2003; Sapra et al., 2006a).

The molecular interactions established by a variable number of amino acids act collectively to form stable structural segments. These amino acids unfold in a cooperative manner over a certain threshold of applied force. There is no general consensus on the number of amino acids required to form a stable structural segment, since this would depend on the amino acids, the interacting amino acids in the immediate vicinity, the lipid type and the nature of protein-protein and protein-lipid interactions. The results from unfolding membrane proteins, however, indicate that the smallest segment contains ~6 amino acids and the largest one more than 20 amino acids (Müller et al., 2002b). Stable structural segments do not necessarily correlate to the secondary structure elements of the protein, since a transmembrane helix together with a polypeptide loop could establish a mechanical barrier. These barriers may be the determining factors during the folding process, folding in modules and are independent of each other, and in the final step start interacting to form a functional protein (Dinner et al., 2000; Dobson, 2003). Mapping these stable structural segments on the secondary structure of a protein helps to localize the regions stabilized by collective molecular interactions. Measuring the force required to unfold the stable structural segments gives a direct measure of the stabilizing molecular interactions in these regions. It is possible to determine unfolding forces under different conditions of pH, temperature, ligands, metal ions, lipids and different point mutations. Since protein activity, function and structure are directly related to the changes in their molecular interactions, it is possible to detect regions of altered molecular interactions under the aforementioned environmental factors and the contribution of each of these factors on different structural segments.

Besides the force required to unfold a structural segment, the probability to unfold a certain structural segment could be taken as an indicator of changed molecular interactions. The probability for a structural segment to unfold is a stochastic process and it indicates the numerous pathways a protein can take in the unfolding energy landscape. These pathways differ just in the energy barriers crossed during unfolding (Janovjak et al., 2004; Müller et al., 2002b). The same stable structural segment can be unfolded in one or multiple steps. Thus depending on the number of steps the unfolding pathways would include one or two or more energy barriers.

Using these analytical methods it has been possible to unfold BR at different temperatures and determine the preference of the molecule to unfold via a certain pathway at a specific temperature (Janovjak et al., 2003); to probe the energy landscape of BR and measure the unfolding rates and the width of potential barriers for individual structural segments (Janovjak et al., 2004); to measure the contribution of dissipative energy and elastic forces during BR unfolding by force modulation spectroscopy (Janovjak et al., 2005); a plausible reason for the differences and similarities in the unfolding pathways of the homologous light-driven ion pumps of *Halobacterium salinarum* (***H. salinarum***), halorhodopsin and BR, which gave intriguing insights into the mechanism of structural segments formation (Cisneros et al., 2005); to dissect protein-protein interactions and the contribution of inter and intra-molecular interactions in different BR assemblies (**Chapter 3**) (Sapra et al., 2006a); to determine the effect of single point mutations in BR on the unfolding energy landscape (**section 7.2**); to unfold membrane proteins from either the N- or C- terminal which further shed light on a possible mechanism on how membrane proteins establish stable structural segments (Kedrov et al., 2004; Kessler and Gaub, 2006); to locate the ligand binding site in the Na^+/H^+ antiporter NhaA and correlate it with its activation in a pH dependent manner (Kedrov et al., 2005); to unfold and refold NhaA (Kedrov et al., 2006a) and BR (Kessler et al., 2006) which proved that individual structural segments could refold in the membrane against an external force and choose between various refolding pathways; to unravel the molecular interactions between different structural segments and consequently detect different structural and functional states of native bovine rhodopsin (**Chapter 4**) (Sapra et al., 2006b); and very recently to correlate the effect of zinc binding on the functional state of native bovine rhodopsin and its likely contribution in the stabilization of the disulfide bridge and promotion of the rhodopsin dimer formation (**Chapter 5**).

Chapter

3

DISSECTING THE INTER- AND INTRAMOLECULAR INTERACTIONS OF BACTERIORHODOPSIN

3.1 INTRODUCTION

BR is a light-driven proton pump which forms highly ordered 2-D hexagonal lattices in the plasma membrane of archaebacterium *H. salinarum*. 248 amino acids long and with a molecular weight of 26,788 Da, architecturally BR is a seven TM α-helical protein (Oesterhelt and Stoeckenius, 1971) similar to the GPCRs (Baldwin, 1993; Filipek et al., 2003b; Hargrave, 1991) (**Figure 3.1**). An all-*trans*-retinal group covalently linked to Lys216 via a protonated Schiff base gives BR its unique purple color (λ_{max} = 568 nm) (Grigorieff et al., 1996; Kimura et al., 1997). On absorbing a photon of light[21] BR isomerizes from the all-*trans* to the 13-*cis* form. The energy stored in the molecule leads to a cascade of thermal reactions, forming spectrally distinct structural intermediates resulting in proton pumping from the cytoplasmic side to the extracellular side of the membrane, subsequently returning to the ground state (Lanyi, 2004).

The elucidation and availability of various refined structural models (Essen et al., 1998; Grigorieff et al., 1996; Luecke et al., 1999a; Mitsuoka et al., 1999) has made BR a very good model system for biophysical and biological characterization, and thus one of the most extensively studied membrane proteins (Haupts et al., 1999; Lanyi, 2004; Subramaniam et al., 1993). BR provides a unique opportunity to investigate relevant questions pertaining to thermodynamic and kinetic characterization of folding and assembly not just on the folding of this particular protein (Booth, 2000; Compton et al., 2006; Engelman et al., 1990; Huang et al., 1981; Hunt et al., 1997; Kim et al., 2001), but also on the factors governing folding of TM α-helical proteins in general.

---

[21] The quantum yield of BR is ~60% (Schneider et al., 1989).

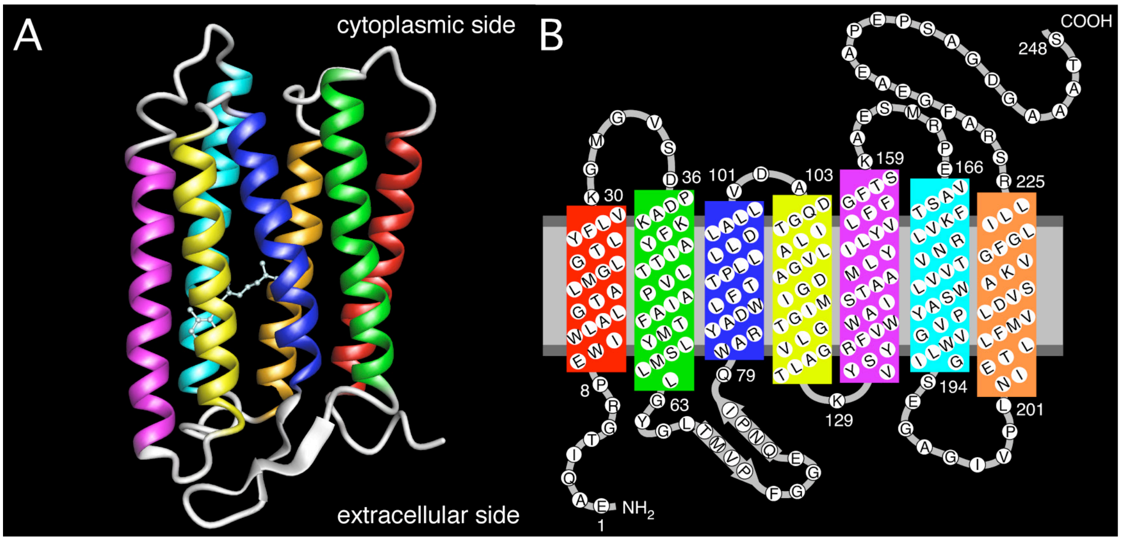

Figure 3.1 Structure of bacteriorhodopsin

(**A**) The X-ray crystal structure of BR (PDB: 1AT9) (Kimura et al., 1997) showing the 3-D arrangement of its seven helices surrounding the retinal chromophore. (**B**) Secondary structure of BR with its primary amino acid sequence. The two anti-parallel arrows on the extracellular side denote the β-sheet structure in loop BC between helices B and C.

In native conditions BR assembles into trimers that are arranged as a 2-D hexagonal lattice (Blaurock and Stoeckenius, 1971). Recrystallization of BR in the presence of n-dodecyl trimethylammonium chloride (DTAC) yields BR dimers arranged in well-ordered 2-D crystals establishing $p22_12_1$ symmetry in an orthorhombic lattice (Michel et al., 1980). Single BR monomers could be potentially formed by the substitution of tryptophans at amino acid positions 12 and 80 with isoleucines, which leads to the collapse of the 2-D assembly of BR. The mutation at amino acid position 12 alters trimer-trimer interactions, and the one at position 80 monomer-monomer interactions within the trimer (**Figure 3.2**) (Weik et al., 1998).

As mentioned in **section 1.3.2**, the problem of how membrane proteins assemble and form thermodynamically stable structures *in vivo* is intriguing and challenging for molecular biologists, biochemists and biophysicists (Engelman et al., 2003; Engelman and Steitz, 1981; White, 2003; White and Wimley, 1999). It is now known that protein folding is driven by intramolecular interactions, which most probably contribute more than intermolecular interactions in maintaining the functional and structural integrity of the protein (White and Wimley, 1999). The interaction forces stabilizing a structural segment in a membrane protein are additive,

$$F_{tot} = F_{inter} + F_{intra}\ (+\, F_{coupling}) \tag{3.1}$$

F_{tot} reflects the total force stabilizing a structural segment, F_{inter} the intermolecular contribution, F_{intra} the intramolecular one, and $F_{coupling}$ the contribution due to coupling of the two.

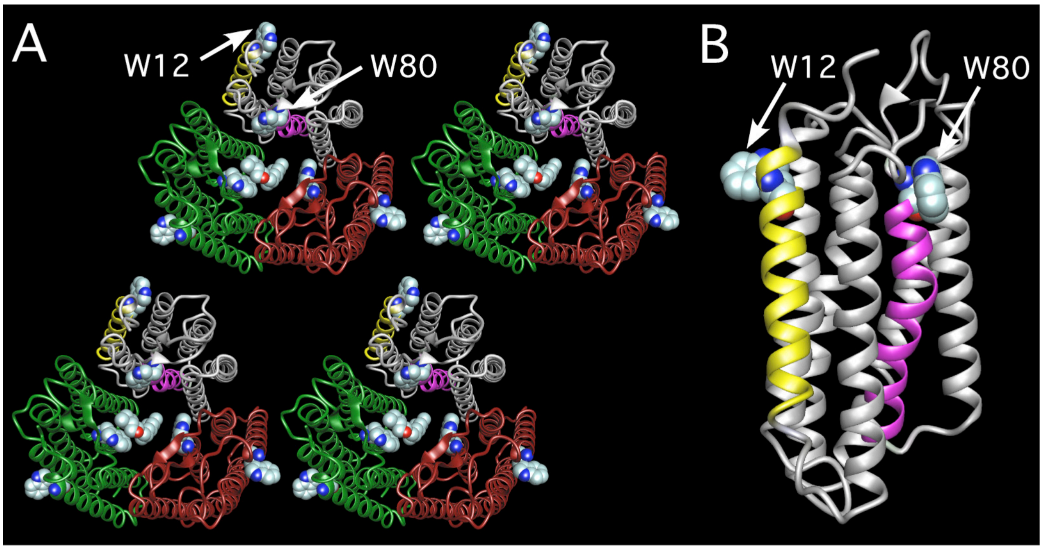

Figure 3.2 Crystal structure of the BR trimer showing the mutations W12I and W80I

(**A**) To emphasize the positions of the mutations at the interfaces of BR trimer, BR in its trigonal lattice (PDB: 1BRR) (Mitsuoka et al., 1999) is displayed. However, the mutant BR was not able to form a crystalline lattice nor did I observe the BR trimers as shown in (**Figure 3.4**(**C**)). (**B**) Side-view of the BR monomer showing the mutations W12I and W80I in helices A and C, respectively.

Hence, it is important to explore the nature of intra- and intermolecular interactions not only to understand how these proteins have evolved to form structurally stable elegant architectures and efficient functional machines (Haltia and Freire, 1995), but also to increase our knowledge of how proteins are driven into misfolded conformations in disease states (Dobson, 2002; Martin, 1999; Prusiner, 1997). An attempt to dissect the individual contribution of these interactions would explain the observed independent stability of secondary structures, as proposed by the two-stage folding model of transmembrane proteins (Popot and Engelman, 1990).

The effects of changes in the BR assembly and membrane lipid content on the structural stability of BR have been investigated till now using conventional kinetic and equilibrium methods (Heyes and El-Sayed, 2002; Mukhopadhyay et al., 1996) and by neutron diffraction (Weik et al., 1998), which are indirect and give an average of the ensemble measurements. To characterize the intra- and intermolecular interactions in the most widely used membrane protein model system, BR, I studied the mechanical unfolding of single BR molecules from three different BR oligomers using SMFS with

AFM. Previous mechanical unfolding experiments performed on BR have revealed that single helices, polypeptide loops and certain structural regions of helices could establish sufficiently strong molecular interactions to form independently stable units (Cisneros et al., 2005; Janovjak et al., 2004; Müller et al., 2002b; Oesterhelt et al., 2000). Such stable structural segments which can be represented by grouped, single or parts of secondary structure elements build unfolding barriers and stabilize the whole membrane protein.

The nature of molecular interactions that establish such stable structural segments within a membrane protein is not well understood though and important questions remain to be answered. Are the locations and stability of these structural segments the result of intermolecular interactions (monomer-monomer or oligomer-oligomer, i.e., trimer-trimer in the case of BR), or intramolecular interactions (within the secondary structure elements) or both? How does the protein assembly exhibit an effect on the unfolding forces? Does it influence the dimensions and positions of the structural segments that form the unfolding barriers? How, if at all, is the statistical nature of the different unfolding pathways altered for molecules from different membrane protein assemblies? To reveal insights into these questions, I unfolded trimeric, dimeric and monomeric BR assemblies using a combination of AFM imaging and SMFS (Oesterhelt et al., 2000).

3.2 EXPERIMENTAL PROCEDURES

3.2.1 Purple membrane preparation, dimerization and monomerization of BR

Trimeric (WT BR in purple membrane), dimeric and monomeric BR samples were a kind gift of Prof. Dieter Oesterhelt (Max Planck Institute of Biochemistry, Martinsried, Germany). WT purple membrane (PM) was extracted from *H. salinarum* and purified as described (Oesterhelt and Stoeckenius, 1974). Dimerization of BR with DTAC was carried out following the procedure of Michel et al. (Michel et al., 1980). Monomeric BR was formed in the cell membrane of *H. salinarum* after introducing point mutations at positions 80 and 12 (W 12/80 I) (Weik et al., 1998). The respective tryptophans were substituted by isoleucines. Cells were lysed and membranes fractionated on sucrose density gradients. As no purple membranes were formed in the mutant strains, the fractions containing the highest BR content were used for the AFM experiments. The mutations introduced only disrupted trimer-trimer interactions (W12I) and monomer-

monomer interactions (W80I) within the trimer, and did not alter the structure-function relationship of BR as characterized by the unchanged photocycle. All buffer solutions were prepared using nanopure water (PureLab Plus, ELGA, Germany) of 18 MΩ•cm conductivity, and p.a. grade chemicals from Sigma/Merck.

3.2.2 Preparation of supports for single-molecule force spectroscopy

AFM measurements do not require any special staining, labeling or fixation of the sample in general. A prerequisite for obtaining reliable information from imaging and SMFS experiments is a specially designed support to immobilize the sample (**Figure 3.3**). A good support should have an atomically flat surface. Materials that fulfill this criterion and are commonly used are mica, graphite, gold and glass. For imaging and SMFS measurements of bacteriorhodopsin, I used mica as the supporting surface (Müller et al., 1997).

To prepare a supporting surface for measurements, 8 mm diameter magnetic steel discs (Agar Scientific, Stansted, UK) were first treated with 37% hydrochloric acid for ~5 mins, and washed intensively with deionized water. Teflon discs of 10 mm diameter were punched and glued onto the cleaned steel discs with instant glue Loctite 770 (Koenig, Dietikon, Switzerland). A 0.2-0.3 mm thick slice of muscovite mica (Shree G. R. Exports, Kolkata, India) was punched into discs of 5 mm diameter. To obtain an atomically flat surface, the upper layer of the mica disc was cleaved using a tape and this side glued onto the Teflon disc with a water-insoluble, two-components epoxy glue (Konrad Electronic, Hischau, Germany).

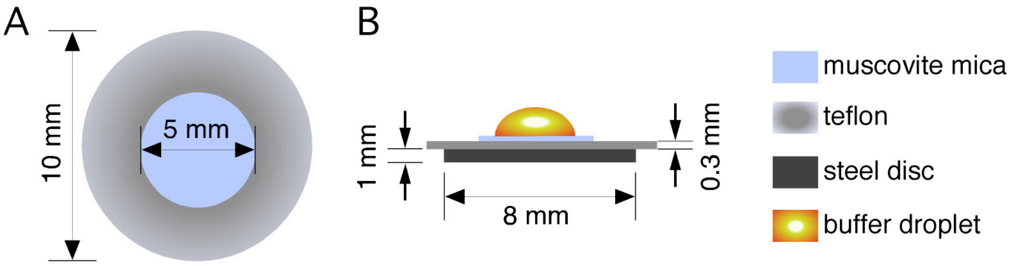

Figure 3.3 Sample support for AFM single-molecule measurements

(**A**) Top-view and (**B**) side-view showing the dimensions and arrangement of mica and teflon discs on a magnetic steel disc. Teflon being highly hydrophobic prevents the buffer droplet from spilling into the piezoelectric transducer.

Since single-molecule measurements are prone to molecular contaminations, just prior to the experiments the mica surface of a support was cleaved using a tape to obtain an atomically flat surface. To check the integrity of the surface and the cantilever tip, the freshly cleaved surface was imaged with AFM. This helped control the flatness of the surface and to ensure if the tip had the desirable properties. Only those supports that showed a height variation of ≤ 5 nm were used to adsorb the membrane patches.

3.2.3 AFM setup for measurements

A commercial Nanoscope IIIa (Veeco Metrology, Santa Barbara, USA) was optimized for high-resolution imaging. The piezoelectric actuator of the AFM was calibrated in x, y, and z dimensions using a calibration grid. AFM equipped with a 50 μm X-Y piezo scanner with a closed-loop 20 μm vertical axis was used for SMFS measurements (Multimode PicoForce, Nanoscope IIIa; Veeco Metrology, Santa Barbara, USA). Before and after every experiment, the contact mode fluid cell was cleaned with a detergent (Pril, Henkel GmbH, Germany), rinsed 4-5 times alternatively with p.a. grade ethanol and nanopure water and dried with filtered nitrogen flow. High-resolution imaging was performed in the contact mode using thin long-legged V-shaped NP-S cantilevers (Veeco Metrology, USA) with nominal values, $\kappa \approx 0.08$ N/m, $\nu \approx 4.0$ kHz, $L \approx 200$ μm, $w \approx 23$ μm and $t \approx 0.6$ μm. Spring constants of cantilevers were calibrated on Nanoscope IIIa equipped with the PicoForce module in 300 mM KCl, 20 mM Tris-HCl, pH 7.8 (**buffer A**) away from the surface using thermal fluctuation analysis (Butt and Jaschke, 1995; Florin et al., 1995**.** All cantilevers used were from the same cantilever batch and exhibited similar spring constants within the uncertainty of this method (~10%).

3.2.4 Single-molecule force spectroscopy and imaging

Single-molecule AFM imaging and force spectroscopy were performed as described earlier (Müller et al., 2002b; Oesterhelt et al., 2000). 5 μl of the purple membrane sample (150 μg/ml), diluted in a 1:10 ratio in buffer A, was adsorbed onto a freshly cleaved mica surface covered by ~30 μl of buffer A. After 5-7 mins, the adsorption process was quenched by washing the mica surface atleast 6 times with ~40 μl buffer A to remove loosely bound and excess membrane patches. To determine the BR assembly, membrane patches were imaged at high-resolution using contact mode AFM (Möller et al., 2000;

Müller et al., 1999c). For force measurements, the AFM tip was approached to the membrane protein surface while applying a constant force of ~1 nN for ~1s between the two. This led to the non-specific attachment of a single BR molecule to the silicon nitride cantilever in most cases. This method has been shown to provide equivalent results and allows a much higher throughput as compared to the specific attachment via thiol-gold linkage (Müller et al., 2002b). After a contact time of ~1 s, the tip was retracted from membrane surface at a constant velocity of 300 nm/s. In about 10% (trimeric BR), ~5% (dimeric BR) and ~2% (monomeric BR) cases one or more adhesion peaks were detected. All experiments were performed in buffer A at room temperature (24 ± 1°C). To rule out statistical errors due to cantilever spring constant deviations, the force spectroscopy experiments were performed on each BR assembly using at least 3 different cantilevers from the same batch.

3.2.5 Selection of force-distance curves

In SMFS experiments the AFM tip can attach non-specifically to any of the solvent exposed parts of the folded polypeptide chain, thus leading to F-D curves of various lengths. This necessitates an extremely careful analysis procedure of the F-D curves due to the complexity of the unfolding process, i.e., of the different types of interactions between the tip, the protein and the surface. Besides attaching at various regions of the molecule, the tip can pick up none[22], one or few molecules of interest, thus contributing very different force curves encoded with varied information. Simultaneous pickup of multiple proteins creates multiple parallel and therefore additive springs between the tip and the surface leading to higher forces and steep slopes to each peak. Any F-D curves displaying an offset in the force indicate multiple parallel springs, i.e., multiple molecule pick-up (**Figure 3.4**(**A**)). These curves were discarded from analysis to ensure single-molecule manipulation. The statistical nature of the picking process unavoidably leads to an experimental situation where most of the force curves have to be discarded due to various artifacts. Thus the first step in analyzing F-D curves is to sort out good curves from the bad ones.

---

[22] The tip can potentially attach to misfolded or unfolded molecules on/in the membrane giving spurious F-D curves.

A suitable and unambiguous criterion that can be used to distinguish curves of BR molecules attached to the tip of the AFM cantilever with different regions of their polypeptide backbone is the overall length of the force curve, which reflects the tip-sample distance at which the last force peak occurs (Müller et al., 2002b; Oesterhelt et al., 2000). It is intuitive that a molecule attached to the cantilever by one of its loops or if it loses the molecular bridge that connects it to the tip would result in a F-D curve of smaller overall length than a molecule attached by one of its termini. The length of a fully stretched molecule upon unfolding can be easily calculated from the secondary structure. **Figure 3.4**(**B**) demonstrates the method applied to determine the length of the stretched polypeptide upon forced unfolding. Depending on the amino acid residue at the C-terminal end where the cantilever tip attaches, the length of the resulting polypeptide chain would differ. It was previously shown that F-D curves exhibiting an overall length between 60 and 70 nm result from completely unfolded and extended BR molecules attached with their C-terminus to the AFM tip (Müller et al., 2002b; Oesterhelt et al., 2000), and were used for analyses.

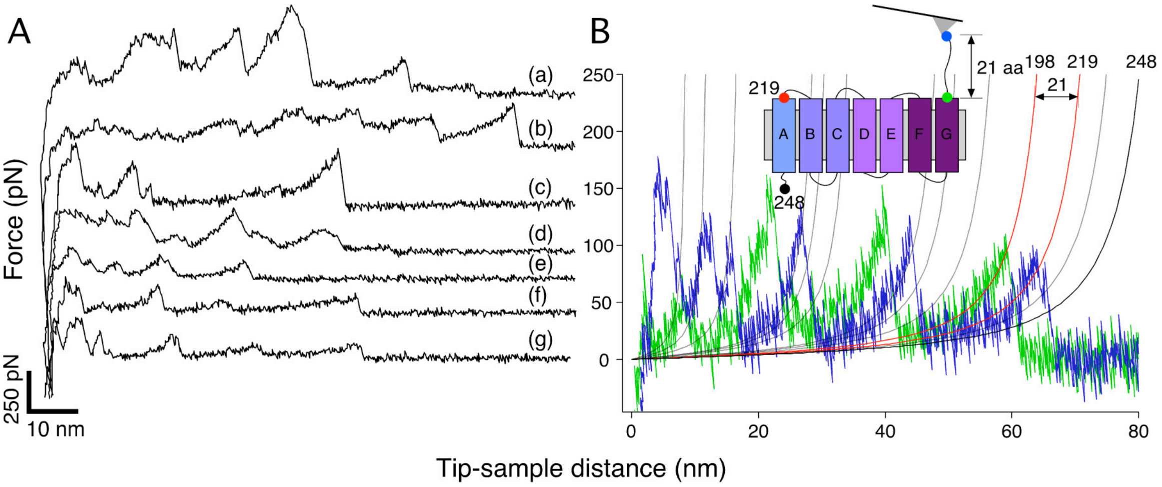

Figure 3.4 Selection of force-distance curves

(**A**) A variety of F-D traces that can be obtained in an SMFS experiment. Curves due to multiple attachment of the molecules to cantilever show an offset in the force (a) & (b). Attachment of misfolded molecules or native molecules give F-D traces that are difficult to interpret (c) & (d). The tip sometimes detaches from the terminus during unfolding giving a F-D trace with a few well defined peaks (e). All the curves falling in the above mentioned and other ambiguous categories were not included in the analysis. (f) & (g) represent F-D traces originating from a native BR molecule which unfolded from its C-terminus as shown in (**B**). The criterion used to select curves with well defined peaks is shown schematically in (**B**). The tip could attach at any position along the length of the terminus. Considering the two extreme cases – attachment of the tip at the two ends of the terminus (blue and green dots) – the lengths of the F-D curves will differ by the length of the terminal end, 21 amino acids (aa) in BR. The F-D traces shown in blue and green correspond to the unfolding of the BR molecule from either end of the terminus (the colors of dots and F-D traces correspond). The WLC fits (red) show the observed difference in the lengths (219-198 = 21) is equal to the terminus length. The numbers at the end of the WLC fit show the length of the unfolded polypeptide in amino acids. The black WLC trace (248) corresponds to the complete length of the BR molecule shown by a black dot at the other end (N-terminus) of the BR molecule.

3.2.6 Analysis of force-distance curves

The force measured in a raw F-D curve during SMFS is displayed as a function of the vertical displacement, z, of the piezoelectric actuator. However, the end-to-end distance of the stretched molecule is smaller than z due to the deflection, Δx, of the cantilever, which can be several nanometers for soft cantilevers (κ = 50-80 pN/nm) used in these experiments. To compensate the z value for the cantilever deflection, the force is presented as the tip-sample separation (*tss*), i.e., versus the distance between the tip and the sample surface (**Figure 3.5**),

$$tss = z - \Delta x \tag{3.2}$$

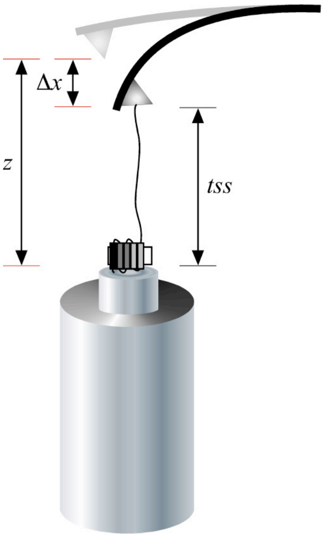

Figure 3.5 Schematic drawing showing the tip-sample separation

The actual length of the unfolded polypeptide is given by *tss*, and not *z*, due to the bending motion of the cantilever as explained in the text.

All force curves exhibiting overall lengths of 60-70 nm and similar unfolding patterns were selected and aligned manually using the software Igor Pro (Wavemetrics Inc., Oregon, USA), taking the adhesion peak which occurred at a tip-to-membrane separation of ~25 nm as the reference (**Figure 3.4**(**B**)). This method of alignment also compensates for attachment at multiple and/ or different sites of the C terminus. To assign events in the force spectra to secondary structural elements I used the mechanical unfolding pathways of BR as described by Müller et al. (Müller et al., 2002b).

Models used to describe stretching under force

Modeling the extension behavior of polymers like proteins, polysaccharides and nucleic acids under force is required to extract meaningful information from forced unfolding or stretching experiments. It is intuitive that to keep a polymer at a certain extension at constant temperature, it is necessary to apply a force where the work done by stretching the polymer chain goes into the reduction of the conformational entropy, i.e., the polypeptide chain acts as an entropic spring. This explains the ascending part of a F-D curve. Once a folded structure has unfolded, an extra-length of the unfolded part of the chain is available for stretching. Entropic contributions, which dominate at small extensions, are subdued on extending the molecule, which limits its conformational states and consequently reduces the entropy. The frustration in the system leads to entropic elasticity. The decrease in entropy is balanced by an increased enthalpic elasticity, which dominates at larger extensions and can be traced to the tensions in the backbone bonds due to the applied force. To ascertain the nature of unfolding of a molecule and polypeptide extension fitting procedures based on certain models are routinely used.

Freely jointed chain (**FJC**)[23] and the worm-like chain (**WLC**) model are two such models (**Figure 3.6**) developed to predict entropic and enthalpic restoring forces. The FJC model can be used to explain the structure or lack of structure of unfolded proteins, structure and mechanical properties of DNA (Bustamante et al., 1994; Smith et al., 1992) and flexible proteins like titin (Kellermayer et al., 1997; Rief et al., 1997a). A freely jointed chain in which short, rigid segments are connected by swivels (**Figure 3.6**(**A**)), is an extreme case of a flexible rod. The many segments ought to behave qualitatively the same as a very flexible slender rod. Such a rod is called a worm-like chain. Although in the absence of an external force the worm-like chain and freely jointed chain are similar[24], there are small differences in the way the two chains elongate when an external force is applied (Bustamante et al., 1994). I used the WLC model and describe it briefly.

Each extension segment between force peaks on the F-D curves is well described by the WLC model. It relates the force, F, of the stretched chain to its extension, x, using two characteristic parameters: the contour length of the chain, L_c, and its persistence length, l_p, (Bustamante et al., 1994) by the equation,

---

[23] The FJC model can be used to understand the mechanics of proteins that have segmental flexibility, e.g., antibodies and motor proteins (Howard, 2001).

[24] Under zero force, $2l_p = s$, where l_p is the persistence length of the worm-like chain and s is the segment length of a freely jointed chain. The equivalent segment length, b, for a worm-like chain is called the Kuhn length (Howard, 2001).

$$F(x) = \frac{k_B T}{l_p}\left[\frac{1}{4}\left(1 - \frac{x}{L_c}\right)^{-2} + \frac{x}{L_c} - \frac{1}{4}\right] \tag{3.3}$$

The WLC model was first used to describe the behavior of DNA (Bustamante et al., 1994) and that of polypeptide chains (Oesterhelt et al., 2000; Rief et al., 1997a). The most important parameter describing a filament's resistance to thermal forces is the persistence length, l_p. Its intuitive meaning is the length of filament over which thermal bending becomes appreciable[25]. The persistence length of a polypeptide chain is defined as (**Figure 3.6**(**B**)),

$$\left\langle \cos\left[\theta(s) - \theta(0)\right]\right\rangle = \exp\left(-\frac{s}{2l_p}\right) \tag{3.4}$$

In an nutshell what this equation tell us is that the thermal fluctuations in shape resulting from the thermal bending of flexible rods can be described using the length, s, over which the tangent angle of the rod changes appreciably, which is nothing but the persistence length of the filament (Howard, 2001).

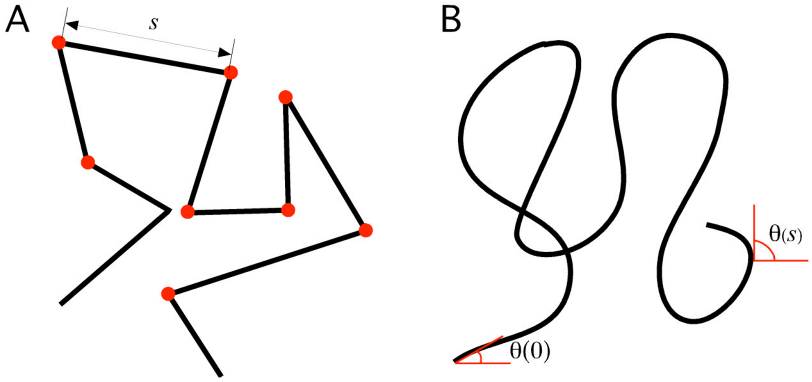

Figure 3.6 Different types of polymer chains

(**A**) A freely jointed chain (FJC) and (**B**) a worm-like chain (WLC) under zero force. Red dots in (**A**) denote joints between the segments with length *s*, which are free to swivel. In the absence of a force WLC is similar to FJC. Small differences, however, exist between the two under an external force (Howard, 2001).

---

[25] For a DNA molecule, l_p ~50 nm, and for a polypetide chain, l_p ~0.4 nm, about the size of a single amino acid.

Every peak of a single F-D curve was fitted using the WLC model with a persistence length of 0.4 nm and a monomer length of 0.36 nm (Rief et al., 1997a). The number of amino acids in the polypeptide extended at each peak was then calculated using the contour length obtained from the WLC fits. Since the fit describes the stretching of an already unfolded part of the protein, comparison of the polypeptide lengths with the BR structure, and marking the end of the preceding and the starting point of the subsequent stable structural segment allows to identify intrinsic mechanical unfolding barriers, to assign unfolding events and identification of the unfolding intermediates of BR (Müller et al., 2002b). The atomic model of Mitsuoka et al. (PDB: 1BRR) (Mitsuoka et al., 1999) was chosen for this purpose. If an unfolding barrier is located within the lipid bilayer or on the side adsorbed to the mica, the bilayer screens a part of the polypeptide chain that results in a shorter apparent length. Although there is no objective criterion at the moment to locate the precise position of an unfolding barrier within the membrane, nevertheless, to compensate for this screening the bilayer thickness of ~ 4 nm, i.e., 11 amino acids, was taken into account when locating the barrier (Müller et al., 2002b).

To measure the unfolding force of each individual structural segment and percent probability, P_e, with which the unfolding intermediates occurred, every event of each curve was analyzed. To determine if the average forces represent the true means of the given population and are statistically different, the data were tested against one-way ANOVA analysis followed by Bonferroni's post-test. The p value obtained from this is the probability (from 0 to 1) of observing a difference as large or larger than one would observe if the null hypothesis were true. The error in percent probability, P_e, of unfolding intermediates was calculated as,

$$P_e = \sqrt{\frac{P(1-P)}{n}} \tag{3.5}$$

where n is the total number of F-D curves.

3.3 RESULTS

3.3.1 High-resolution AFM imaging of monomeric, dimeric and trimeric BR assemblies

Before performing SMFS, I observed the samples at high-resolution using AFM in buffer solution (**Figure 3.7**). The average protrusion of BR molecules from the mica support was 5.9 ± 0.4 nm (Müller and Engel, 1997). High-resolution imaging revealed molecular details in different BR assemblies. While BR of purple membrane was arranged as trimers (**Figure 3.7**(**A**)), the dimers assembled into an orthorhombic lattice (**Figure 3.7**(**B**)) (Müller et al., 1999c). Overview topographs of the mutant proteins (**Figure 3.7**(**C**)) suggested that less than 20% of the lipid membrane area (height ~4.1 ± 0.4 nm) was occupied with membrane proteins (height ~5.7 ± 0.4 nm). This lower packing density of the membrane is in good agreement with the sucrose gradient experiments performed by Dr. Hüseyin Besir (Prof. Dieter Oesterhelt laboratory, Martinsried, Germany) (data not shown). Additionally, the membranes containing the BR double mutant (W 12/80 I) showed no apparent crystalline structure (**Figure 3.7**(**C**), bottom); instead loosely packed assemblies were observed. High-resolution topographs of the mutant BR assembly did not reveal single or even groups of BR trimers such as observed previously for bacterio-opsin (Möller et al., 2000). Individual objects in this protein assembly had dimensions of single BR molecules and since the membrane contained only BR, these objects were assumed to be monomeric BR. It was, however, difficult to observe sub-structural details of these BR monomers due to the reduced BR packing density and consequently free diffusion of the BR molecules in the membrane (Müller et al., 2003).

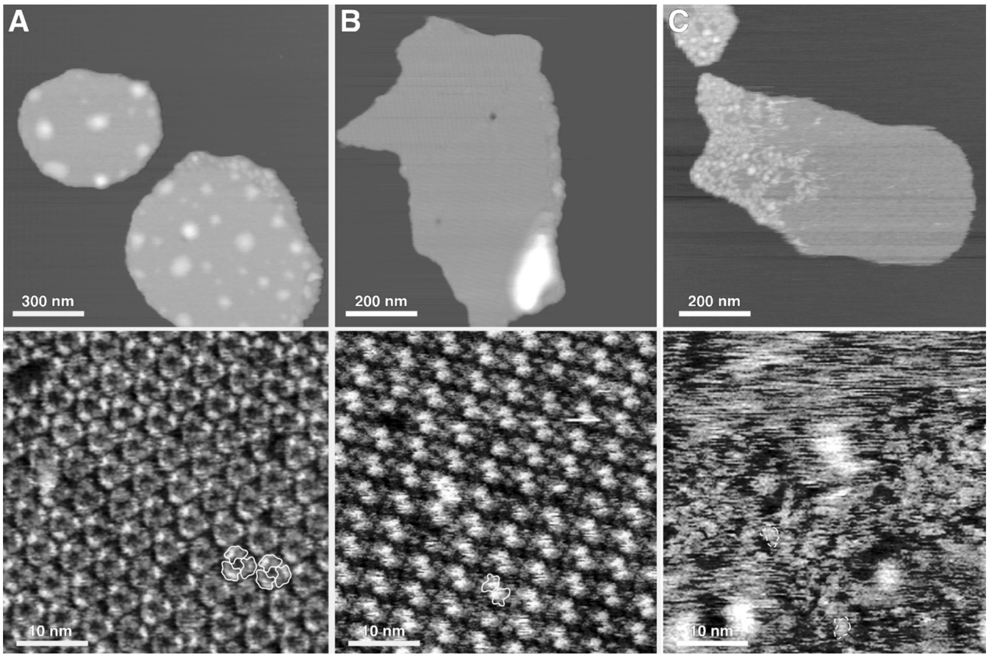

Figure 3.7 High-resolution AFM topographs of different BR assemblies

BR molecules assembled into (**A**) trimers, (**B**) dimers and (**C**) monomers. Top row, membranes being flatly adsorbed on mica. The membranes exhibited heights between 5.5 ± 0.6 nm and 6.4 ± 0.5 nm. Bottom row, membrane surfaces imaged at high-resolution. Due to a lower concentration in the membrane as compared to the crystalline BR assemblies, monomeric BR (**C**) could not be resolved as single molecules as in the case of trimeric (**A**) and dimeric (**B**) assemblies. The outlined BR shapes shown in the high-resolution topographs (bottom) represent 0.1 nm thick slices of the cytoplasmic BR surface. In (**C**) the dashed outlines show possible arrangements of single BR monomers. Topographs are displayed in full gray scale corresponding to vertical heights of 20 nm (top row) and 1.2 nm (bottom row).

3.3.2 Unfolding pathway of a single BR molecule

A schematic interpretation of a typical F-D curve exhibiting common features observed among all curves is shown in **Figure 3.8**(A). The spectrum shows the unfolding pattern of a single BR molecule from a dimeric assembly (Müller et al., 2003). After attachment of the C-terminal end of a BR molecule to the AFM tip and subsequent separation of the tip from the purple membrane surface, the polypeptide was extended. Further separation of the tip and membrane stretched the C-terminal end leading to a force build-up in a gradual non-linear manner. At a certain threshold force the first pair of transmembrane helices - G and F - unfolded. This unfolding event, however, in most cases is masked by non-specific interactions between the tip and the membrane surface occurring at tip-sample separations ≤ 20 nm (Müller et al., 2002b; Oesterhelt et al., 2000). Unfolding of helices G and F increased the length of the molecular bridge between the tip and membrane causing the cantilever to relax as the force dropped abruptly (shown by black arrows). The polypeptide chain of the unfolded structural elements was extended on further separating the AFM tip and membrane surface. As soon as the polypeptide was stretched again the force increased as detected by the cantilever deflection. At a certain critical force, the next secondary structure element (in terms of the polypeptide chain) unfolded. The F-D traces defined by unfolding and stretching of helices could be well fitted using the WLC model with only one free parameter: the contour length of the stretched portion of the molecule (**section 3.2.6**) (Rief et al., 1997a). The fitted contour length of the F-D curve and the secondary structure model of BR show that three peaks at amino acid positions 88, 148 and 220 occurred predominantly suggesting that helices E & D, helices B & C, and helix A with the N-terminus preferred to unfold in a pairwise manner (Müller et al., 2002b; Oesterhelt et al., 2000). The last seventh helix A was then pulled out from the membrane in a single step. Beyond an extension of ~70 nm no interaction could be measured (see **Figure 3.9** for a detailed description).

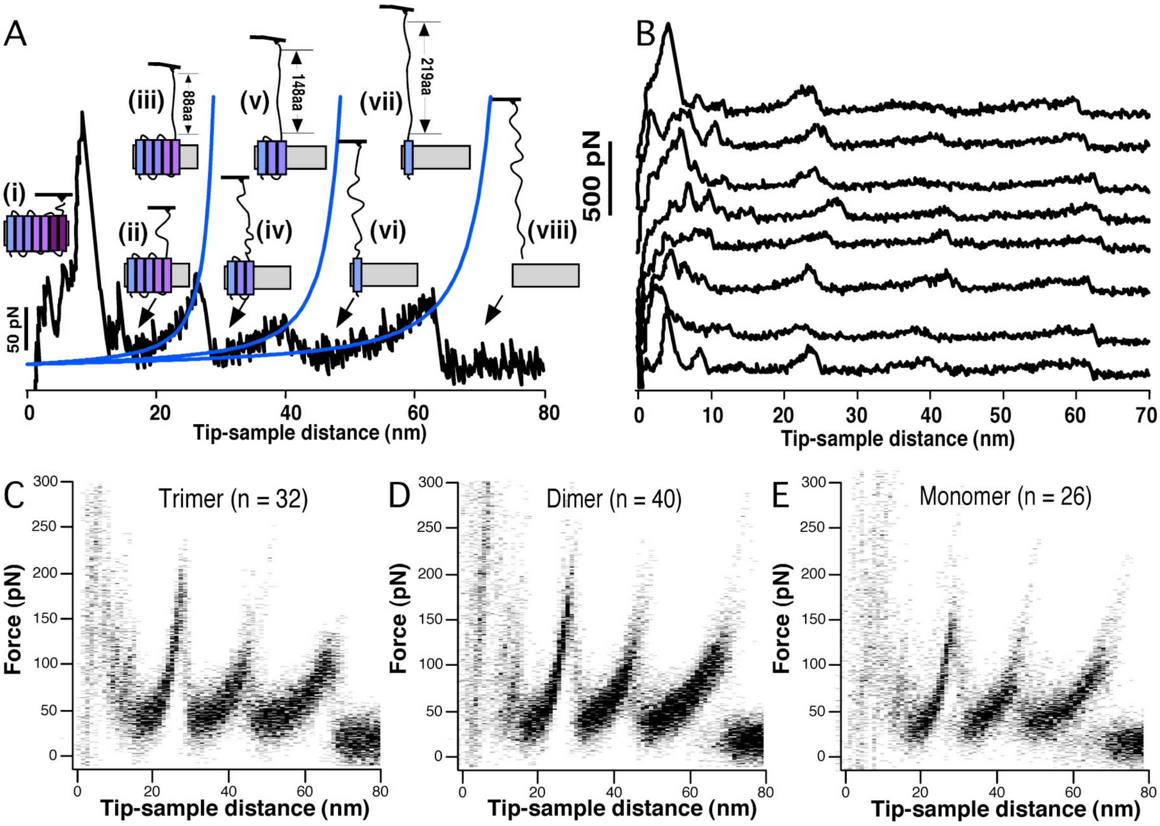

Figure 3.8 Unfolding pathways of BR trimer, dimer and monomer

(**A**) The spectrum shows a representative pairwise unfolding pathway of a single BR dimer molecule. The schematic drawings show the unfolding pathways at different positions as unfolding proceeds. Blue curves represent WLC fits to individual force peaks. (**B**) Individual force spectrum of single BR dimer molecules. Superimpositions show a common unfolding pattern for trimeric BR (**C**), dimeric BR (**D**), and monomeric BR (**E**). The width (spread) of the single peaks is determined by the experimental noise and by standard deviations of these peaks from their average values (**Figure 3.8** and **Table 1**).

3.3.3 Unfolding pathways do not depend on BR assembly

Figure 3.8(**C-E**) shows superimpositions of typical F-D traces obtained on unfolding single BR molecules. Superimposition of unfolding traces highlights the common unfolding pattern through the accumulation of measured data points (densely plotted areas) and at the same time conserves the individualism of single unfolding events (less densely plotted areas). All single-molecule F-D traces from trimeric (**Figure 3.8**(**C**)), dimeric (**Figure 3.8**(**D**)), and monomeric (**Figure 3.8**(**E**)) BR assemblies showed three peaks at amino acid positions 88 (helices E & D), 148 (helices B & C) and 220 (helix A). I call these three as main peaks since they occurred with a probability of 100% (Janovjak et al., 2004; Müller et al., 2002b). Apart from the main unfolding peaks, some F-D curves of all BR assemblies exhibited side peaks at polypeptide lengths of 94, 105, 158, 175 and 232 amino acids (**Figure 3.9**).

Side peaks occurred with lower probabilities, ranging between 10 and 60%. Curves where the main peaks occurred without side peaks denote the pairwise unfolding of helices and their connecting loops. F-D curves which showed both main peak and side peaks occurring simultaneously are attributed to the stepwise unfolding of single helices, the connecting loops or of fragments hereof (Janovjak et al., 2003; Müller et al., 2002b). Thus, the secondary structures of the protein can unfold either in a collective process such as observed by the pairwise unfolding of transmembrane α-helices (see above) or in a stepwise manner. Each of these partially unfolded structures during unfolding denotes an intermediate in the unfolding pathway. The similar contour lengths of the unfolded polypeptide chains of single BR molecules as signified by the peaks in segments of F-D curves (**Figure 3.9**) show that these molecules from different oligomeric assemblies unfold via the same pathways.

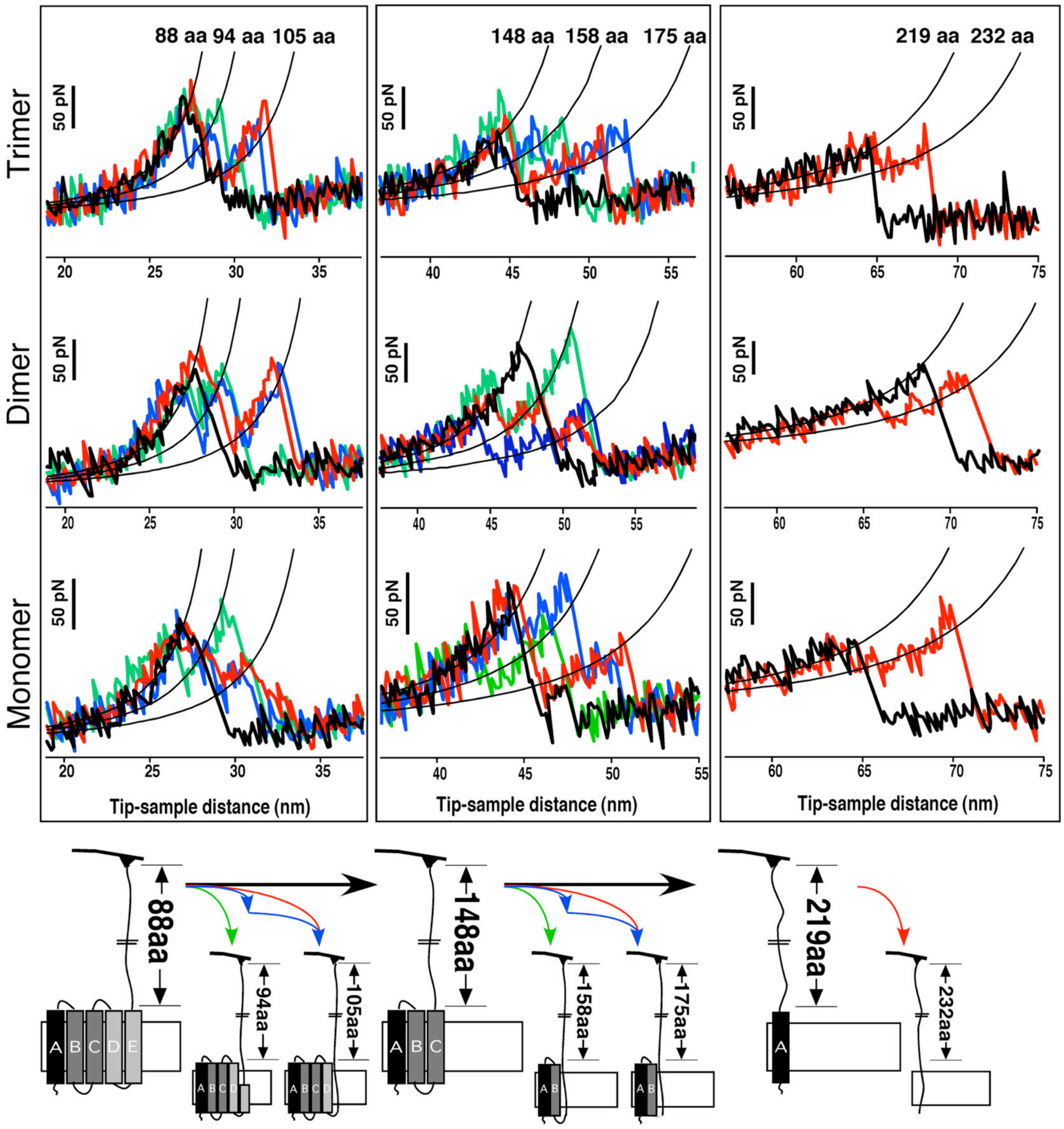

Figure 3.9 Similar unfolding pathways of trimeric, dimeric and monomeric BR

Each horizontal row shows the unfolding pathways of individual secondary structure elements for trimer, dimer and monomer. Black smooth curves represent average WLC fits of force peaks. Single peaks deviate from the average values within the standard deviation (SD) (**Table 3.1**). Occasionally, the first unfolding peak at 88 aa shows two shoulder peaks (first column), indicating the stepwise unfolding of the helical pair. If both shoulders occur, the peak at 88 aa indicates the unfolding of helix E, that at 94 of loop DE, and the peak at 105 corresponds to the unfolding of helix D. The shoulder peaks of the second major peak at 148 aa indicate the stepwise unfolding of helices C and B and loop BC. The peak at 148 aa indicates the unfolding of helix C, that at 158 of loop BC, and the peak at 175 aa represents unfolding of helix B. The unfolding scheme via the different pathways is shown at the bottom. The arrows indicate the observed unfolding pathways. In certain pathways (black arrows), a pair of transmembrane helices and their connecting loop unfolded in a single step. In other unfolding pathways (coloured arrows), these structural elements unfolded in several intermediate steps. The colour code of the F-D curves corresponds to that of the arrows in the pathways shown below. In the given probabilities, average forces and contour lengths of unfolded polypeptides (**Figures 3.10** and **3.11**, **Table 3.1**), an individual unfolding curve can show deviations from the one represented here.

3.3.4 Single BR molecules from different assemblies unfold at different forces

The magnitude of unfolding forces of each main and each side peak observed for BR assembled into monomeric, dimeric and trimeric forms is shown in **Figure 3.10**.

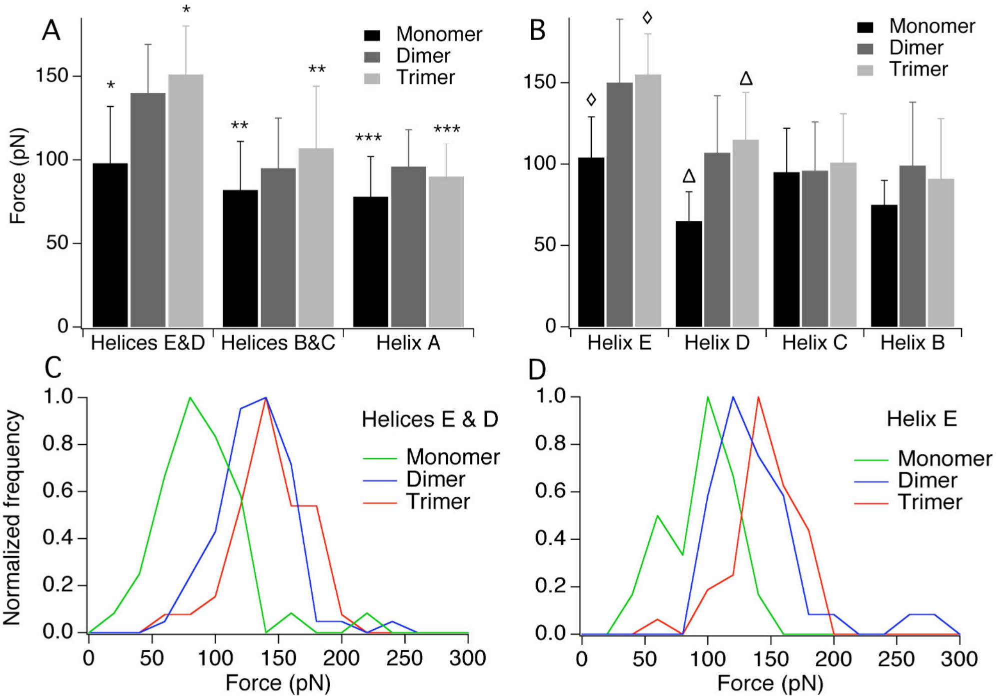

Figure 3.10 Unfolding forces of secondary structure elements in trimeric, dimeric and monomeric BR

(**A**) Category plot showing the forces for the pairwise unfolding of transmembrane α-helices E & D (88 aa), B & C (148 aa) and of helix A (219 aa). (*) $p < 0.0001$, (**) $p = 0.0003$, (***) $p = 0.01$ (one-way ANOVA followed by Bonferroni's post-test). For helices E & D, $p < 0.0001$ comparing monomer with dimer and trimer respectively, and $p = 0.2$ on dimer-trimer comparison. For helices B & C, $p = 0.0003$ on monomer-trimer comparison, $p = 0.1$ comparing dimer with trimer and monomer respectively. For helix A, $p = 0.01$ for trimer-monomer, $p = 0.08$ for dimer-trimer, and $p < 0.0001$ for dimer-monomer comparisons. (**B**) Except for single α-helices E and D, the unfolding forces for single helices were similar for all three BR types. (◊) $p < 0.0001$, (Δ) $p = 0.0032$. Error bars are the standard deviations. (**C**) & (**D**) are normalized histograms of unfolding forces of helices E & D, and single helix E, respectively, showing a clear peak shift towards higher unfolding forces from monomer to dimer to trimer. $n = 77$ (monomer), $n = 176$ (dimer) and $n = 124$ (trimer).

For all three BR oligomers, the most noticeable change in unfolding force was observed for the grouped unfolding of helices E & D (**Figure 3.10**(**A**), **Table 3.1**). For unfolding a single BR molecule out of a trimer, the average unfolding force of the helical pair E & D (151 pN, $n = 39$), was larger than that for helices B & C (107 pN, $n = 51$), and for the unfolding of helix A including N-terminal (90 pN, $n = 103$). A similar trend was observed for unfolding a BR molecule from the BR dimer. The unfolding force of paired helices E & D (140 pN, $n = 74$) was higher than that for helices B & C (95 pN, $n = 66$) and for helix A (96 pN, $n = 171$). The pattern was observed again for unfolding of BR monomer. Forces to unfold the helical pair E & D (98 pN, *n* = 43) were above those required to unfold helices B & C (82 pN, *n* = 54) and helix A (with N-terminus) (78 pN, *n* = 65).

Helices unfolded	Average unfolding force ± SD (pN)			Occurrence ± error (%)			Average contour length ± SD (aa)		
	Trimer [a]	*Dimer* [b]	*Monomer* [c]	*Trimer*	*Dimer*	*Monomer*	*Trimer*	*Dimer*	*Monomer*
E $^{\Diamond}$	155 ± 25	150 ± 39	104 ± 25	33 ± 4	22 ± 3	22 ± 5	106 ± 9	108 ± 10	105 ± 5
D $^{\Delta}$	115 ± 29	107 ± 35	65 ± 18	51 ± 5	40 ± 4	30 ± 5	146 ± 4	144 ± 5	146 ± 5
E & D *	151 ± 29	140 ± 29	98 ± 34	32 ± 4	42 ± 4	56 ± 6	-	-	-
C	101 ± 30	96 ± 30	95 ± 27	36 ± 4	34 ± 4	16 ± 4	159 ± 2	152 ± 3	159 ± 3
B	91 ± 37	99 ± 39	75 ± 15	32 ± 4	39 ± 4	20 ± 5	216 ± 7	211 ± 6	217 ± 7
B & C **	107 ± 37	95 ± 30	82 ± 29	41 ± 4	38 ± 4	70 ± 5	-	-	-
C & loop BC	99 ± 30	98 ± 28	93 ± 34	23 ± 4	29 ± 3	14 ± 4	170 ± 4	164 ± 4	173 ± 3
loop BC & B	100 ± 50	120 ± 56	103 ± 33	27 ± 4	24 ± 3	10 ± 4	216 ± 7	211 ± 6	217 ± 7
loop BC	117 ± 35	94 ± 29	85 ± 17	9 ± 3	10 ± 2	5 ± 3	-	-	-
A (N terminal) ***	90 ± 20	96 ± 22	78 ± 24	83 ± 3	97 ± 1	84 ± 4	Molecule extracted from the membrane (248 aa)		

Table 3.1 Unfolding forces, contour lengths and occurrence probabilities of stable structural segments unfolding in a pairwise or stepwise manner

Within the same BR assembly (trimer, dimer and monomer), forces for pairwise unfolding of helices E & D are higher than for pairwise unfolding of helices B & C and helix A (and N terminal). (for BR trimer, $p < 0.0001$ on comparing unfolding of helices E & D with helices B & C and helix A respectively, $p = 0.0005$ comparing helices B & C with helix A; for BR dimer, $p < 0.0001$ comparing helices E & D with helices B & C and helix A respectively, $p = 1$ for helices B & C with helix A comparison; for BR monomer, $p = 0.02$ on comparing helices E & D with helices B & C, $p = 0.003$ comparing helices E & D with helix A, $p = 1$ comparing helices B & C with helix A). *, **, ***, $^{\Diamond}$, $^{\Delta}$ denote the same as given in legend of **Figure 3.10**.

The average unfolding forces (**Figure 3.10**(**A**), **Table 3.1**) suggested that the unfolding force for the paired helices E & D was the highest for BR trimer (151 pN), decreased for dimer (140 pN), and was the least for monomer (98 pN). Similarly, the force for unfolding of helices B & C in a pairwise manner dropped from trimeric (107 pN) to monomeric (82 pN) BR assembly. In agreement with the above observations the grouped unfolding force of helix A and its N-terminal end was higher for the trimeric assembly (90 pN) than for the monomer (78 pN). As observed previously (Müller et al., 2002b), the rupture forces of helical pairs decreased with the number of structural elements that have been unfolded before. **Figure 3.10**(**B**) and **Table 3.1** show the magnitude of unfolding forces of each side peak for all BR types. The unfolding forces for individual secondary structure elements in the different BR assemblies were approximately the same.

3.3.5 Unfolding probability via a certain trajectory depends on BR assembly

The fact that the unfolding pathways of BR molecules from different assemblies do not change implies that BR unfolding through the various unfolding trajectories in the energy landscape always involves the same stable intermediates. Since unfolding of a protein molecule is a highly stochastic process, it is of crucial importance to determine if the occurrence frequency of these intermediates changes for the different oligomeric forms. Any change in the probability of occurrence of the unfolding intermediates would signify an altered energetics of the unfolding process for that BR assembly as compared to the native trimeric form.

As shown in **Figure 3.11**, the probability of occurrence of different unfolding pathways depended on the BR assemblies. Of all three BR assemblies the probability of transmembrane helices to unfold in a pairwise manner was the highest for monomeric BR. For pairwise unfolding of helices E & D and helices B & C, the probability increased from trimer to monomer. The probability for unfolding of helical pair E & D was 32% (*n* = 39) for trimeric BR, 4% (*n* = 74) for dimeric BR and 56% (*n* = 43) for monomeric BR. In the same order the probability for pairwise unfolding of helices B & C increased from BR trimer, 41% (*n* = 51), to BR monomer, 70% (*n* = 54).

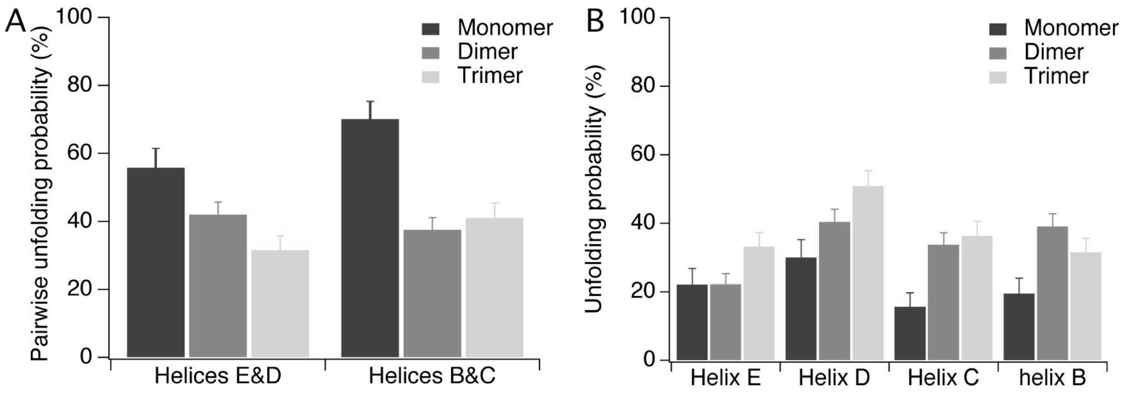

Figure 3.11 Probability of unfolding pathways

(**A**) Probability of pairwise unfolding of helices increased from trimer to monomer. (**B**) Probability of secondary structure elements being unfolded individually followed a reverse trend. Error bars show the absolute errors. The number of unfolding curves analyzed were *n* = 77 (monomer), *n* = 176 (dimer) and *n* = 124 (trimer).

3.4 DISCUSSION

3.4.1 Unfolding pathways remain the same but their probability depends on BR assembly

All BR assemblies investigated showed similar subsets of F-D curves recorded upon unfolding single molecules (**Figures 3.8** and **3.9**). This indicates that the BR molecules could choose among identical unfolding pathways. However, the probability of a BR molecule to choose one individual unfolding pathway from the various unfolding pathways strongly depended on its assembly. From the probability histogram in **Figure 3.11**, it can be concluded that oligomerization of BR supports unfolding of structural segments individually, while unfolding in BR monomer occurs predominantly in a pairwise fashion. A similar trend was observed on unfolding single BR molecules from the trimeric assembly at temperatures ranging from 8 °C - 52 °C (Janovjak et al., 2003). While at low temperatures the single helices and loops exhibited an enhanced probability to unfold in single events, their probability to unfold groupwise increased with temperature. Since temperature like force serves as a denaturant (Brouillette et al., 1989; Jackson and Sturtevant, 1978) it can be conveniently assumed that in both cases the reduction of mechanical stability supports pathways with groupwise unfolding of structural segments. A consequential argument could be that the reduced mechanical stability in the two cases represents minimal interhelical interactions, a state similar to the initial states of membrane protein folding as proposed in the ‘two-stage model’ (Popot and Engelman, 1990). Since in the initial stages of folding the helices are paired and still not a complete part of the whole molecule, in the forced unfolding experiments the predominant pairwise unfolding of helices at high temperature and from the monomeric assembly might imply a mimicking of these initial stages of membrane protein folding.

Furthermore, these results strongly suggest that unfolding pathways of BR depend on whether the membrane proteins are unfolded from their trimer, dimeric or monomeric assembly. Considering that not only the oligomeric state but also the lipid environment of the BR establishes the overall system, which guides the membrane protein to populate certain unfolding pathways, important conclusions may be drawn for unfolding experiments in general. In most unfolding experiments of membrane proteins the protein is removed from the membrane by detergent (Booth et al., 2001b). Albeit, being functional in detergent it can be assumed here that the altered environment of the membrane protein may change the population of certain unfolding pathways in these experiments. The same can be concluded if the oligomeric state of the solubilized membrane protein unfolded is not the native one. Thus, to prevent the characterization of unfolding pathways a membrane protein would not necessarily take *in vivo,* with mechanical, chemical or thermal unfolding experiments, unfolding experiments should be performed in the native or at least in the native-like environment of the membrane protein.

3.4.2 Location of stable structural segments is independent of BR assembly

F-D curves of BR unfolding from monomeric, dimeric and trimeric assemblies exhibited force peaks at identical positions (**Figure 3.9**). This suggests that a change in the oligomeric state and of the lateral assembly of the BR oligomers within the membrane do not influence the position of the unfolding barriers. Thus, it can be concluded that in these measurements intermolecular interactions occurring between proteins or between proteins and lipids did not change the location of structural segments that stabilize the protein and establish the unfolding barriers. Considering that the tertiary structure of BR did not change significantly upon oligomerization (Brouillette et al., 1989; Michel et al., 1980) it may be concluded that the stable segments and the secondary structures may be somehow related (Cisneros et al., 2005). Currently it is difficult to understand how they are linked to each other since some of the stable structural segments can bridge two or more secondary structures while in some cases they only stabilize one third of a helix (Cisneros et al., 2005; Müller et al., 2002b).

3.4.3 Membrane protein assembly changes stability of structural segments

Unfolding of BR from three different oligomeric assemblies allows to conclude that BR assembled in a trimeric arrangement is mechanically more stable than BR assembled in dimeric or monomeric forms as suggested by the forces required to unfold paired or single secondary structure elements (**Table 3.1**). In apparent contrast, size and location of structural segments establishing the unfolding barriers within the membrane are the same as observed for the native trimeric assembly. Thus, it can be suggested that BR molecules do not establish new unfolding barriers by introducing new interactions or deleting old interactions within or between molecules in their monomeric or dimeric assemblies, but that interactions establishing these barriers are strengthened by the increasing complexity of the assembly.

It is important to mention here that changing the membrane protein assembly of BR is associated with changing the lipids directly attached to the protein. Thus, the lipid environment mainly determines whether the BR molecules form monomeric, dimeric or trimeric arrangements. Possible contributions of lipids should be therefore considered when investigating the influence of different BR oligomeric states on the unfolding barriers. Structural investigations suggest that lipid molecules stabilize BR trimers by specific interactions of their head group moieties (Essen et al., 1998; Grigorieff et al., 1996). Since the exact lipid environment and arrangement of the BR assemblies investigated here are not resolved yet, I exclude these considerations.

3.4.4 Deciphering contributions of inter- and intramolecular interactions

As tabulated in **Table 3.1** the forces required to unfold individual secondary structure elements vary depending on the BR assembly. Except for individual helices E and D, for which the unfolding force decreased significantly from trimer to monomer, unfolding of the corresponding individual secondary structure elements occurred at slightly decreasing forces (**Figure 3.10**). It is intriguing that inspite the differences in BR assemblies almost the same forces are required to unfold helices C, B and A individually. This similarity can be attributed to the unaltered intramolecular interactions which may dominate these secondary structure elements against destabilizing or stabilizing factors from the environment. This leads to an important conclusion. Besides the change in assembly, a possible reason for decreased unfolding forces in monomeric BR could be a change in the internal structure of the BR molecule. The similar forces of individual helices suggest that, in any case, this change is caused by an alteration in the long range or intermolecular interactions, thus making unwinding of the helices from the monomer easier.

The analyses of the experimental data allow insights into the complex contributions of inter- and intramolecular interactions to the overall stability of a structural segment. Due to the absence of surrounding molecules, stable structural segments established in monomeric BR are mostly the result of intramolecular interactions. As mentioned in the previous sections, oligomerization of BR can significantly contribute to its stability. Simple subtraction of forces allows to determine the contribution of intermolecular interactions that enhance the mechanical stability of structural segments that stabilize secondary structure elements. E.g., trimerization of BR contributes ~50 pN to the stability of helix E and ~25 pN to loop BC. Division of the absolute unfolding force values from two oligomeric assemblies allows calculation of the percentage of increasing stability due to intermolecular interactions.

3.4.5 Can the results from single-molecule measurements correlated to chemical and thermal denaturation experiments?

Conventional unfolding of BR by chemical or thermal denaturation have shown that lipids (Dracheva et al., 1996; Mukhopadhyay et al., 1996), detergents (Huang et al., 1980; Michel et al., 1980), electrolytes (Mukhopadhyay et al., 1996; Sternberg et al., 1992), could have strong influences on BR assembly, stability and function. It was also shown that monomeric BR unfolds at lower temperatures compared to trimeric BR. The denaturational transition at ~100^0 C of BR trimer as measured by differential scanning calorimetry exhibited an enthalpy change of 100 kcal/mol (Brouillette et al., 1987; Jackson and Sturtevant, 1978; Kahn et al., 1992). Monomeric BR in detergent is denatured with a nearly identical enthalpy change (95 kcal/mol), although at a lower temperature of 80^0 C (Brouillette et al., 1989). This suggests that trimeric BR is marginally more stable and has a higher activation energy of transition as compared to monomeric BR. The possible reasons for this behavior could be trimer formation of BR and hence more favourable energetics of association between trimers in the lattice. Pairwise unfolding forces of helices E & D and helices B & C are higher for BR trimer than for dimer and monomer. The probability for pairwise unfolding of these helices, on the other hand, is lowest for BR assembled into a trimer. Though a comparison of conventional (bulk measurements) and forced unfolding experiments is not relevant, it can be suggested based on these data that the higher stability of trimeric and dimeric BR as compared to monomeric BR is due to stronger monomer-monomer and monomer-lipid interactions leading to higher intrinsic stability of the two systems.

3.5 FUNCTIONAL IMPLICATIONS AND OUTLOOK

As suggested by the lower unfolding force and higher probability, the unfolding pathway of a monomer existing independently in the membrane is energetically and kinetically more favorable than in a trimeric assembly. Stabilization of monomers is hence achieved by trimer formation and arrangement into a crystal lattice structure for its efficient function as a proton pump. The long life cycle of this molecule is a guarantee for photosynthetic growth in nature over a period of months under intense sunshine without photochemical destabilization. Nevertheless the unfolding data presented here suggest that the BR monomer is a structurally stable biological unit, which also occurs in some halobacterial species as the functional unit (Otomo et al., 1992). Thus it seems that in *H.*

salinarum the lattice formation of the purple membrane serves a purpose of functional stabilization, which may or may not be due to structural stabilization, whereas in other strains intramolecular forces may provide this stabilization. It will be interesting to test this hypothesis by force spectroscopy experiments with the Mexican or Australian halobacterial strains mex, port or shark (Otomo et al., 1992).

3.6 CONCLUSIONS

Using SMFS I characterized the inter- and intramolecular interactions stabilizing individual structural segments of single BR molecules assembled into trimers, dimers and monomers. While the assembly of BR did not vary the location of these structural segments, their intrinsic stability could change up to 70% increasing from monomer to dimer to trimer. Since each stable structural segment established one unfolding barrier, I conclude that the locations of unfolding barriers were determined by intramolecular interactions, but their strengths were strongly influenced by intermolecular interactions. Subtracting molecular interactions established in the BR trimer from that of monomer allowed to calculate the contribution of inter- and intramolecular interactions to the membrane protein stabilization. Statistical analyses showed that the unfolding pathways of differently assembled BR molecules did not differ in their appearance but in their population. This suggests that the membrane protein assembly does not necessarily change the location of unfolding barriers within the protein, but certainly their strength, and thus shifts the probability of a protein to choose certain unfolding pathways. Recently, an independent study using molecular dynamic simulations has corroborated the results presented here (Seeber et al., 2006).

Chapter

4

UNRAVELING MOLECULAR INTERACTIONS THAT STABILIZE NATIVE BOVINE RHODOPSIN

4.1 BACKGROUND & SCOPE

GPCRs constitute by far the largest family of cell surface receptors that provide molecular links between extracellular signals and intracellular processes (Bockaert et al., 2002; Gether and Kobilka, 1998; Lefkowitz, 1998). Hundreds of GPCRs found in tissues throughout the human body respond to a range of sensory, chemotactic, hormonal and neuronal signals, and couple these to internal signal transduction systems via heterotrimeric guanylate nucleotide-binding proteins (**G proteins**). All GPCRs share a common architecture of a seven TM α-helical domain linked together by loops on the extracellular and the cytoplasmic surfaces. The external signal acts on the extracellular side of these molecules and causes them to undergo a conformational change on the intracellular surface of the receptor, mediated through the transmembrane domain, resulting in the binding and activation of several hundreds of G protein molecules by a universal mechanism (Bhandawat et al., 2005; Heck and Hofmann, 2001). The GPCR superfamily[26] modulates an extremely wide range of physiological processes, and mutations in the genes encoding these receptors have been implicated in numerous diseases. It, thus, comes as no surprise that these receptors form the largest class of therapeutic targets (Dahl and Sylte, 2005). GPCRs share highly conserved residues (80-100%), such as the D(E)RY and NPXXY motifs and a stabilizing Cys-Cys disulfide bond, that play important functional roles. GPCRs can exist either as homo- or hetero-oligomers, thereby increasing their functional variability (Breitwieser, 2004; Milligan and Bouvier, 2005; Park et al., 2004; Park and Palczewski, 2005; Salahpour et al., 2000).

---

[26] The GPCR superfamily encompasses ~950 genes in the human genome, which translates into >600 non-sensory and 1000s of sensory GPCRs (Mirzadegan et al., 2003; Takeda et al., 2002).

4.1.1 Rhodopsin

One of the most widely studied GPCRs is rhodopsin (**Figure 4.1**), the light receptor that initiates phototransduction in the rod outer segments (**ROS**) of the retinal rod cells (photoreceptor cells) present in the eye. On the basis of the predicted structure, conservation of few amino acids in the region critical for G protein activation, and activation by small ligand, rhodopsin belongs to GPCRs family A – the largest subfamily of GPCRs[27] (Mirzadegan et al., 2003). The overall topology of rhodopsin is similar to bacteriorhodopsin (Ovchinnikov Yu, 1982). Rhodopsin, having a molecular mass of 42,002 Da, is composed of a seven TM[28] apoprotein, opsin, with a polypeptide chain of 348 amino acids, and a chromophore, 11-*cis*-retinal, covalently bound via a protonated Schiff base to Lys296 in helix VII (Filipek et al., 2003a). The counter ion for the protonated Schiff base, Glu113 in helix III, is highly conserved among all known vertebrate visual pigments (Mirzadegan et al., 2003). Absorption of a photon causes the photoisomerization of 11-*cis*-retinylidene to all-*trans*-retinylidene triggering conformational changes in the opsin from its inactive to active conformation[29]. This is accompanied by conformational changes in the protein that result in a binding site on its cytoplasmic surface for its cognate G protein, transducin (**Gt**) (Hamm, 2001; Meng and Bourne, 2001). Once activated, the α-subunit of Gt activates a phosphodiesterase that converts cyclic-GMP to GMP. Ion channels gated by cyclic-GMP then close, leading to a hyperpolarized cell that can initiate a nerve signal from the retina to the brain. A variety of biophysical and chemical techniques including AFM, transmission electron microscopy, chemical cross-linking, SDS-polyacrylamide gel electrophoresis and proteolysis experiments have shown that rhodopsin consists mainly of dimers and higher oligomers in disc membranes (Fotiadis et al., 2003; Jastrzebska et al., 2004; Medina et al., 2004; Suda et al., 2004).

---

[27] Mammalian GPCRs are usually grouped by amino acid sequence similarities into three distinct families – A, B, and C (Lefkowitz, 2004; Pierce et al., 2002).

[28] The helices differ on the level of irregularities and are tilted at various angles with respect to the expected membrane surface (Teller et al., 2001).

[29] Bovine rhodopsin in the inactive state has a λ_{max}= 500 nm which shifts to 465 nm when the *cis*-retinal converts to all-*trans*-retinal. The activation happens through multiple intermediates, such as photorhodopsin, bathorhodopsin, lumirhodopsin, Meta I, Meta II and Meta III, before the chromophore hydrolyzes and leaves the binding pocket (Okada et al., 2001; Palczewski, 2006).

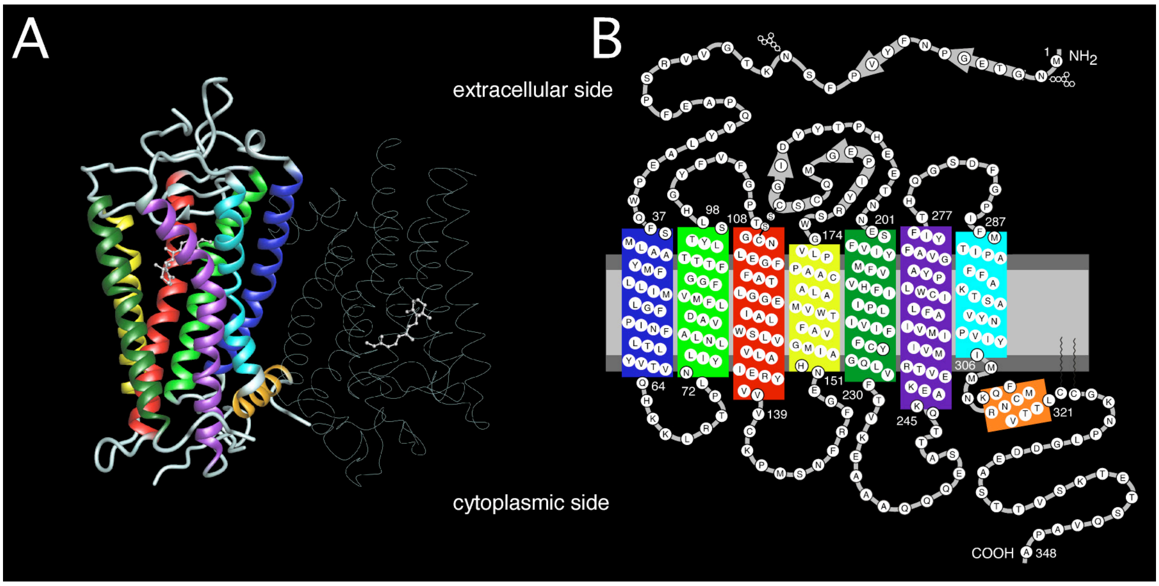

Figure 4.1 Structure of bovine rhodopsin

(**A**) 3D structure of bovine rhodopsin at 2.8 Å resolution (PDB: 1F88) (Palczewski et al., 2000) showing the dimeric assembly of rhodopsin. The dimer in the crystal structure cannot be physiologically relevant since one monomer is rotated by ~160° in relation to the second. The molecule shown in ball and stick is the retinal chromophore. (**B**) Secondary structure of rhodopsin showing the amino acid sequence. The N-terminal end is on the extracellular side and the C-terminal end on the cytoplasmic side. Helix I is colored dark blue to the extreme left and helix 8 is colored orange anchored to the lipid bilayer on the cytoplasmic side. The arrows in the beginning of the N-terminus and in the extracellular loop between helix IV (yellow) and helix V (dark green) represent the structured β-sheet regions.

The specific localization of rhodopsin in the internal discs of the ROS, its high expression level in the retina (constituting >90% of all proteins in disc membranes), and the lack of other highly abundant membrane proteins have facilitated studies in this system with a number of biochemical, biophysical and molecular biological methods that cannot be carried out with any other GPCR system (Filipek et al., 2003a). Since the elucidation of its X-ray crystal structure[30], rhodopsin has served as a structural basis and template for studying and understanding this family of receptors and the signaling systems that they regulate (Filipek et al., 2003b; Ridge et al., 2003).

A number of diseases are associated with mutations that cause destabilization and misfolding of GPCRs (Dryja and Li, 1995). Understanding the molecular interactions that stabilize or destabilize GPCRs is therefore fundamental to our understanding of their function. However, little is known about the underlying molecular mechanisms. The majority of these types of mutations in rhodopsin lead to the neurodegenerative disease

---

[30] Bovine rhodopsin is currently the only GPCR for which a crystal structure has been solved (Li et al., 2004a; Okada et al., 2004; Palczewski et al., 2000; Teller et al., 2001).

retinitis pigmentosa[31] (Liu et al., 1996b; Rader et al., 2004). Most mutations target the TM and extracellular domains of rhodopsin (Mirzadegan et al., 2003) and induce misfolding by the replacement of the conserved Cys110-Cys187 disulfide (**S-S**) bond with an abnormal disulfide bond Cys185-Cys187 or Cys110-Cys185 (Hwa et al., 2001; Hwa et al., 1999). Mass spectrometry studies have shown the importance of the Cys110-Cys187 disulfide bridge and its implication in the maintenance of the structural and functional stability of rhodopsin. These studies also reported the presence of the abnormal disulfide bond Cys185-Cys187 in misfolded *retinitis pigmentosa* mutants in the TM domain (Hwa et al., 2001). The rhodopsin structure has provided opportunities to identify regions critical for proper folding by computational approaches (Jacobs et al., 2001; Rader et al., 2004). The extracellular domain, which is also the folding core of rhodopsin, is tightly coupled functionally and structurally to the TM domain of the molecule (Rader et al., 2004). This has led to the hypothesis that rhodopsin folding involves long-range interactions apart from inter-helical interactions (Klein-Seetharaman, 2005). However, insights into the molecular interactions that stabilize and destabilize the protein in native membranes are currently limited due to the lack of experimental approaches that allow for direct measurements of those interactions.

Here, I describe the characterization of molecular interactions established within rhodopsin embedded in native ROS disc membranes from bovine retina. These interactions could be mapped onto the rhodopsin structure clearly resolving the stable structural segments. The map showed the highly conserved residues among GPCRs (Mirzadegan et al., 2003) to be located at the interior of these stable structural segments in rhodopsin. In absence of the stabilizing Cys110-Cys187 bond, the molecular interactions establishing structural segments changed their strengths and locations. Such changes may build a molecular mechanism of protein destabilization, misfolding and malfunction.

---

[31] About 0.05% of the global population is affected by this disease leading to photoreceptor degradation and loss of vision (Rattner et al., 1999).

4.2 EXPERIMENTAL PROCEDURES

4.2.1 Preparation of ROS disc membranes

Though I did the ROS disc membranes prep a couple of times myself for some experiments, the disc membranes were mainly prepared and provided by Dr. Paul S.-H. Park (Palczewski laboratory, Case Western Reserve University, Ohio, USA). All experimental procedures were carried out under dim red light. Centrifugation steps were performed at 4°C. ROS discs were purified from fresh bovine retinas (Papermaster, 1982) and stored at –80 °C. To obtain the disc membranes, ROS membranes were resuspended using a glass hand-held homogenizer in 13 ml of buffer A (2 mM Tris-HCl, pH 7.4) and incubated overnight at 4 °C. The membrane suspension was centrifuged at 26,500×g for 30 min. The membranes were washed twice with 13 ml of buffer A and three times with 3 ml of buffer B (2 mM Tris-HCl, 150 mM NaCl, 2mM EDTA, pH 7.4). Membranes were collected each time by centrifugation at 26,500×g for 30 min. The membranes were then resuspended in buffer A and used for SMFS and AFM imaging. Alternatively, membranes were resuspended in buffer C (67 mM potassium phosphate, 1 mM magnesium acetate, 0.1 mM EDTA, 1 mM DTT, 18% sucrose, pH 7.0) and stored at –80 °C. Membranes stored in buffer C were washed twice with buffer A or nanopure water prior to SMFS studies.

For cleavage experiments, ROS membrane sample was prepared by Dr. Paul S.-H. Park (Case Western Reserve University, USA). 2 mg/ml of ROS membranes were resuspended in Ringer's buffer (10 mM Hepes, 130 mM NaCl, 3.6 mM KCl, 2.4 mM $MgCl_2$, 1.2 mM $CaCl_2$, 0.02 mM EDTA, pH 7.4) and treated with endoproteinase Glu-C (Roche Applied Science, Indianapolis, IN, USA) at a substrate to enzyme ratio of 10:1 (w/w). Membranes were digested with the enzyme for 2 h at room temperature and 1.5 h on ice. The reaction was terminated by washing membranes three times with Ringer's buffer containing 5 mM benzamidine (1 ml) and one time with buffer A (1 ml). Membranes were resuspended in buffer A for SMFS studies. For solubilization of rhodopsin, ROS membranes were resuspended in 20 mM BTP, 150 mM NaCl, 1% *n*-dodecyl-*β*-D-maltoside, pH 7.4. The membrane suspension was shaken at room temperature for 10 min and then centrifuged to remove insoluble material at 164,000×g for 30 min. Protein concentration was determined using the Bradford Protein Assay Kit from Bio-Rad Laboratories (Hercules, CA, USA).

4.2.2 Attaching a single rhodopsin molecule to the AFM cantilever tip

As in the case of bacteriorhodopsin unfolding, rhodopsin was attached nonspecifically to Si_3N_4 cantilever by applying a contact force of ~1 nN for ~1 s between the AFM tip and the membrane surface (Cisneros et al., 2005; Kedrov et al., 2004; Möller et al., 2003; Müller et al., 2002b).

4.2.3 Imaging and single-molecule force spectroscopy

All AFM imaging and force spectroscopy were performed in a completely dark room, and sample preparation was carried out under dim red light (Fotiadis et al., 2003; Fotiadis et al., 2004). 50 μl of disc membrane stock solution (0.5 mg/ml) was diluted in 500 μl deionized water and centrifuged at 13,200 rpm for 5 mins. The supernatant was discarded and pellet resuspended in 500 μl deionized water and centrifuged once again at 13,200 rpm for 5 mins. In the final step, the pellet was resuspended in 500 μl deionized water and stored in fridge at 4 ^{o}C and used for not more than 1 week. 10-20 μl of this sample was adsorbed directly onto freshly cleaved mica surface and incubated for ~15 mins (Liang et al., 2003). The mica surface was then rinsed 6-7 times with ~40 μl buffer D (150 mM KCl, 25 mM $MgCl_2$, 20 mM Tris, pH 7.8) to remove the unadsorbed membrane discs.

Rhodopsin constitutes > 90% of the proteins found in the disc membranes (Filipek et al., 2003a). The periphery of the disc contains relatively high levels of peripherin, which are proteins involved in maintaining the regular stacking of the discs (Molday et al., 1987). To avoid complications in the interpretation of the data, force spectroscopy was restricted to the interior regions of the discs where rhodopsin is the predominant protein species. For force measurements, the AFM tip was approached to the rhodopsin surface while applying a constant force of ~1 nN. After a contact time of ~1 s, the tip was retracted from membrane surface at a constant velocity of 300 nm/s. In about 38% of cases one or more adhesion peaks were detected. All experiments were performed in buffer D at room temperature 24 ± 1 ^{o}C. This buffer was supplemented with either DTT (100 mM) or NEM (50 mM or 100 mM) in studies involving those reagents. Data were indistinguishable for studies performed in the presence of either 50 mM or 100 mM NEM. Although the red laser on the AFM promoted minimal bleaching of rhodopsin, force curves were collected over a period of ≤ 1h. ROS membranes solubilized in *n*-

dodecyl-β-D-maltoside were bleached less than 5% after incubation under the AFM laser for 1 h.

To rule out statistical errors due to deviations in the cantilever spring constant, SMFS experiments were performed on each rhodopsin sample using ~100 different cantilevers from different batches. Also, the experiments were performed using two different AFM equipments, viz., Picoforce (dI-Veeco, USA) and Multimode (dI-Veeco, USA). Experiments on the Multimode were performed by Dr. Paul S.-H. Park (Case Western Reserve University, USA). F-D curves obtained from the two instruments were analyzed separately. The unfolding forces measured in the two cases agreed within < 20% and that of WLC fits were the same. Spring constants of the 200 μm long silicon nitride AFM cantilevers (NPS, Veeco Metrology; nominal spring constant ~0.08 N/m) were calibrated in buffer solution using equipartition theorem (Butt and Jaschke, 1995; Florin et al., 1995). All cantilevers exhibited similar spring constants within ~10% uncertainty of the calibration method. The large number of cantilevers was also necessary due to the extremely fast contamination of the AFM cantilever during the experiments thus necessitating their frequent replacement.

4.2.4 Selection of force-distance curves and data analyses

As for bacteriorhodopsin, in the first step F-D curves were exported to Igor Pro software (Wavemetrics, Inc., Oregon, USA) and separated manually based on their lengths. Following this procedure I was able to group the curves into two classes based on length: one class had a length of ~65 nm and the other ~95 nm. Of the total curves collected, 11% belonged to the ~65 nm length class and 4% to the ~95 nm length class (n = 670). The length selection helped in the classification of curves from rhodopsin molecules with an intact native S-S bond (Cys110-Cys187, ~65 nm, **S-S intact curves**) and an absent native S-S bond (~95 nm, **S-S broken curves**). Functional rhodopsin requires a conserved disulfide bond between Cys110 and Cys187 for proper folding and stability of the receptor (Davidson et al., 1994; Karnik and Khorana, 1990; Karnik et al., 1988). An intact S-S bond will shorten the effective length of the protein in F-D curves to ~65 nm due to the extraction/ unfolding of the helical hairpin constituted by helices III and IV. A fully extended rhodopsin polypeptide chain without the Cys110-Cys187 bond is however expected to produce F-D curves that are ~95 nm in length. The length of F-D curves for the two most frequently observed classes of curves are consistent with the unfolding of rhodopsin in the presence and absence of the conserved Cys110-Cys187 disulfide bond. F-D curves exhibiting an overall length of ~65 nm (or ~95 nm) reflect completely unfolded and extended rhodopsin molecules attached with their N-terminal end to the AFM tip (Müller et al., 2002b; Oesterhelt et al., 2000)[32].

As explained in details in **section 3.2.5**, a good fraction of curves have smaller lengths due to attachment of the AFM tip to one of the loops or detachment of the molecule from the tip during unfolding. To ensure that the F-D curves were from rhodopsin with an intact S-S bond, which adhered to the AFM tip by its termini and not by one of its loops, as the first step of my analyses I selected only force curves with a length of ~65 nm and discarded the shorter curves (< 65 nm)[33]. All F-D curves exhibiting similar overall unfolding spectra and lengths were selected and aligned using identical procedures and criteria established previously (Müller et al., 2002b). Due to the long termini of rhodopsin (N-terminus is 35 amino acids long and C-terminus 40 amino acids), it is difficult to assign the first unfolding peak in the F-D curve to a structural segment in the secondary structure since the tip could attach at any amino acid along the length of the terminus. Thus a suitable criterion is to determine the relative distances of the peaks with respect to a peak in the centre or the last peak. I used the peak at amino acid position 108 and the last peak to align the F-D curves. Each peak of every force curve was fitted with the WLC model with a persistence length of 0.4 nm and a monomer length of 0.36 nm (Rief et al., 1997a). The number of extended amino acids at each peak was then calculated using the contour length obtained from the WLC fits. This allowed the assignment of unfolding events to structural segments of rhodopsin and to locate molecular interactions established in the protein as also described for bacteriorhodopsin (Müller et al., 2002b) (**section 3.3.2**). Individual F-D curves showed variations between each other (**Figure 4.3(B)).** More than 100 F-D curves were collected in multiple experiments using different cantilevers of the same type to obtain statistically significant results.

---

[32] This conclusion could only be made after analyzing and comparing the F-D curves from the enzymatically digested rhodopsin sample, where the third cytoplasmic loop C-III was cleaved, with those from the uncleaved sample.

[33] Some of the shorter curves were used for further analysis later to determine the sidedness of rhodopsin pulling, i.e., N- or C-terminal (**section 4.3.3**).

To measure the unfolding force and probability of unfolding for each individual structural segment, every event of each curve was analyzed. Statistical analyses showed that each unfolding pattern exhibited a certain probability to occur (**Table 4.1**). The frequency of occurrence of each structural segment provides an estimate of whether a single rhodopsin molecule will select a certain intermediate during unfolding or not. The combination of intermediates taken during unfolding defines the unfolding pathway of the molecule.

As mentioned above the molecule could detach from the AFM tip during unfolding. Therefore, for the cleavage experiments with endoproteinase Glu-C it was important to be certain that the ≤ 40 nm length F-D curves were mainly from the N-terminal fragment of the molecule and not from the detached molecule. To get a comparative statistics for the cleavage experiments, I estimated the percentage of curves showing the same molecular unfolding pattern (peaks at aa 19, 26, 37 and 97, 108, 123) due to the detachment of the molecule from the total number of curves obtained from the uncleaved native rhodopsin sample, and compared it to the fraction of curves obtained from the enzymatically treated sample. Of the total curves obtained, the fraction of short curves (≤ 40 nm) obtained was 23% in the case of untreated sample and 55% for the digested sample, whereas the fraction of ~65 nm and ~95 nm long curves decreased to 2% in the enzymatically treated sample. The F-D curves from the digested molecules, therefore, were mainly due to the truncated C-III loop and not due to the detachment of the molecule.

4.2.5 Assigning the stable structural segments in rhodopsin

The unfolding curve of a single rhodopsin can be interpreted in the following manner. Separation of the AFM tip from the surface of the sample results in the unraveling of the polypeptide chain until this process is opposed by molecular interactions within the protein. These molecular interactions that constitute the so-called unfolding barriers are a result of a small segment, a complete, or a group of secondary structure elements. The first structural segment established an unfolding barrier beginning at amino acid 19 and required an average unfolding force of 131 pN. This force provides a direct measure of the strength of molecular interactions that stabilizes this structural segment. When the externally applied force exceeds the stability of the structural segment all residues in that segment unfold cooperatively[34]. This increases the length of the unfolded polypeptide chain bridging the AFM tip and the sample surface, keeping the other secondary structure elements of the protein folded in the membrane. Further separation of the tip stretches the unfolded protein until the unfolding barrier of the subsequent structural segment is detected. The beginning of such an unfolding barrier can be determined within an accuracy of 2-8 amino acids by fitting the force peaks with the WLC model (**Table 4.1**). The number of residues contributing to a structural segment is determined by the distance between the first amino acid of the unfolding barrier and that of the forthcoming one. Thus, the first structural segment of rhodopsin was established between amino acids 20 and 26 of the N-terminal region. In this manner all stable structural segments were mapped onto the secondary structure model of rhodopsin (**Figure 4.3**(**D**), **section 4.3.4**).

4.3 RESULTS

4.3.1 Imaging native ROS disc membranes

Prior to SMFS studies, native ROS disc membranes containing rhodopsin were imaged in buffer D by AFM (**Figure 4.2**).

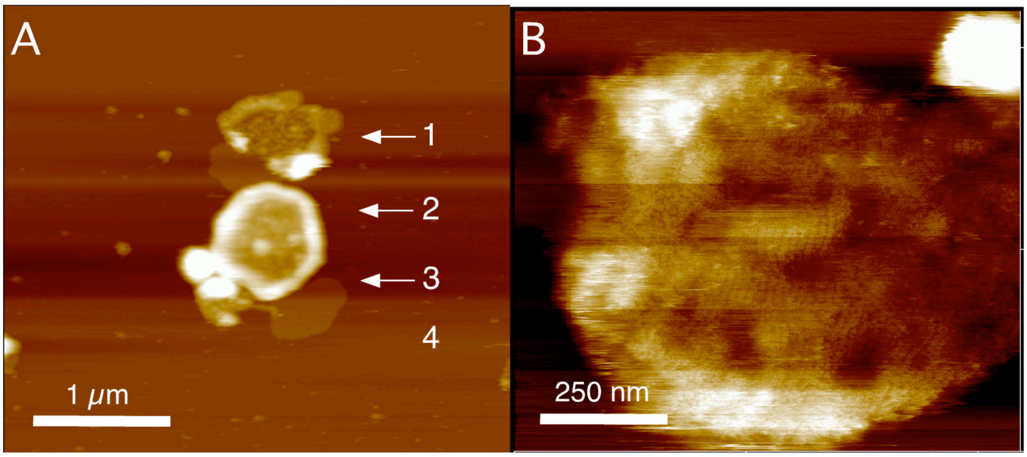

Figure 4.2 AFM imaging of native ROS disc membranes

(**A**) Overview showing a typical ensemble in ROS disc membrane preparations adsorbed onto mica (4). Arrow 1 points at a single layered protein membrane, arrow 2 at a double-layered intact ROS disc, and arrow 3 points at a co-isolated lipid bilayer containing no proteins. The topograph is displayed in full gray scale corresponding to a vertical height of 20 nm. (**B**) A topograph showing the arrangement of rhodopsin molecules as dimeric arrays (Fotiadis et al., 2003).

---

[34] The cooperative unfolding of a structural segment depends on the unfolding speed. It is common to see a structural segment unfolding in multiple steps at higher speeds than at lower speeds (Janovjak et al., 2004).

In most cases, burst disc membranes adsorbed to mica resulting in single-layered protein membranes (arrow 1), exhibiting an average height of 8.2 ± 0.9 nm (*n* = 61). Co-isolated lipid bilayers had an average thickness of 4.0 ± 0.6 nm (*n* = 24).

4.3.2 Mechanical unfolding of single native rhodopsin molecules

A single rhodopsin molecule was attached to the AFM tip via a polypeptide loop or terminal end by bringing the tip in close contact with the surface of a single-layered disc membrane and applying a contact force of ~1 nN for ~1 s (Janovjak et al., 2005; Müller et al., 2002b). The attached terminal of rhodopsin could then be used as a molecular bridge to exert a mechanical pulling force to unfold the protein. The two classes of F-D curves observed most frequently exhibited a length of ~65 nm (S-S intact) (**Figure 4.3**) and ~95 nm (S-S broken) (**Figure 4.5**). To further confirm the nature of rhodopsin molecules from which the F-D curves were obtained, I calculated the ratio between the two classes of curves. In buffer, without dithiothreitol (**DTT**) or *N*-ethylmaleimide (**NEM**), the ratio between S-S intact and S-S broken was 2:1 (*n* = 274). The presence and absence of the disulfide bond is supported by the change in this ratio when F-D curves were obtained in the presence of either DTT or NEM. The ratio of S-S intact and S-S broken curves in the presence of DTT was 1:2 (*n* = 180) and in the presence of NEM was 7:1 (*n* = 139).

DTT and NEM most probably act during the unfolding of rhodopsin since the residues modified by these reagents are buried in the membrane and not accessible in the native structure of the protein (Palczewski et al., 2000). DTT most likely disrupts the Cys110-Cys187 bond in rhodopsin during unfolding, thereby increasing the number of curves that exhibit a length of ~95 nm. NEM causes the acetylation of Cys 185 thus blocking it and preventing the rearrangement reaction during unfolding (**Figure 4.7**) (Hwa et al., 2001). This is manifested as an increase in the number of curves with length ~65 nm.

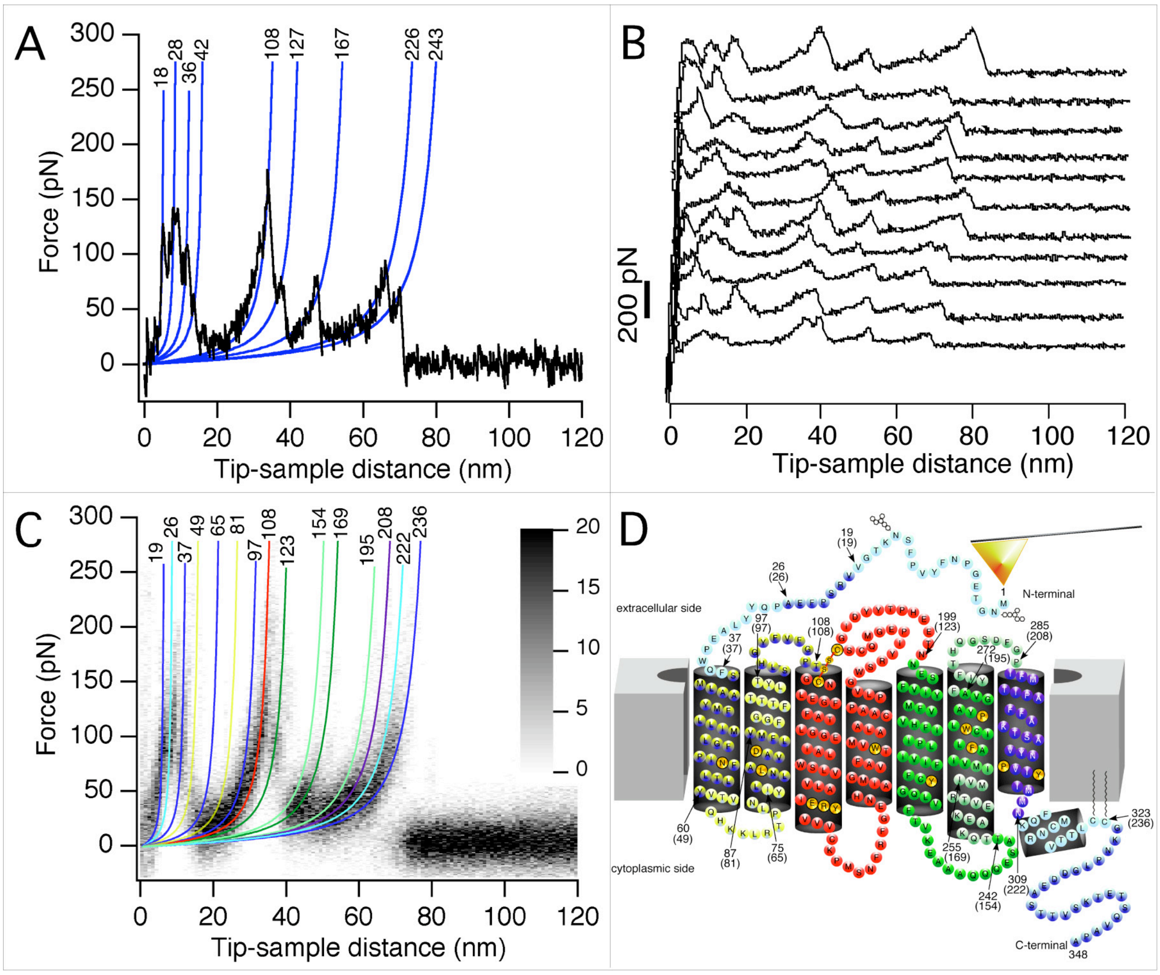

Figure 4.3 Single-molecule force spectroscopy curves recorded on native ROS disc membranes

(**A**) A representative F-D curve of length ~65 nm corresponding to the unfolding of a single rhodopsin molecule with an intact Cys110-Cys187 bond. The values obtained from the WLC model (blue lines) are shown at the end of each fit and denote the unfolded length of the polypeptide segment in amino acids. (**B)** A selection of F-D curves recorded under identical experimental conditions. A comparison of the force curves reveals that some force peaks occur in the majority of curves (main peaks) and some occur in only a small fraction of curves (minor peaks) (**Table 4.1**). Force curves exhibiting the same major and minor force peaks indicate that rhodopsin molecules unfolded taking the same pathways. (**C)** The superimposition of several force curves (*n* = 42) enhanced common features among the curves. Major (black) and minor peaks (grey shaded) were fitted using the WLC model as above. (**D)** Secondary structure of rhodopsin mapped with structural segments that constitute the unfolding barriers in SMFS. Arrows locate the starting and end of each structural segment. Numbers in brackets are the amino acid values obtained from WLC fitting, and numbers without brackets are the corresponding residue numbers in the rhodopsin sequence. Equally colored WLC fits of force peaks (**C**) and structural segments correlate to each other. Highly conserved residues are highlighted in gold.

The characteristic sequence of force peaks in an unfolding spectrum describes a unique unfolding pathway followed by a rhodopsin molecule in the unfolding energy landscape. Statistical analyses help to calculate the frequency with which a rhodopsin molecule selects a particular unfolding pathway. The superimposition of many F-D curves following different unfolding pathways enhances the most frequently occurring unfolding events (**Figure 4.3**(**C**)), while the rarely occurring single events are masked by the noise. The cluster of force peaks in the superimposition were fitted using the WLC model, which correlated well with the averages obtained from fitting each peak in individual curves (**Table 4.1**). The values obtained from fitting the peaks with the WLC model were then mapped onto the secondary structure of rhodopsin (**Figure 4.3**(**D**)) to demarcate the structural segments that establish molecular interactions strong enough to be detected in the experiments.

4.3.3 Unfolding rhodopsin from the N-terminal end

To interpret the results obtained from SMFS experiments and map the molecular interactions on the 3-D structure of the protein it is very important to know the side from which the membrane protein is being pulled, i.e., does the molecule attach to the AFM tip at the C- or N-terminal end. This is not a trivial problem since disc membranes can potentially adsorb onto mica exposing either the N- or the C-terminus of rhodopsin. To determine if the protein molecules were pulled from the extracellular or the cytoplasmic side of the membranes, a strategy involving the enzymatic digestion of ROS membranes with endoproteinase Glu-C from *Staphylococcus aureus* V8 was used. Controlled digestion by endoproteinase Glu-C leads to specific cleavage of the third cytoplasmic loop C-III at residue E239 and the C-terminal at residue E341 leading to the formation of three fragments (**Figures 4.4**(**A**) and (**B**)) (Findlay et al., 1981; Palczewski et al., 1991). Depending on the side from which digested rhodopsin is being pulled the F-D curves would be different. If pulled from the extracellular side (N-terminal), the F-D curves would show only one pattern with curves of shorter lengths, and if pulled from the cytoplasmic side (C-terminal), the F-D curves would show three different populations[35] (Kedrov et al., 2004). The SMFS data confirmed that the curves exhibited only an interaction range of ≤ 40 nm, which corresponds to the stretching of 124 amino acids from the N-terminal fragment of rhodopsin (**Figure 4.4**(**C**)). A single pattern was observed that exhibited two sets of triple peaks, one at amino acid positions 19, 26, and 36, and the other at amino acids 97, 108, and 123. Within the same extension range this characteristic pattern was also observed for the unfolding of undigested rhodopsin from the terminus of the molecule (**Figure 4.3**(**C**), **Table 4.1**). Taken together, these results suggest that the F-D curves from both digested and undigested rhodopsin preparations originate from attachment of the AFM tip to the N-terminus of rhodopsin. The conditions used to prepare samples on mica therefore appear to favor the adsorption of disc membranes exposing the extracellular surface of rhodopsin.

---

[35] Cleaving the third cytoplasmic loop results in the creation of two extra ends both of which could adsorb non-specifically to the tip.

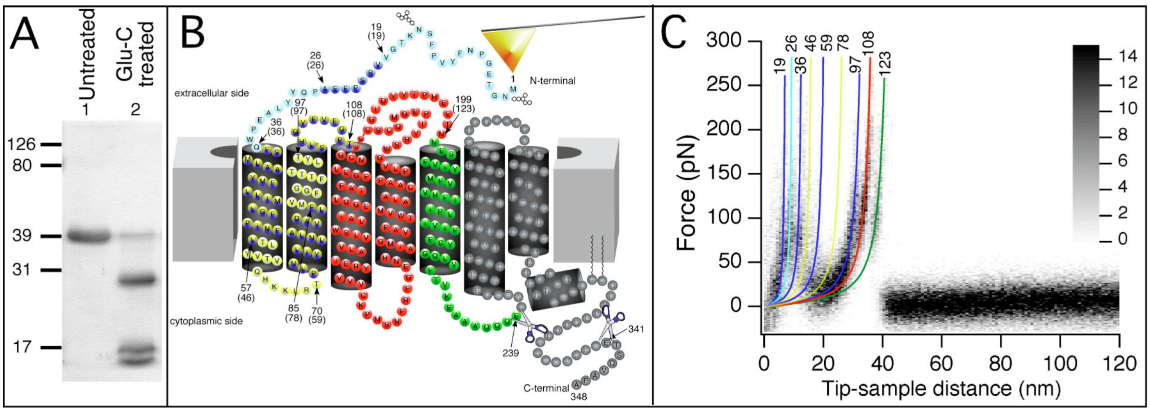

Figure 4.4 Unfolding rhodopsin after enzymatic cleavage by endoproteinase Glu-C confirms the N-terminal unfolding of rhodopsin

(**A**) Silver stained SDS-PAGE gel showing intact (lane 1) and enzymatically cleaved (lane 2) rhodopsin. **(B)** Schematic model of rhodopsin after cleavage. The C-terminal end, and the loop C-3 connecting transmembrane α-helices V and VI have been truncated. (**C**) F-D curves recorded from the cleaved rhodopsin showed the two characteristic triple peaks at amino acid positions 19, 26, and 36, and at 97, 108, and 123. These peaks were also observed with intact rhodopsin (**Figure 4.3**). Beyond amino acid 123 no peaks were observed which agreed with the Glu-C digestion pattern of rhodopsin.

4.3.4 Mapping the stable structural segments in dark state native rhodopsin

In **section 4.2.3**, I described the procedure used to assign the stable structural segments and the strength of their stabilizing molecular interactions (unfolding force for that segment) in native rhodopsin unfolded in the dark state. A secondary structure element could establish a stable structural segment in many ways. While some secondary structure elements established a stable structural segment independently, in other cases a secondary structure element hosted two or more structural segments. Also, a group of secondary structure elements or parts of two different structure elements could constitute one stable structural segment. The polypeptide segments forming the structural segments, the unfolding force and the occurrence probability of each stable structural segment are given in **Table 4.1**.

Secondary structure [a]	Structural segment [b]	Polypeptide segment (aa) [c]			Average contour length ± SD (aa)			Average unfolding force ± SD (pN)			Occurrence ± error (%)		
		Native	C3	S≠S	Native	C3	S≠S	Native	C3	S≠S	Native	C3	S≠S
N terminal region	**N1**	20-26	20-26	20-26	19±2	19±2	19±2	131±38	112±47	133±44	57±4	55±7	49±5
N terminal region	**N2**	27-37	27-36	27-35	26±2	26±2	26±3	139±38	112±44	146±48	65±3	63±7	59±5
Helix I	**H1**	38-60	37-57	36-57	37±3	36±3	35±3	132±46	126±67	136±45	62±4	65±7	61±5
Loop C-I	**C1**	61-75	58-70	58-75	49±5	46±4	46±4	117±47	126±55	130±44	22±3	43±7	39±5
Helix II	**H2.1**	76-87	71-85	76-87	65±5	59±5	64±5	96±34	92±41	92±47	14±3	41±7	20±4
Helix II	**H2.2**	88-97	86-97	88-97	81±4	78±8	82±3	89±34	69±27	62±7	12±2	24±6	7±3
Loop E-I	**E1**	98-108	98-108	98-108	97±4	97±3	97±3	106±38	124±31	106±33	63±4	76±6	60±5
Helices III & IV, loops C-II & E-II	**H3, H4, C2, E2**		109-199	----		109±2	----	158±53	169±42	----	100	100	----
Helix III	**H3**		----	109-133		----	108±2	----	----	157±55	----	----	100
Loop C-II & helix IV	**C2, H4**		----	134-170		----	123±4	----	----	135±55	----	----	66±5
Loop E-II	**E2.1**	----	----	171-181	----	----	159±3	----	----	96±32	----	----	10±3
Loop E-II	**E2.2**	----	----	182-199	----	----	169±5	----	-----	77±28	----	----	29±5
Helix V	**H5**	----	----	200-229	----	----	199±6	----	----	103±29	----	----	63±5
Helix V & loop C-III	**H5, C3**	200-242	200-239	----	123±5	123±4	----	136±45	162±56	----	78±3	71±6	-----
Loop C-III & Helix VI	**C3, H6.1**	----	----	230-255	----	----	219±6	----	----	97±50	----	----	24±5
Helix VI	**H6.1**	243-255	----	----	154±4	----	----	85±34	----	----	9±2	----	----
Helix VI	**H6.2**	256-272	----	256-272	169±6	----	243±6	81±34	----	84±30	68±3	----	44±5
Loop E-III	**E3**	273-285	----		195±5	----	----	79±32	----	----	16±3	----	----
Loop E-III & helix VII	**E3, H7**	----	----	273-308	----	----	262±6	----	----	85±42	----	----	15±4
Helix VII	**H7**	286-309	----		208±3	----	----	99±40	----	----	25±3	----	----
Helix 8	**H8**	310-323	----	309-323	222±6	----	296±8	104±44	----	112±39	76±3	----	78±4
C terminal region	**CT**	324-348	----	324-348	236±6	----	314±8	109±47	----	105±44	61±4	----	40±5

Table 4.1 Stability, location and occurrence of structural segments

[a] Secondary structure(s) contributing to the stable structural segment. [b] Name of each stable structural segment. [c] Polypeptides that establish a structural segment. Native – rhodopsin with Cys110-Cys187, C3 – loop C-III cleaved, S≠S – Cys110-Cys187 bond missing.

4.3.5 Unfolding rhodopsin in absence of the structurally stabilizing native Cys110-Cys187 bond

To determine the difference between S-S intact (~65 nm) and S-S broken (~95 nm) curves, which correspond to the unfolding of rhodopsin molecules without the stabilizing Cys110-Cys187 bond, I analyzed F-D curves exhibiting a length of ~95 nm (**Figure 4.5**). While the force peaks at a separation < 40 nm, i.e., till the S-S bond, essentially remained at the same positions as observed for intact rhodopsin, they were clearly different at higher separations. A procedure similar to that of S-S intact curves was followed to assign the stable structural segments for S-S broken curves. Assignment of the stable structural segments showed that the structural domain stabilized by the disulfide bridge consisted of four structural segments. In absence of the Cys110-Cys187 bond, the structural segment held together by the S-S bond could be unfolded in individual steps. In contrast to Cys110-Cys187 intact rhodopsin, helix V established a single stable segment, and loop C-III, which formed a stable structural segment with helix V in Cys110-Cys187 intact rhodopsin, now established a segment together with the cytoplasmic part of helix VI. Thus, these secondary structures were stabilized by significantly different structural regions and forces compared to Cys110-Cys187 intact rhodopsin. The stable structural segment established within the extracellular region of helix VI was not influenced by the Cys110-Cys187 disulfide bond and remained at the same position. In absence of the stabilizing S-S bond, the extracellular loop E-III established a stable structural segment together with the entire helix VII. The stable structural segment formed by helix 8 did not depend on the Cys110-Csy187 bond, and maintained its location. The same was observed for the C-terminal region, which did not change position or stability of its segments (**Figures 4.3**(**D**) and **4.5**(**D**), **Table 4.1**).

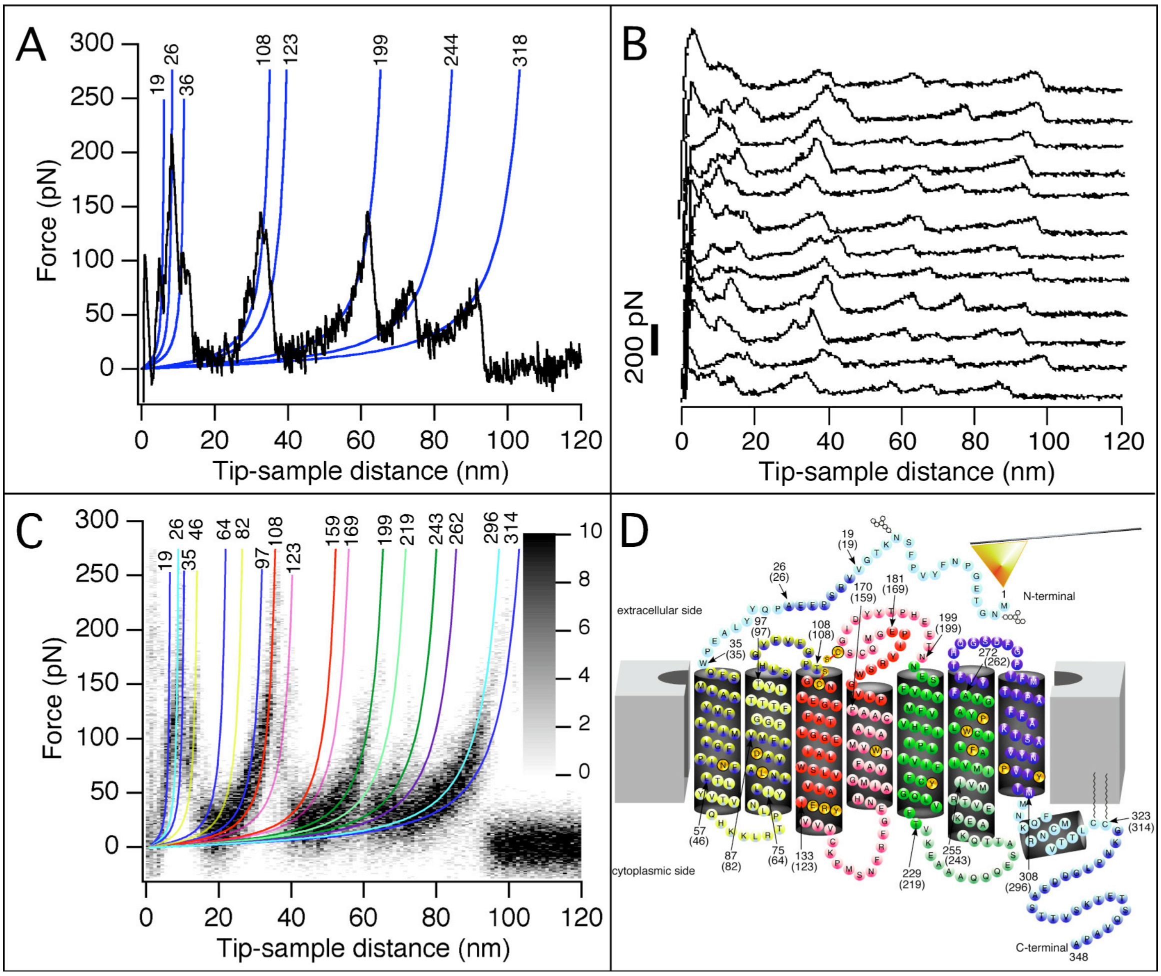

Figure 4.5 Detecting molecular interactions within rhodopsin in absence of the stabilizing Cys110-Cys187 bond

(**A**) A representative F-D curve with a length of ~95 nm corresponds to the unfolding of a rhodopsin molecule in absence of the Cys110-Cys187 disulfide bond. The values obtained from the WLC model (blue lines) are shown at the end of each fit. (**B**) A selection of F-D curves recorded under identical experimental conditions. A comparison of the force curves reveals that some force peaks occur in the majority of curves (main peaks) and some occur in only a small fraction of curves (minor peaks). Force curves exhibiting the same major and minor force peaks indicate that rhodopsin molecules unfolded taking the same pathways. (**C**) The superimposition of several F-D curves (*n* = 25) enhanced the common features among the curves. Major (black) and minor peaks (grey shaded) were fitted using the WLC model as above. The analysis of force curves reveals the strengths and locations of molecular interactions established within rhodopsin (**D** and **Table 4.1**). (**D**) Secondary structure of rhodopsin mapped with stable structural segments observed by SMFS. Arrows locate the starting and end of each structural segment. Numbers in brackets are the amino acid values obtained from WLC fitting and the numbers without brackets are the corresponding residue number in the rhodopsin sequence. Equally colored WLC fits of force peaks (**C**) and structural segments correlate to each other. Highly conserved residues are highlighted in gold.

4.4 DISCUSSION

The unfolding pathways of rhodopsin from native ROS disc membranes as detected by SMFS reveals stable structural segments that stabilize rhodopsin. These unfolding barriers can then be mapped onto the 3-D structure of rhodopsin (**Figure 4.6**). The variety of unfolding patterns highlight a complex unfolding pathway of the rhodopsin molecule with each force peak representing an unfolding intermediate in the unfolding pathway.

Here I discuss the possible reasons for observing these barriers and their origin during unfolding of rhodopsin.

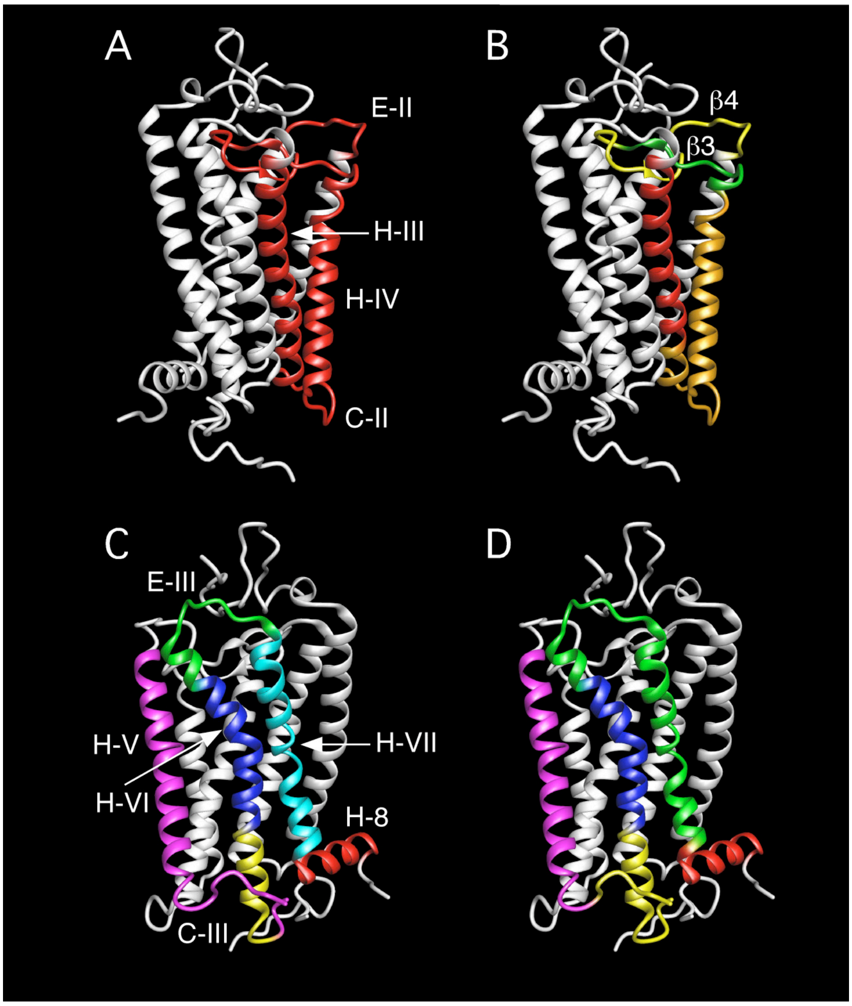

Figure 4.6 Stable structural segments mapped onto the tertiary structure of rhodopsin

Each panel highlights only a subset of structural segments indicated by different coloring. Retinal is not shown. (**A**) and (**C**) show stable structural segments in presence of the native Cys110-Cys187 disulfide bond, whereas (**B**) and (**D**) in absence of the Cys110-Cys187 disulfide bond. The stable structural segment H3, H4, C2, E2, constituted by H-III, H-IV, C-II and E-II (red), unfolds together as a helical hairpin in presence of the native Cys110-Cys187 disulfide bond (**A**). In (**B**) is shown the same stable structural segment being unfolded in steps as H-III (red), C-II & H-IV (orange), β3 (green) and β4 (yellow) in absence of the Cys110-Cys187 disulfide bond. H-V, which unfolds with cytoplasmic loop C-III (pink) in presence of the disulfide bond (**C**), unfolds individually in absence of the disulfide bond (pink) (**D**). Similarly H-VII (cyan) forms an individual stable structural segment in presence of the Cys110-Cys187 bond (**C**), whereas it unfolds with the extracellular loop E-III (green) in the absence of this disulfide bridge.

4.4.1 Molecular interactions in the N-terminal region and transmembrane helix I

The N-terminal region establishes two stable structural segments (N1 and N2) with sufficiently strong molecular interactions providing a barrier against mechanical unfolding. It is interesting to note that the unfolding forces for each of the two structural segments reached values required to unfold transmembrane helices (**Table 4.1**). No other membrane protein studied so far by SMFS showed a comparably stable region within one of its terminal regions (Cisneros et al., 2005; Kedrov et al., 2004; Möller et al., 2003; Müller et al., 2002b). A possible reason for this could be the β-hairpin structure (β1 and β2) in the N-terminal region (amino acids: **aa** 22-25, 28-32) (Filipek et al., 2003a). Additionally, it may be due to the fact that the N-terminal region and polypeptide loops of the extracellular surface associate to form a compact structure which forms a structural "lid" or "plug" that holds the retinal chromophore in place (Bourne and Meng, 2000; Palczewski et al., 2000). The formation of these surface structures is important for proper folding and assembly of the receptor (Anukanth and Khorana, 1994; Doi et al., 1990). The unfolding spectra show that transmembrane helix I mainly unfolded in one single step (H1).

4.4.2 Unfolding of helices I and II with extracellular loop C-I: Proof of 'third stage' of membrane protein folding

Molecular interactions that stabilize the subsequent structural segment (aa 61-75) bridge two secondary structures - loop C-I and short cytoplasmic regions of helices I and II (C1). In the 'three-stage hypothesis' of membrane protein folding it has been suggested that stabilizing interactions between helices via loops could be established during the third step of folding (**section 1.3.2**) (Engelman et al., 2003; Klein-Seetharaman, 2005). It has also been proposed that during folding of rhodopsin and like GPCRs long-range interactions might play an equally important role as inter-helical interactions, thus making rhodopsin folding a cooperative process unlike that of bacterial membrane proteins like bacteriorhodopsin (Klein-Seetharaman, 2005). The unification of transmembrane helices I and II to form a stable segment suggests that the peptide loop connecting the two secondary structures likely pulls and holds them together into the functional structure. This may be a general feature for all loops of rhodopsin since all the structural segments constituted by the loops contain some part of a transmembrane helix (**Figure 4.6**).

4.4.3 Origin of two stable structural segments in transmembrane helix II

Two structural segments were detected after the short cytoplasmic region of helix II unfolded together with loop C-I. The first was a short structural segment (aa 76–87, H2.1) with the highly conserved residues Leu79 and Asp83 centered in this structural segment.

Stability simulations on rhodopsin unfolding suggest that the region around Asp83 establishes interactions leading to enhanced stability, which might be implicated in rhodopsin folding (Rader et al., 2004). The last structural segment of helix II (aa 88-97, H2.2) includes the kink inducing Gly-Gly sequence at positions 89 and 90, which causes an enhanced flexibility of helix II (Palczewski et al., 2000).

4.4.4 Stability of extracellular loop E-I

The stable structural segment established by loop E-I covers the entire loop up to the Cys110-Cys187 bond (E1). Extracellular loop stability is functionally important since it establishes together with the N-terminal region a compact structure that forms a “plug” for the retinal chromophore. The Cys110-Cys187 disulfide bridge is an important part of this “plug”. It has been suggested the extracellular region forms the core of rhodopsin folding (Rader et al., 2004). Any mutation in this region disturbs the seven transmembrane domain of the molecule resulting in misfolding of rhodopsin and causing diseases like *retinitis pigmentosa* (Hwa et al., 2001).

4.4.5 Extracting the helical hairpin structure held together by the native Cys110-Csy187 bond

In native rhodopsin the region constituted by helix III, cytoplasmic loop C-II, helix IV, and extracellular loop E-II (H3, H4, C2 and E2) could be extracted together in one step due the Cys110-Cys187 bond connected helix III and loop C-II. A force of 158 pN was required to remove this large domain from the membrane, which is significantly higher than the forces measured for the removal of any other structural segment. This enhanced stability appears to originate mostly from helix III since in the absence of the native S-S bond a structural segment formed by helix III alone still requires an unfolding force of 157 pN. Helix III runs parallel to the retinal chromophore and provides a wall for one side of the binding cavity (Palczewski et al., 2000). The maintenance of helix III structure is therefore critical and might play a large part in maintaining the cavity of the chromophore.

It should be mentioned here that the peak corresponding to this structural segment occurs in every F-D curve, i.e., the occurrence probability for this peak is 100% (**Table 4.1**). Interestingly, it appears that helices I-III and V-VII, with helix IV connected to either of the two fragments, form active rhodopsin, suggesting the existence of two independent intradomain interactions (Filipek et al., 2003a). The 100% occurrence of this structural segment (H3, H4, C2, E2) in all the unfolding pathways suggests a maximum stability for this intermediate, also reflected in the force measurements. I propose that the formation of this intermediate during the folding of rhodopsin is crucial for maintaining the structural stability of the molecule.

4.4.6 Stable structural segments of helix V and cytoplasmic loop C-III, and helix VI

Helix V and cytoplasmic loop C-III could be removed in a single step (aa 200-242, H5 and C3). Cleavage of cytoplasmic loop C-III does not significantly affect the structural integrity of rhodopsin (Palczewski et al., 1991). The similar unfolding forces of the structural segments in this region of the molecule (< 40 nm) upon cleavage by endoproteinase Glu-C as compared to the undigested molecule further support the idea that this loop does not significantly affect the structural stability of the protein. Helix VI establishes two structural segments, one by the cytoplasmic half of helix VI (aa 243-255, H6.1) and the other by the extracellular half of helix VI (aa 256-272, H6.2) of relatively low mechanical strengths. The low mechanical stability of a structural segment is an indication of the minimal interactions it maintains with the neighboring helices and lipid environment. Interestingly it has been suggested that during the activation of rhodopsin, the cytoplasmic part of helix VI undergoes a rigid body movement with respect to helix III (Farrens et al., 1996). A structural segment of low mechanical stability would be more suited for such a function than a rigid rod which requires a large input of energy to overcome the interaction hindrance of its environment. The role of helix VI in rhodopsin activation and its low mechanical stability are corroborated by the fact that helix VI is the most loosely associated with other helices in rhodopsin (Filipek et al., 2003a).

4.4.7 Extracellular loop E-III, helix VII, and cytoplasmic helix VIII establish independently stable structural segments

The fact that the extracellular loop E-III forms a stable structural segment individually (aa 273-285, E3) and resists mechanical unfolding even after complete unfolding of the other extracellular loops suggests that each extracellular loop has an intrinsic mechanical strength that contributes in the maintenance of the compact “plug” structure in the extracellular region. The entire helix VII establishes a single structural segment (aa 286-

309, H7). This segment encompasses the highly conserved residues Pro303 and Tyr306, which together with Asn302 establish the NPXXY domain of rhodopsin. The stable structural segment established entirely by helix 8 (aa 310-323, H8) is anchored by palmitoyl moieties at residues 322 and 323 to the cytoplasmic surface of the membrane. This helical structure plays an important role in the interaction with transducin (Konig et al., 1989; Wakamatsu et al., 1992), and therefore likely requires some intrinsic stability. Since the C-terminal region, which constitutes the final structural segment (aa 324-348, CT), is highly flexible and devoid of any structure it does not show any intrinsic stability. The unfolding force measured for this region could therefore be attributed to the two palmitoyl groups that anchor this region to the lipid membrane. I, however, did not check if breaking these anchors by harsh treatment with N-hydroxylamine causes this unfolding barrier to disappear.

4.4.8 Molecular interactions are altered in absence of the native disulfide bond

The native Cys110-Cys187 bond is critical for the stability and function of the receptor. The stabilizing molecular interactions in rhodopsin are altered in absence of the native S-S bond. Though the structural segments between the N-terminal region and extracellular loop E-I were not influenced by the absence of the highly conserved and stabilizing Cys110-Cys187 bond, a dramatic difference was observed in the position of structural segments that occurred after Thr108 (**Figures 4.3** and **4.5**). This may suggest that the native disulfide bond remained intact during unfolding of the structural segment until Thr108. However, in some instances after this point the formation of a non-native S-S bond between adjacent Cys185 and Cys187 in loop E-II may be favored (Kono et al., 1998). The pattern and amplitude of the peaks corresponding to structural segments N1 to E1, H8, and CT, i.e., the beginning and the end parts of the molecule, are the same for both S-S intact and S-S broken curves (**Table 4.1**). The difference in the two types of curves, therefore, occurs in the unfolding of the polypeptide connecting these two regions.

The S-S bond can not be possibly broken by the mechanical force applied during the unfolding of rhodopsin since the force required to break a covalent bond is ~2 nN (Grandbois et al., 1999), which is atleast an order of magnitude higher than the maximal force required to unfold the stable structural segments in rhodopsin. What could be the reason for F-D curves with lengths corresponding to the unfolding of rhodopsin molecules with an absent Cys110-Cys187 bond? I give here two explanations that could account for this. The first possibility is that a population of rhodopsin molecules in the disc membranes does not contain the S-S linkage. Since the occurrence of the S-S broken curves is about 2-fold less than that of the S-S intact curves, the stoichiometry between rhodopsin molecules with and without the native S-S bond would have to be 2:1 in the disc membranes. An alternative explanation involves the replacement of the native S-S bond between Cys110 and Cys187 by a non-native S-S bond linking Cys185 to Cys187. This has been observed under certain conditions (Hwa et al., 2001; Kono et al., 1998; Ridge et al., 1995b) though the exact mechanism of how this happens has not been deciphered. The unfolding of the rhodopsin molecule under force in some instances may lead to a bond rearrangement promoting a non-native S-S bridge between adjacent Cys residues 185 and 187 (**Figure 4.7**). This latter hypothesis could be supported by the effect of NEM on the unfolding of rhodopsin, where a 3.5-fold increase in the proportion of S-S intact curves was observed. NEM alkylates Cys185 thus preventing the formation of the non-native Cys185-Cys187 bond (Kono et al., 1998).

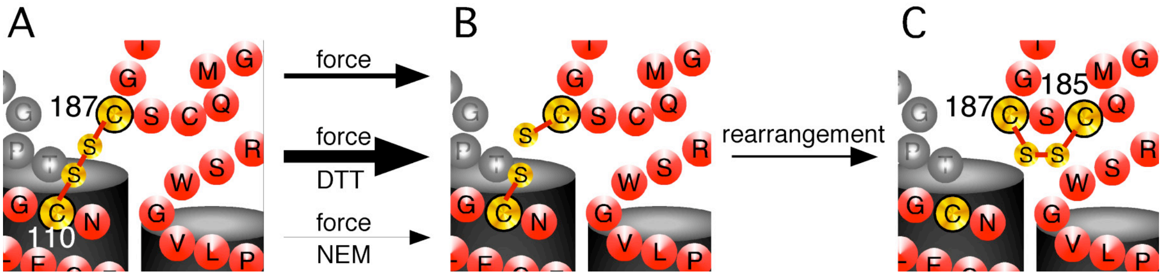

Figure 4.7 Effect of force on the native disulfide bridge during rhodopsin unfolding

(**A**) The intact disulfide bridge between Cys110 and Cys187 in native rhodopsin. It is assumed that under an external force during unfolding this bond might break to state (**B**), possibly rearranging to form a non-native disulfide bond between Cys185 and Cys187 (**C**). The ratio of the two populations represented by (**A**) & (**C**) or (**B**) shows a noticeable change when pulled in the presence of DTT and NEM. The thickness of arrows indicate the tendency of population (**A**) to convert to (**B**) and subsequently to (**C**) (thicker arrow indicates a greater tendency). Though the experiment with NEM points to a rearranged state (**C**), it is difficult to predict unambiguously the population of this state under the three conditions.

An intact disulfide bond between Cys110 and Cys187 would mask any potential structural segments formed within helices III, IV, and the connecting loops. In absence of the native S-S bond, this structural domain unfolded via various intermediates and never in a single step (**Figures 4.5**(**D**) and **4.6**). The structural segments revealed in absence of the native Cys110-Cys187 bond may also have been present in rhodopsin with the native S-S intact or may be the by-product of the release of the constraint and changed interactions between helix III and helix IV. Surprisingly, helix III established the most stable segment (aa 109-133), which unfolded at a force of 157 pN. While the beginning of this domain was near the extracellular surface, the end was determined by the D(E)RY motif which regulates rhodopsin and G protein interactions. In functional rhodopsin, the D(E)RY motif establishes salt bridges between Glu134, Glu247, and Arg135.

In absence of the native S-S bond, extracellular loop E-II could be unfolded in two steps (**Figures 4.5**(**D**) and **4.6**). The intrinsic mechanical stability of loop E-II can be attributed to the two β-sheet structures (β3 and β4) establishing stable structural segments in absence of the native S-S bond.

In presence of the Cys110-Cys187 bond, helix V establishes a stable segment together with loop C-III. In absence of the native S-S bond, helix V establishes an independent stable segment along the entire secondary structural element independent of loop C-III (**Figure 4.6**). Cytoplasmic loop C-III forms a stable structural segment together with the cytoplasmic part of helix VI, whereas cytoplasmic part of helix VI forms an independent stable structural segment in presence of the native S-S bond. The remainder of helix VI forms an independent stable segment. The extracellular loop E-III and helix VII each form independent stable structural segments in presence of the native S-S bond. In absence of this covalent bond, both secondary structures combine to form one stable structural segment. I propose that the change in the positions of stable structural segments reflects a shift in the underlying molecular interactions in the regions after Thr108 as a result of the missing native Cys110-Cys187 bridge. In contrast, the absence of this bond does not affect the structural segments containing H8 and the C-terminal region. Though it is easy to conclude from these results that these regions are not linked to the changes in molecular interactions that occur as a result of altering the Cys110-Cys187 bond, it should be bore in mind that mechanically unfolding a molecule destroys it as it is unfolded, thus removing the preceding interactions and as a result minimizing the effect of different interactions that occur simultaneously and are important in maintaining the functional and structural integrity of a molecule.

4.4.9 Functional implications of changing molecular interactions

Packing of transmembrane domains, folding of the extracellular region and maintenance of the stabilizing Cys110-Cys187 bond are coupled events that lead to functional rhodopsin (Hwa et al., 1997). Several mutations localized within the transmembrane helices or the extracellular loops and N-terminal region are associated with *retinitis pigmentosa*. These mutations result in complete or partial misfolding of the GPCR molecule (Garriga et al., 1996; Hwa et al., 1997; Liu et al., 1996b). In addition, mutations in both transmembrane and extracellular regions result in the replacement of the native Cys110-Cys187 bond with the non-native Cys185-Cys187 bond (Hwa et al., 2001). The effects observed in the F-D curves of rhodopsin lacking the native disulfide bond may therefore underlie the disruption of molecular interactions that occur in these point mutations leading to *retinitis pigmentosa.* In addition, these data suggest that the native S-S bond (Cys110-Cys187), extracellular and cytoplasmic loops, and transmembrane domains are structurally coupled since absence of the native S-S bond leads to altered interactions in most regions of the molecule.

4.4.10 Cleaving cytoplasmic loop C-III does not affect molecular interactions

It has been shown that splitting rhodopsin at the second and third cytoplasmic loops leads to two-fragment rhodopsin that shows properties similar to the wild-type (Ridge et al., 1995a; Ridge et al., 1999). This and alike limited proteolysis studies suggest that connecting subsequent cytoplasmic loops II and III only have a small stabilizing effect on rhodopsin (Filipek et al., 2003a). In the current SMFS study, to determine if rhodopsin was being pulled from the N- or C-terminal end, cytoplasmic loop C-III was cleaved using endoproteinase Glu-C from *S.aureus* V8. This cleavage resulted in three fragments – one constituted of the N-terminus and helices I-V with the connecting loops ending at E239 in the cytoplasmic loop C-III, the second fragment consisted of the remaining part of loop C-III and helices VI-VIII until E341 in the C-terminal end, and the third fragment was the end tail of the C-terminus. SMFS measurements on the first fragment of cleaved rhodopsin showed that the positions of all stable structural segments remained the same, but the unfolding forces of majority of stable structural segments in this fragment changed as compared to structural segments in native uncleaved rhodopsin (**Table 4.1**).

This suggests that although cleaving the cytoplasmic loop C-III does not alter the nature of interactions, it probably is important for the structural integrity of the molecule.

In **Chapter 3**, I showed that single bacteriorhodopsin molecules from different assemblies unfold at different forces indicating a change in their packing and long-range interactions in these assemblies. Thus, it can be concluded that the packing and the strength of molecular interactions are changed in rhodopsin after cleavage since the unfolding forces change. This connects well with the cooperative folding model of rhodopsin (Klein-Seetharaman, 2005) and the 'three-stage hypothesis' of membrane protein folding (Engelman et al., 2003) since SMFS measurements show a change in unfolding forces of transmembrane helices on cleaving the cytoplasmic loop. However the fact that the positions of stable structural segments are maintained is supported by the fact that rhodopsin retains its spectrum after extensive proteolysis of its exposed loops by pronase in native membranes or in detergent solutions (Filipek et al., 2003a).

4.4.11 Conserved residues are localized within stable structural segments

An interesting observation was that none of the highly conserved residues among GPCRs (80-100%) lie at the borders of the unfolding barriers. Instead, they are located in the interior of the stable structural segments. What could be the molecular origin for a mechanism embedding conserved residues in a structurally stabilized environment? Conserved residues play an important functional and/or structural role in all proteins. Their position is critical and a mechanism is required to ensure their maintenance. Establishing a stable structural segment that hosts the conserved residues would provide an efficient method of stabilizing and orienting these residues in precisely the right place.

Interestingly, this hypothesis collapses in absence of the native disulfide bond. E.g., without the native disulfide bond, the D(E)RY motif is no longer centered in the stable structural segment of helix III, but situated at the end of this structural segment. This shift in the position of the D(E)RY motif in absence of the native disulfide bond may be an improper positioning causing altered molecular interactions that prevent the proper functioning of the receptor.

4.5 CONCLUSIONS & OUTLOOK

The molecular details of the structure and organization of rhodopsin and other GPCRs in native membranes are not fully known. SMFS with the help of bioinformatics tools could be used to predict the structure of membrane proteins and the nature of molecular interactions in the native membrane environment. SMFS is an upcoming method that could provide a map of molecular interactions in the native membrane environment of a protein. In the present study I showed the use of SMFS in detecting two states of rhodopsin – a native state and a non-native state. It was also possible to detect molecular interactions in the native state and a shift in these interactions in the non-native state, implying a possible cause of diseases like *retinitis pigmentosa*. To my knowledge this is the first time someone has deciphered molecular interactions in a different structural state of the same molecule in the absence of an X-ray crystal structure for that state. The current study highlights the importance of the native Cys110-Cys187 covalent linkage and the effect it has on protein stability. Understanding the factors that affect these molecular interactions will provide greater insight into the function and dysfunction of the rhodopsin molecule. Further studies investigating how molecular interactions drive different functional states of rhodopsin will provide a more precise understanding of molecular mechanisms determining structure-function relationships of GPCRs. Though X-ray crystal structures of different conformational states would provide a wealth of most accurate information on these and related questions, obtaining crystals for X-ray studies possesses a serious challenge. In the mean time, biophysical methods like SMFS could lend a helping hand to understand the underlying mechanisms of this versatile group of protein sensors. E.g., SMFS makes it possible to decipher the interactions in the activated state of rhodopsin. Establishing the current approach for rhodopsin could act as a template for other GPCRs, opening opportunities to understand and gain mechanistic insights into receptors at a molecular level.

Chapter

5

ZINC MEDIATED INCREASE IN STABILITY OF NATIVE BOVINE RHODOPSIN

5.1 INTRODUCTION

In the last chapter, I showed the characterization of rhodopsin unfolding in native ROS disc by SMFS to reveal the molecular interactions that stabilize the dark state of the receptor, touching just the tip of the iceberg. Many fundamental questions in relation to the activation mechanism of GPCRs, the specificity and recognition of interacting proteins and their mechanisms of activation by GPCRs, the role of GPCR dimerization and its functions during signaling, to mention a few, remain unsolved. In the current study, I have monitored the effect of zinc on the molecular interactions stabilizing dark state rhodopsin using the same SMFS assay. Interestingly, it was found that zinc could be a key player in the dimerization of rhodopsin, the functional unit during the signaling process.

5.1.1 Role of zinc in biology

Zinc (Zn^{2+}) has been recognized as an essential element for plants and animals (Prasad, 1995). It is the second most abundant trace element found in the human body[36] (Weiss et al., 2000), influences cell metabolism through a variety of mechanisms and is required for the function of numerous proteins, serving both as a part of the active site, e.g., in metalloenzymes, and acting to stabilize protein domains, such as the Zn^{2+} finger-binding motif in transcription factors (Schwabe and Klug, 1994; Vallee and Falchuk, 1993). The largest pools of Zn^{2+} exist in the muscle, bone, skin, hair and liver (Aggett and Comerford, 1995). Several neurodegenerative disorders - Alzheimer's disease, Parkinson's disease, familial amyotrophic lateral sclerosis, and the transmissible spongiform encephalopathies (TSEs) - share a common pathogenesis involving the misfolding and aggregation of specific proteins. The effect of trace metal ions like Zn^{2+}, copper (Cu^{2+}) and iron (Fe^{3+}) is implicated in the formation of amyloid plaques in these neurodegenerative disorders (Huang et al., 2004; Moir et al., 1999). Mounting evidence demonstrates direct binding of Zn^{2+} to the β-amyloid (Alzheimer's disease), α-synuclein (Parkinson's disease), superoxide dismutase (amyotrophic lateral sclerosis), and prion (TSE) proteins, linking either the gain or loss of Zn^{2+} binding to the progression of these severe protein misfolding disorders (Jobling et al., 2001).

---

[36] The total content is ~2 g (Aggett and Comerford, 1995).

Recent studies have identified Zn^{2+} as an allosteric modulator of structure and function for a number of GPCRs, including the dopamine (Schetz and Sibley, 1997), adrenergic (Swaminath et al., 2003; Swaminath et al., 2002), melanocortin (Holst et al., 2002), and chemokine (Gerlach et al., 2003) receptors. Besides, there is experimental evidence indicating the presence of naturally occurring Zn^{2+} binding sites in several GPCR proteins (Schetz et al., 1999; Schetz and Sibley, 1997).

Many GPCRs modulate activities in the central nervous system (CNS). The brain contains high concentrations of Zn^{2+} with an estimated concentration of 150 μM (Weiss et al., 2000). It has been suggested that the release of Zn^{2+} into the synapses of hippocampal neurons can increase the local concentrations to as high as 300 μM (Assaf and Chung, 1984). Several GPCRs in the brain have been reported to bind Zn^{2+} with micromolar binding affinities, and to modulate the binding properties of agonists, antagonists and inverse agonists (Holst et al., 2002; Liu et al., 2006; Schetz et al., 1999; Schetz and Sibley, 1997; Swaminath et al., 2003), thereby suggesting a possible physiological role of Zn^{2+} on the action of these receptors.

5.1.2 Physiological role of Zn^{2+} in the eye

Zn^{2+} is found in high concentrations in the retina, retinal pigment epithelium (**RPE**) and choroid in ocular tissues (Grahn et al., 2001; Karcioglu, 1982; Ugarte and Osborne, 2001) serving several important functions. Zn^{2+} deficiency in a number of species has been shown to result in a variety of ultrastructural and electrophysiologic ocular manifestations (Grahn et al., 2001). The bivalent metal ion interacts with taurine and vitamin A in the retina, regulates the light-rhodopsin reaction within the photoreceptor[37] and modulates synaptic transmission. The role of Zn^{2+} as an anti-oxidant in both the retina and RPE is

---

[37] Significant levels of chelatable Zn^{2+} were found in photoreceptors cells using histochemical methods that label free or loosely bound Zn^{2+} (Hirayama, 1990; Ugarte and Osborne, 1998; Ugarte and Osborne, 1999).

well suited since the photoreceptors are particularly susceptible to oxidative damage because of their high-polyunsaturated fatty acid content, high metabolic rate and constant bombardment by light (Sarma et al., 1994). A critical function for Zn^{2+} in the outer segments of photoreceptors may be related to its effect on plasma membrane functions by modulating membrane protein conformation and protein-protein interactions (Bettger and O'Dell, 1993).

It is speculated that the role of Zn^{2+} in vision is related, in part, to rhodopsin. Direct association of rhodopsin with the bivalent metal ion (Shuster et al., 1992; Stojanovic et al., 2004) increases the level of rhodopsin phosphorylation (Shuster et al., 1996). In addition, higher Zn^{2+} concentrations (50-200 μM) reduce the thermal stability of rhodopsin and regeneration of the protein with 11-*cis*-retinal (del Valle et al., 2003; Stojanovic et al., 2004). The dissociation constant of Zn^{2+} for rhodopsin in the disc membrane and purified rhodopsin in the dark has been estimated to be 2-10 μM (Shuster et al., 1992), and the maximal regeneration of rhodopsin by its chromophore is reduced in the presence of Zn^{2+} (del Valle et al., 2003). This suggests that Zn^{2+} can bind to rhodopsin and other GPCRs under physiological conditions and may play a role in the signaling process. Zn^{2+} therefore appears to play an important functional and structural role in rhodopsin. Despite the numerous studies, the exact role of Zn^{2+} in the visual cycle and specifically in its interaction with rhodopsin remains unclear.

Changes in the unfolding force as detected by SMFS under different experimental conditions are an indicator of altered molecular interactions promoted by those changes (Janovjak et al., 2003; Kedrov et al., 2005). Recently, it was possible to detect ligand and inhibitor binding to the membrane protein NhaA using SMFS (Kedrov et al., 2005; Kedrov et al., 2006b). F-D curves recorded in absence of the native Cys110-Cys187 disulfide in rhodopsin showed that some of the molecular interactions established within the molecule changed their structural positions and strengths (**Chapter 4**). Such changes of interactions within the GPCR may therefore provide insights into the molecular mechanism causing destabilization that occurs with *retinitis pigmentosa* point mutations like His211Pro. A direct binding of Zn^{2+} to rhodopsin would manifest as a change in unfolding force or the unfolding probability of different stable structural segments. The effect of Zn^{2+} on the unfolding of rhodopsin was examined to understand further the role of the bivalent ion in the receptor.

5.2 EXPERIMENTAL PROCEDURES

5.2.1 ROS disc membrane preparation

The ROS disc membranes were prepared in the same way as described in **section 4.2.1**.

5.2.2 AFM imaging and SMFS

AFM imaging and SMFS were performed as described in **sections 4.2.2** and **4.2.3**. All experiments were performed in the SMFS assay buffer (150 mM KCl, 25 mM $MgCl_2$, 20 mM Tris, pH 7.8) at room temperature. In experiments where membranes were treated with $ZnCl_2$ (Fluka, Sigma), $CaCl_2$ (Merck, Sigma), $CdCl_2$ (Sigma), $CoCl_2$ (Sigma), or $CuCl_2$ (Sigma), the assay buffer was supplemented with the specified concentrations of the reagent and the pH adjusted to 7.8. ROS disc membranes were diluted in the assay buffer supplemented with the various metal ions and incubated on ice for 40 – 60 min in complete darkness. When membranes were treated with EDTA (Sigma), $MgCl_2$ was excluded from the assay buffer. All dilutions were carried out under dim red light, and experiments performed in a completely dark room. Force curves were collected over a period of less than 1h to prevent bleaching of rhodopsin.

To rule out statistical errors due to cantilever spring constant deviations, the SMFS experiments were performed on each rhodopsin sample using ~20 different cantilevers from the same batch. Experiments were performed using two different AFM equipments, viz., Picoforce (dI-Veeco, USA) and Multimode (dI-Veeco, USA). F-D curves obtained from both the instruments were analyzed separately. The unfolding forces of at least 80% of the force peaks measured in the two cases agreed within <20%[38], and the WLC fits gave the same lengths of unfolded polypeptides. Spring constants of the 200 μm long silicon nitride AFM cantilevers (NPS, Veeco Metrology; nominal spring constant ~0.08 N/m) were calibrated in buffer solution using the equipartition theorem (Butt and Jaschke, 1995; Florin et al., 1995). All cantilevers exhibited similar spring constants within the uncertainty of the above calibration method (~10%).

---

[38] For only 10 μM $ZnCl_2$, 3 in 15 stable structural segments showed >20% difference in unfolding force.

5.2.3 Selection and analysis of force-extension curves

The selection criterion and the analysis procedure was exactly the same as that mentioned in **section 4.2.4**.

5.2.4 Molecular dynamics simulations

Molecular dynamics (**MD**) simulations and free energy calculations were performed by the group of Dr. Slawomir Filipek (IIMCB, Warsaw, Poland). Rhodopsin monomer and dimers were immersed in a membrane composed of dipalmitoylphosphatidyl-choline (**DPPC**) phospholipids. The final system contained 153 DPPC molecules in the case of rhodopsin monomer (PD: 1U19), and 105 for rhodopsin dimer (PDB: 1N3M). Positions of Zn^{2+} ions were taken from the most updated rhodopsin crystal structures: pair 1 from 1GZM; pairs 2, 3 and 4 from 1U19. The periodic box dimensions were 6.33 x 6.33 x 11.0 nm for rhodopsin monomer, and 10.0 x 6.33 x 11.0 nm for the dimer. A charge of +2 was set for each Zn^{2+} ion. Water TIP3P was used and counterions were added to maintain the overall charge zero. PME procedure (Darden et al., 1993; Essmann et al., 1995) was used for treatment of long-range electrostatic interactions. Initial equilibration of the system was performed by 500 ps molecular dynamics with C_α atoms of rhodopsin and all the Zn^{2+} ions frozen. During subsequent 1000 ps MD, the C_α atoms and Zn^{2+} ions were restrained to their initial positions using harmonic potentials. MD simulations were conducted in Gromacs (Van der Spoel et al., 2005) using the standard FFGMX modified for describing lipids forcefield (Berger et al., 1997).

5.2.5 Free energy calculations

Free energy calculations were performed by using the free energy perturbation (**FEP**) method (Van der Spoel et al., 2005) with slow perturbation of the system from initial to final state. The “slow-growth” thermodynamic integration method in Gromacs was used. The initial and final states differed by the location of Zn^{2+} ions. Zn^{2+} ions were initially located at the Zn^{2+} binding sites in rhodopsin (positions found in crystal structures of rhodopsin) and subsequently transferred to bulk water during FEP. This was not a physical transfer but transformation of properties of Zn^{2+} ions both in protein binding sites and in bulk water. During FEP, all parameters (charge and van der Waals) of Zn^{2+} ions in rhodopsin were gradually diminished to zero and simultaneously the parameters for dummy atoms with fixed positions in bulk water were increased from zero. Fixed positions were necessary to prevent the nearly non-interacting atoms (all parameters close to zero) from uncontrolled movements throughout the entire system. For the same reason the positions of Zn^{2+} ions in protein binding sites were also fixed. No other constraints were used in the system so amino acids in binding sites as well as water molecules adjacent to Zn^{2+} ions in bulk water had enough freedom for tight binding Zn^{2+} ions. All calculations were performed in a periodic box with explicit membrane and water molecules. Parameters were changed very slowly at each step of the simulation (1 fs). Such a procedure ensures near-equilibrium conditions during FEP.

In order to minimize error in ΔG calculations, each perturbation was divided into three phases and the parameters changed for only one type during each phase. In the first phase (400 ps), the van der Waals parameters of Zn^{2+} ions bound to the protein were diminished. In the second phase (800 ps), the charges on both sets of Zn^{2+} ions (in protein and in bulk water) were exchanged (the overall sum of charges was the same during the whole FEP). In the third phase (400 ps), the van der Waals parameters of Zn^{2+} ions in bulk water were increased to their final values.

5.3 RESULTS

5.3.1 Unfolding single native rhodopsin molecules in presence of Zn^{2+}

Rhodopsin in native ROS disc membranes in buffer solution containing Zn^{2+} was imaged and studied by SMFS as described in **Chapter 4**. No apparent change in the morphology of the flatly adsorbed burst discs was observed, and a raft-like organization of rhodopsin was seen even in the presence of Zn^{2+} (Fotiadis et al., 2003).

Unfolding rhodopsin molecules in the presence of Zn^{2+} again yielded two major classes of F-D curves corresponding to the unfolding of rhodopsin polypeptide chain with an intact native disulfide bond between Cys110 and Cys187, ~65 nm long, and without this disulfide bond, ~95 nm long (**Chapter 4**). F-D spectra obtained in the presence of $ZnCl_2$ revealed the same location for each stable structural segment as that detected in the absence of $ZnCl_2$ (**Figures 5.1** and **5.2**, **Table 5.1**). The presence of Zn^{2+}, therefore, does not alter the positions of stable structural segments.

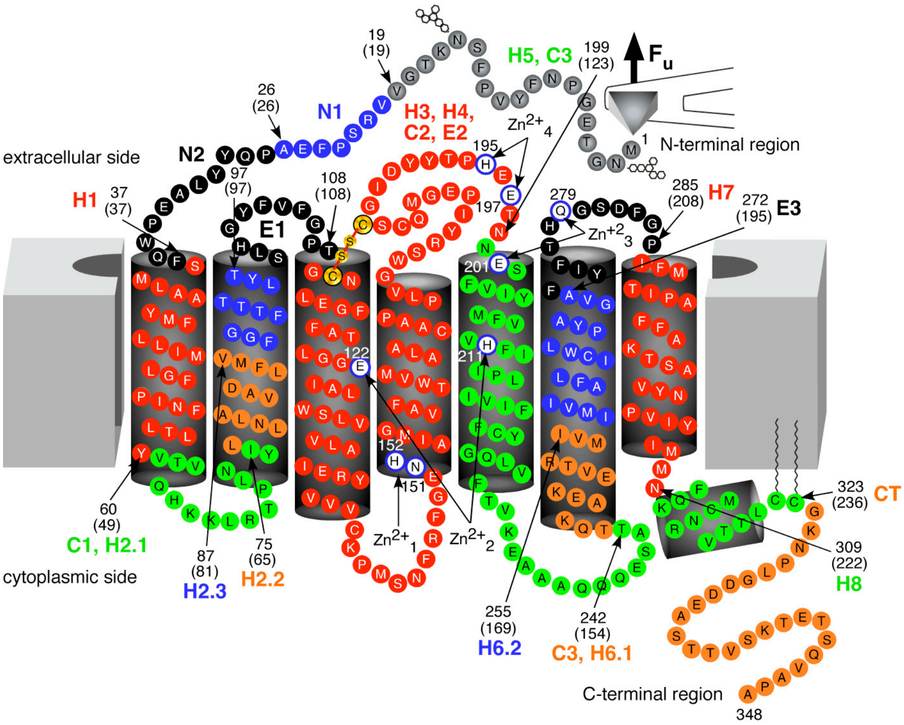
19
(19)
H5, C3
199
(123)
F_u
26
(26)
N1
H3, H4,
C2, E2
$Zn^{2+}{}_4$
1
N-terminal region
extracellular side
N2
195
97
(97)
108
(108)
197
279
285
(208)
H7
272
(195)
E3
H1
37
(37)
E1
$Zn^{+2}{}_3$
201
122
211
152
151
60
(49)
C1, H2.1
87
(81)
H2.3
75
(65)
H2.2
$Zn^{2+}{}_1$
$Zn^{2+}{}_2$
323
(236)
CT
309
(222)
H8
cytoplasmic side
255
(169)
H6.2
242
(154)
C3, H6.1
C-terminal region
348

Figure 5.1 Mapping stable structural regions of bovine rhodopsin in the presence of Zn^{2+}

Unfolding rhodopsin by pulling from the N-terminus helped deciphering the molecular interactions and localizing them in the molecule. Arrows indicate the starting and end of each structural segment. Numbers in brackets are the amino acid values obtained from fitting the peaks in the F-D curves to the WLC model (**Figure 5.2**), and the numbers without brackets are the corresponding residue numbers in the rhodopsin sequence. The amino acid residues encircled blue denote the putative Zn^{2+} binding sites. Asn151 and His152 at the cytoplasmic end of helix IV constitute a Zn^{2+} binding site ($Zn^{2+}{}_1$). The second site ($Zn^{2+}{}_2$) is embedded in the membrane and is formed by Glu122 and His211 in helices III and V respectively. The third Zn^{2+} binding site ($Zn^{2+}{}_3$) is formed by Glu201 in helix V and Gln279 in the extracellular loop EIII. The extracellular loop EII hosts the last Zn^{2+} binding site ($Zn^{2+}{}_4$) formed by residues His195 and Glu197.

Individual F-D curves showed small variations between each other (**Figures 5.2**(**A**) and (**C**)). Moreover, the F-D curves from experiments done in the presence of Zn^{2+} exhibited an overall pattern similar to those performed without Zn^{2+} (**Chapter 4**). Thus, ROS discs in the presence of Zn^{2+} adsorbed predominantly exposing the extracellular surface of rhodopsin as in the absence of Zn^{2+}. Also, in a recent study on BR unfolding by SMFS, it was shown that unfolding BR molecules from the N- and C-terminal ends gave non-identical F-D curves (Kessler and Gaub, 2006). It can, therefore, be safely concluded that rhodopsin unfolding occurred from the N-terminal region, which is important for a comparative study.

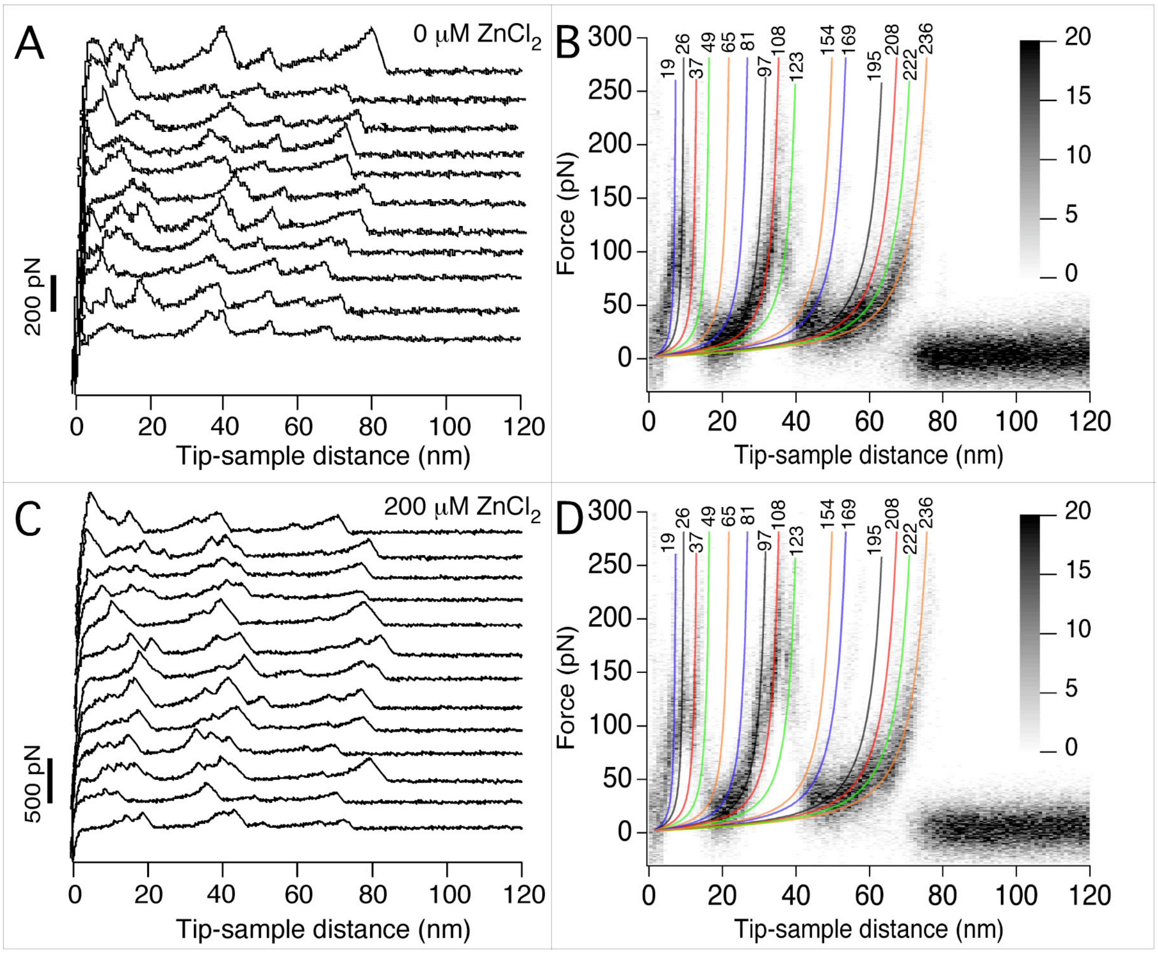

Figure 5.2 Single-molecule force spectroscopy curves recorded on native ROS disc membranes

F-D curves recorded in the absence, (**A**) 0 µM, and in the presence, (**C**) 200 µM, of Zn^{2+}. The curves exhibit lengths of ~65 nm corresponding to that of an entirely unfolded rhodopsin peptide having an intact Cys110-Cys187 bond. Individual force curves can show considerable variations. Some force peaks occur in the majority of curves (major peaks), while others occur only in a small fraction of force curves (minor peaks). The characteristic combination of different force peaks in a F-D curve represents the molecular interactions detected during unfolding. F-D curves exhibiting the same major and minor force peaks indicate that rhodopsin molecule unfolded via the same pathway. Superimpositions of several force curves for 0 µM Zn^{2+} (n=42) (**B**), and 200 µM Zn^{2+} (n=34) (**D**) enhance their common features. Major (black) and minor (grey shaded) peaks were fitted using the WLC model. Fits shown are average values obtained on fitting each peak of individual force curves, and reveal the unfolded and stretched polypeptide length. Subtracting this length from the terminal end pulled allows locating the molecular interaction established within the rhodopsin structure (**Figure 5.1** and **Table 5.1**). Average forces and locations of the molecular interactions detected by SMFS are shown at the end of each fit. Equally colored WLC fits of force peaks in (**B**) and (**D**) and structural segments in **Figure 5.1** correlate to each other.

Secondary structure[a]	Structural segment[b]	Polypeptide segment (aa)[c]	Average contour length ± SD (aa)[d]		Average unfolding force ± SD (pN)										
			ZnCl$_2$ (μM)		ZnCl$_2$ (μM)							1 mM EDTA	200 μM CaCl$_2$	200 μM CdCl$_2$	200 μM CoCl$_2$
			0[e]	200	0[e]	10	25	50	100	200	400				
N-terminal region	**N1**	20-26	19±2	19±2	131±38 (106)	109±37 (117)	108±31 (141)	129±43 (122)	134±40 (93)	130±39 (63)	130±39 (76)	116±33 (65)	109±30 (51)	125±39 (56)	104±28 (62)
N-terminal region	**N2**	27-37	26±2	27±2	139±38 (121)	121±36 (117)	120±38 (128)	151±51 (138)	147±43 (89)	152±40 (67)	139±41 (81)	126±32 (70)	125±37 (57)	125±40 (58)	112±28 (59)
Helix I	**H1**	38-60	37±3	37±3	132±46 (116)	124±38 (122)	124±41 (121)	155±49 (136)	146±50 (98)	159±53 (68)	141±44 (77)	119±37 (66)	126±40 (60)	125±35 (56)	112±35 (51)
Loop C-I	**C1**	61-75	49±5	49±5	117±47 (41)	98±39 (50)	112±51 (49)	135±57 (82)	128±51 (47)	125±59 (48)	112±55 (42)	112±56 (26)	113±46 (28)	106±43 (30)	91±40 (23)
Helix II	**H2.1**	76-87	65±5	66±6	96±34 (26)	89±41 (22)	74±25 (14)	100±45 (29)	90±31 (37)	108±62 (16)	99±47 (20)	90±47 (11)	74±32 (14)	97±51 (8)	80±41 (9)
Helix II	**H2.2**	88-97	81±4	82±4	89±34 (23)	76±27 (38)	82±30 (76)	90±36 (63)	104±39 (67)	103±45 (24)	100±40 (48)	82±48 (17)	94±41 (22)	94±31 (10)	75±30 (14)
Loop E-I	**E1**	98-108	97±4	96±3	106±38 (118)	103±31 (146)	119±35 (161)	132±45 (175)	142±49 (130)	152±44 (85)	136±41 (114)	101±36 (70)	103±30 (59)	117±37 (67)	99±32 (57)
Helices III & IV, loops C-II & E-II	**H3, H4, C2, E2**			107±1	158±53 (187)	146±37 (165)	153±40 (175)	184±53 (198)	198±54 (139)	198±50 (105)	197±52 (129)	148±42 (87)	149±40 (82)	174±42 (84)	146±41 (73)
Helix V & loop C-III	**H5, C3**	200-242	123±5	121±4	136±45 (146)	136±40 (131)	151±47 (153)	167±53 (156)	182±58 (119)	180±57 (92)	177±50 (94)	127±41 (72)	152±48 (68)	173±44 (68)	126±42 (64)
Helix VI	**H6.1**	243-255	154±4	138±6	85±34 (17)	85±31 (25)	103±42 (30)	103±34 (32)	114±41 (33)	125±27 (10)	119±34 (23)	86±20 (11)	90±41 (9)	78±12 (4)	94±43 (10)
Helix VI	**H6.2**	256-272	169±6	170±7	81±34 (127)	70±35 (91)	63±20 (98)	79±35 (122)	90±47 (86)	93±47 (44)	77±38 (56)	63±14 (72)	67±33 (53)	81±31 (35)	66±37 (42)
Loop E-III	**E3**	273-285	195±5	192±6	79±32 (30)	69±30 (35)	65±24 (52)	85±43 (48)	76±34 (44)	92±44 (34)	81±45 (45)	64±26 (14)	73±31 (12)	77±36 (19)	92±41 (15)
Helix VII	**H7**	286-309	208±3	209±3	99±40 (46)	83±30 (49)	81±30 (75)	94±38 (78)	97±34 (71)	93±37 (46)	96±50 (58)	91±36 (40)	81±24 (39)	80±32 (32)	77±35 (25)
Helix 8	**H8**	310-323	222±6	223±5	104±44 (142)	88±37 (97)	96±37 (132)	107±44 (135)	122±47 (106)	118±43 (78)	108±42 (98)	89±37 (69)	99±34 (55)	97±45 (59)	89±41 (49)
C-terminal region	**CT**	324-348	236±6	236±5	109±47 (114)	94±33 (109)	120±40 (117)	119±54 (115)	133±62 (73)	139±43 (46)	128±48 (75)	103±39 (55)	113±43 (35)	107±46 (51)	101±33 (40)

Table 5.1 Unfolding forces of stable structural segments with and without Zn^{2+}

[a] Secondary structure(s) involved in the stable structural segment. [b] Names of stable structural segments. [c] Polypeptides that establish a structural segment. [d] Average number of aa stretched. [e] These data are from **Chapter 4**.

5.3.2 Zn^{2+} binding increases the mechanical stability of rhodopsin

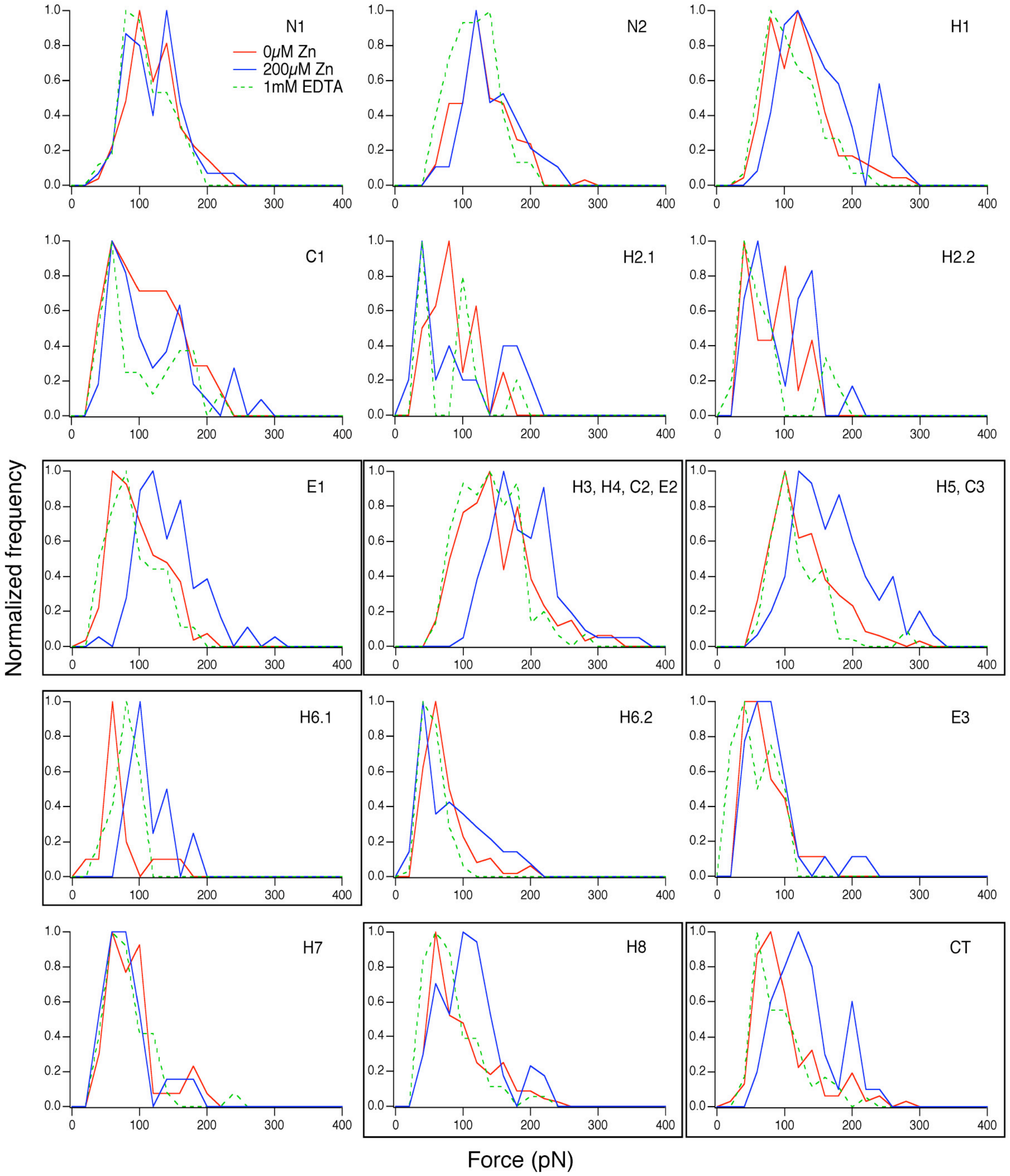

Figure 5.3 Histograms of unfolding forces

The histograms show the unfolding forces of the different stable structural segments of rhodopsin in the presence of 0 μM (red solid line), 200 μM (blue solid line) Zn^{2+} and 1 mM EDTA (green dashed line). For the stable structural segments E1; H3, H4, C2, E2; H5, C3; and H6.1 (in boxes) a clear shift in unfolding forces could be observed in the presence of 200 μM Zn^{2+} as compared to 0 μM Zn^{2+} (compare blue and red solid traces). The unfolding forces for 0 μM Zn^{2+} and 1 mM EDTA remained the same for all stable structural segments (red solid and green dashed lines).

To check if Zn^{2+} has any effect on rhodopsin unfolding, SMFS was performed in the presence of 200 μM $ZnCl_2$. Though no change in the position of stable structural segments was observed, the inclusion of Zn^{2+} however changed the forces required to unfold the various stable structural segments (**Figure 5.3**). An increase in force could be observed for all stable structural segments except for the first structural segment of the N-terminal region (N1) and the one involving helix VII (H7). The largest increase in unfolding forces was observed in the four structural segments between extracellular loop E1 and helix VI (E1; H3, H4, C2, & E2; H5, C3; C3, H6.1) (**Figure 5.4**, **Table 5.1**).

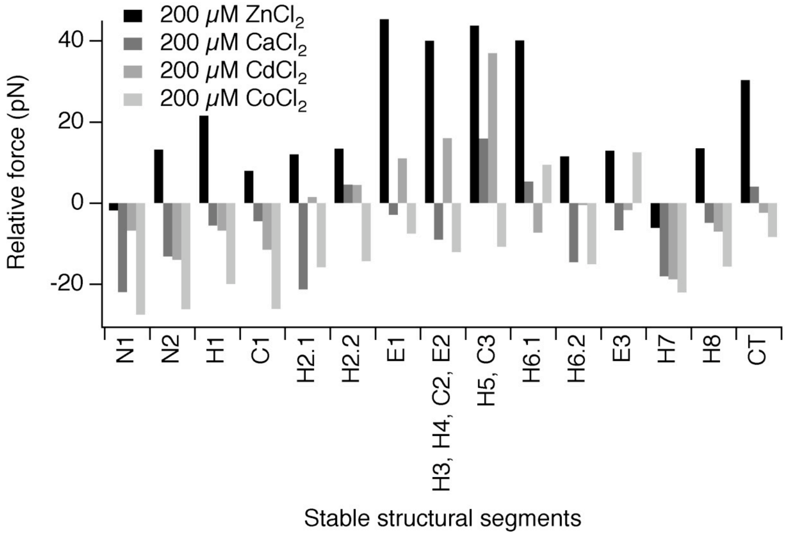

Figure 5.4 Zn^{2+} binding to rhodopsin is specific

Specificity of Zn^{2+} in increasing the stability of structural segments was tested by unfolding rhodopsin in the presence of different bivalent ions. Changes in unfolding forces for all the stable structural segments with and without different bivalent ions were determined. The figure shows a plot of the change in unfolding forces for all the stable structural segments in the presence of 200 μM Zn^{2+}, Ca^{2+}, Co^{2+} and Cd^{2+} in comparison to 0 μM Zn^{2+}. The maximum increase in unfolding forces for all stable structural segments occurred in the presence of 200 μM Zn^{2+}.

Forces required to unfold these segments are 40-46 pN higher in the presence of 200 μM $ZnCl_2$. The structural segment E1 showed an increase in force from 106 pN to 152 pN constituting a 43% increase in stability. The group of structural segments constituted by H3, H4, C3 & E2 showed a 25% increase in stability as indicated by the increase in unfolding force from 158 pN to 198 pN. The unfolding force of region H5 & C3 increased from 136 pN to 180 pN thus increasing its stability by 32%. C3 & H6.1 showed an increase in force from 85 pN to 125 pN and in stability of 47%. Other structural segments with appreciable increases in unfolding forces include, helix I (H1, 27 pN) and the cytoplasmic tail (CT, 30 pN), corresponding to an increase in the strength of their stabilizing molecular interactions by 20% and 28%, respectively. All other structural regions showed minor increase in stability. The increase in forces required to overcome unfolding barriers in the presence of 200 μM $ZnCl_2$ points to a stabilizing effect of Zn^{2+} on the molecular interactions in those structural regions.

Disc membranes were prepared in buffer containing 2 mM EDTA, and therefore most of the free and solvent exposed Zn^{2+} should be chelated. To test the completeness of Zn^{2+} chelation by EDTA, F-D curves were collected in the presence of added 1 mM EDTA. Since all F-D curves were collected in a buffer containing 25 mM $MgCl_2$ (see materials and methods), which would interfere with the chelation of Zn^{2+} by EDTA, SMFS experiments in the presence of EDTA were therefore performed in a buffer without $MgCl_2$. It was observed that the absence of $MgCl_2$ did not change the forces required to unfold stable structural segments (**Figure 5.5**). The inclusion of EDTA resulted in a minor decrease in the externally applied forces required to unfold all stable structural segments except for segment C3, H6.1. This suggests that chelation of Zn^{2+} was possibly incomplete after processing of disc membranes.

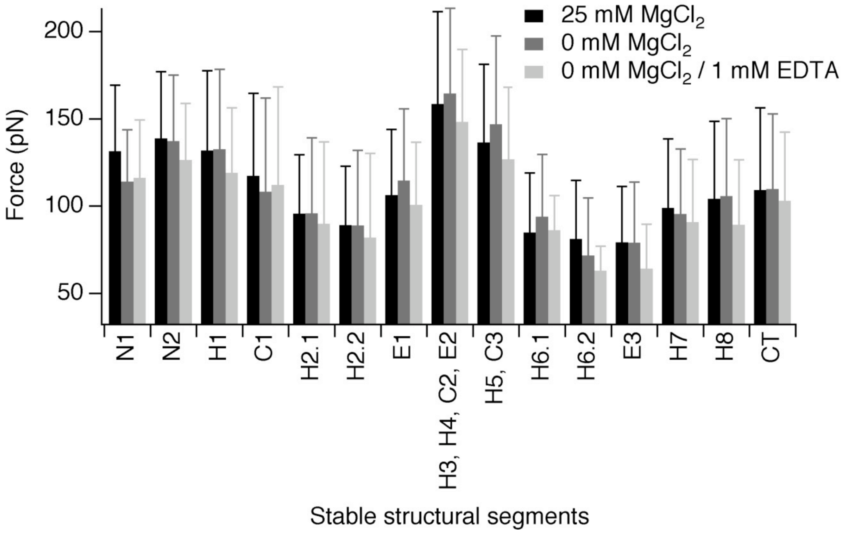

Figure 5.5 Effect of $MgCl_2$ and EDTA on unfolding forces

Additional unfolding experiments were done with 1 mM EDTA (0 mM $MgCl_2$) to validate the 0 μM $ZnCl_2$ results. To rule out any effect of $MgCl_2$, rhodopsin was unfolded in the SMFS buffer without $MgCl_2$. The unfolding forces for all the structural segments were ≤ 20 pN (within the errors of SMFS measurements) with and without 1 mM EDTA and $MgCl_2$, thus confirming the 0 μM $ZnCl_2$ results. The maximal increase for 200 μM Zn^{2+} shows that Zn^{2+} binding to rhodopsin is highly specific and responsible for the observed increase in stability though non-specific action of other bivalent ions cannot be completely ruled out.

The concentration dependence of the apparent stabilization of stable structural segments was characterized by performing SMFS at concentrations of $ZnCl_2$ ranging from 0-400 μM (**Figure 5.6**). All structural segments exhibiting an appreciable increase in stability in the presence of 200 μM $ZnCl_2$ showed a clear concentration dependent relationship with saturation occurring at ~100 μM of the bivalent cation. The EC_{50} value for the Zn^{2+} binding sites hosting structural segment H3, H4, C2, E2 is 40 μM, and that for the structural segment H5, C3 is 37 μM, obtained manually from the concentration dependent curves of these two segments in **Figure 5.6**(**B**). The effect of Zn^{2+} is therefore saturable, and the EC_{50} values revealed from SMFS measurements are in excellent agreement with the equilibrium dissociation constant (K_D) of 2-10 μM determined biochemically for the binding of Zn^{2+} to rhodopsin (Shuster et al., 1992).

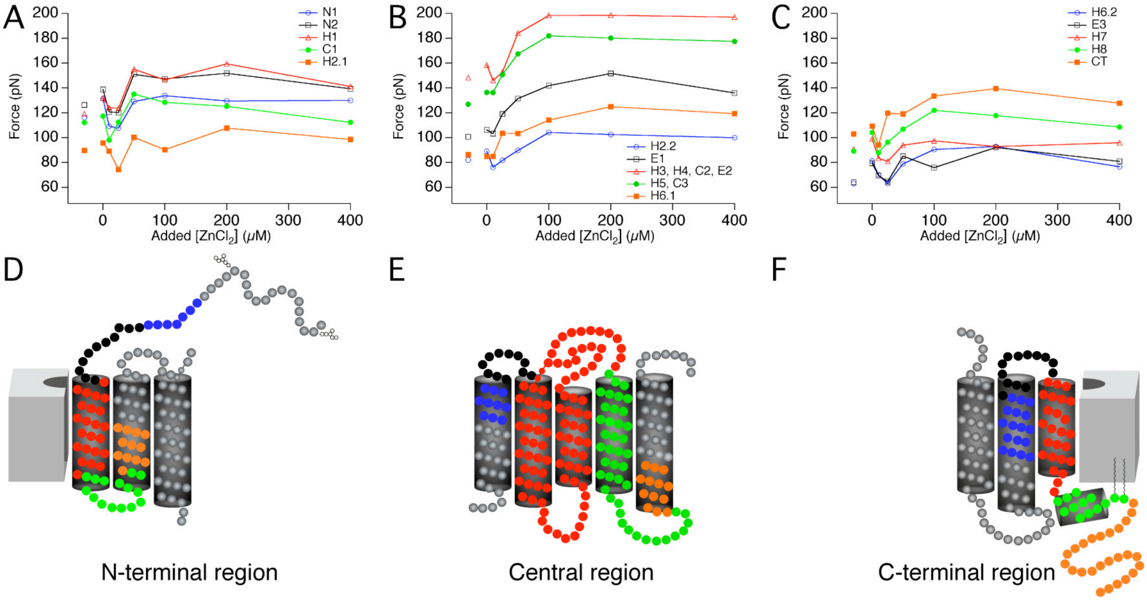

N-terminal region

Central region

C-terminal region

Figure 5.6 Dependence of unfolding forces on $ZnCl_2$ concentrations

SMFS was performed at $ZnCl_2$ concentrations from 0-400 μM, and the average unfolding force determined for each structural segment (**A-C**). Data points below 0 μM added $ZnCl_2$ on the x-axis denote average unfolding forces from experiments done without $MgCl_2$ but in the presence of 1 mM EDTA. The colors of the titration curves correspond to the stable structural segments shown in **D-F**. The standard deviations of the unfolding forces of each stable structural segment at different Zn^{2+} concentrations are given in **Table 5.1**.

5.3.3 Stabilization of rhodopsin by Zn^{2+} is specific

To determine whether the apparent stabilization of structural segments was due to an effect specifically related to Zn^{2+} binding rather than to its positive charge, I did SMFS experiments with other bivalent cations. The SMFS assay was performed in the presence of 200 μM $CaCl_2$, $CdCl_2$, $CoCl_2$ and $CuCl_2$. The F-D curves obtained in the presence of 200 μM $CuCl_2$ did not show any specific peaks for the different secondary structural segments like the other metal ions. The appearance of F-D curves resembled an irregular unfolding pattern observed when multiple molecules are attached to the tip. Therefore these curves were not included in the analyses. It can be speculated here that Cu^{2+} binding to rhodopsin, or some other unknown effect, causes rhodopsin molecules to aggregate thus preventing them from unfolding in a specific reproducible manner, though this warrants further investigation. The unfolding of rhodopsin in presence of each of the other bivalent metal ions showed the same stable structural segments as in the absence and presence of 200 μM Zn^{2+} (**Figure 5.1**, **Table 1**). Though none of the bivalent metal ions was able to mimic the full effects on the magnitude of forces observed in the presence of $ZnCl_2$, the increase in force required to overcome unfolding barriers observed in the presence of 200 μM $ZnCl_2$ was partially reproducible for a couple of stable structural segments in the presence of $CdCl_2$ and $CoCl_2$ (**Figure 5.4**).

In the presence of $CoCl_2$, F-D curves displayed an equal increase in unfolding force for structural segment E3 as that observed in the presence of $ZnCl_2$. F-D curves recorded in the presence of $CdCl_2$ showed a marked but lower increase in unfolding force compared to those obtained with $ZnCl_2$ in segment H5, C3. The ability of Co^{2+} and Cd^{2+} to partially mimic the effects of Zn^{2+} in those specific segments may indicate that these ions may be able to bind, to some extent, to Zn^{2+} binding sites responsible for those regions. These results suggest that the apparent stabilization of rhodopsin in the presence of Zn^{2+} is predominantly due to specific binding of Zn^{2+} though a non-specific electrostatic effect cannot be ruled out completely.

5.3.4 Zn^{2+} stabilizes the native disulfide bond between Cys110-Cys187

The presence of the highly conserved Cys110-Cys187 disulfide bond is of crucial importance for rhodopsin stability as illustrated by the destabilization and misfolding in some mutant forms of the receptor due to breaking of the disulfide bond resulting in *retinitis pigmentosa* (Hwa et al., 2001). As shown in **Chapter 4**, the presence or absence of the native disulfide bond between Cys110 and Cys187 is reflected in the length of the F-D curves. The ratio between the S-S intact and S-S broken curves was 2:1 (n = 274) for unfolding dark-state rhodopsin molecules from native ROS disc membranes in the SMFS assay buffer (150 mM KCl, 25 mM $MgCl_2$, 20 mM Tris, pH 7.8).

The ratio of the two classes of F-D curves was determined for each of the different $ZnCl_2$ concentrations (**Figure 5.7**). The proportion of curves representing the unfolding of rhodopsin with an intact Cys110-Cys187 disulfide bond became greater as the concentration of $ZnCl_2$ was increased in the assay buffer. Zn^{2+}, therefore, appears to stabilize or favor the maintenance of this disulfide bond. Surprisingly, the proportion of curves corresponding to the unfolding of rhodopsin with the Cys110-Cys187 bond also changed in the presence of $CaCl_2$, $CdCl_2$, or $CoCl_2$.

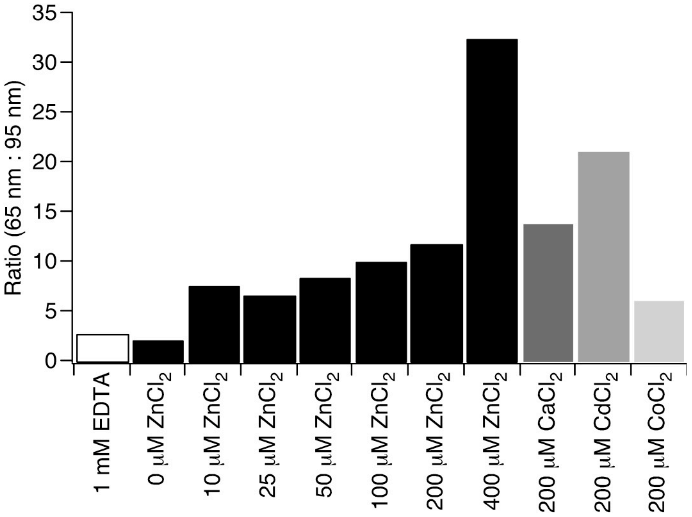

Figure 5.7 Ratio of force curves in presence and absence of the native Cys110-Cys187 disulfide bond

The ratios of F-D curves with and without the functionally important Cys110-Cys187 bond increased as the Zn^{2+} concentration was increased from 0 to 400 μM. Besides stabilizing the rhodopsin structure, Zn^{2+} ions might play an important role in maintaining the integrity of Cys110-Cys187 bond. However, an increase in ratio, similar to that in the presence of 200 μM Zn^{2+}, was also observed with 200 μM of Ca^{2+}, Cd^{2+} and Co^{2+}. This points to possible non-specific interactions of these bivalent ions with the disulfide bond of rhodopsin or the bilayer membrane. It may be assumed that th4 electrostatic interactions due to the presence of bivalent ions might act as a stabilizing factor for the Cys110-Cys187 bond.

While the stabilization of rhodopsin indicated by an increase in the unfolding forces of structural segments appears to be a specific effect of Zn^{2+}, the stabilization and preservation of the Cys110-Cys187 disulfide bond appears to be a result of non-specific electrostatic effects at the level of the membrane, receptor, or both. Another possibility is that the disulfide bridge is switched between the intact and broken states with a change in the stress in the lipid bilayer. A change in the local concentration of charges with excess added bivalent ions would influence the lipid bilayer stress resulting in a structural change of rhodopsin. However, it remains to be seen if these hypotheses would stand the test of experimental results.

5.3.5 Unfolding probability of secondary structure elements is altered on Zn^{2+} binding

The characteristic fingerprint of force peaks in a F-D spectrum describes a unique unfolding pathway of the rhodopsin molecule. Statistical analyses allow calculations of the frequency with which a rhodopsin molecule selects a particular unfolding pathway (**Chapter 4**). I calculated the occurrence probabilities of unfolding pathways including structural segments between N1 and the structural segment constituted by H5, C3, since these include the Zn^{2+} binding sites. Rhodopsin was observed to unfold via 72 unique unfolding pathways observed in the absence of $ZnCl_2$ (0 μM). Each unfolding pathway was assigned a pathway index number in a descending order based on the frequency with which that pathway occurred, '0' being the pathway occurring with the highest frequency and '72' with the lowest frequency. The same pathway index number was used to classify unfolding pathways in the presence of 10-400 μM $ZnCl_2$ (**Figure 5.8**).

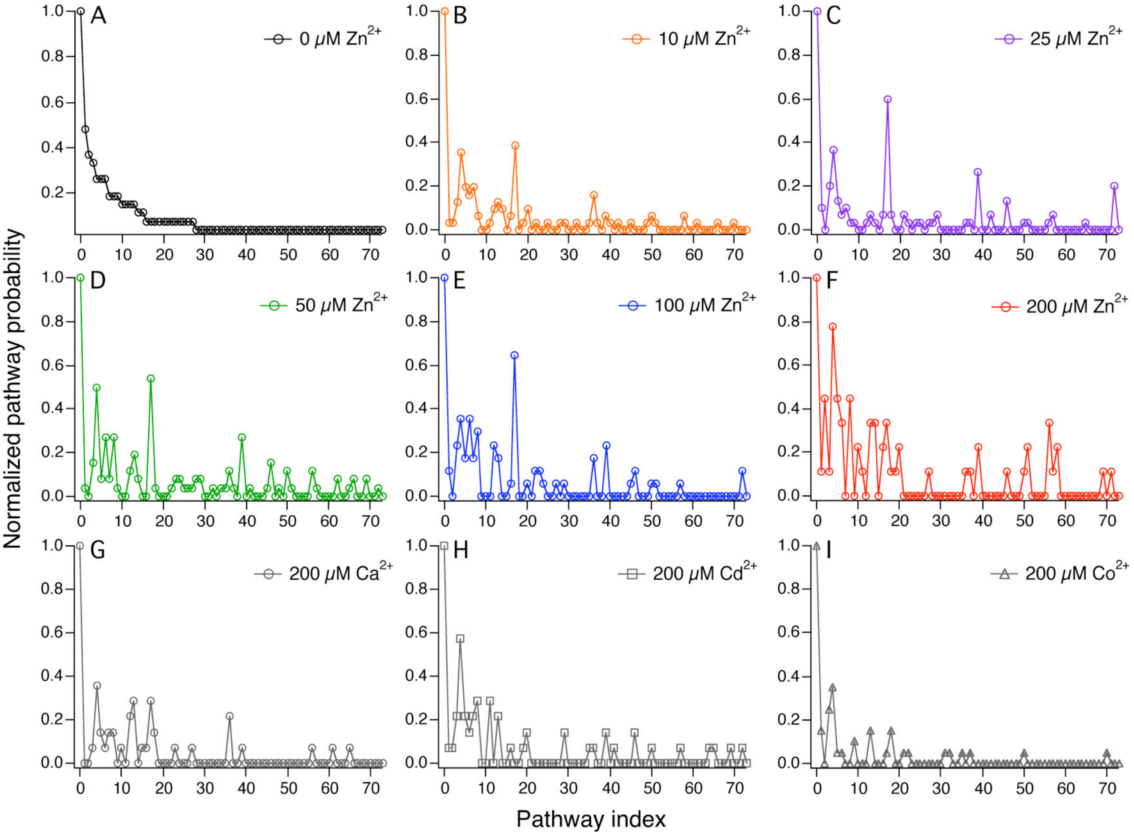

Figure 5.8 Probability of unfolding pathways of rhodopsin in the presence of $ZnCl_2$ and control metal ions

The unfolding pathways of rhodopsin without, 0 μM (**A**), and with, 10-200 μM (**B-F**), $ZnCl_2$ show a change in the occurrence probabilities, suggesting that Zn^{2+} binding leads to altered molecular interactions. It is easy to see a trend in the changing occurrence probabilities of unfolding pathways between pathway indices 0-20 (**A-F**). On the contrary, in the presence of control metal ions the probabilities did not show a dramatic shift as for 200 μM $ZnCl_2$ (**G-I**). The control plots are similar to the plots observed for low $ZnCl_2$ (10 and 25 μM).

The cumulative probability of these unfolding pathways in the presence of 0, 10, 25, 50, 100, 200 and 400μM Zn^{2+} is shown in **Figure 5.9**(**A**). The total cumulative probability decreases exponentially with increasing concentrations of $ZnCl_2$ **Figure 5.9**(**B**). Fitting the data to a single exponential decay function provides an EC_{50} of 9.6 μM, in good agreement with EC_{50} values derived from concentration dependence plots of unfolding forces, and the K_D value from biochemical measurements.

Increase in the unfolding force upon Zn^{2+} binding is a measure of altered molecular interactions. Modulating the interactions would consequently change the unfolding pathways of rhodopsin. I propose that the different unfolding probabilities of secondary structural segments, and hence the unfolding pathways in the Zn^{2+} experiments, could be attributed to changes in molecular interactions with increasing Zn^{2+} concentration. With the present resolution of the SMFS technique it is difficult to define the energy associated with the unfolding pathways under each condition.

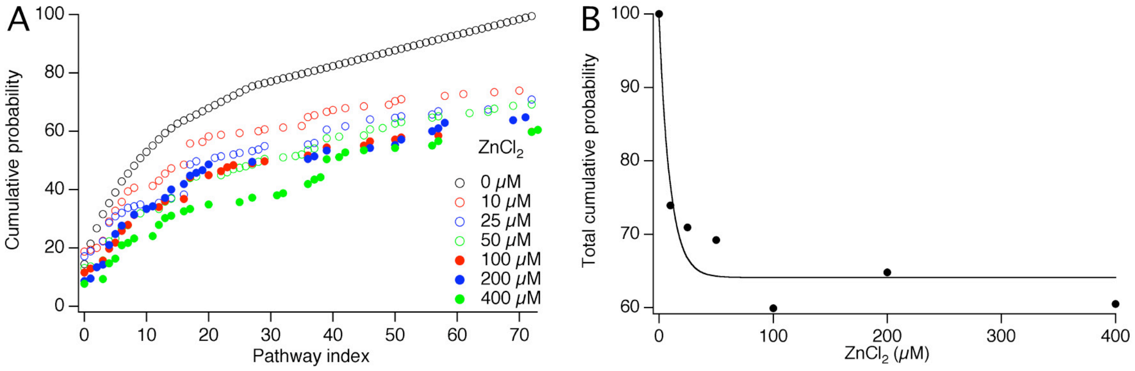

Figure 5.9 Change in unfolding pathways with increasing Zn^{2+} concentration

The unfolding pathways of rhodopsin were determined from stable structure segment N1 to H5, C3 for Zn^{2+} concentrations ranging from 0 μM to 400 μM. The 0 μM concentration was taken as the reference state to assign each unfolding pathway a number denoted as unfolding pathway index, '0' being the index number denoting the highest occurring pathway. The occurrence probability of each pathway was then calculated for all Zn^{2+} concentrations. A plot of cumulative percentage vs. unfolding pathway index (**A**) shows that the total cumulative percentage of pathways decreases with increasing Zn^{2+} concentration (**B**) possibly due to changes in molecular interactions in the presence of higher Zn^{2+} concentrations. An exponential fit to the data gave an EC_{50} value of ~9.6 μM.

5.3.6 Effect of Zn^{2+} on the free energy of rhodopsin

The stabilizing role of Zn^{2+} in rhodopsin was investigated computationally using the FEP method implemented in Gromacs (Van der Spoel et al., 2005). Putative Zn^{2+} binding sites considered in rhodopsin are shown in **Figure 5.10** (Li et al., 2004a; Okada et al., 2002; Okada et al., 2004; Palczewski et al., 2000; Teller et al., 2001)[39].

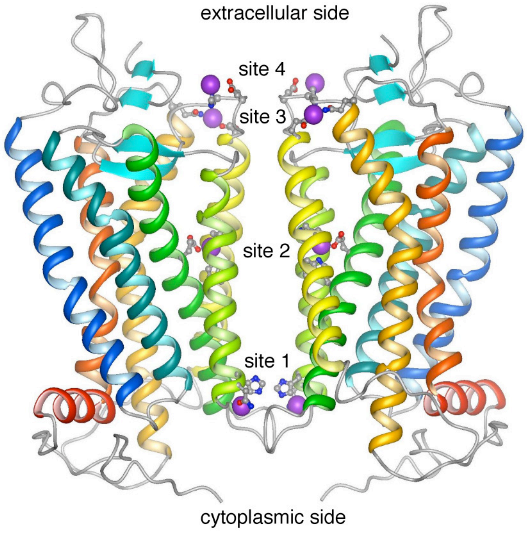

Figure 5.10 Putative Zn^{2+} binding sites in rhodopsin dimer

Zn^{2+} ions have a strong preference to bind along the dimeric interface of rhodopsin (sites 1-4), thus suggesting a possible role in the dimerization process of rhodopsin. (Figure courtesy: Dr. Slawomir Filipek, IIMCB, Poland).

In addition, MD simulations were used to determine the stability of Zn^{2+} in their putative binding sites in a single rhodopsin molecule. Zn^{2+} ions were initially positioned in their putative binding sites and were free to move. C_α atoms of rhodopsin were restrained to their initial positions with a harmonic potential. Zn^{2+} ions in positions 2, 3 and 4 did not change locations in their binding sites and are therefore considered to be stable. In contrast, Zn^{2+} in position 1 moved out of its binding site away from His152 by 0.41 nm. An additional 200 ps MD simulation performed without any restraints however showed that Zn^{2+} in position 1 was still moving out of its binding site. Zn^{2+} binding at this site is most probably unstable and non-specific.

Estimates of Zn^{2+} affinity at each putative binding site were determined by calculating the difference in free energy (ΔG) for the transfer of a Zn^{2+} atom from its putative binding site to bulk water. Free energy values were computed for single and paired Zn^{2+} shown in **Figure 5.10** for monomeric and dimeric rhodopsin, respectively (**Table 5.2**). In monomeric rhodopsin site 3 seems to be the most stable, whereas site 1 is unstable, whereas in dimeric rhodopsin Zn^{2+} binds with highest affinity at the site within the transmembrane helices (position 2). A negative ΔG value was computed for Zn^{2+} binding to the cytoplasmic region of rhodopsin (site 1), suggesting that binding at this site is unfavorable both in the monomer and dimer. This is consistent with the MD simulations and this site was therefore excluded in subsequent calculations.

---

[39] The 1GZM structure of rhodopsin (Li et al., 2004a) displayed only a single Zn^{2+} binding site located at the cytoplasmic side (position 1). The earliest crystal structure of rhodopsin, 1F88 (Palczewski et al., 2000), displayed the extracellular binding sites (positions 3 and 4). Crystal structures 1HZX (Teller et al., 2001), 1L9H (Okada et al., 2002), and 1U19 (Okada et al., 2004) displayed Zn^{2+} binding sites within the transmembrane helices and extracellular surface (positions 2-4).

Zn^{2+} binding site	$\Delta G_{monomer}$ (kJ/mol)	ΔG_{dimer} (kJ/mol)
1	- 74	-163
2	91	251
3	136	197
4	70	200

Table 5.2 Change in free energy for Zn^{2+} transfer from its binding sites to bulk water

Free energy values were calculated for the transfer of a single Zn^{2+} ion from its particular binding site in monomeric rhodopsin to bulk water, or for the transfer of a pair of Zn^{2+} ions in dimeric rhodopsin to bulk water. Each site was investigated in the absence of bound Zn^{2+} at the other sites. Zn^{2+} binding sites are shown in **Figure 5.10**.

The change in free energy of the system introduced by the binding of Zn^{2+} (positions 2-4) was computed for both monomeric rhodopsin and dimeric rhodopsin. The difference in free energy between the unbound and bound states of a rhodopsin monomer (ΔG_1) is –309 kJ/mol and that for rhodopsin dimer (ΔG_2) is –596 kJ/mol. This suggests that in both cases the Zn^{2+} bound state of rhodopsin is thermodynamically more stable than the unbound state. These calculations support my experimental SMFS results suggesting the stabilizing effect of Zn^{2+}on rhodopsin.

5.4 DISCUSSION

Free and loosely bound Zn^{2+} was most likely absent in disc membrane preparations used in previous and current SMFS studies since EDTA was included in buffers used to prepare those membranes (**Chapter 4**). F-D curves obtained from the membranes, therefore, represent the pulling of rhodopsin in the absence of Zn^{2+} ions, except for those bound to transmembrane region of the receptor, which is inaccessible to the Zn^{2+} chelator EDTA, and perhaps some residual loosely bound Zn^{2+}. The inclusion of $ZnCl_2$ in the assay buffer resulted in an increase in the unfolding forces for most of the stable structural segments. The location of the stable structural segments, however, remained unchanged. The increase in force required to unfold each stable structural segment is concentration dependent, and the maximal increase was attained at ~100 μM of added $ZnCl_2$. The additional force required to unfold the various segments of rhodopsin in the presence of Zn^{2+} suggests that the bivalent ion stabilizes the receptor.

5.4.1 Specific effect of Zn^{2+}

The apparent stabilizing effect of Zn^{2+} cannot be mimicked by the bivalent ions Ca^{2+}, Co^{2+}, Cd^{2+}, and Cu^{2+}. Zn^{2+} can bind to purified rhodopsin, rhodopsin in disc membranes, (Shuster et al., 1992; Stojanovic et al., 2004) and rhodopsin in three-dimensional crystals (Li et al., 2004a; Okada et al., 2002; Okada et al., 2004; Palczewski et al., 2000; Teller et al., 2001). The binding of Zn^{2+} appears to be specific since no other bivalent ion except Cu^{2+} can fully compete off radioactive labeled Zn^{2+} bound to rhodopsin in disc membranes (Shuster et al., 1992). Cd^{2+} and Co^{2+} can partially compete with Zn^{2+}, providing an explanation for the ability of these metal ions to mimic the effect of Zn^{2+} at some of the structural segments. The specificity of the Zn^{2+} binding sites is further supported by the observation that Zn^{2+} induced effects on the thermal bleaching of rhodopsin cannot be mimicked by any of the bivalent ions considered here (del Valle et al., 2003). This suggests that the apparent stabilizing effect of Zn^{2+} on the rhodopsin structure occurs through specific interactions of the receptor with the bivalent metal ion.

5.4.2 Zn^{2+} binding has a global effect on rhodopsin

Studies on *retinitis pigmentosa* causing point mutations in rhodopsin revealed the tight functional and structural coupling of transmembrane domains and the extracellular folding core (Hwa et al., 1997; Hwa et al., 2001; Rader et al., 2004). Mutations in the transmembrane domain lead to breaking of the native Cys110-Cys187 bond causing misfolding and malfunctioning of the receptor. In such a scenario it is difficult to imagine the independent co-existence of these two domains in the molecule. It has, therefore, been proposed that the folding of rhodopsin is a highly cooperative process and that long-range interactions contribute to the stability and function of the protein (Klein-Seetharaman, 2005). Within such a framework, the effect of changes at one location in the protein will not be localized or confined to that region, but rather propagate to other areas resulting in global effects rather than only local ones.

There are no studies so far that address whether the effect of Zn^{2+} on rhodopsin is local or global. The global changes in the molecular interactions upon Zn^{2+} binding, as observed in the SMFS study presented here, corroborates with the hypothesis of cooperative folding of rhodopsin. The binding of Zn^{2+} does not change the molecular interactions of a single stable structural segment, but increases the force required to unfold most of the detected stable structural segments. This points to a stabilizing effect that is not confined locally to regions in close proximity to Zn^{2+} binding sites, but rather being relayed throughout the molecule. In contrast to rhodopsin, binding of the ligand Na^{+} to the *E.coli* Na^{+}/H^{+} antiporter NhaA results in a highly localized effect without altering the molecular interactions in the neighboring helices as detected by SMFS (Kedrov et al., 2005). The localized effect of Na^{+} binding significantly enhances an existing molecular interaction detected by a single force peak in the F-D spectra. This effect is not observed in absence of the ligand. The increased force peak likely results from interactions established within the region of the ligand-binding site in NhaA (Kedrov et al., 2005).

Although the global effect of Zn^{2+} increases the unfolding forces of stable structural segments, the magnitude of these changes differs across the segments. Surprisingly, the C-terminal region (CT) showed a marked increase in stability in the presence of Zn^{2+}. Since most of the receptor molecule is unfolded out of the membrane, all of the molecular interactions with the rest of the receptor will be absent. Neglecting a memory effect, what could be the origin of this stability effect at the C-terminal end? Assuming a dimeric model of rhodopsin, the C-terminal region would be in contact with an adjacent rhodopsin molecule (Fotiadis et al., 2004). The increase in force of this segment may therefore derive from molecular interactions involving regions in the partner rhodopsin molecule. It is evident that the global effect of Zn^{2+} manifests in different ways at each of the stable structural segments. The relation of these changes to the functional role of the molecule requires further investigation.

5.4.3 Is the effect of Zn^{2+} binding in rhodopsin physiologically relevant?

Zn^{2+} binding sites considered in the computation of free energy values are those that have been determined from high-resolution crystal structures of rhodopsin in its inactive state (Li et al., 2004a; Okada et al., 2002; Okada et al., 2004; Palczewski et al., 2000; Teller et al., 2001). However, a site that bridges a non-physiological dimer interface occurring only in 3-D crystals was ignored in the computational calculations (Okada et al., 2002; Palczewski et al., 2000). Since the concentration of Zn^{2+} under crystallization conditions is extremely high (65-90 mM), all of the sites considered here may not be physiologically relevant. The Zn^{2+} binding site buried within the transmembrane helices (Glu122 and His211) has been confirmed by mutagenesis studies (Stojanovic et al., 2004), and therefore is a likely physiologically relevant site. The naturally occurring point mutation, His211Pro, in this region causes misfolding and leads to *retinitis pigmentosa*.

Misfolding of this and other point mutations results in the replacement of the native stabilizing disulfide bond between Cys110 and Cys187 for the non-native disulfide bond between Cys185 and Cys187 (Hwa et al., 2001). The disruption of the Zn^{2+} binding site involving His211 has been proposed to underlie the mechanism of these effects (Stojanovic et al., 2004). The effect of Zn^{2+} on the ratio of F-D curves corresponding to the pulling of rhodopsin in presence of the native disulfide bond to the pulling of rhodopsin in absence of the native disulfide bond is consistent with this proposal. Increasing the Zn^{2+} concentration favors the F-D curves of length ~65 nm, indicating an apparent stabilizing effect of Zn^{2+} in maintaining the native Cys110-Cys187 disulfide bond. This points to a physiological role for Zn^{2+} in the structure and function of rhodopsin that involves the stabilization and promotion of proper folding of the receptor molecule.

5.4.4 Increase in thermodynamic stability by Zn^{2+}

It has been shown in previous studies on soluble proteins that there need not exist a correlation between mechanical stability and thermodynamic stability of a protein (Brockwell et al., 2002). A protein may be mechanically stable but unstable thermodynamically or vice-versa. To determine if, similar to an increase in the unfolding forces, addition of Zn^{2+} resulted in increased thermodynamic stability, FEP method was used to calculate the difference in the free energy between monomeric and dimeric rhodopsin in the presence and absence of bound Zn^{2+}. The negative ΔG value obtained from these computations indicates a more thermodynamically stable receptor molecule when Zn^{2+} occupies sites on the protein. This supports the notion that Zn^{2+} plays a stabilizing role on the structure of rhodopsin.

Stability of rhodopsin inferred from thermal bleaching studies suggests a decreased thermal stability of the protein in the presence of 15-100 μM Zn^{2+}, as shown by an increased rate of thermal bleaching in solution and in ROS membranes (del Valle et al., 2003; Stojanovic et al., 2004). The effect of low Zn^{2+} concentration (10 μM) during rhodopsin folding in COS-1 cells, on the other hand, suggests the presence of a stabilizing Zn^{2+} binding site in a solvent inaccessible transmembrane site, as determined by a decreased rate of thermal bleaching (Stojanovic et al., 2004). Thus, based on thermal bleaching measurements it was concluded that rhodopsin consists of destabilizing low-affinity Zn^{2+} binding sites exposed at the extracellular and cytoplasmic domains, and a stabilizing high-affinity site buried in the transmembrane domain. The discrepancy in the determination of receptor stability from thermal bleaching data and that by SMFS measurements and FEP calculations from the current study can be attributed to the difference in the two experimental assays. Thermal bleaching assays detect the effects on the structure of the receptor indirectly by measuring the hydrolysis of the chromophore. Whereas, SMFS detects the molecular interactions directly occurring within a protein, and may therefore provide a better measure of protein stability. Moreover, it would be wrong to assume a direct correlation between the hydrolysis rate of the chromophore and the structural stability of rhodopsin. Though a ‘destructive’ assay, the higher resolution and sensitivity of SMFS enables to probe the origin of molecular interactions at the level of a single helix to a few amino acids.

5.4.5 Zn^{2+} binding and dimerization of rhodopsin

A closer examination of the putative Zn^{2+} binding sites considered in the current study shows that the sites line up along the dimer interface of rhodopsin, which has been proposed based on the packing constraints from AFM studies (**Figure 5.10**) (Fotiadis et al., 2004; Liang et al., 2003). Oligomerization of rhodopsin and other GPCRs has only recently become an appreciated concept, and likely plays a central role in the signaling process (Park et al., 2004). Little is known of the structural impact of oligomerization in rhodopsin or any other GPCR.

The binding of Zn^{2+} changes the electrostatic potential of the putative dimer interface of rhodopsin (**Figure 5.11**). The electrostatic interaction at the dimer interface must be optimized for dimerization to occur. Two contact areas determine the interface between rhodopsin monomers (**Figure 5.10**). In the absence of bound Zn^{2+} (**Figure 5.11**(**A**)), the contact area at the cytoplasmic side is characterized with a slightly positive electrostatic potential that will not prevent the dimerization of rhodopsin. In contrast, the contact area at the extracellular side has a strong negative potential which will introduce a strong repulsion and thereby hinder dimerization. Binding of Zn^{2+} to all 8 sites determined from crystal structures eliminates the repulsive negative electrostatic potential at the extracellular contact area (**Figure 5.11**(**B**)). However, the electrostatic potential at the cytoplasmic contact area becomes strongly positive and therefore repulsive. The optimal electrostatic potential at the dimer interface of rhodopsin occurs when all the Zn^{2+} binding sites are occupied except for the site at the cytoplasmic surface (**Figure 5.11**(**C**)). The binding of Zn^{2+} therefore appears to be required for the optimization of electrostatic interactions at the dimer interface of rhodopsin.

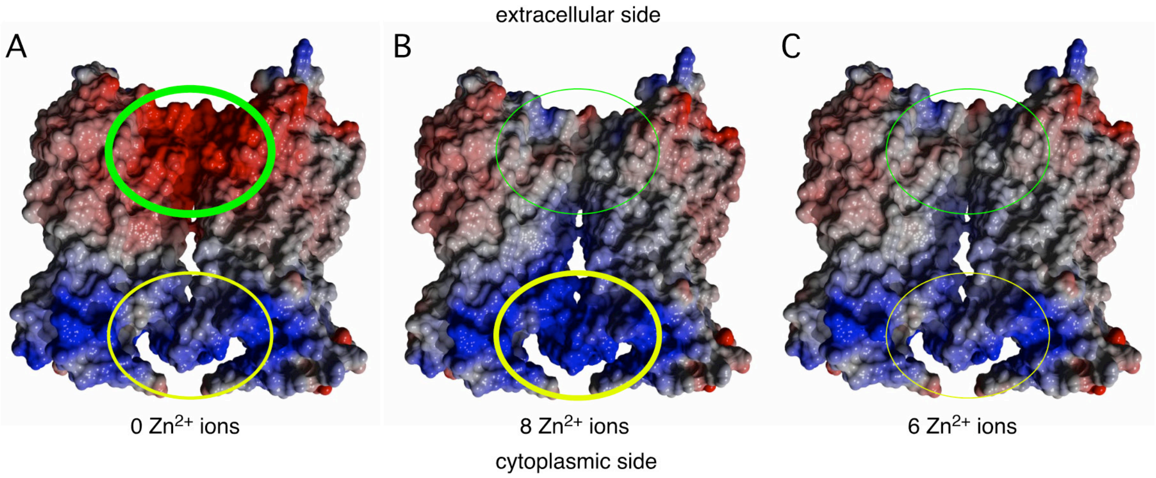

Figure 5.11 Changes in electrostatic potential of rhodopsin dimer in the presence of Zn^{2+} ions

A high negative potential (red region outlined by bold green oval), on the extracellular side of a rhodopsin, in the absence of Zn^{2+} ions might be detrimental to the dimerization of rhodopsin. A slight positive potential (blue region outlined by yellow oval) at the dimer interface may not interfere in the dimerization process. (**B**) On binding 8 Zn^{2+} ions, the extracellular side of rhodopsin shows a decreased negative potential and an increased positive potential (blue area outline by bold yellow oval) on the cytoplasmic side. The optimum electrostatic potential for dimerization could be reached on binding 6 Zn^{2+} ions (**C**). The thickness of the green and yellow ovals denotes the favorable and unfavorable electrostatic interactions (bold – unfavorable, thin – favorable). (Images courtesy of Dr. Slawomir Filipek, IIMCB, Poland).

The negative ΔG values on Zn^{2+} binding in both monomeric and dimeric rhodopsin suggest a stabilizing role for Zn^{2+} in both the forms. The ΔG for the dimer is even smaller than that for two monomers, implying a possible role of Zn^{2+} in promoting and stabilizing rhodopsin dimers. This presents an intriguing proposal of Zn^{2+} as a determinant for the oligomerization of rhodopsin and other GPCRs. However, further studies are required to experimentally confirm this concept.

Oligomerization of bacteriorhodopsin appears to stabilize the structure of each protein molecule. SMFS on monomeric, dimeric and trimeric forms of bacteriorhodopsin in purple membranes displays similar mechanisms of membrane protein stabilization as that observed in the current investigation (**Chapter 3**). F-D curves of bacteriorhodopsin show higher forces to unfold stable structural segments with increasing oligomeric complexity. Bacteriorhodopsin molecules present as monomers exhibit the lowest stability, while those forming trimers exhibit the highest stability. The naturally occurring oligomerization of bacteriorhodopsin into trimers enhances the stability of almost every structural segment established within the molecule. Similar to rhodopsin, some structural segments were stabilized to a greater extent than others. The assembly of bacteriorhodopsin into trimers appears to be a natural mechanism to enhance the stability of the protein, thereby allowing for proper function under the harsh environmental conditions of *H. salinarum*. A similar stabilizing mechanism may also be present in rhodopsin dimers or oligomers. The localization of putative Zn^{2+} binding sites at the dimer interface of rhodopsin suggests that the metal bivalent ion modulates the interaction between adjacent rhodopsin molecules, thereby enhancing the stability and function of the receptor.

5.5 CONCLUSIONS & FUTURE GOALS

Vision-related disorders, such as impaired dark adaptation, night blindness and retinal degeneration symptoms reminiscent of *retinitis pigmentosa*, caused by mutant forms of rhodopsin reported in human Zn^{2+} deficiency[40] (McClain et al., 1985; Morrison et al., 1978) could occur due to decreased rhodopsin formation (Dorea and Olson, 1986), a process that can be correlated to the stability of the molecule. The study described here clearly shows a specific effect of Zn^{2+} on the mechanical and thermodynamic stability of rhodopsin. Although the free concentration of Zn^{2+} in the photoreceptor cells is unknown[41], if the concentration is comparable to that found in the brain then it could

---

[40] It is possible that Zn^{2+} deficiency depresses the level of plasma and liver retinol binding proteins, resulting in a failure to mobilize vitamin A from liver stores (Grahn et al., 2001). The impact of Zn^{2+} deficiency on vitamin A metabolism in the retina has not been studied.

[41] The mean Zn^{2+} concentration in the adult human retina is ~464 μg/g dry weight (Grahn et al., 2001).

potentially be in the micromolar range (Frederickson, 1989). From a Zn^{2+} concentration titration curve I could determine the EC_{50} values for the stable structural segments containing the putative Zn^{2+} binding sites. The unfolding pathways of rhodopsin at different Zn^{2+} ion concentrations suggest a change in molecular interactions upon Zn^{2+} binding; a similar effect for Ca^{2+}, Cd^{2+} or Co^{2+} could not be observed. The most common *retinitis pigmentosa* mutant, His211Pro, results in the disruption of the native disulfide bond between Cys110 and Cys187 and the mechanism of its action has been proposed to involve disruption of Zn^{2+} binding (Stojanovic et al., 2004). Though at high Zn^{2+} concentrations the native disulfide bridge was preserved, however, the effect of an electrostatic effect can not be completely ruled out. The Zn^{2+} ions were found to line up along the dimeric interface of rhodopsin suggesting a possible role of the bivalent ion in dimerization of rhodopsin. Thus, the stabilizing effect of Zn^{2+} on rhodopsin, observed under the experimental conditions of the current study, suggest a physiological relevance. Since rhodopsin is a prototypical member of the GPCR superfamily (Filipek et al., 2003b), the potential physiological role of Zn^{2+} in signaling and stability may therefore not be restricted to rhodopsin, but may also extend to other members of the GPCR family. All in all, the results presented here could have far reaching implications on the dimerization process and the associated signaling process of rhodopsin and other GPCRs.

One of my next goals is to develop a novel experimental approach to determine the thermal noise of a single rhodopsin molecule in the presence and absence of bound Zn^{2+} ions using a very sensitive AFM cantilever as the probe. Promising results have been obtained with initial MD simulations where a change in the RMSD (root mean square deviation) values was seen with and without Zn^{2+} for some regions of rhodopsin. The development of such a method would enable one to detect ligand binding for any membrane protein without mechanically destroying it.

Chapter

6

GENERAL CONCLUSIONS

Since its advent, the AFM has proved to be an indispensable tool to biophysicists in studying protein mechanics. SMFS with AFM has given valuable insights into the interactions network of soluble and membrane proteins in conjunction with helping to determine the validity of protein (un)folding energy landscapes.

In the work presented here, using BR and rhodopsin as model membrane systems, I have convincingly shown that with the proper design of experiments and controls, SMFS could shed light on important physiological processes at the single-molecule level so far hidden in the complexity of a whole population. Interesting details about the stabilizing mechanisms of membrane proteins were obtained from unfolding studies of BR using different oligomeric assemblies, viz., trimer, dimer and monomer (**Chapter 3**). I found that the force required to unfold a single BR molecule from a trimeric assembly was higher than that from a monomeric assembly, indicating an increase in the intrinsic stability of up to 70% from monomer to dimer to trimer. From the difference in the unfolding forces of BR in the trimeric and monomeric assemblies it was possible to calculate the contribution of inter- and intramolecular interactions to the membrane protein stabilization. In contrast, the different BR assemblies had no influence on the unfolding intermediates although the occurrence probability of unfolding a BR molecule via a certain pathway changed, suggesting different energetic or kinetic contributions of the preferred unfolding pathways in the different assemblies.

Native bovine rhodopsin was unfolded in the dark or the inactive state to decipher the stabilizing interactions between helices. I could detect two structural states corresponding to the presence and the absence of the native disulfide bond between Cys110 and Cys187 (**Chapter 4**). It was found that the interhelical interactions in rhodopsin changed in absence of the Cys110-Cys187 bond as compared to when it is present. The interactions in the Cys110-Cys187 bond absent structural state could be extrapolated to the rhodopsin mutants which lead to the breakage of this highly conserved bond leading to diseases like *retinitis pigmentosa*. Thus the altered interactions underscore the significance of the disulfide bridge in maintaining the functional and structural integrity of the molecule. Interestingly, it was seen that the highly conserved residues among GPCRs were located in the interior of individual stable structural segments in the state where the Cys110-Cys187 bond was intact. In absence of the disulfide bridge, most of the conserved residues shifted their positions to the ends of the structural segments suggesting a possible structural role for the conserved residues in maintaining the interactions between the stable structural segments.

As a next step, I studied the effect of Zn^{2+} on the stability of rhodopsin (**Chapter 5**). Whereas biochemical experiments have suggested a decrease in thermal stability of rhodopsin in the presence of Zn^{2+}, single-molecule unfolding experiments showed on the contrary. I found that the mechanical stability of most stable structural segments of rhodopsin was specific for Zn^{2+} binding and increased with increasing Zn^{2+} concentrations (0 - 400 μM). The EC_{50} values derived from the concentration-dependent curves, 40 μM and 37 μM for the two stable structural segments suggested to have the putative Zn^{2+} binding sites, approximated the equilibrium dissociation constant, 2-10 μM, for the binding of Zn^{2+} to rhodopsin. The validity of the SMFS experiments was proved computationally by calculating the free energy values using the free energy perturbation method, which showed an increase in the thermodynamic stability of the GPCR in the Zn^{2+} bound state. Moreover, the calculations suggested an enhanced stability for the Zn^{2+}-rhodopsin dimer complex as opposed to the Zn^{2+}-rhodopsin monomer complex, though both were significantly stabilized as compared to the no Zn^{2+} state. In light of the fact that the putative Zn^{2+} binding sites were found to line the dimer interface of rhodopsin, these results suggest a possible contribution of Zn^{2+} ions in the stabilization and the dimeric status of the molecule, important during the signaling process. The success of the SMFS assay here demonstrates that such a technique could be used to identify the interactions of trace metal ions with protein precursors, and would be of tremendous help to study proteins aggregation in various neurodegenerative diseases.

Chapter
7

OUTLOOK & FUTURE GOALS: MECHANICAL UNFOLDING OF MEMBRANE PROTEINS – AN UNEXPLORED GOLDMINE?

7.1 MECHANISM OF HELIX UNFOLDING UNDER FORCE – A HYPOTHESIS

The unfolding mechanism of a transmembrane helix under an externally applied force is still debatable. Does a helix unfold inside the membrane and the unfolded polypeptide chain is extracted (Janovjak et al., 2004), is it extracted from the membrane and then spontaneously unfolds once in the aqueous medium, or is it partially extracted from the water-membrane interface and then unfolds as it is extracted (Ganchev et al., 2004)? All three scenarios are equally possible. Though unfolding simulations suggest that a transmembrane helix is most likely to unfold inside the membrane (Seeber et al., 2006) (unpublished results on rhodopsin in collaboration with Dr. Slawomir Filipek, IIMCB, Warsaw), it should be noted that these MD simulations are done at least six orders of magnitude faster than the unfolding speed in a laboratory experiment[42]. Though a likely scenario under force, under physiological conditions it is highly unlikely that a transmembrane helix unfolds inside the lipid-bilayer and is then extracted, since the entropic costs of such a process would be too high. Though extraction in a first step and spontaneous unfolding in a second step cannot be completely ruled out, the most likely mechanism of unfolding should be a partial extraction at the aqueous-lipid interface and simultaneous unfolding. This mechanism was proposed recently based on AFM SMFS measurements on synthetic transmembrane peptides (Ganchev et al., 2004).

The similar unfolding force of ~160 pN for the helical hairpin constituted by helices III and IV with their connecting loops, and single helix III[43], in two different structural states of rhodopsin detected in SMFS experiments (**Chapter 4**) suggest that the unfolding mechanism in the two cases should be similar. Since transmembrane helices connected by a 'locking' bond (a Cys-Cys bond in this case) cannot be unfolded inside the membrane, nor a transmembrane helix can maintain its helicity in aqueous environment, the best explanation is that the helices are partially extracted and simultaneous unfolded during extraction.

---

[42] It has been shown for bacteriorhodopsin that with increasing loading rates stable structural segments unfold predominantly step-wise rather than in a single step (Janovjak et al., 2004).

[43] The two cases of helix III unfolding could be observed for the two different structural states of rhodopsin, with an intact disulfide bridge between Cys110-Cys187 and with this disulfide bridge broken (**Chapter 4**).

Dynamic force spectroscopy (**DFS**) with AFM involves unfolding a protein at different pulling speeds (Evans, 1999). Plotted as the most probable unfolding force *vs*. $\log_e$ (loading rate), the force spectrum maps the most prominent energy barriers traversed in the energy landscape along the force-driven pathway and exposes the differences in energy between barriers (Evans, 1998; Evans and Ritchie, 1997). The most probable unfolding force, F_p, can be described as,

$$F_p = \frac{k_B T}{x_u} \ln\left(\frac{x_u r_f}{k_B T k_u}\right) \tag{7.1}$$

where r_f is the loading rate and the other symbols have the same meaning as before (**section 2.2.1**).

DFS measurements on rhodopsin molecules with the Cys110-Cys187 intact disulfide state showed that the x_u values for most stable structural segments were similar (**Figure 7.1**, **Table 7.1**). For the stable structural segment constituted of H3, H4, C2 and E2 together, $x_u = 0.21 \pm 0.02$ Å, and for the structural segment made of H5, C3, $x_u = 0.25 \pm 0.03$ Å. These values further support my argument that the unfolding mechanism for the two cases cannot be different and helices are extracted and unfolded simultaneously. However, it should be noted that the x_u values range between 0.21 and 0.47 Å. This variation could be a result of the different amino acid sequences of the structural segments. Pulling polypeptide chains of amino acid sequences exhibiting varied hydrophobicity would help understand the contribution of different amino acids in determining the unfolding intermediates during mechanical unfolding.

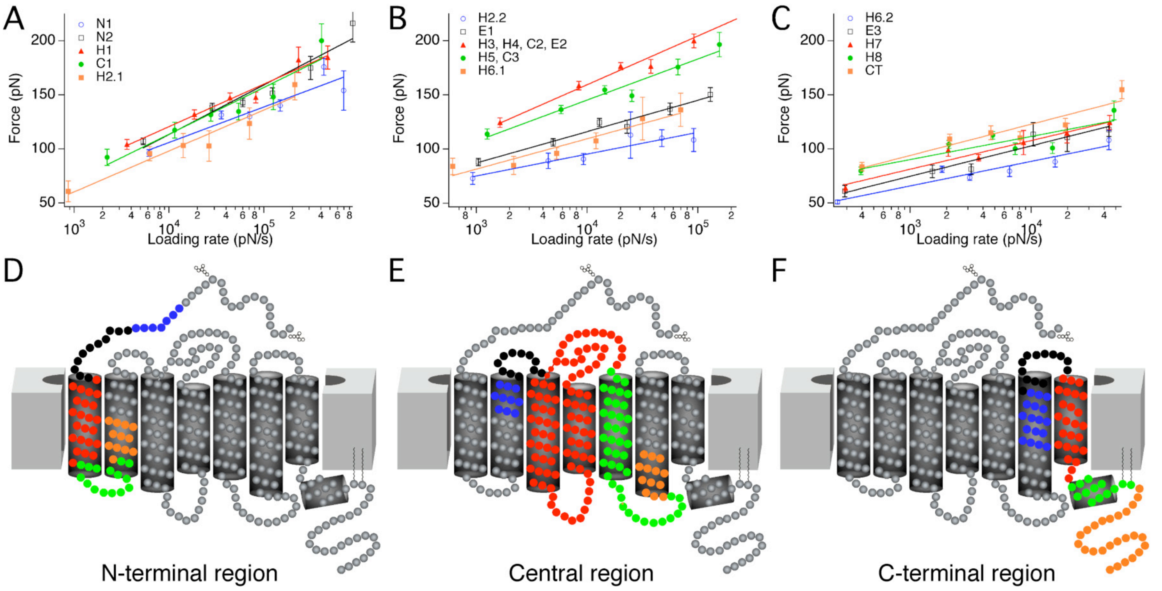

Figure 7.1 Dynamic force spectroscopy of rhodopsin with the Cys110-Cys187 disulfide bridge intact

Unfolding rhodopsin at different pulling speeds gives a measure of the width of the potential barrier x_u, and the unfolding rate k_u for the different stable structural segments by fitting the data to equation 7.1. Colors of the data points and the fits (**A-C**) correspond to the color code of the stable structural segments in **D-F**. Error bars shown are standard errors of the mean (SEM).

Stable structural segment	x_u (± SD) (Å)	t_u (± SD) (s)
N1	0.29 ± 0.06	2.4 ± 4.4
N2	0.21 ± 0.03	0.6 ± 0.6
H1	0.24 ± 0.02	2 ± 1.5
C1	0.22 ± 0.04	0.8 ± 0.8
H2.1	0.25 ± 0.03	0.6 ± 0.5
H2.2	0.47 ± 0.09	47.2 ± 91.2
E1	0.33 ± 0.03	12.7 ± 9.5
H3, H4, C2, E2	0.21 ± 0.02	6.8 ± 4.3
H5, C3	0.25 ± 0.03	11.1 ± 10.1
H6.1	0.34 ± 0.05	9.9 ± 11.4
H6.2	0.42 ± 0.07	7.8 ± 9.6
E3	0.34 ± 0.04	5.5 ± 5.1
H7	0.36 ± 0.04	13.5 ± 12.7
H8	0.44 ± 0.14	152.5 ± 513
CT	0.33 ± 0.06	22.2 ± 34.2

Table 7.1 Values of widths of potential barriers (x_u) and stability (t_u) of stable structural segments of native rhodopsin

The x_u is calculated from the slopes of the fits in **Figure 7.1**. t_u is the inverse of the unfolding rates (k_u) also derived from the linear fits in **Figure 7.1**.

Futhermore, the pairwise unfolding of helices, e.g., helices E and D, and helices B and C, in bacteriorhodopsin could be assumed to be similar to the unfolding of helices III and IV connected with the disulfide bond Cys110-Cys187 in rhodopsin. The unfolding forces for helices E and D together and individual helix E in BR are similar, ~151 pN and

~155 pN, respectively. Also, the unfolding forces for helices B and C together and individual helix B (or C) are similar, ~107 pN and ~91 pN (~101 pN), respectively (**Chapter 3**). Moreover, the force for pairwise unfolding of helices E and D of native trimeric bacteriorhodopsin at 300 nm/s, ~150 pN, is the same as that for unfolding the stable structural segment H3, H4, C2 and E2 in rhodopsin, ~158 pN, at a similar speed of 349 nm/s. These results indicate that the unfolding of a pair of helices or an individual helix inside the membrane and then being pulled out of the lipid bilayer, as proposed previously, may not be a likely scenario (Janovjak et al., 2004). Though the amino acid sequences of these structural segments from different membrane proteins are not identical, in the light of above arguments it could be suggested that unfolding of stable structural segments follows a mechanism of simultaneous extraction from the membrane bilayer while being unfolded in the aqueous environment.

7.2 EFFECT OF POINT MUTATIONS ON THE COMPLEX UNFOLDING ENERGY LANDSCAPE OF BR

In **Chapter 1**, I discussed the importance of studying protein folding. To understand the nature of membrane protein folding and why a given sequence evolves to a particular structure, the function of a structural domain, and what leads it to misfold or misassemble, it is very crucial to explore the molecular interactions within the molecule. An important and necessary step to understand protein folding is to establish, as far as possible, a generalized functional, structural and stability role of each amino acid or a protein domain. The widespread occurrence of proline residues in the TM α-helices of integral membrane proteins, as compared to the α-helices of soluble proteins (Barlow and Thornton, 1988; Brandl and Deber, 1986; Reiersen and Rees, 2001), underscores their importance in structural and functional roles (Labro et al., 2001; Sansom and Weinstein, 2000; Shelden et al., 2001; Williams and Deber, 1991). Furthermore, it has been suggested that proline residues may play an important role in the folding of membrane proteins (Lu et al., 2001).

To understand the contribution of single amino acids in membrane protein unfolding under force, I unfolded five different single point mutants of BR - P50A, P91A, P186A, M56A and Y57A (**Figure 7.2**(**A**)) (Faham et al., 2004; Yohannan et al., 2004b). These mutations presented an opportunity to answer many relevant questions. The point mutations in the kinked helix B (P50A, M56A and Y57A), kinked helix C (P91A) and kinked helix F (P186A) which do not change the structure but alter the stability of BR differently[44], offer clear advantages to confirm the role of the kinks in the kinetic stability and unfolding landscapes with relation to their thermodynamic stability. All the mutants have well preserved structural features (the kink) similar to WT BR.

Using a combination of DFS with AFM and bioinformatics tools, I identified the molecular nature of the unfolding barriers hosting the mutations. Moreover, the idea was to determine the effect of mutations on the unfolding energy landscapes. The one most important question – how does changing a single amino acid alters, if at all, the energy landscape of the molecule? – was answered by characterizing the unfolding barriers by a comparative analysis of the atomic details of the packing interactions that surround the evolutionarily conserved proline kinks.

7.2.1 Changes in intramolecular interactions alter the preferred unfolding routes on the energy landscape

Since the intermediates that occur during unfolding could be determined, it was possible to construct the complete unfolding pathways of single BR molecules taking into consideration all the secondary structure elements (helices A to G). It should be noted that in the previous studies, the unfolding pathways of paired helices instead of the whole molecule have been considered (**Chapter 3**) (Janovjak et al., 2004; Müller et al., 2002b). Statistical analyses of all the possible unfolding pathways for each BR sample showed the existence of a major pathway and an exponentially decreasing distribution of all the pathways. At all unfolding speeds[45], I observed that certain pathways occurred with a higher frequency in WT BR than in a given mutant and vice-versa. The distribution of unfolding pathways at 87.2 nm/s clearly shows that the probability of unfolding pathways is drastically changed for all mutants (**Figure 7.2**). **Table 7.2** shows the occurrence probabilities of the most statistically significant unfolding pathways for WT BR and the mutants P50A and M56A.

---

[44] SDS unfolding experiments have shown that replacing the kink-inducing proline at position 50 with alanine (P50A) did not alter BR stability ($\Delta\Delta G_u = 0.1 \pm 0.1$ kcal/mol) or the kink angle. M56A, on the other hand, was found to be the most stabilizing mutation ($\Delta\Delta G_u = 1.4 \pm 0.1$ kcal/mol), whereas Y57A had the maximum destabilizing effect with an associated change in ΔG_u of -3.7 ± 0.5 kcal/mol (Faham et al., 2004). Both P91A and P186A were found to be destabilizing with $\Delta\Delta G_u$ values of -1.3 ± 0.3 and -0.9 ± 0.1 kcal mol^{-1}, respectively. However, no global changes in the X-ray crystal structures of P91A and P186A were seen, though local structural alterations around the kink region of the helices were observed (Yohannan et al., 2004b).

[45] Each BR mutant was unfolded at 6 different speeds, viz., 87.2 nm/s, 300 nm/s, 600 nm/s, 1310 nm/s, 2320 nm/s and 5230 nm/s.

The difference in frequency of the same unfolding pathway between the WT and the mutants suggested that a small change in the sequence and consequently structural rearrangements, leading to changes in inter- and intra-helical interactions, might be responsible for this observed difference. In order to investigate this relationship, the intramolecular contacts within a given unfolding barrier or stable structural segment in WT BR and the mutants were determined (**Figure 7.3**). In these analyses, the probabilities of different unfolding pathways only at the two lower speeds of 87.2 nm/s and 300 nm/s were analyzed since at lower speeds the molecule possibly probes more unfolding intermediates as compared to higher speeds. Although forced unfolding is a process carried out far from equilibrium, unfolding at a lower speed would occur under quasi-equilibrium conditions mimicking native like unfolding. It is important to mention that at all speeds no differences in the unfolding forces of the stable structural segments of the mutants as compared to WT BR were seen.

	Contour length from C-terminus (aa)								Speed (nm/s)	Probability (%)		
	88	94	105	148	158	175	219	232		WT	P50A	M56A
Peak occurrence in unfolding pathways	1	1	1	1	1	0	1	0	**87.2**	10.1	1.9	1
	1	0	1	1	1	1	1	0		8.9	5.8	2.1
	1	1	1	1	1	1	1	0		7.6	1.9	4.2
	1	0	0	1	0	1	1	0		7.6	15.3	11.4
	1	1	1	1	0	1	1	1		5.1	1.9	2.1
	1	0	0	1	0	0	1	0	**300**	18.2	9.3	35.5
	1	0	1	1	1	0	1	0		9.9	4.2	2.6
	1	1	0	1	0	0	1	0		9.9	1.7	6.6
	1	0	1	1	0	0	1	0		9.4	2.5	9.3
	1	0	0	1	0	1	1	0		5	16.9	11.8

Table 7.2 Unfolding pathways of WT BR, P50A and M56A

The various unfolding barriers that occur during unfolding of WT BR were described in **Chapter 3**. The occurrence probabilities of the unfolding pathways change for the mutants P50A and M56A as compared to WT BR. ‘1’ denotes the presence of a peak and ‘0’ denotes a missing peak at the specified positions. The occurrence of certain peaks in these mutants could be correlated to molecular interactions in the corresponding unfolding barriers (**Figure 7.3**).

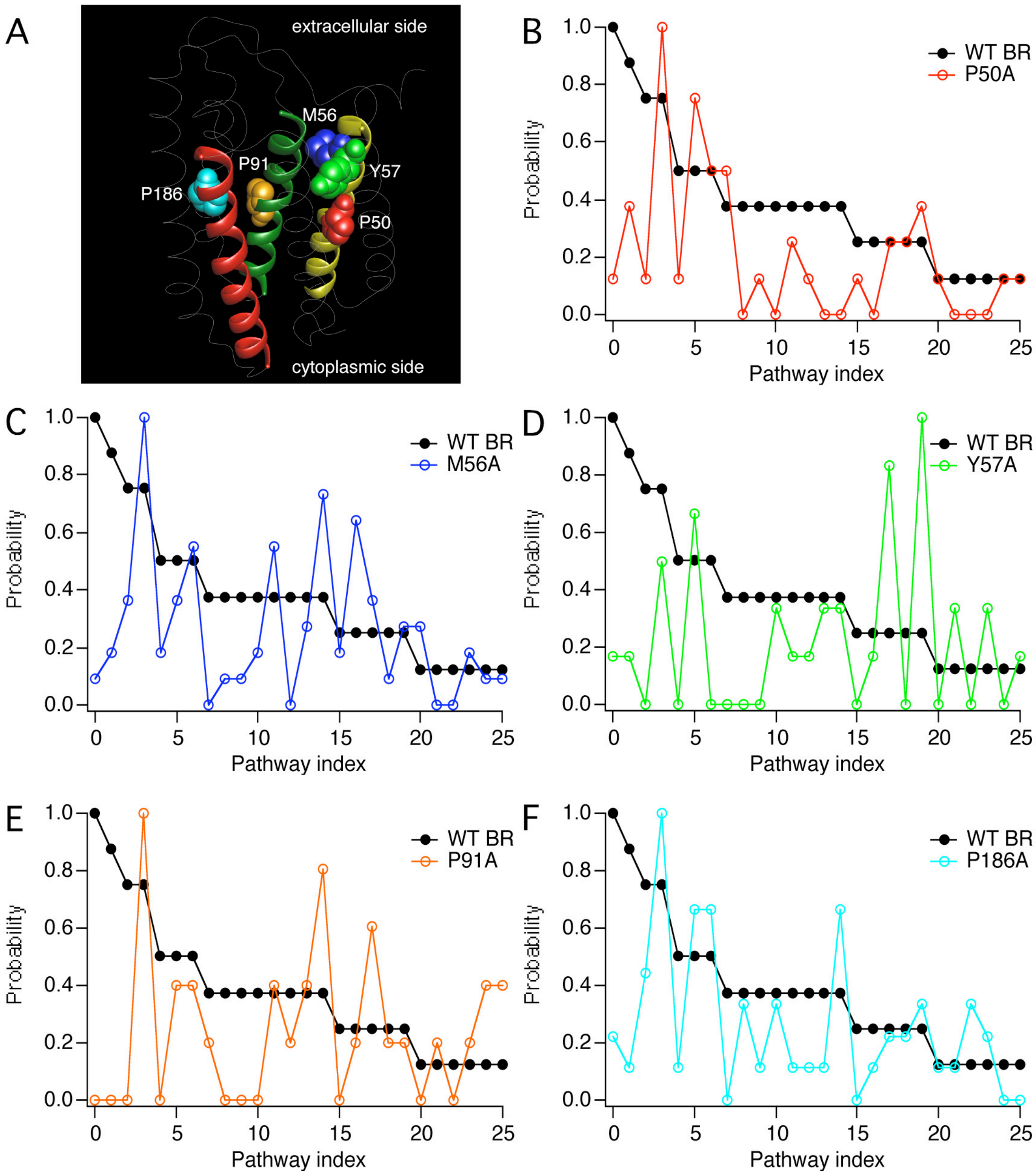

Figure 7.2 Occurrence probabilities of unfolding pathways of WT BR and the mutants

(**A**) BR monomer (PDB: 1AT9) (Kimura et al., 1997) showing the mutations at positions P50 (red), M56 (blue), Y57 (green) in helix B, P91 (orange) in helix C, and P186 (cyan) in helix F. (**B-F**) Unfolding pathways of WT BR and the mutants were constructed from the unfolding intermediates. Each pathway was codified as a string of '0' and '1', where '1' corresponds to a sequence position denoting the presence of a peak, and '0' corresponds to a sequence position where the given peak is missing (**Table 7.2**). To determine the speed dependence of the pathways, as a first step, the unfolding pathways of WT BR were determined at every unfolding speed. For a specific unfolding speed, these pathways were then arranged in a descending order of occurrence and given an index number, '1' being the pathway occurring with the highest probability. The unfolding pathways of the mutants at that speed were arranged in the same order irrespective of the occurrence probability. A similar procedure was followed at all speeds. A comparison of the occurrence probabilities between the mutants and WT BR is shown in (**B-F**) for 87.2 nm/s. As shown, the probabilities varied considerably for some unfolding pathways due to changes in intramolecular interactions. The colors of the amino acids in (**A**) correspond to the traces in (**B-F**).

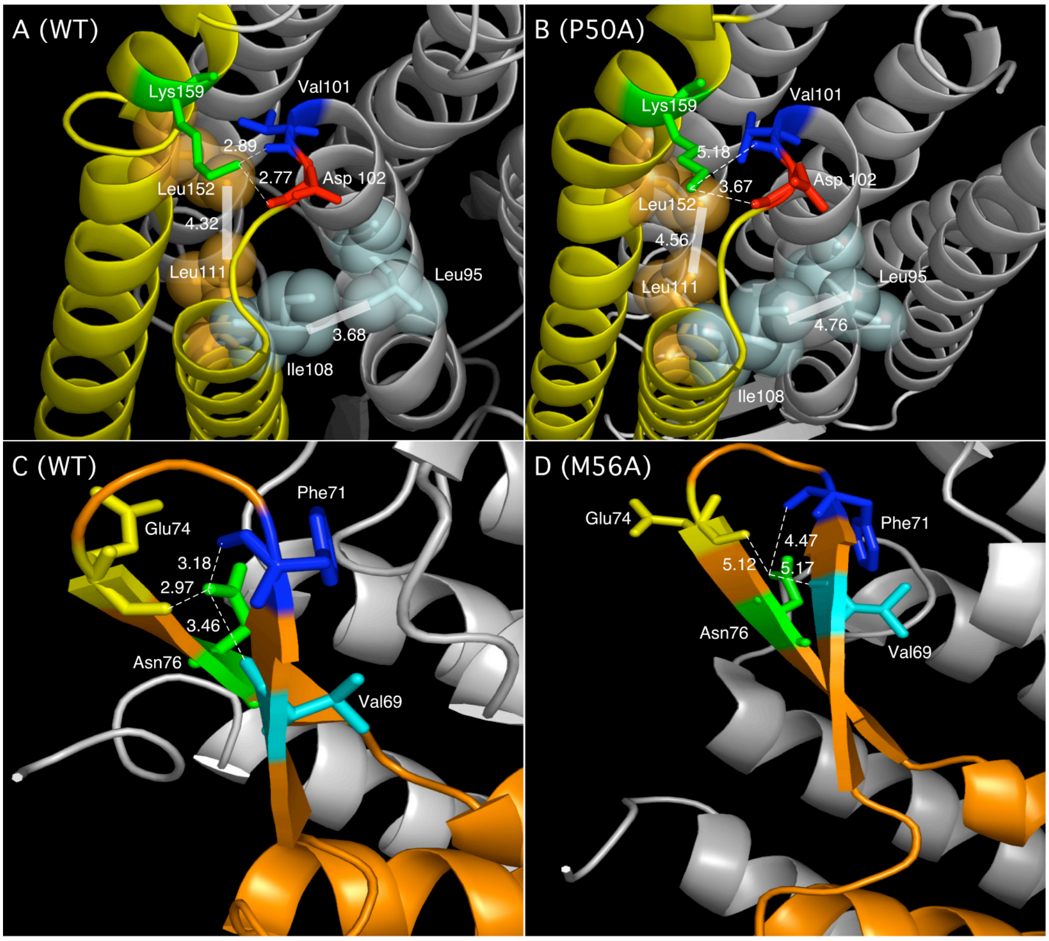

Figure 7.3 Changes in molecular interactions in WT BR, P50A and M56A

(**A**) In the WT, a small network of hydrogen bonds is present at the cytoplasmic ends of helices E and D (Asp102-Lys159-Val101). This small network could be the reason for the high occurrence probability of the peak at amino acid 94 in most unfolding pathways of the WT compared to the mutant. This network is completely missing in mutant P50A, due to the fact that the Lys159 side chain is oriented in the opposite side with respect to the oxygen atoms of residues Asp102 and Val101 (**B**). The distances between the atoms under such a scenario exceed the allowed threshold for a hydrogen bond (3.5 Å). The representation in spheres denotes the hydrophobic interactions, which are again altered in P50A. The distances between these non-polar amino acids is increased in P50A. (**C**) In WT BR there is a small network of hydrogen bonds in the extra-cellular loop BC, involving residues Val69, Glu74, Asn76 and Phe71. This network correlates very well with the presence of the force peak at amino acid 158 in many of the possible unfolding pathways of the WT. This network of polar contacts is completely missing in loop BC of the mutant M56A (**D**). A possible reason could be the orientation of Asn76 side chain in the opposite direction, with respect to its position in the WT, making bond formation with the backbone oxygen atoms of Val69, Glu74 and Asn76 highly unlikely. The lack of this network in mutant M56A can be associated to the very low probability of the peak at amino acid 158 in the unfolding pathways of this mutant. The numbers denote the distances (Å) between the atoms involved in polar and non-polar contacts.

7.2.2 Mutations and unfolding energy landscape

It is known for proteins like the heat-shock transcription factor of *Kluyveromyces lactis* and the factor for inversion stimulation, Fis, that hydrogen bonding and van der Waals interactions in helix-helix packing interactions, which fix the orientation of each segment of the kinked helices independently, are mediated by highly conserved amino acid residues (Ceruso and Weinstein, 2002). It is easy to imagine that mutating the conserved residues in a protein would change the network of the intra- and interhelical interactions, most likely leading to altered structure, function or both. Unfolding of rhodopsin in presence and absence of the native disulfide bridge Cys110-Cys187 emphasizes the importance of mutations in changing the interhelical interactions between conserved residues leading to a change in the unfolding pathways (**Chapter 4**). In corroboration, the current results suggest that a change in the free energy associated with a single amino acid change is enough to perturb the unfolding landscape of the molecule, which might affect the folding efficiency of a protein. As a first approximation, if folding involves the same interactions as detected in unfolding, the high occurrence of certain intermediates, which might be energetically unfavorable, could denote the pathways leading to misfolding or misassembly of the molecule. However, at present it is difficult to ascertain which pathways lead to the native folded state and which to the non-native or misfolded states. More elaborate experimental work in conjunction with MD simulations is needed to shed light on the contribution of each pathway in the folding, misfolding and misassembly of a protein.

7.2.3 Physiological relevance of energy landscapes

The physiological relevance of such a study could be immense. Protein folding/misfolding in the ER happens via multiple steps, involving both chemical reactions and multiple protein molecules. Different combinations of these steps would give rise to multiple folding and misfolding pathways, as seen *in vitro* with SMFS measurements. The modest folding efficiency for wild-type eukaryotic integral membrane proteins[46] indicates that the energetic balance between folding and misassembly pathways for many proteins is delicate enough to be tipped in a pathological direction by various mutations (Sanders and Myers, 2004). It has been shown that a number of proteins not implicated in diseases could form amyloid like plaques if given the optimum environmental factors like pH, temperature and solvent (Dobson, 2003; Fandrich et al., 2003). Since a mutational change tilts the energy landscape by changing the probability of the preferred unfolding pathways, the effect of small molecules, ligands or other environmental factors could be studied on these mutations to shift the unfolding landscape of the mutant to that of the native one. An example of such an approach could be that of Zn^{2+} binding to rhodopsin, which stabilizes the native Cys110-Cys187 disulfide bridge in the protein increasing the population of native molecules as compared to molecules without the disulfide bond, which is the implicated diseased state. Also, the occurrence probability of different unfolding pathways of native rhodopsin changed with increasing Zn^{2+} concentration as compared to the native state without Zn^{2+}. In my opinion, this could be a very fascinating approach to 'treat' misfolded proteins.

---

[46] <50% for WT CFTR (Kopito, 1999; Seibert et al., 1997) and ~20% for PMP22 (Pareek et al., 1997).

7.3 CAN WE PROBE THE RELATIONSHIP BETWEEN MEMBRANE PROTEIN STABILITY AND FOLDING EFFICIENCY WITH SMFS?

It is still an open question if the molecular identity of the unfolding barriers (stable structural segments) detected during unfolding of a membrane protein using SMFS could be correlated to the intermediates during the folding of the membrane protein. With the advent of force-clamp AFM it is now possible to measure the lifetimes of different conformational states of a protein, and the data corroborated with *in vivo* studies (Bullard et al., 2006; Fernandez and Li, 2004; Wiita et al., 2006). One of the many exciting opportunities that force-clamp offers is determining the lifetimes of (un)folding intermediates in a stable, functional protein and in an unstable, non-functional protein. The *in vivo* implications of such a study would be enormous. Since unstable proteins spend more time in non-native conformations, the ER quality control can probe the stability by measuring the lifetimes of intermediates for these proteins (Sanders and Myers, 2004). If the thermodynamic stability of an integral membrane protein is defined as the equilibrium between the fully folded protein and the Popot-Engelman unfolded state[47], then by measuring the lifetime of intermediates, quality control is effectively probing membrane protein stability. Thus the cell by disposing unstable proteins eliminates proteins that have a high propensity to misfold into kinetically trapped conformations. These steps, though difficult to reconstitute *in vitro*, could be easy to mimic with AFM force-clamp experiments. Such measurements would help identify the kinetically trapped misfolded states, which may be difficult for the cell to degrade.

---

[47] The prefolded state of a polytopic transmembrane domain inserted into the ER membrane by the translocon may have a native-like secondary structure and correct membrane topology, but incomplete or non-native like tertiary and quaternary structure. This state could be similar to the 'unfolded state' defined in the 'two-stage model' for membrane protein folding proposed by Popot and Engelman (Popot and Engelman, 2000).

7.4 THE KLONDIKE GOLD RUSH?

The emerging success of chemical and pharmacological chaperones in “rescuing” membrane proteins from inefficient assembly (Bernier et al., 2004; Morello et al., 2000) presents an exciting opportunity with tremendous medical applications to apply the potential of SMFS and force-clamp to measure the effects of these artificial chaperones on membrane proteins. Confirming a general correlation between membrane protein stability and *in vivo* folding efficiency will be useful because conditions and reagents that enhance protein stability will also increase productive assembly in the ER. Rational drug design based on the principle of stabilizing native membrane proteins could prove to be a powerful strategy in drug discovery. Using SMFS and force-clamp techniques it may be easy to identify trapped conformations or misassembled proteins, and help design and study the effect of new small-molecule drugs, ligands and mutations, and test new conditions where abnormal conformational states can be reversed or avoided. The effect of Zn^{2+} in maintaining the integrity of the Cys110-Cys187 disulfide bond as detected by SMFS proves the validity of this approach (**Chapter 5**). The challenge lies in studying mutations that cause misfolding but are not destabilizing. An interesting strategy could be to use a map of the occurrence probability of unfolding pathways on the energy landscape of the molecule to determine the nature of altered molecular interactions in the misfolded or misassembled states of the protein. I have demonstrated the first examples of such an approach in **Chapter 5** for rhodopsin by showing the effect of Zn^{2+} binding in altering the unfolding energy landscape of rhodopsin leading to increased mechanical and thermodynamic stabilization, and in **section 7.2** for single point mutants of BR.

The human brain has always been fascinated by the unknown, in the search of exploring difficult paths in the hope of something unexpected and ‘big’. Whether the assays based on single-molecule unfolding measurements will bring us out of the ‘depression’ and help us design and screen the so-called ‘golden bullets’ of medicine or would just prove to be another dead-end, it is only with time that we shall have an answer to these questions.

BIBLIOGRAPHY

Abramson, J., Iwata, S., and Kaback, H. R. (2004). Lactose permease as a paradigm for membrane transport proteins. Mol Memb Biol *21*, 227-236.

Abramson, J., Smirnova, I., Kasho, V., Verner, G., Kaback, H. R., and Iwata, S. (2003). Structure and mechanism of the lactose permease of Escherichia coli. Science *301*, 610-615.

Adams, P. D., Arkin, I. T., Engelman, D. M., and Brunger, A. T. (1995). Computational searching and mutagenesis suggest a structure for the pentameric transmembrane domain of phospholamban. Nat Struct Biol *2*, 154-162.

Adams, P. D., Engelman, D. M., and Brunger, A. T. (1996). Improved prediction for the structure of the dimeric transmembrane domain of glycophorin A obtained through global searching. Proteins *26*, 257-261.

Aggett, P. J., and Comerford, J. G. (1995). Zinc and human health. Nutr Rev *53*, S16-22.

Alberts, B., Johnson, A., Lewis, J., Raff, M., Roberts, K., and Walter, P. (2002). Molecular Biology of the Cell, 4th Edition edn (New York, Garland Science).

Allen, S. J., Kim, J. M., Khorana, H. G., Lu, H., and Booth, P. J. (2001). Structure and function in bacteriorhodopsin: the effect of the interhelical loops on the protein folding kinetics. J Mol Biol *308*, 423-435.

Altenbach, C., Greenhalgh, D. A., Khorana, H. G., and Hubbell, W. L. (1994). A collision gradient method to determine the immersion depth of nitroxides in lipid bilayers: application to spin-labeled mutants of bacteriorhodopsin. Proc Natl Acad Sci U S A *91*, 1667-1671.

Altenbach, C., Klein-Seetharaman, J., Cai, K., Khorana, H. G., and Hubbell, W. L. (2001). Structure and function in rhodopsin: mapping light-dependent changes in distance between residue 316 in helix 8 and residues in the sequence 60-75, covering the cytoplasmic end of helices TM1 and TM2 and their connection loop CL1. Biochemistry *40*, 15493-15500.

Altenbach, C., Marti, T., Khorana, H. G., and Hubbell, W. L. (1990). Transmembrane protein structure: spin labeling of bacteriorhodopsin mutants. Science *248*, 1088-1092.

Altenbach, C., Yang, K., Farrens, D. L., Farahbakhsh, Z. T., Khorana, H. G., and Hubbell, W. L. (1996). Structural features and light-dependent changes in the cytoplasmic interhelical E-F loop region of rhodopsin: a site-directed spin-labeling study. Biochemistry *35*, 12470-12478.

Anfinsen, C. B., and Haber, E. (1961). Studies on the reduction and re-formation of protein disulfide bonds. J Biol Chem *236*, 1361-1363.

Anukanth, A., and Khorana, H. G. (1994). Structure and function in rhodopsin. Requirements of a specific structure for the intradiscal domain. J Biol Chem *269*, 19738-19744.

Aridor, M., and Hannan, M. L. (2000). Traffic jam: a compendium of human diseases that affect intracellular transport processes. Traffic *1*, 836-851.

Aridor, M., and Hannan, M. L. (2002). Traffic jams II: an update of diseases of intracellular transport. Traffic *3*, 781-790.

Arkin, I. T., Brunger, A. T., and Engelman, D. M. (1997). Are there dominant membrane protein families with a given number of helices? Proteins *28*, 465-466.

Arselin, G., Giraud, M. F., Dautant, A., Vaillier, J., Brethes, D., Coulary-Salin, B., Schaeffer, J., and Velours, J. (2003). The GxxxG motif of the transmembrane domain of subunit e is involved in the dimerization/oligomerization of the yeast ATP synthase complex in the mitochondrial membrane. Eur J Biochem *270*, 1875-1884.

Ashkin, A. (1997). Optical trapping and manipulation of neutral particles using lasers. Proc Natl Acad Sci U S A *94*, 4853-4860.

Ashkin, A., Schutze, K., Dziedzic, J. M., Euteneuer, U., and Schliwa, M. (1990). Force generation of organelle transport measured in vivo by an infrared laser trap. Nature *348*, 346-348.

Assaf, S. Y., and Chung, S. H. (1984). Release of endogenous Zn2+ from brain tissue during activity. Nature *308*, 734-736.

Badola, P., and Sanders, C. R. (1997). Escherichia coli diacylglycerol kinase is an evolutionarily optmized membrane enzyme and catalyzes direct phosphoryl transfer. J Biol Chem *272*, 24176:24182.

Bahatyrova, S., Frese, R. N., Siebert, C. A., Olsen, J. D., Van Der Werf, K. O., Van Grondelle, R., Niederman, R. A., Bullough, P. A., Otto, C., and Hunter, C. N. (2004). The native architecture of a photosynthetic membrane. Nature *430*, 1058-1062.

Baker, A. A., Helbert, W., Sugiyama, J., and Miles, M. J. (2000). New insight into cellulose structure by atomic force microscopy shows the i(alpha) crystal phase at near-atomic resolution. Biophys J *79*, 1139-1145.

Baker, T. S., and Henderson, R. (2001). Electron cryomicroscopy (The Netherlands, Kluwer Academic Publishers).

Baldwin, J. M. (1993). The probable arrangement of the helices in G protein-coupled receptors. EMBO J *12*, 1693-1703.

Baldwin, R. L., and Rose, G. D. (1999a). Is protein folding hierarchic? I. Local structure and peptide folding. Trends Biochem Sci *24*, 26-33.

Baldwin, R. L., and Rose, G. D. (1999b). Is protein folding hierarchic? II. Folding intermediates and transition states. Trends Biochem Sci *24*, 77-83.

Barlow, D. J., and Thornton, J. M. (1988). Helix geometry in proteins. J Mol Biol *201*, 601-619.

Bell, G. I. (1978). Models for the specific adhesion of cells to cells. Science *200*, 618-627.

Benoit, M., Gabriel, D., Gerisch, G., and Gaub, H. E. (2000). Discrete interactions in cell adhesion measured by single-molecule force spectroscopy. Nat Cell Biol *2*, 313-317.

Berger, O., Edholm, O., and Jahnig, F. (1997). Molecular dynamics simulations of a fluid bilayer of dipalmitoylphosphatidylcholine at full hydration, constant pressure, and constant temperature. Biophys J *72*, 2002-2013.

Berman, H. M., Westbrook, J., Feng, Z., Gilliland, G., Bhat, T. N., Weissig, H., Shindyalov, I. N., and Bourne, P. E. (2000). The Protein Data Bank. Nucleic Acids Res *28*, 235-242.

Bernier, V., Bichet, D. G., and Bouvier, M. (2004). Pharmacological chaperone action on G-protein-coupled receptors. Curr Opin Pharmacol *4*, 528-533.

Best, R. B., Li, B., Steward, A., Daggett, V., and Clarke, J. (2001). Can non-mechanical proteins withstand force? Stretching barnase by atomic force microscopy and molecular dynamics simulation. Biophys J *81*, 2344-2356.

Bettger, W. J., and O'Dell, B. L. (1993). Physiological roles of zinc in the plasma membrane of mammalian cells. J Nutr Biochem *4*, 194-207.

Bezanilla, M., Drake, B., Nudler, E., Kashlev, M., Hansma, P. K., and Hansma, H. G. (1994). Motion and enzymatic degradation of DNA in the atomic force microscope. Biophys J *67*, 2454-2459.

Bhandawat, V., Reisert, J., and Yau, K. W. (2005). Elementary response of olfactory receptor neurons to odorants. Science *308*, 1931-1934.

Bieri, O., Wirz, J., Hellrung, B., Schutkowski, M., Drewello, M., and Kiefhaber, T. (1999). The speed limit for protein folding measured by triplet-triplet energy transfer. Proc Natl Acad Sci U S A *96*.

Bigelow, H. R., Petrey, D. S., Liu, J., Przybylski, D., and Rost, B. (2004). Predicting transmembrane beta-barrels in proteomes. Nucleic Acids Res *32*, 2566-2577.

Binnig, G., Quate, C. F., and Gerber, C. (1986). Atomic force microscope. Phys Rev Lett *56*, 930-933.

Binnig, G., Rohrer, H., Gerber, C., and Weibel, E. (1982). Tunneling through a controllable vacuum gap. Appl Phys Lett *40*, 178.

Blaurock, A., and Stoeckenius, W. (1971). Structure of the purple membrane. Nat New Biol *233*, 152-155.

Blobel, G., and Dobberstein, B. (1975). Transfer of proteins across membranes. I. Presence of proteolytically processed and unprocessed nascent immunoglobulin light chains on membrane-bound ribosomes of murine myeloma. J Cell Biol *67*, 835-851.

Bockaert, J., Claeysen, S., Becamel, C., Pinloche, S., and Dumuis, A. (2002). G protein-coupled receptors: dominant players in cell-cell communication. Int Rev Cytol *212*, 63-132.

Bogdanov, M., and Dowhan, W. (1999). Lipid assisted protein folding. J Biol Chem *274*, 36827-36830.

Bongrand, P., Capo, C., Mege, J.-L., and Benoliel, A.-M. (1988). Use of hydrodynamic flows to study cell adhesion. In Physical basis of cell adhesion, P. Bongrand, ed. (Boca Raton, Florida, CRC Press), pp. 125-156.

Booth, P. J. (2000). Unravelling the folding of bacteriorhodopsin. Biochim Biophys Acta *1460*, 4-14.

Booth, P. J. (2003). The trials and tribulations of membrane protein folding in vitro. Biochim Biophys Acta *1610*, 51-56.

Booth, P. J., and Curran, A. R. (1999). Membrane protein folding. Curr Opin Struct Biol *9*, 115-121.

Booth, P. J., Templer, R. H., Curran, A. R., and Allen, S. J. (2001a). Can we identify the forces that drive the folding of integral membrane proteins? Biochem Soc Trans *29*, 408-413.

Booth, P. J., Templer, R. H., Meijberg, W., Allen, S. J., Curran, A. R., and Lorch, M. (2001b). In vitro studies of membrane protein folding. Crit Rev Biochem Mol Biol *36*, 501-603.

Borbat, P. P., McHaourab, H. S., and Freed, J. H. (2002). Protein structure determination using long-distance constraints from double-quantum coherence ESR: study of T4 lysozyme. J Am Chem Soc *124*, 5304-5314.

Bourne, H. R., and Meng, E. C. (2000). Structure. Rhodopsin sees the light. Science *289*, 733-734.

Bowie, J. U. (1997). Helix packing in membrane proteins. J Mol Biol *272*, 780-789.

Bowie, J. U. (2001). Stabilizing membrane proteins. Curr Opin Struct Biol *11*, 397-402.

Bowie, J. U. (2005). Solving the membrane protein folding problem. Nature *438*, 581-589.

Brandl, C. J., and Deber, C. M. (1986). Hypothesis about the function of membrane-buried proline residues in transport proteins. Proc Natl Acad Sci U S A *83*, 917-921.

Breitwieser, G. E. (2004). G protein-coupled receptor oligomerization: implications for G protein activation and cell signaling. Circ Res *94*, 17-27.

Breyton, C., Haase, W., Rapoport, T. A., Kuhlbrandt, W., and Collinson, I. (2002). Three-dimensional structure of the bacterial protein-translocation complex SecYEG. Nature *418*, 662-665.

Brockwell, D. J., Beddard, G. S., Clarkson, J., Zinober, R. C., Blake, A. W., Trinick, J., Olmsted, P. D., Smith, D. A., and Radford, S. E. (2002). The effect of core destabilization on the mechanical resistance of I27. Biophys J *83*, 458-472.

Brodsky, J. L., and McCracken, A. A. (1999). ER protein quality control and proteasome-mediated protein degradation. Semin Cell Dev Biol *10*, 507-513.

Brouillette, C., McMichens, R., Stern, L., and Khorana, H. (1989). Structure and thermal stability of monomeric bacteriorhodopsin in mixed phospholipid/detergent micelles. Proteins *5*, 38-46.

Brouillette, C., Muccio, D., and Finney, T. (1987). pH dependence of bacteriorhodopsin thermal unfolding. Biochemistry *26*, 7431-7438.

Bullard, B., Garcia, T., Benes, V., Leake, M. C., Linke, W. A., and Oberhauser, A. F. (2006). The molecular elasticity of the insect flight muscle proteins projectin and kettin. Proc Natl Acad Sci U S A *103*, 4451-4456.

Bustamante, C., Marko, J. F., Siggia, E. D., and Smith, S. (1994). Entropic elasticity of lambda-phage DNA. Science *265*, 1599-1600.

Butt, H.-J., and Jaschke, M. (1995). Calculation of thermal noise in atomic force microscopy. Nanotechnology *6*, 1-7.

Cai, K., Itoh, Y., and Khorana, H. G. (2001). Mapping of contact sites in complex formation between transducin and light-activated rhodopsin by covalent crosslinking: use of a photoactivatable reagent. Proc Natl Acad Sci U S A *98*, 4877-4882.

Carrion-Vazquez, M., Oberhauser, A. F., Fowler, S. B., Marszalek, P. E., Broedel, S. E., Clarke, J., and Fernandez, J. M. (1999). Mechanical and chemical unfolding of a single protein: a comparison. Proc Natl Acad Sci U S A *96*, 3694-3699.

Ceruso, M. A., and Weinstein, H. (2002). Structural mimicry of proline kinks: Tertiary packing interactions support local structural distortions. J Mol Biol *318*, 1237-1249.

Chen, X., Davies, M. C., Roberts, C. J., Shakesheff, K. M., Tendler, S. J. B., and Williams, P. M. (1996). Dynamic surface events measured by simultaneous probe microscopy and surface plasmon detection. Anal Chem *68*, 1451-1455.

Chothia, C., Levitt, M., and Richardson, D. (1981). Helix to helix packing in proteins. J Mol Biol *272*, 780-789.

Christensen, K., Bose, H. S., Harris, F. M., Miller, W. L., and Bell, J. D. (2001). Binding of steriodogenic acute regulatory protein to synthetic membranes suggests an active molten globule. J Biol Chem *276*, 17044-17051.

Cieplak, M., Filipek, S., Janovjak, H., and Krzysko, K. A. (2006). Pulling single bacteriorhodopsin out of a membrane: Comparison of simulation and experiment. Biochim Biophys Acta *1758*, 537-544.

Cisneros, D. A., Oesterhelt, D., and Müller, D. J. (2005). Probing origins of molecular interactions stabilizing the membrane proteins halorhodopsin and bacteriorhodopsin. Structure (Camb) *13*, 235-242.

Clausen-Schaumann, H., Seitz, M., Krautbauer, R., and Gaub, H. E. (2000). Force spectroscopy with single bio-molecules. Curr Opin Chem Biol *4*, 524-530.

Cleveland, J. P., Manne, S., Bocek, D., and Hansma, P. K. (1993). A nondestructive method for determining the spring constant of cantilevers for scanning force microscopy. Rev Sci Instrum *64*, 403-405.

Compton, E. L. R., Farmer, N. A., Lorch, M., Mason, J. M., Moreton, K. M., and Booth, P. J. (2006). Kinetics of an individual transmembrane helix during bacteriorhodopsin folding. J Mol Biol *357*, 325-338.

Cotton, R. G., and Horaitis, O. (2002). The HUGO Mutation Database Initiative. Human Genome Organization. Pharmacogenomics J *2*, 16-19.

Cramer, W. A., Heymann, J. B., Schendel, S. L., Deriy, B. N., Cohen, F. S., Elkins, P. A., and Stauffacher, C. V. (1995). Structure-function of the channel-forming colicins. Annu Rev Biophys Biomol Struct *24*, 611-641.

Cui, Y., and Bustamante, C. (2000). Pulling a single chromatin fiber reveals the forces that maintain its higher-order structure. Proc Natl Acad Sci U S A *97*, 127-132.

Curran, A. R., and Engelman, D. M. (2003). Sequence motifs, polar interactions and conformational changes in helical membrane proteins. Curr Opin Struct Biol *13*, 412-417.

Czajkowsky, D. M., Hotze, E. M., Shao, Z., and Tweten, R. K. (2004). Vertical collapse of a cytolysin prepore moves its transmembrane beta-hairpins to the membrane. EMBO J *23*, 3206-3215.

Daggett, V., and Fersht, A. (2003a). Is there a unifying mechanism for protein folding. Trends Biochem Sci *28*, 19-26.

Daggett, V., and Fersht, A. (2003b). The present view of the mechanism of protein folding. Nat Rev Mol Cell Biol *4*, 497-502.

Dahl, S. G., and Sylte, I. (2005). Molecular modelling of drug targets: the past, the present and the future. Basic Clin Pharmacol Toxicol *96*, 151-155.

Dale, H., and Krebs, M. P. (1999). Membrane insertion kinetics of a protein domain in vivo. The bacterioopsin N terminus inserts co-translationally. J Biol Chem *274*, 22693-22698.

Darden, T., York, D., and Pedersen, L. (1993). Particle Mesh Ewald - an N.Log(N) Method for Ewald Sums in Large Systems. J Chem Phys *98*, 10089-10092.

Davidson, F. F., Loewen, P. C., and Khorana, H. G. (1994). Structure and function in rhodopsin: replacement by alanine of cysteine residues 110 and 187, components of a conserved disulfide bond in rhodopsin, affects the light-activated metarhodopsin II state. Proc Natl Acad Sci U S A *91*, 4029-4033.

del Valle, L. J., Ramon, E., Canavate, X., Dias, P., and Garriga, P. (2003). Zinc-induced decrease of the thermal stability and regeneration of rhodopsin. J Biol Chem *278*, 4719-4724.

Dempsey, C. E. (1990). The actions of melittin on membranes. Biochim Biophys Acta *1031*, 143-161.

Dietz, H., and Rief, M. (2004). Exploring the energy landscape of GFP by single-molecule mechanical experiments. Proc Natl Acad Sci U S A *101*, 16192-16197.

Dietz, H., and Rief, M. (2006). Protein structure by mechanical triangulation. Proc Natl Acad Sci U S A *103*, 1244-1247.

Dill, K. A. (1999). Polymer principles and protein folding. Protein Sci *8*, 1166-1180.

Dill, K. A., and Chan, H. S. (1997). From Levinthal to pathways to funnels. Nat Struct Biol *4*, 10-19.

Dinner, A. R., Sali, A., Smith, L. J., Dobson, C. M., and Karplus, M. (2000). Understanding protein folding via free-energy surfaces from theory and experiment. Trends Biochem Sci *25*, 331-339.

Dobson, C. M. (1999). Protein misfolding, evolution and disease. Trends Biochem Sci *24*, 329-332.

Dobson, C. M. (2002). Getting out of shape. Nature *418*, 729-730.

Dobson, C. M. (2003). Protein folding and misfolding. Nature *426*, 884-890.

Doi, T., Molday, R. S., and Khorana, H. G. (1990). Role of the intradiscal domain in rhodopsin assembly and function. Proc Natl Acad Sci U S A *87*, 4991-4995.

Dorea, J. G., and Olson, J. A. (1986). The rate of rhodopsin regeneration in the bleached eyes of zinc-deficient rats in the dark. J Nutr *116*, 121-127.

Doyle, D. A., Morais Cabral, J., Pfuetzner, R. A., Kuo, A., Gulbis, J. M., Cohen, S. L., Chait, B. T., and MacKinnon, R. (1998). The structure of the potassium channel: molecular basis of K^+ conduction and selectivity. Science *280*, 69-77.

Dracheva, S., Bose, S., and Hendler, R. (1996). Chemical and functional studies on the importance of purple membrane lipids in bacteriorhodopsin photocycle behavior. FEBS Lett *382*, 209-212.

Dryja, T. P., and Li, T. (1995). Molecular genetics of retinitis pigmentosa. Hum Mol Genet *4 Spec No*, 1739-1743.

Dugdale, T. M., Dagastine, R., Chiovitti, P., Mulvaney, P., and Wetherbee, R. (2005). Single adhesive nanofibers from a live diatom have the signature fingerprint of modular proteins. Biophys J *89*, 4252-4260.

Dunlap, D. D., Maggi, A., Soria, M. R., and Monaco, L. (1997). Nanoscopic structure of DNA condensed for gene delivery. Nucl Acids Res *25*, 3095.

Dutzler, R., Campbell, E. B., Cadene, M., Chait, B. T., and MacKinnon, R. (2002). X-ray structure of a ClC chloride channel at 3 A^o reveals the molecular basis of anion selectivity. Nature *415*, 287-294.

Eidelman, O., BarNoy, S., Razin, M., Zhang, J., McPhie, P., Lee, G., Huang, Z., Sorscher, E. J., and Pollard, H. B. (2002). Role for phospholipid interactions in the trafficking defect of Delta F508-CFTR. Biochemistry *41*, 11161-11170.

Eilers, M., Ying, W., Reeves, P. J., Khorana, H. G., and Smith, S. O. (2002). Magic angle spinning nuclear magnetic resonance of isotopically labeled rhodopsin. Methods Enzymol *343*, 212-222.

Eng, L. M., Seuret, C., Looser, H., and Günter, P. (1996). Approaching the liquid/air interface with scanning force microscopy. J Vac Sci & Technol B *14*, 1386-1389.

Engel, A., and Müller, D. J. (2000). Observing single biomolecules at work with the atomic force microscope. Nat Struct Biol *7*, 715-718.

Engelman, D. M. (2005). Membranes are more mosaic than fluid. Nature *438*, 578-580.

Engelman, D. M., Adair, B. D., Hunt, J. F., Kahn, T. W., and Popot, J.-L. (1990). Bacteriorhodopsin folding in membranes: a two stage process. Curr Topics Membr Transport *36*, 71-78.

Engelman, D. M., Chen, Y., Chin, C. N., Curran, A. R., Dixon, A. M., Dupuy, A. D., Lee, A. S., Lehnert, U., Matthews, E. E., Reshetnyak, Y. K., *et al.* (2003). Membrane protein folding: beyond the two stage model. FEBS Lett *555*, 122-125.

Engelman, D. M., and Steitz, T. A. (1981). The spontaneous insertion of proteins into and across membranes: the helical hairpin hypothesis. Cell *23*, 411-422.

Essen, L.-O., Siegert, R., Lehmann, W. D., and Oesterhelt, D. (1998). Lipid patches in membrane protein oligomers: Crystal structure of the bacteriorhodopsin-lipid complex. Proc Natl Acad Sci U S A *95*, 11673-11678.

Essmann, U., Perera, L., Berkowitz, M. L., Darden, T., Lee, H., and Pedersen, L. G. (1995). A Smooth Particle Mesh Ewald Method. J Chem Phys *103*, 8577-8593.

Evans, E. (1998). Energy landscapes of biomolecular adhesion and receptor anchoring at interfaces explored with dynamic force spectroscopy. Faraday Discuss *111*, 1-16.

Evans, E. (1999). Looking inside molecular bonds at biological interfaces with dynamic force spectroscopy. Biophys Chem *82*, 83-97.

Evans, E. (2001). Probing the relation between force-lifetime-and chemistry in single molecular bonds. Annu Rev Biophys Biomol Struct *30*, 105-128.

Evans, E., and Ritchie, K. (1997). Dynamic strength of molecular adhesion bonds. Biophys J *72*, 1541-1555.

Evans, E., Ritchie, K., and Merkel, R. (1995). Sensitive force technique to probe molecular adhesion and structural linkages at biological interfaces. Biophys J *68*, 2580-2587.

Faham, S., Yang, D., Bare, E., Yohannan, S., Whitelegge, J. P., and Bowie, J. U. (2004). Side-chain contributions to membrane protein structure and stability. J Mol Biol *335*, 297-305.

Fandrich, M., Forge, V., Buder, K., Kittler, M., Dobson, C. M., and Diekmann, S. (2003). Myoglobin forms amyloid fibrils by association of unfolded polypeptide segments. Proc Natl Acad Sci U S A *100*, 15463-15468.

Farahbakhsh, Z. T., Ridge, K. D., Khorana, H. G., and Hubbell, W. L. (1995). Mapping light-dependent structural changes in the cytoplasmic loop connecting helices C and D in rhodopsin: a site-directed spin labeling study. Biochemistry *34*, 8812-8819.

Farrens, D. L., Altenbach, C., Yang, K., Hubbell, W. L., and Khorana, H. G. (1996). Requirement of rigid-body motion of transmembrane helices for light activation of rhodopsin. Science *274*, 768-770.

Fernandez, J. M., and Li, H. (2004). Force-clamp spectroscopy monitors the folding trajectory of a single protein. Science *303*, 1674-1678.

Filipek, S., Krzysko, K. A., Fotiadis, D., Liang, Y., Saperstein, D. A., Engel, A., and Palczewski, K. (2004). A concept for G protein activation by G protein-coupled receptor dimers: the transducin/rhodopsin interface. Photochem Photobiol Sci *3*, 628-638.

Filipek, S., Stenkamp, R. E., Teller, D. C., and Palczewski, K. (2003a). G protein-coupled receptor rhodopsin: a prospectus. Annu Rev Physiol *65*, 851-879.

Filipek, S., Teller, D. C., Palczewski, K., and Stenkamp, R. (2003b). The crystallographic model of rhodopsin and its use in studies of other G protein-coupled receptors. Annu Rev Biophys Biomol Struct *32*, 375-397.

Findlay, J. B., Brett, M., and Pappin, D. J. (1981). Primary structure of C-terminal functional sites in bovine rhodopsin. Nature *293*, 314-317.

Fisher, L. E., Engelman, D. M., and Sturgis, J. N. (2003). Effect of detergents on the association of the glycophorin A transmembrane helix. Biophys J *85*, 3097-3105.

Fisher, T. E., Marszalek, P. E., and Fernandez, J. M. (2000). Stretching single molecules into novel conformations using the atomic force microscope. Nat Struct Biol *7*, 719-724.

Fleishman, S. J., Unger, V. M., and N., B.-T. (2006). Transmembrane protein structures without X-rays. Trends Biochem Sci *31*, 106-113.

Fleming, K. G., Ackerman, A. L., and Engelman, D. M. (1997). The effect of point mutations on the free energy of transmembrane α-helix dimerization. J Mol Biol *272*, 266-275.

Florin, E.-L., Moy, V. T., and Gaub, H. E. (1994). Adhesion forces between individual ligand-receptor pairs. Science *264*, 415-417.

Florin, E.-L., Rief, M., Lehmann, H., Ludwig, M., Dornmair, C., Moy, V. T., and Gaub, H. E. (1995). Sensing specific molecular interactions with the atomic force microscope. Biosens Bioelectron *10*, 895-901.

Fotiadis, D., Liang, Y., Filipek, S., Saperstein, D. A., Engel, A., and Palczewski, K. (2003). Atomic-force microscopy: Rhodopsin dimers in native disc membranes. Nature *421*, 127-128.

Fotiadis, D., Liang, Y., Filipek, S., Saperstein, D. A., Engel, A., and Palczewski, K. (2004). The G protein-coupled receptor rhodopsin in the native membrane. FEBS Lett *564*, 281-288.

Fotiadis, D., Müller, D. J., Tsiotis, G., Hasler, L., Tittmann, P., Mini, T., Jenö, P., Gross, H., and Engel, A. (1998). Surface analysis of the photosystem I complex by electron and atomic force microscopy. J Mol Biol *283*, 83-94.

Frank, J. (1996). Three-dimensional electron microscopy of macromolecular assemblies (London, Academic Press).

Frederickson, C. J. (1989). Neurobiology of zinc and zinc-containing neurons. Int Rev Neurobiol *31*, 145-238.

Frederix, P. L., Gullo, M. R., Akiyama, T., Tonin, A., de Rooij, N. F., Staufer, U., and Engel, A. (2005). Assessment of insulated conductive cantilevers for biology and electrochemistry. Nanotechnology *16*, 997-1005.

Fritz, J., Katopodis, A. G., Kolbinger, F., and Anselmetti, D. (1998). Force-mediated kinetics of single P-selectin/ligand complexes observed by atomic force microscopy. Proc Natl Acad Sci U S A *95*, 12283-12288.

Fritz, M., Radmacher, M., Allersma, M. W., Cleveland, J. P., Stewart, R. J., Hansma, P. K., and Schmidt, C. F. (1995). Imaging microtubles in buffer solution using tapping mode atomic force microscopy. SPIE *2384*, 150-157.

Fu, D., Libson, A., Miercke, L. J., Weitzman, C., Nollert, P., Krucinski, J., and Stroud, R. M. (2000). Structure of a glycerol-conducting channel and the basis for its selectivity. Science *290*, 481-486.

Fukuma, T., Kobayashi, K., Matsushige, K., and Yamada, H. (2005). True atomic resolution in liquid by frequency-modulation atomic force microscopy. Appl Phys Lett *87*, 034101.

Ganchev, D. N., Rijkers, D. T., Snel, M. M., Killian, J. A., and de Kruijff, B. (2004). Strength of integration of transmembrane alpha-helical peptides in lipid bilayers as determined by atomic force spectroscopy. Biochemistry *43*, 14987-14993.

Garriga, P., Liu, X., and Khorana, H. G. (1996). Structure and function in rhodopsin: correct folding and misfolding in point mutants at and in proximity to the site of the retinitis pigmentosa mutation Leu-125-->Arg in the transmembrane helix C. Proc Natl Acad Sci U S A *93*, 4560-4564.

Gelman, M. S., Kannegaard, E. S., and Kopito, R. R. (2002). A principal role for the proteasome in endoplasmic reticulum-associated degradation of misfolded intracellular cystic fibrosis transmembrane conductance regulator. J Biol Chem *277*, 11709-11714.

Gelman, M. S., and Kopito, R. R. (2002). Rescuing protein conformation: prospects for pharmacological therapy in cystic fibrosis. J Clin Invest *110*, 1591-1597.

Gerlach, L. O., Jakobsen, J. S., Jensen, K. P., Rosenkilde, M. R., Skerlj, R. T., Ryde, U., Bridger, G. J., and Schwartz, T. W. (2003). Metal ion enhanced binding of AMD3100 to Asp262 in the CXCR4 receptor. Biochemistry *42*, 710-717.

Gether, U., and Kobilka, B. K. (1998). G protein-coupled receptors. II. Mechanism of agonist activation. J Biol Chem *273*, 17979-17982.

Gibson, C. T., Watson, G. S., and Myhra, S. (1996). Determination of the spring constants of probes for force microscopy/spectroscopy. Nanotechnology *7*, 259-262.

Goder, V., Junne, T., and Spiess, M. (2004). Sec61p contributes to signal sequence orientation according to the positive-inside rule. Mol Biol Cell *15*, 1470-1478.

Goncalves, R. P., Busselez, J., Levy, D., Seguin, J., and Scheuring, S. (2005). Membrane insertion of Rhodopseudomonas acidophila light harvesting complex 2 investigated by high resolution AFM. J Struct Biol *149*, 79-86.

Gorzelle, B. M., Nagy, J. K., Oxenoid, K., Lonzer, W. L., Cafiso, D. S., and Sanders, C. R. (1999). Reconstitutive refolding of diacylglycerol kinase, an integral membrane protein. Biochemistry *38*, 16373-16382.

Grahn, B. H., Paterson, P. G., Gottschall-Pass, K. T., and Zhang, Z. (2001). Zinc and the eye. J Am Coll Nutr *20*, 106-118.

Grandbois, M., Beyer, M., Rief, M., Clausen-Schaumann, H., and Gaub, H. E. (1999). How strong is a covalent bond? Science *283*, 1727-1730.

Grasberger, B., Minton, A. P., DeLis, C., and Metzger, H. (1986). Interaction between proteins localized in membranes. Proc Natl Acad Sci U S A *83*, 6258-6262.

Gratkowski, H., Lear, J. D., and DeGrado, W. F. (2001). Polar side chains drive the association of model transmembrane peptides. Proc Natl Acad Sci U S A *98*, 880-885.

Grigorieff, N., Ceska, T. A., Downing, K. H., Baldwin, J. M., and Henderson, R. (1996). Electron-crystallographic refinement of the structure of bacteriorhodopsin. J Mol Biol *259*, 393-421.

Guthold, M., Zhu, X., Rivetti, C., Yang, G., Thomson, N. H., Kasas, S., Hansma, H. G., Smith, B., Hansma, P. K., and Bustamante, C. (1999). Direct observation of one-dimensional diffusion and transcription by *Escherichia coli* RNA polymerase. Biophys J *77*, 2284-2294.

Gutsmann, T., Fantner, G. E., Kindt, J. H., Venturoni, M., Danielsen, S., and Hansma, P. K. (2004). Force spectroscopy of collagen fibers to investigate their mechanical properties and structural organization. Biophys J *86*, 3186-3193.

Haltia, T., and Freire, F. (1995). Forces and factors that contribute to the structural stability of membrane proteins. Biochim Biophys Acta *1228*, 1-27.

Hamm, H. E. (2001). How activated receptors couple to G proteins. Proc Natl Acad Sci U S A *98*, 4819-4821.

Hampton, R. Y. (2002). ER-associated degradation in protein quality control and cellular regulation. Curr Opin Cell Biol *14*, 476-482.

Han, W., Lindsay, S. M., Dlakic, M., and Harrington, R. E. (1997). Kinked DNA. Nature *386*, 563.

Han, W., Mou, J., Sheng, J., Yang, J., and Shao, Z. (1995). Cryo-Atomic Force Microscopy: a new approach for biological imaging at high resolution. Biochemistry *34*, 8215-8220.

Hargrave, P. (1991). Seven-helix receptors. Curr Opin Struct Biol *1*, 575-581.

Haupts, U., Tittor, J., and Oesterhelt, D. (1999). Closing in on bacteriorhodopsin: progress in understanding the molecule. Annu Rev Biophys Biomol Struct *28*, 367-399.

Heck, M., and Hofmann, K. P. (2001). Maximal rate and nucleotide dependence of rhodopsin-catalyzed transducin activation: initial rate analysis based on a double displacement mechanism. J Biol Chem *276*, 10000-10009.

Henderson, R., and Unwin, P. N. T. (1975). Three-dimensional model of purple membrane obtained by electron microscopy. Nature *257*, 28-32.

Hessa, T., Kim, H., Bihlmaier, K., Lundin, C., Boekel, J., Andersson, H., Nilsson, I., White, S. H., and von Heijne, G. (2005a). Recognition of transmembrane helices by the endoplasmic reticulum translocon. Nature *433*, 377-381.

Hessa, T., White, S. H., and von Heijne, G. (2005b). Membrane insertion of a potassium-channel voltage sensor. Science *307*, 1427.

Heyes, C., and El-Sayed, M. (2002). The role of the native lipids and lattice structure in bacteriorhodopsin protein conformation and stability as studies by temperature-dependent Fourier transform-infrared spectroscopy. J Biol Chem *277*, 29437-29443.

Hinterdorfer, P., Baumgartner, W., Gruber, H. J., Schilcher, K., and Schindler, H. (1996). Detection and localization of individual antibody-antigen recognition events by atomic force microscopy. Proc Natl Acad Sci U S A *93*, 3477-3481.

Hirayama, Y. (1990). Histochemical localization of zinc and copper in rat ocular tissues. Acta Histochem *89*, 107-111.

Hoh, J. H., Lal, R., John, S. A., Revel, J.-P., and Arnsdorf, M. F. (1991). Atomic force microscopy and dissection of gap junctions. Science *253*, 1405-1408.

Holst, B., Elling, C. E., and Schwartz, T. W. (2002). Metal ion-mediated agonism and agonist enhancement in melanocortin MC1 and MC4 receptors. J Biol Chem *277*, 47662-47670.

Howard, J. (2001). Mechanics of motor proteins and the cytoskeleton (Sunderland, Massachusetts, Sinauer Associates Inc.).

Huang, K., Bayley, H., and Khorana, H. (1980). Delipidation of bacteriorhodopsin and reconstitution with exogenous phospholipids. Proc Natl Acad Sci USA *77*, 323-327.

Huang, K. S., Bayley, H., Liao, M. J., London, E., and Khorana, H. G. (1981). Refolding of an integral membrane protein. Denaturation, renaturation, and reconstitution of intact bacteriorhodopsin and two proteolytic fragments. J Biol Chem *256*, 3802-3809.

Huang, X., Atwood, C. S., Moir, R. D., Hartshorn, M. A., Tanzi, R. E., and Bush, A. I. (2004). Trace metal contamination initiates the apparent auto-aggregation, amyloidosis, and oligomerizatoin of Alzheimer's Aβ peptides. J Biol Inorg Chem *9*, 954-960.

Hunt, J. F., Earnest, T. N., Bousche, O., Kalghatgi, K., Reilly, K., Horvath, C., Rothschild, K. J., and Engelman, D. M. (1997). A biophysical study of integral membrane protein folding. Biochemistry *36*, 15156-15176.

Huschilt, J., Millman, B., and Davis, J. (1989). Orientation of alpha-helical peptides in a lipid bilayer. Biochim Biophys Acta *979*, 139-141.

Hutter, J. L., and Bechhoefer, J. (1993). Manipulation of van der Waals forces to improve image resolution in atomic-force microscopy. J Appl Phys *73*, 4123.

Hwa, J., Garriga, P., Liu, X., and Khorana, H. G. (1997). Structure and function in rhodopsin: packing of the helices in the transmembrane domain and folding to a tertiary structure in the intradiscal domain are coupled. Proc Natl Acad Sci U S A *94*, 10571-10576.

Hwa, J., Klein-Seetharaman, J., and Khorana, H. G. (2001). Structure and function in rhodopsin: Mass spectrometric identification of the abnormal intradiscal disulfide bond in misfolded retinitis pigmentosa mutants. Proc Natl Acad Sci U S A *98*, 4872-4876.

Hwa, J., Reeves, P. J., Klein-Seetharaman, J., Davidson, F., and Khorana, H. G. (1999). Structure and function in rhodopsin: further elucidation of the role of the intradiscal cysteines, Cys-110, -185, and -187, in rhodopsin folding and function. Proc Natl Acad Sci U S A *96*, 1932-1935.

Israelachvili, J. (1991). Intermolecular & surface forces, Second edn (London, Academic Press Limited).

Jackson, M., and Sturtevant, J. (1978). Phase transitions of the purple membranes of Halobacterium halobium. Biochemistry *17*, 911-915.

Jacobs, D. J., Rader, A. J., Kuhn, L. A., and Thorpe, M. F. (2001). Protein flexibility predictions using graph theory. Proteins *44*, 150-165.

Jacobs, R. E., and White, S. H. (1989). The nature of the hydrophobic binding of small peptides at the bilayer interface: implications for the insertion of transbilayer helices. Biochemistry *28*, 3421-3437.

Jaenicke, R. (1995). Folding and association versus misfolding and aggregation of proteins. Philos Trans R Soc Lond B Biol Sci *348*, 97-105.

Janovjak, H., Kedrov, A., Cisneros, D. A., Sapra, K. T., and Müller, D. J. (2006). Imaging and detecting molecular interactions of single transmembrane proteins. Neurobiol of Aging *27*, 546-561.

Janovjak, H., Kessler, M., Oesterhelt, D., Gaub, H. E., and Müller, D. J. (2003). Unfolding pathways of native bacteriorhodopsin depend on temperature. EMBO J *22*, 5220-5229.

Janovjak, H., Müller, D. J., and Humphris, A. D. (2005). Molecular force modulation spectroscopy revealing the dynamic response of single bacteriorhodopsins. Biophys J *88*, 1423-1431.

Janovjak, H., Struckmeier, J., Hubain, M., Kedrov, A., Kessler, M., and Müller, D. J. (2004). Probing the energy landscape of the membrane protein bacteriorhodopsin. Structure (Camb) *12*, 871-879.

Jastrzebska, B., Maeda, T., Zhu, L., Fotiadis, D., Filipek, S., Engel, A., Stenkamp, R. E., and Palczewski, K. (2004). Functional characterization of rhodopsin monomers and dimers in detergents. J Biol Chem *279*, 54663-54675.

Jiang, S., and Vakser, I. A. (2004). Shorter side chains optimize helix-helix packing. Protein Sci *13*, 1426-1429.

Jo, E., Fuller, N., Rand, R. P., George-Hyslop, P., and Fraser, P. E. (2002). Defective membrane interactions of familial Parkinson's disease mutant A30P alpha-synuclein. J Mol Biol *315*, 799-807.

Jobling, M. F., Huang, X., Stewart, L. R., Barnham, K. J., Curtain, C., Volitakis, I., Perugini, M., White, A. R., Cherny, R. A., Masters, C. L., *et al.* (2001). Copper and zinc binding modulates the aggregation and neurotoxic properties of the prion peptide PrP106-126. Biochemistry *40*, 8073-8084.

Junker, J. P., Hell, K., Schlierf, M., Neupert, W., and Rief, M. (2005). Influence of substrate binding on the mechanical stability of mouse dihydrofolate reductase. Biophys J *89*, L46-L48.

Kaback, H. R., Sahin-Toth, M., and Weinglass, A. B. (2001). The kamikaze approach to membrane transport. Nat Rev Mol Cell Biol *2*, 610-620.

Kahn, T., Sturtevant, J., and Engelman, D. (1992). Thermodynamic measurements of the contributions of helix-connecting loops and of retinal to the stability of bacteriorhodopsin. Biochemistry *31*, 8829-8839.

Karcioglu, Z. A. (1982). Zinc in the eye. Surv Ophthalmol *27*, 114-122.

Karlin, A. (1993). Structure of nicotinic acetylcholine receptors. Curr Opin Neurbiol *3*, 299-309.

Karnik, S. S., and Khorana, H. G. (1990). Assembly of functional rhodopsin requires a disulfide bond between cysteine residues 110 and 187. J Biol Chem *265*, 17520-17524.

Karnik, S. S., Sakmar, T. P., Chen, H. B., and Khorana, H. G. (1988). Cysteine residues 110 and 187 are essential for the formation of correct structure in bovine rhodopsin. Proc Natl Acad Sci U S A *85*, 8459-8463.

Karrasch, S., Dolder, M., Hoh, J., Schabert, F., Ramsden, J., and Engel, A. (1993). Covalent binding of biological samples to solid supports for scanning probe microscopy in buffer solution. Biophys J *65*, 2437-2446.

Kaushal, S., and Khorana, H. G. (1994). Structure and function in rhodopsin. 7. Point mutations associated with autosomal dominant retinitis pigmentosa. Biochemistry *33*, 6121-6128.

Kawakami, M., Byrne, K., Khatri, B., Mcleish, T. C., Radford, S. E., and Smith, D. A. (2004). Viscoelastic properties of single polysaccharide molecules determined by analysis of thermally driven oscillations of an atomic force microscope cantilever. Langmuir *20*, 9299-9303.

Kazlauskaite, J., Sanghera, N., Sylvester, I., Venien-Bryan, C., and Pinheiro, T. J. (2003). Structural changes of the prion protein in lipid membranes leaading to aggregation and fibrillization. Biochemistry *42*, 3295-3304.

Kedrov, A., Janovjak, H., Ziegler, C., Kühlbrandt, W., and Müller, D. J. (2006a). Observing folding kinetics and pathways of single antiporters. J Mol Biol *355*, 2-8.

Kedrov, A., Krieg, M., Ziegler, C., Kuhlbrandt, W., and Müller, D. J. (2005). Locating ligand binding and activation of a single antiporter. EMBO Rep *6*, 668-674.

Kedrov, A., Ziegler, C., Janovjak, H., Kuhlbrandt, W., and Müller, D. J. (2004). Controlled unfolding and refolding of a single sodium-proton antiporter using atomic force microscopy. J Mol Biol *340*, 1143-1152.

Kedrov, A., Ziegler, C., and Müller, D. J. (2006b). Differentiating ligand and inhibitor interactions of a single antiporter. J Mol Biol *362*, 925-932.

Kellermayer, M. S., Smith, S. B., Granzier, H. L., and Bustamante, C. (1997). Folding-unfolding transitions in single titin molecules characterized with laser tweezers. Science *276*, 1112-1116.

Kessler, M., and Gaub, H. (2006). Unfolding barriers in bacteriorhodopsin probed from the cytoplasmic and the extracellular side by AFM. Structure *14*, 521-527.

Kessler, M., Gottschalk, K. E., Janovjak, H., Muller, D. J., and Gaub, H. E. (2006). Bacteriorhodopsin folds into the membrane against an external force. J Mol Biol *357*, 644-654.

Kiefhaber, T., Rudolph, R., Kohler, H. H., and Buchner, J. (1991). Protein aggregation in vitro and in vivo: a quantitative model of the kinetic competition between folding and aggregation. Biotechnology *9*, 825-829.

Kim, J. M., Booth, P. J., Allen, S. J., and Khorana, H. G. (2001). Structure and function in bacteriorhodopsin: the role of interhelical loops in the folding and stability of bacteriorhodopsin. J Mol Biol *308*, 409-422.

Kimura, Y., Vassylyev, D. G., Miyazawa, A., Kidera, A., Matsushima, M., Mitsuoka, K., Murata, K., Hirai, T., and Fujiyoshi, Y. (1997). Surface of bacteriorhodopsin revealed by high-resolution electron crystallography. Nature *389*, 206-211.

Klein-Seetharaman, J. (2005). Dual role of interactions between membranous and soluble portions of helical membrane receptors for folding and signaling. Trends Phramacol Sci *26*, 183-189.

Klein-Seetharaman, J., Reeves, P. J., Loewen, M. C., Getmanova, E. V., Chung, J., Schwalbe, H., Wright, P. E., and Khorana, H. G. (2002). Solution NMR spectroscopy of [alpha -15N]lysine-labeled rhodopsin: The single peak observed in both conventional and TROSY-type HSQC spectra is ascribed to Lys-339 in the carboxyl-terminal peptide sequence. Proc Natl Acad Sci U S A *99*, 3452-3457.

Kleinschmidt, J. H., and Tamm, L. K. (2002). Secondary and tertiary structure formation of the beta-barrel membrane protein OmpA is synchronized and depends on membrane thickness. J Mol Biol *324*, 319-330.

Konig, B., Arendt, A., McDowell, J. H., Kahlert, M., Hargrave, P. A., and Hofmann, K. P. (1989). Three cytoplasmic loops of rhodopsin interact with transducin. Proc Natl Acad Sci U S A *86*, 6878-6882.

Kono, M., Yu, H., and Oprian, D. D. (1998). Disulfide bond exchange in rhodopsin. Biochemistry *37*, 1302-1305.

Kopito, R. R. (1999). Biosynthesis and degradation of CFTR. Physiol Rev *79*, S167-S173.

Kreusch, A., and Schulz, G. E. (1994). Refined structure of the porin from *Rhodopseudomonas blastica*. Comparison with the porin from *Rhodobacter capsulatus*. J Mol Biol *243*, 891-905.

Kühlbrandt, W., and Wang, D. N. (1991). Three-dimensional structure of plant light-harvesting complex determined by electron crystallography. Nature *350*, 130-134.

Labro, A. J., Raes, A. L., Ottschytsch, N., and Snyders, D. J. (2001). Role of the S6 tandem proline motif in gating of Kv channels. Biophys J *80*, 1875.

Langosch, D., and Heringa, J. (1998). Interaction of transmembrane helices by a knobs-into-holes packing characteristic of soluble coiled coils. Proteins *31*, 150-159.

Lanyi, J. K. (2004). Bacteriorhodopsin. Annu Rev Physiol *66*, 665-688.

Leckband, D. E., Israelachvili, J. N., Schmitt, F. J., and Knoll, W. (1992). Long-range attraction and molecular rearrangements in receptor-ligand interactions. Science *255*, 1419-1421.

Lee, G., Abdi, K., Jiang, Y., Michaely, P., Bennett, V., and Marszalek, P. E. (2006). Nanospring behaviour of ankyrin repeats. Nature *440*, 246-249.

Lee, G. U., Chrisey, L. A., and Colton, R. J. (1994). Direct measurement of the forces between complementary strands of DNA. Science *266*, 771-773.

Lee, H. J., Choi, C., and Lee, S. J. (2002). Membrane-bound alpha-synuclein has a high aggregation propensity and the ability to seed the aggregation of the cytosolic form. J Biol Chem *277*, 671-678.

Lefkowitz, R. J. (1998). G protein-coupled receptors. III. New roles for receptor kinases and beta-arrestins in receptor signaling and desensitization. J Biol Chem *273*, 18677-18680.

Lefkowitz, R. J. (2004). Historical review: A brief history and personal retrospective of seven-transmembrane receptors. Trends Pharmacol Sci *25*, 413-422.

Lehnert, U., Xia, Y., Royce, T. E., Goh, C. S., Liu, Y., Senes, A., Yu, H., Zhang, Z. L., Engelman, D. M., and Gerstein, M. (2004). Computational analysis of membrane proteins: genomic occurrence, structure prediction and helix interactions. Q Rev Biophys *37*, 121-146.

Lemmon, M. A., Flanagan, J. M., Hunt, J. F., Adair, B. D., Bormann, B. J., Dempsey, C. E., and Engelman, D. M. (1992). Glycophorin A dimerization is driven by specific interactions between transmembrane α-helices. J Biol Chem *267*, 7683-7689.

Levinthal, C. (1968). Are there pathways for protein folding? J Chim Phys *65*, 44-45.

Li, H., Carrion-Vazquez, M., Oberhauser, A. F., Marszalek, P. E., and Fernandez, J. M. (2000). Point mutations alter the mechanical stability of immunoglobulin modules. Nat Struct Biol *7*, 1117-1120.

Li, J., Edwards, P. C., Burghammer, M., Villa, C., and Schertler, G. F. (2004a). Structure of bovine rhodopsin in a trigonal crystal form. J Mol Biol *343*, 1409-1438.

Li, R., Gorelik, R., Nanda, V., Law, P. B., Lear, J. D., DeGrado, W. F., and Bennett, J. S. (2004b). Dimerization of the transmembrane domain of intergrin alpha IIb subunit in cell membranes. J Biol Chem *279*, 26666-26673.

Liang, Y., Fotiadis, D., Filipek, S., Saperstein, D. A., Palczewski, K., and Engel, A. (2003). Organization of the G protein-coupled receptors rhodopsin and opsin in native membranes. J Biol Chem *278*, 21655-21662.

Liu, L. P., Li, S. C., Goto, N. K., and Deber, C. M. (1996a). Threshold hydrophobicity dictates helical conformations of peptides in membrane environments. Biopolymers *39*, 465-470.

Liu, X., Garriga, P., and Khorana, H. G. (1996b). Structure and function in rhodopsin: correct folding and misfolding in two point mutants in the intradiscal domain of rhodopsin identified in retinitis pigmentosa. Proc Natl Acad Sci U S A *93*, 4554-4559.

Liu, Y., Teeter, M. M., DuRand, C. J., and Neve, K. A. (2006). Identification of a Zn2+-binding site on the dopamine D2 receptor. Biochem Biophys Res Commun *339*, 873-879.

Lu, H., and Booth, P. J. (2000). The final stages of folding of the membrane protein bacteriorhodopsin occur by kinetically indistinguishable parallel folding paths that are mediated by pH. J Mol Biol *299*, 233-243.

Lu, H., Marti, T., and Booth, P. J. (2001). Proline residues in transmembrane alpha helices affect the folding of bacteriorhodopsin. J Mol Biol *308*, 437-446.

Luecke, H., Schobert, B., Richter, H., Cartailler, J., and Lanyi, J. (1999a). Structure of Bacteriorhodopsin at 1.55 A resolution. J Mol Bio *291*, 899-911.

Luecke, H., Schobert, B., Richter, H.-T., Certailler, J.-P., and Lanyi, J. K. (1999b). Structural changes in bacteriorhodopsin during ion transport at 2 Angstrom resolution. Science *286*, 255-260.

MacKenzie, K. R., Prestegard, J. H., and Engelman, D. M. (1997). A transmembrane helix dimer: structure and implications. Science *276*, 131-133.

Marszalek, P. E., Li, H., Oberhauser, A. F., and Fernandez, J. M. (2002). Chair-boat transitions in single polysaccharide molecules observed with force-ramp AFM. Proc Natl Acad Sci U S A *99*, 4278-4283.

Marszalek, P. E., Lu, H., Li, H., Carrion-Vazquez, M., Oberhauser, A. F., Schulten, K., and Fernandez, J. M. (1999). Mechanical unfolding intermediates in titin modules. Nature *402*, 100-103.

Martin, J. (1999). Molecular basis of the neurodegenerative disorders. N Engl J Med *340*, 1970-1980.

McClain, C. J., Kasarskis, E. J., and Allen, J. J. (1985). Functional consequences of zinc deficiency. Prog Food Nutr Sci *9*, 185-226.

McCloskey, M. A., and Poo, M. M. (1986). Rates of membrane-associated reactions: reduction of dimensionality revisited. J Cell Biol *102*, 88-96.

McDonnell, P. A., Shon, K., Kim, Y., and Opella, S. J. (1993). fd coat protein structure in membrane environments. J Mol Biol *233*, 447-463.

Medina, R., Perdomo, D., and Bubis, J. (2004). The hydrodynamic properties of dark- and light-activated states of n-dodecyl beta-D-maltoside-solubilized bovine rhodopsin support the dimeric structure of both conformations. J Biol Chem *279*, 39565-39573.

Melnyk, R. A., Partridge, A. W., and Deber, C. M. (2002). Transmembrane domain mediated self-assembly of major coat protein subunits from Ff bacteriophage. J Mol Biol *315*, 63-72.

Mendrola, J. M., Berger, M. B., King, M. C., and Lemmon, M. A. (2002). The single transmembrane domains of ErbB receptors self-associate in cell membranes. J Biol Chem *277*, 4704-4712.

Meng, E. C., and Bourne, H. R. (2001). Receptor activation: what does the rhodopsin structure tell us? Trends Pharmacol Sci *22*, 587-593.

Merkel, R., Nassoy, P., Leung, A., Ritchie, K., and Evans, E. (1999). Energy landscapes of receptor-ligand bonds explored with dynamic force spectroscopy. Nature *397*, 50-53.

Meyer, E., Hug, H. J., and Bennewitz, R. (2003). Scanning Probe Microscopy - The Lab on a Tip (Berlin, Springer).

Michel, H., Oesterhelt, D., and Henderson, R. (1980). Orthorhombic two-dimensional crystal form of purple membrane. Proc Natl Acad Sci USA *77*, 338-342.

Milligan, G., and Bouvier, M. (2005). Methods to monitor the quaternary structure of G protein-coupled receptors. Febs J *272*, 2914-2925.

Mirzadegan, T., Benko, G., Filipek, S., and Palczewski, K. (2003). Sequence analyses of G-protein-coupled receptors: similarities to rhodopsin. Biochemistry *42*, 2759-2767.

Mitsuoka, K., Hirai, T., Murata, K., Miyazawa, A., Kidera, A., Kimura, Y., and Fujiyoshi, Y. (1999). The structure of bacteriorhodopsin at 3.0 Å resolution based on electron crystallography: implication of the charge distribution. J Mol Biol *286*, 861-882.

Moir, R. D., Atwood, C. S., Huang, X., Tanzi, R. E., and Bush, A. I. (1999). Mounting evidence for the involvement of zinc and copper in Alzheimer's disease. Eur J Clin Invest *29*, 569-570.

Molday, R. S., Hicks, D., and Molday, L. (1987). Peripherin. A rim-specific membrane protein of rod outer segment discs. Invest Ophthalmol Vis Sci *28*, 50-61.

Möller, C., Allen, M., Elings, V., Engel, A., and Müller, D. J. (1999). Tapping-mode atomic force microscopy produces faithful high-resolution images of protein surfaces. Biophys J *77*, 1150-1158.

Möller, C., Büldt, G., Dencher, N., Engel, A., and Müller, D. J. (2000). Reversible loss of crystallinity on photobleaching purple membrane in presence of hydroxylamine. J Mol Biol *301*, 869-879.

Möller, C., Fotiadis, D., Suda, K., Engel, A., Kessler, M., and Müller, D. J. (2003). Determining molecular forces that stabilize human aquaporin-1. J Struct Biol *142*, 369-378.

Morello, J. P., Salahpour, A., Laperriere, A., Bernier, V., Arthus, M. F., Lonergan, M., Petaja-Repo, U., Angers, S., Morin, D., Bichet, D. G., and Bouvier, M. (2000). Pharmacological chaperones rescue cell-surface expression and function of misfolded V2 vasopressin receptor mutants. J Clin Invest *105*, 887-895.

Moriki, T., Maruyama, H., and Maruyama, I. N. (2001). Activation of preformed EGF receptor dimers by ligand-induced rotation of the transmembrane domain. J Mol Biol *311*, 1011-1026.

Morrison, S. A., Russell, R. M., Carney, E. A., and Oaks, E. V. (1978). Zinc deficiency: a cause of abnormal dark adaptation in cirrhotics. Am J Clin Nutr *31*, 276-281.

Mukhopadhyay, A., Dracheva, S., Bose, S., and Hendler, R. (1996). Control of the integral membrane protein pump, bacteriorhodopsin, by purple membrane lipids of Halobacterium halobium. Biochemistry *35*, 9245-9252.

Müller, D. J., Amrein, M., and Engel, A. (1997). Adsorption of biological molecules to a solid support for scanning probe microscopy. J Struct Biol *119*, 172-188.

Müller, D. J., Baumeister, W., and Engel, A. (1999a). Controlled unzipping of a bacterial surface layer with atomic force microscopy. Proc Natl Acad Sci U S A *96*, 13170-13174.

Müller, D. J., Büldt, G., and Engel, A. (1995). Force-induced conformational change of bacteriorhodopsin. J Mol Biol *249*, 239-243.

Müller, D. J., and Engel, A. (1997). The height of biomolecules measured with the atomic force microscope depends on electrostatic interactions. Biophys J *73*, 1633-1644.

Müller, D. J., and Engel, A. (1999). Voltage and pH-induced channel closure of porin OmpF visualized by atomic force microscopy. J Mol Biol *285*, 1347-1351.

Müller, D. J., and Engel, A. (2002). Conformations, flexibility, and interactions observed on individual membrane proteins by atomic force microscopy. Methods Cell Biol *68*, 257-299.

Müller, D. J., Engel, A., Matthey, U., Meier, T., Dimroth, P., and Suda, K. (2003). Observing membrane protein diffusion at subnanometer resolution. J Mol Biol *327*, 925-930.

Müller, D. J., Fotiadis, D., Scheuring, S., Muller, S. A., and Engel, A. (1999b). Electrostatically balanced subnanometer imaging of biological specimen by atomic force microscopy. Biophys J *76*, 1101-1111.

Müller, D. J., Hand, G. M., Engel, A., and Sosinsky, G. (2002a). Conformational changes in surface structures of isolated connexin26 gap junctions. EMBO J *21*, 3598-3607.

Müller, D. J., Kessler, M., Oesterhelt, F., Möller, C., Oesterhelt, D., and Gaub, H. (2002b). Stability of bacteriorhodopsin alpha-helices and loops analyzed by single-molecule force spectroscopy. Biophys J *83*, 3578-3588.

Müller, D. J., Sapra, K. T., Scheuring, S., Kedrov, A., Frederix, P. L., Fotiadis, D., and Engel, A. (2006). Single molecule studies of membrane proteins. Curr Opin Struc Biol *16*, 1-7.

Müller, D. J., Sass, H. J., Muller, S. A., Buldt, G., and Engel, A. (1999c). Surface structures of native bacteriorhodopsin depend on the molecular packing arrangement in the membrane. J Mol Biol *285*, 1903-1909.

Nagy, J. K., Lonzer, W. L., and Sanders, C. R. (2001). Kinetic study of folding and misfolding of diacylglycerol kinase in model membranes. Biochemistry *40*, 8971-8980.

Nagy, J. K., and Sanders, C. R. (2002). A critical residue in the folding pathway of an integral membrane protein. Biochemistry *41*, 9021-9025.

Nagy, J. K., and Sanders, C. R. (2004). Destabilizing mutations promote membrane protein misfolding. Biochemistry *43*, 19-25.

Nakayama, T. A., and Khorana, H. G. (1990). Orientation of retinal in bovine rhodopsin determined by cross-linking using a photoactivatable analog of 11-cis-retinal. J Biol Chem *265*, 15762-15769.

Nevo, R., Brumfeld, V., Kapon, R., Hinterdorfer, P., and Reich, Z. (2005). Direct measurement of protein energy landscape roughness. EMBO Rep *6*, 482-486.

Oberhauser, A. F., Badilla-Fernandez, C., Carrion-Vazquez, M., and Fernandez, J. M. (2002). The mechanical hierarchies of fibronectin observed with single-molecule AFM. J Mol Biol *319*, 433-447.

Oberhauser, A. F., Hansma, P. K., Carrion-Vazquez, M., and Fernandez, J. M. (2001). Stepwise unfolding of titin under force-clamp atomic force microscopy. Proc Natl Acad Sci U S A *98*, 468-472.

Oberhauser, A. F., Marszalek, P. E., Carrion-Vazquez, M., and Fernandez, J. M. (1999). Single protein misfolding events captured by atomic force microscopy. Nat Struct Biol *6*, 1025-1028.

Oberhauser, A. F., Marszalek, P. E., Erickson, H. P., and Fernandez, J. M. (1998). The molecular elasticity of the extracellular matrix protein tenascin. Nature *393*, 181-185.

Oesterhelt, D., and Stoeckenius, W. (1971). Rhodopsin-like protein from the purple membrane of Halobacterium halobium. Nat New Biol (London) *233*, 149-152.

Oesterhelt, D., and Stoeckenius, W. (1974). Isolation of the cell membrane of Halobacterium halobium and it fraction into red and purple membrane. Methods Enzymol *31*, 667-678.

Oesterhelt, F., Oesterhelt, D., Pfeiffer, M., Engel, A., Gaub, H. E., and Müller, D. J. (2000). Unfolding pathways of individual bacteriorhodopsins. Science *288*, 143-146.

Okada, T., Ernst, O. P., Palczewski, K., and Hofmann, K. P. (2001). Activation of rhodopsin: new insights from structural and biochemical studies. Trends Biochem Sci *26*, 318-324.

Okada, T., Fujiyoshi, Y., Silow, M., Navarro, J., Landau, E. M., and Shichida, Y. (2002). Functional role of internal water molecules in rhodopsin revealed by X-ray crystallography. Proc Natl Acad Sci U S A *99*, 5982-5987.

Okada, T., Sugihara, M., Bondar, A. N., Elstner, M., Entel, P., and Buss, V. (2004). The retinal conformation and its environment in rhodopsin in light of a new 2.2 A crystal structure. J Mol Biol *342*, 571-583.

Opella, S. J., and Marassi, F. M. (2004). Structure determination of membrane proteins by NMR spectroscopy. Chem Rev *104*, 3587-3606.

Oroudjev, E., Soares, J., Arcdiacono, S., Thompson, J. B., Fossey, S. A., and Hansma, H. G. (2002). Segmented nanofibers of spider dragline silk: atomic force microscopy and single-molecule force spectroscopy. Proc Natl Acad Sci U S A *99*, 6460-6465.

Otomo, J., Tomioka, H., and Sasabe, H. (1992). Bacterial rhodopsins of newly isolated halobacteria. J Gen Microbiol *138*, 1027-1037.

Ovchinnikov Yu, A. (1982). Rhodopsin and bacteriorhodopsin: structure-function relationships. FEBS Lett *148*, 179-191.

Overton, M. C., Chinault, S. L., and Blumer, K. J. (2003). Oligomerization, biogenesis, and signaling is promoted by a glycophorin A-like dimerization motif in transmembrane domain 1 of a yeast G protein-coupled receptor. J Biol Chem *278*, 49369-49377.

Pace, C. N. (1986). Determination and analysis of urea and guanidine hydrochloride denaturation curves. Methods Enzymol *131*, 266-280.

Palczewski, K. (2006). G protein-coupled receptor rhodopsin. Annu Rev Biochem *75*, 743-767.

Palczewski, K., Buczylko, J., Kaplan, M. W., Polans, A. S., and Crabb, J. W. (1991). Mechanism of rhodopsin kinase activation. J Biol Chem *266*, 12949-12955.

Palczewski, K., Kumasaka, T., Hori, T., Behnke, C. A., Motoshima, H., Fox, B. A., Le Trong, I., Teller, D. C., Okada, T., Stenkamp, R. E., *et al.* (2000). Crystal structure of rhodopsin: A G protein-coupled receptor. Science *289*, 739-745.

Papermaster, D. S. (1982). Preparation of retinal rod outer segments. Methods Enzymol *81*, 48-52.

Pareek, S., Notterpek, L., Snipes, G. J., Naef, R., Sossin, W., Laliberte, J., Iacampo, S., Suter, U., Shooter, E. M., and Murphy, R. A. (1997). Neurons promote the translocation of peripheral myelin protein 22 into myelin. J Neurosci *17*, 7754-7762.

Park, P. S.-H., Filipek, S., Wells, J. W., and Palczewski, K. (2004). Oligomerization of G protein-coupled receptors: past, present, and future. Biochemistry *43*, 15643-15656.

Park, P. S.-H., and Palczewski, K. (2005). Diversifying the repertoire of G protein-coupled receptors through oligomerization. Proc Natl Acad Sci U S A *102*, 8793-8794.

Partridge, A. W., Therien, A. G., and Deber, C. M. (2002). Polar mutations in membrane proteins as a biophysical basis for disease. Biopolymers *66*, 350-358.

Petrache, H. I., Grossfield, A., MacKenzie, K. R., Engelman, D. M., and Woolf, T. B. (2000). Modulation of glycophorin A transmembrane helix interactions by lipid bilayers: molecular dynamics calculations. J Mol Biol *302*, 727-746.

Philippsen, A., Im, W., Engel, A., Schirmer, T., Roux, B., and Müller, D. J. (2002). Imaging the electrostatic potential of transmembrane channels: Atomic probe microscopy on OmpF porin. Biophys J *82*, 1667-1676.

Pierce, K. L., Premont, R. T., and Lefkowitz, R. J. (2002). Seven-transmembrane receptors. Nat Rev Mol Cell Biol *3*, 639-650.

Pogoryelov, D., Yu, J., Meier, T., Vonck, J., Dimroth, P., and Müller, D. J. (2005). The c15 ring of the *Spirulina platensis* F-ATP synthase: F1/F0 symmetry mismatch is not obligatory. EMBO Rep *6*, 1040-1044.

Popot, J.-L., Gerchmann, S.-E., and Engelmann, D. M. (1987). Refolding of bacteriorhodopsin in lipid bilayers: a thermodynamically controlled two-stage process. J Mol Biol *198*, 655-676.

Popot, J. L., and Engelman, D. M. (1990). Membrane protein folding and oligomerization: the two-stage model. Biochemistry *29*, 4031-4037.

Popot, J. L., and Engelman, D. M. (2000). Helical membrane protein folding, stability, and evolution. Annu Rev Biochem *69*, 881-922.

Prasad, A. S. (1995). Zinc: an overview. Nutrition *11*, 93-99.

Privalov, P. L. (1992). Physical basis of the stability of the folded conformations of proteins. In Protein folding, T. E. Creighton, ed. (New York, Freeman), pp. 83-126.

Prusiner, S. (1997). Prion diseases and the BSE crisis. Science *278*, 245-251.

Rader, A. J., Anderson, G., Isin, B., Khorana, H. G., Bahar, I., and Klein-Seetharaman, J. (2004). Identification of core amino acids stabilizing rhodopsin. Proc Natl Acad Sci U S A *101*, 7246-7251.

Ramachandran, R., Heuck, A. P., Tweten, R. K., and Johnson, A. E. (2002). Structural insights into the membrane-anchoring mechanism of a cholesterol-dependent cytolysin. Nat Struct Biol *9*, 823-827.

Rapoport, T. A., Goder, V., Heinrich, S. U., and Matlack, K. E. (2004). Membrane-protein intergation and the role of the translocation channel. Trends Cell Biol *14*, 568-575.

Rattner, A., Sun, H., and Nathans, J. (1999). Molecular genetics of human retinal disease. Annu Rev Genet *33*, 89-131.

Rees, D. C., Komiya, H., Yeates, T. O., Allen, J. P., and Feher, G. (1989). The bacterial photosynthetic reaction center as a model for membrane proteins. Annu Rev Biochem *58*, 607-633.

Reiersen, H., and Rees, A. R. (2001). The hunchback and its neighbours: proline as an environmental modulator. Trends Biochem Sci *26*, 679-684.

Rhee, K. H., Morris, E. P., Barber, J., and Kuhlbrandt, W. (1998). Three-dimensional structure of the plant photosystem II reaction centre at 8 A^0 resolution. Nature *396*, 283-286.

Richards, F. M. (1992). Folded and unfolded proteins: an introduction. In Protein folding, T. E. Creighton, ed. (New York, Freeman), pp. 1-58.

Ridge, K. D., Abdulaev, N. G., Sousa, M., and Palczewski, K. (2003). Phototransduction: crystal clear. Trends Biochem Sci *28*, 479-487.

Ridge, K. D., Lee, S. S., and Yao, L. L. (1995a). In vivo assembly of rhodopsin from expressed polypeptide fragments. Proc Natl Acad Sci U S A *92*, 3204-3208.

Ridge, K. D., Lu, Z., Liu, X., and Khorana, H. G. (1995b). Structure and function in rhodopsin. Separation and characterization of the correctly folded and misfolded opsins produced on expression of an opsin mutant gene containing only the native intradiscal cysteine codons. Biochemistry *34*, 3261-3267.

Ridge, K. D., Ngo, T., Lee, S. S., and Abddulaev, N. G. (1999). Folding and assembly in rhodopsin. Effect of mutations in the sixth transmembrane helix on the conformation of the third cytoplasmic loop. J Biol Chem *274*, 21437-21442.

Rief, M., Clausen-Schaumann, H., and Gaub, H. E. (1999a). Sequence-dependent mechanics of single DNA molecules. Nat Struct Biol *6*, 346-349.

Rief, M., Fernandez, J. M., and Gaub, H. E. (1998a). Elastically coupled two-level-systems as a model for biopolymer extensibility. Phys Rev Lett *81*, 4764-4767.

Rief, M., Gautel, M., Oesterhelt, F., Fernandez, J. M., and Gaub, H. E. (1997a). Reversible unfolding of individual titin immunoglobulin domains by AFM. Science *276*, 1109-1112.

Rief, M., Gautel, M., Schemmel, A., and Gaub, H. E. (1998b). The mechanical stability of immunoglobulin and fibronectin III domains in the muscle protein titin measured by atomic force microscopy. Biophys J *75*, 3008-3014.

Rief, M., Oesterhelt, F., Heymann, B., and Gaub, H. (1997b). Single molecule force spectroscopy on polysaccharides by atomic force microscopy. Science *275*, 1295-1297.

Rief, M., Pascual, J., Saraste, M., and Gaub, H. E. (1999b). Single molecule force spectroscopy of spectrin repeats: low unfolding forces in helix bundles. J Mol Biol *286*, 553-561.

Sader, J. E., Larson, I., Mulvaney, P., and White, L. R. (1995). Method for calibration of atomic force cantilevers. Rev Sci Instrum *60*, 3131-3134.

Salahpour, A., Angers, S., and Bouvier, M. (2000). Functional significance of oligomerization of G-protein-coupled receptors. Trends in Endocrinology and Metabolism *11*, 163-168.

Sanders, C. R., and Myers, J. K. (2004). Disease-related misassembly of membrane proteins. Annu Rev Biophys Biomol Struct *33*, 25-51.

Sanders, C. R., and Nagy, J. K. (2000). Misfolding of membrane proteins in health and disease: the lady or the tiger? Curr Opin Struct Biol *10*, 438-442.

Sansom, M. S., and Weinstein, H. (2000). Hinges, swivels and switches: the role of prolines in signalling via transmembrane alpha-helices. Trends Pharm Sci *21*, 445-451.

Sansom, M. S. P., and Kerr, I. D. (1995). Transbilayer pores formed by β-barrels: molecular modeling of pore structures and properties. Biophys J *69*, 1334-1343.

Sapra, K. T., Besir, H., Oesterhelt, D., and Muller, D. J. (2006a). Characterizing molecular interactions in different bacteriorhodopsin assemblies by single-molecule force spectroscopy. J Mol Biol *355*, 640-650.

Sapra, K. T., Park, P. S., Filipek, S., Engel, A., Müller, D. J., and Palczewski, K. (2006b). Detecting molecular interactions that stabilize native bovine rhodopsin. J Mol Biol *358*, 255-269.

Sarma, U., Brunner, E., Evans, J., and Wormald, R. (1994). Nutrition and the epidemiology of cataract and age-related maculopathy. Eur J Clin Nutr *48*, 1-8.

Schetz, J. A., Chu, A., and Sibley, D. R. (1999). Zinc modulates antagonist interactions with D2-like dopamine receptors through distinct molecular mechanisms. J Pharmacol Exp Ther *289*, 956-964.

Schetz, J. A., and Sibley, D. R. (1997). Zinc allosterically modulates antagonist binding to cloned D1 and D2 dopamine receptors. J Neurochem *68*, 1990-1997.

Scheuring, S., Busselez, J., and Levy, D. (2005). Structure of the dimeric PufX-containing core complex of *Rhodobacter blasticus* by in situ atomic force microscopy. J Biol Chem *280*, 1426-1431.

Scheuring, S., Goncalves, R. P., Prima, V., and Sturgis, J. N. (2006). The photosynthetic apparatus of *Rhodopseudomonas palustris*: structures and organization. J Mol Biol *358*, 83-96.

Scheuring, S., Müller, D. J., Stahlberg, H., Engel, H. A., and Engel, A. (2002). Sampling the conformational space of membrane protein surfaces with the AFM. Eur Biophys J *31*, 172-178.

Scheuring, S., Seguin, J., Marco, S., Levy, D., Robert, B., and Rigaud, J. L. (2003). Nanodissection and high-resolution imaging of the Rhodopseudomonas viridis photosynthetic core complex in native membranes by AFM. Proc Natl Acad Sci U S A *100*, 1690-1693.

Scheuring, S., and Sturgis, J. N. (2005). Chromatic adaptation of photosynthetic membranes. Science *309*, 484-487.

Schiffer, M., Chang, C. H., and Stevens, F. J. (1992). The functions of tryptophan residues in membrane proteins. Prot Eng *5*, 213-214.

Schlessinger, J. (2002). Ligand-induced, receptor-mediated dimerization and activation of EGF receptor. Cell *110*, 669-672.

Schlierf, M., Li, H., and Fernandez, J. M. (2004). The unfolding kinetics of ubiquitin captured with single-molecule force-clamp techniques. Proc Natl Acad Sci U S A *101*, 7299-7304.

Schneider, G., Diller, R., and Stockburger, M. (1989). Photochemical quantum yield of bacteriorhodopsin from resonance Raman scattering as a probe for photolysis. Chem Phys *131*, 17-29.

Schoenauer, R., Bertoncini, P., Machaidze, G., Aebi, U., Perriard, J.-C., Hegner, M., and Agarkova, I. (2005). Myomesin is a molecular spring with adaptable elasticity. J Mol Biol *349*, 367-379.

Schwabe, J. W., and Klug, A. (1994). Zinc mining for protein domains. Nat Struct Biol *1*, 345-349.

Schwaiger, I., Schleicher, M., Noegel, A. A., and Rief, M. (2005). The folding pathway of a fast-folding immunoglobulin domain revealed by single-molecule mechanical experiments. EMBO Reports *6*, 46-51.

Seeber, M., Fanelli, F., Paci, E., and Caflisch, A. (2006). Sequential unfolding of individual helices of bacterioopsin observed in molecular dynamics simulations of extraction from the purple membrane. Biophys J *91*, 3276-3284.

Seelert, H., Poetsch, A., Dencher, N. A., Engel, A., Stahlberg, H., and Müller, D. J. (2000). Proton powered turbine of a plant motor. Nature *405*, 418-419.

Seibert, F. S., Loo, T. W., Clarke, D. M., and Riordan, J. R. (1997). Cystic fibrosis: channel, catalytic, and folding properties of the CFTR protein. J Bioenerg Biomembr *29*, 429-442.

Selkoe, D. J. (2001). Alzheimer's disease: genes, proteins, and therapy. Physiol Rev *81*, 741-766.

Senes, A., Ubarretxena-Belandia, I., and Engelman, D. M. (2001). The Calpha-H.O hydrogen bond: a determinant of stability and specificity in transmembrane helix interactions. Proc Natl Acad Sci U S A *98*, 9056-9061.

Shelden, M. C., Loughlin, P., Tierney, M. L., and Howitt, S. M. (2001). Proline residues in two tightly coupled helices of the sulphate transporter, SHST1, are important for sulphate transport. Biochem J *356*, 589-594.

Shin, I., Kreimer, D., Silman, I., and Weiner, L. (1997). Membrane-promoted unfolding of acetylcholinesterase: a possible mechanism for insertion into the lipid bilayer. Proc Natl Acad Sci U S A *94*, 2848-2852.

Shuster, T. A., Martin, F., and Nagy, A. K. (1996). Zinc causes an apparent increase in rhodopsin phosphorylation. Curr Eye Res *15*, 1019-1024.

Shuster, T. A., Nagy, A. K., Conly, D. C., and Farber, D. B. (1992). Direct zinc binding to purified rhodopsin and disc membranes. Biochem J *282 (Pt 1)*, 123-128.

Silvestro, L., and Axelsen, P. H. (2000). Membrane-induced folding of cecropin A. Biophys J *79*, 1465-1477.

Simson, D. A., Ziemann, F., Strigl, M., and Merkel, R. (1998). Micropipet-based picoforce transducer: indepth analysis and experimental verification. Biophys J *74*, 2080-2088.

Singer, S. J., and Nicolson, G. L. (1972). The fluid mosaic model of the structure of cell membranes. Science *175*, 720-731.

Smith, S. B., Finzi, L., and Bustamante, C. (1992). Direct mechanical measurements of the elasticity of single DNA-molecules by using magnetic beads. Science *258*, 1122-1126.

Song, L., Hobaugh, M. R., Shustak, C., Cheley, S., Bayley, H., and Gouaux, J. E. (1996). Structure of staphylococcal α-hemolysin, a heptameric transmembrane pore. Science *274*, 1859-1866.

Stahlberg, H., Muller, D. J., Suda, K., Fotiadis, D., Engel, A., Meier, T., Matthey, U., and Dimroth, P. (2001). Bacterial Na(+)-ATP synthase has an undecameric rotor. EMBO Reports *2*, 229-233.

Steinhoff, H.-J., Mollaaghababa, R., Altenbach, C., Khorana, H. G., and Hubbell, W. L. (1995). Site directed spin labeling studies of structure and dynamics in bacteriorhodopsin. Biophys Chem *56*, 89-94.

Sternberg, B., L'Hostis, C., Whiteway, C., and Watts, A. (1992). The essential role of specific Halobacterium halobium polar lipids in 2D-array formation of bacteriorhodopsin. Biochim Biophys Acta *1108*, 21-30.

Stöffler, D., Goldie, K. N., Feja, B., and Aebi, U. (1999). Calcium-mediated structural changes of native nuclear pore complexes monitored by time-lapse atomic force microscopy. J Mol Biol *287*, 741-752.

Stojanovic, A., and Hwa, J. (2002). Rhodopsin and retinitis pigmentosa: shedding light on structure and function. Recept Channels *8*, 33-50.

Stojanovic, A., Stitham, J., and Hwa, J. (2004). Critical role of transmembrane segment zinc binding in the structure and function of rhodopsin. J Biol Chem *279*, 35932-35941.

Strunz, T., Oroszlan, K., Schumakovitch, I., Guntherodt, H., and Hegner, M. (2000). Model energy landscapes and the force-induced dissociation of ligand-receptor bond. Biophys J *79*, 1206-1212.

Subramaniam, S., Gerstein, M., Oesterhelt, D., and Henderson, R. (1993). Electron diffraction analysis of structural changes in the photocycle of bacteriorhodopsin. EMBO J *12*, 1-8.

Suda, K., Filipek, S., Palczewski, K., Engel, A., and Fotiadis, D. (2004). The supramolecular structure of the GPCR rhodopsin in solution and native disc membranes. Mol Membr Biol *21*, 435-446.

Sui, H., Han, B. G., Lee, J. K., Walian, P., and Jap, B. K. (2001). Structural basis of water-specific transport through the AQP1 water channel. Nature *414*, 872-878.

Swaminath, G., Lee, T. W., and Kobilka, B. (2003). Identification of an allosteric binding site for Zn2+ on the beta2 adrenergic receptor. J Biol Chem *278*, 352-356.

Swaminath, G., Steenhuis, J., Kobilka, B., and Lee, T. W. (2002). Allosteric modulation of beta2-adrenergic receptor by Zn(2+). Mol Pharmacol *61*, 65-72.

Takeda, S., Kadowaki, S., Haga, T., Takaesu, H., and Mitaku, S. (2002). Identification of G protein-coupled receptor genes from the human genome sequence. FEBS Letters *520*, 97-101.

Tamarappoo, B. K., Yang, B., and Verkman, A. S. (1999). Misfolding of mutant aquaporin-2 water channels in nephrogenic diabetes insipidus. J Biol Chem *274*, 34825-34831.

Teller, D. C., Okada, T., Behnke, C. A., Palczewski, K., and Stenkamp, R. E. (2001). Advances in determination of a high-resolution three-dimensional structure of rhodopsin, a model of G-protein-coupled receptors (GPCRs). Biochemistry *40*, 7761-7772.

Torii, A., Sasaki, M., Hane, K., and Okuma, S. (1996). A method for determining the spring constant of cantilevers for atomic force microscopy. Meas Sci Technol *7*, 179-184.

Torres, J., Stevens, T. J., and Samso, M. (2003). Membrane proteins: the 'Wild West' of structural biology. Trends Biochem Sci *28*, 137-144.

Tsai, B., Ye, Y., and Rapoport, T. A. (2002). Retrotranslocation of proteins from the endoplasmic reticulum into the cytosol. Nat Rev Mol Cell Biol *3*, 246-255.

Tskhovrebova, L., Trinick, J., Sleep, J. A., and Simmons, R. M. (1997). Elasticity and unfolding of single molecules of the giant muscle protein titin. Nature *387*, 308-312.

Ubarretxena-Belandia, I., Baldwin, J. M., Schuldiner, S., and Tate, C. G. (2003). Three-dimensional structure of the bacterial multidrug transporter EmrE shows it is an asymmetric homodimer. EMBO J *22*, 6175-6181.

Ugarte, M., and Osborne, N. N. (1998). The localization of endogenous zinc and the in vitro effect of exogenous zinc on the GABA immunoreactivity and formation of reactive oxygen species in the retina. Gen Pharmacol *30*, 297-303.

Ugarte, M., and Osborne, N. N. (1999). The localization of free zinc varies in rat photoreceptors during light and dark adaptation. Exp Eye Res *69*, 459-461.

Ugarte, M., and Osborne, N. N. (2001). Zinc in the retina. Prog Neurobiol *64*, 219-249.

Unger, V. M., Kumar, N. M., Gilula, N. B., and Yeager, M. (1999). Three-dimensional structure of a recombinant gap junction membrane channel. Science *283*, 1176-1180.

Unwin, P. N., and Henderson, R. (1975). Molecular structure determination by electron microscopy of unstained crystalline specimens. J Mol Biol *94*, 425-440.

Vallee, B. L., and Falchuk, K. H. (1993). The biochemical basis of zinc physiology. Physiol Rev *73*, 79-118.

Van den Berg, B., Clemons, W. M. J., Collinson, I., Modis, Y., Hartmann, E., Harrison, S. C., and Rapoport, T. A. (2004). X-ray structure of a protein-conducting channel. Nature *427*, 36-44.

Van der Spoel, D., Lindahl, E., Hess, B., Groenhof, G., Mark, A. E., and Berendsen, H. J. (2005). GROMACS: fast, flexible, and free. J Comput Chem *26*, 1701-1718.

Viani, M. B., Pietrasanta, L. I., Thompson, J. B., Chand, A., Gebeshuber, I. C., Kindt, J. H., Richter, M., Hansma, H. G., and Hansma, P. K. (2000). Probing protein-protein interactions in real time. Nat Struct Biol *7*, 644-647.

Viani, M. B., Schäfer, T. E., Chand, A., Rief, M., Gaub, H., and Hansma, P. K. (1999). Small cantilevers for force spectroscopy of single molecules. J Appl Phys *86*, 2258-2262.

Voet, D., Voet, J. G., and Pratt, C. W. (1999). Fundamentals of biochemistry (New York, John Wiley & Sons, Inc.).

von Heijne, G. (1986). The distribution of positively charged residues in bacterial inner membrane proteins correlates with the transmembrane topology. EMBO J *5*, 3021-3027.

Wakamatsu, K., Okada, A., Miyazawa, T., Ohya, M., and Higashijima, T. (1992). Membrane-bound conformation of mastoparan-X, a G-protein-activating peptide. Biochemistry *31*, 5654-5660.

Wallin, E., and von Heijne, G. (1998). Genome wide analysis of integral membrane proteins from eubacterial, archaean, and eukaryotic organisms. Protein Sci *7*, 1029-1038.

Walz, T., Hirai, T., Murata, K., Heyman, J., Mitsuoka, K., Fujiyoshi, Y., Smith, B. L., Agre, P., and Engel, A. (1997). The three-dimensional structure of aquaporin-1. Nature *387*, 624-627.

Wang, Z., and Moult, J. (2001). SNPs, protein structure, and disease. Hum Mutat *17*, 263-270.

Weik, M., Patzelt, H., Zaccai, G., and Oesterhelt, D. (1998). Localization of glycolipids in membranes by in vivo labeling and neutron diffraction. Mol Cell *1*, 411-419.

Weiss, J. H., Sensi, S. L., and Koh, J. Y. (2000). Zn(2+): a novel ionic mediator of neural injury in brain disease. Trends Pharm Sci *21*, 395-401.

Wen, J., Chen, X., and Bowie, J. U. (1996). Exploring the allowed sequence space of a membrane protein. Nat Struct Biol *3*, 141-148.

White, S. (2003). Translocons, thermodynamics, and the folding of membrane proteins. FEBS Lett *555*, 116-121.

White, S. H. (2004). The progress of membrane protein structure determination. Protein Sci *13*, 1948-1949.

White, S. H., and Wimley, W. C. (1999). Membrane protein folding and stability: Physical principles. Annu Rev Biophys Biomol Struct *28*, 319-365.

Wiener, M. C., and White, S. H. (1992). Structure of a fluid dioleoylphosphatidylcholine bilayer determined by joint refinement of X-ray and neutron diffraction data. III. Complete structure. Biophys J *61*, 437-447.

Wigley, W. C., Corboy, M. J., Cutler, T. D., Thibodeau, P. H., Oldan, J., Lee, M. G., Rizo, J., Hunt, J. F., and Thomas, P. J. (2002). A protein sequence that can encode native structure by disfavoring alternate conformations. Nat Struct Biol *9*, 381-388.

Wiita, A. P., Ainavarapu, S. R., Huang, H. H., and Fernandez, J. M. (2006). Force-dependent chemical kinetics of disulfide bond reduction observed with single-molecule techniques. Proc Natl Acad Sci U S A *103*, 7222-7227.

Williams, K. A., and Deber, C. M. (1991). Proline residues in transmembrane helices: structural or dynamic role? Biochemistry *30*, 8919-8923.

Wimley, W. C. (2003). The versatile beta-barrel membrane protein. Curr Opin Struct Biol *13*, 404-411.

Wimley, W. C., Creamer, T. P., and White, S. H. (1996). Solvation energies of amino acid sidechains and backbone in a family of host-guest pentapeptides. Biochemistry *35*, 5109-5124.

Wimley, W. C., and White, S. H. (1996). Experimentally determined hydrophobicity scale for proteins at membrane interfaces. Nat Struct Biol *3*, 842-848.

Xiong, X., Chong, E., and Skach, W. R. (1999). Evidence that the endoplasmic reticulum (ER)-associated degradation of cystic fibrosis transmembrane conductance regulator is linked to retrograde translocation from the ER membrane. J Biol Chem *274*, 2616-2624.

Yohannan, S., Faham, S., Yang, D., Grosfeld, D., Chamberlain, A. K., and Bowie, J. U. (2004a). A Cα-H---O hydrogen bond in a membrane protein is not stabilizing. J Am Chem Soc *126*, 2284-2285.

Yohannan, S., Faham, S., Yang, D., Whitelegge, J. P., and Bowie, J. U. (2004b). The evolution of transmembrane helix kinks and the structural diversity of G protein-coupled receptors. Proc Natl Acad Sci U S A *101*, 959-963.

Zhan, H., Oh, K. J., Shin, Y.-K., Hubbell, W. L., and Collier, R. J. (1995). Interaction of the isolated transmembrane domain of diphtheria toxin with membranes. Biochemistry *34*, 4856-4863.

Zhou, F. X., Cocco, M. J., Russ, W. P., Brunger, A. T., and Engelman, D. M. (2000). Interhelical hydrogen bonding drives strong interactions in membrane proteins. Nature Structural Biology *7*, 154-160.

Zhou, Y., and Bowie, J. U. (2000). Building a thermostable membrane protein. J Biol Chem *275*, 6975-6979.

Zielenski, J., and Tsui, L. C. (1995). Cystic fibrosis: genotypic and phenotypic variations. Annu Rev Genet *29*, 777-807.

PUBLICATIONS

Peer-reviewed research articles

1) **Sapra, K. T.**, Marsico, A., Balasubramanian, P., Labudde, D., and Müller, D. J. (2006) Effect of point mutations on the complex unfolding energy landscape of bacteriorhodopsin - *manuscript in preparation*

2) Park, P. S.*, **Sapra, K. T.***, Koliski, M., Filipek, S., Palczewski, K., and Müller, D. J. (2006) Stabilizing effect of zinc in native bovine rhodopsin – *submitted* (*equal contribution)

3) Marsico, A., **Sapra, K. T.**, Muller, D. J., Schroeder, M, and Labudde, D. (2006) A structure-based analysis of single-molecule force spectroscopy (SMFS) data for bacteriorhodopsin and four mutants. *Complife2006, LNBI*, 162-172.

4) Marsico, A., Labudde, D., **Sapra, K. T.**, Müller, D. J., and Schroeder, M. (2006) A novel pattern recognition algorithm to classify membrane protein unfolding pathways with high-throughput single molecule force spectroscopy. *Bioinformatics – in press*

5) **Sapra K. T.*,** Park, P. S.*, Filipek, S., Engel, A., Muller, D. J., and Palczewski, K. (2006) Detecting molecular interactions that stabilize native bovine rhodopsin. *J Mol Biol* 358(1), 225-269 (*equal contribution)

6) **Sapra, K. T.**, Besir, H., Oesterhelt, D., and Müller, D. J. (2006) Characterizing molecular interactions in different bacteriorhodopsin assemblies by single-molecule force spectroscopy. *J Mol Biol* 355(4), 640-50

7) Janovjak, H., **Sapra, K.T.**, and Müller, D.J. (2005) Complex stability of single proteins explored by forced unfolding experiments. *Biophys J* 88(5), L37-L39

8) Ohi, R., **Sapra, K. T.**, Howard, J., and Mitchison, T. J. (2004) Differentiation of cytoplasmic and meiotic spindle assembly MCAK functions by Aurora B-dependent phosphorylation. *Mol Biol Cell* 15(6), 2895-2906

Reviews

9) Kedrov, A., Janovjak, H., **Sapra, K. T.**, and Müller, D. J. (2006) Deciphering molecular interactions of native membrane proteins by single-molecule force spectroscopy. *Annu Rev Biophys and Biomol Struct – submitted*

10) Müller, D. J., **Sapra, K. T.**, Scheuring, S., Kedrov, A., Frederix, P. L., Fotiadis, D., and Engel, A. (2006) Single-molecule studies of membrane proteins. *Curr Opin Struct Biol* 16(4), 489-495

11) Janovjak, H., Kedrov, A., Cisneros, D. A., **Sapra, K. T.**, Struckmeier, J., and Müller, D. J. (2006) Imaging and detecting molecular interactions of single transmembrane proteins. *Neurobiol of Aging* 27(4), 546-61

ACKNOWLEDGEMENTS

A PhD involves the work and support of many people. I would like to express my deep felt gratitude to the man who made all this possible - my PhD advisor, guide, friend and an excellent man, Prof. Dr. Daniel J. Müller. There are no words to express my gratefulness to Daniel. When I was all dejected and down without any hopes, Daniel believed in me and helped me gain my confidence and get back on my feet. I still remember that winter evening in January 2004 when I went to meet him in his laboratory and he was so kind and supportive. Though I had an unusual and unexpected start in his laboratory on January 16, 2004, let me put it in simple words that I was destined to do my PhD under Daniel. It was always my dream to work in a beautiful place, on the subject I love to do the most, and with a 'cool' supervisor. The whole experience in Daniel's laboratory has just been like a dream come true! The most important things in science - to finish a project and publish it, to make perfect figures, to write a clear and concise scientific story, I have learnt from Daniel. He has been a terrific mentor, and I sincerely hope that we continue and maintain our professional and personal relationship for many years to come.

I am extremely grateful to Prof. Petra Schwille for accepting to be in my thesis advisory committee, and taking the time out of her busy schedule for scientific meetings.

I would like to thank my colleagues Alexej Kedrov and Harald Janovjak for introducing me to atomic force microscope when I joined the lab. Thanks to Alexej again for accompanying me to several conferences in Europe and making all of those extremely memorable and pleasant trips. I am thankful to David Cisneros for his funny comments and a lively presence in the lab. I am greatly indebted to all the members of the lab for providing a wonderful working environment. It has been a great pleasure to know Jonne 'Master' Helenius, Pierre-H. Peuch, Clemens Franz, Michael 'Michi Boy' Krieg, Jens Friedrichs, Christian Bippes, Natalya Baltrukovich, Anna Taubenberger, Jana Doehner, Steffi Lennhard, Suzanne Wegmann, Isabel Richter, Helena Knaus and many others whom I forget to mention here. Everyone made the daily tisch-fuβball games extremely enjoyable. It was a great experience supervising Prakash Balasubramanian during his Master's thesis, and I would like to thank him for the cooperation. It was a great pleasure working with Dirk Labudde and Annalisa Marsico and my thanks to both for their help and hard work in the BR mutant project. My gratitude to our secretary Barbara Lindemann for all her hard work and struggle to save us from the daily bureaucracy.

My sincere thanks to Prof. Krzysztof Palczewski and Dr. Paul Park for their absolutely wonderful collaboration on the rhodopsin project. Without them the two big rhodopsin stories would not have been possible. I hope we continue to churn out many more interesting results in the coming future.

Above all, I would like to thank my mum and dad, Sangita Sapra and Dr. Rohit Sapra, for their constant support and encouragement in whatever I chose to do since childhood. I am very fortunate to have such liberal and caring parents, who have let me lead my life the way I want. My brother, Mohit Sapra, has always been a great source of encouragement to me, and more since I left India in 1999. He has always supported me in every step I have taken in my life. I don't want to belittle his contributions by thanking him; I would always be indebted to him. I am thankful to Nilu for taking care of us like a sister and helping the whole family with full devotion. Finally, I am thankful from the bottom of my heart to the beautiful doctor in my life, Edna Holz, whose love, patience and constant support in every possible way during the last two years gave me the strength to keep going.

Declaration

I herewith declare that I have produced this paper without the prohibited assistance of third parties and without making use of aids other than those specified; notions taken over directly or indirectly from other sources have been identified as such. This paper has not previously been presented in identical or similar form to any other German or foreign examination board.

The thesis work was conducted from **January 2004** to **July 2006** under the supervision of **Prof. Dr. Daniel J. Müller** at the Center for Biotechnology, University of Technology, Dresden.

K. Tanuj Sapra

Dresden, November 9, 2006